



Universidade do Minho
Escola de Engenharia

José Miguel Alves Pires

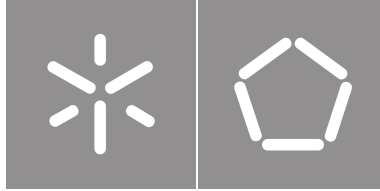
**Functional design and manufacturing of 3D
Multi-Material structures using SLS/SLM**

Functional design and manufacturing of 3D
Multi-Material structures using SLS/SLM

José Pires

UMinho | 2023

December, 2023



Universidade do Minho

Escola de Engenharia

José Miguel Alves Pires

**Functional design and manufacturing of
3D Multi-Material structures using
SLS/SLM**

Doctorate Thesis

Doctorate in Mechanical Engineering

Work developed under the supervision of:

Professor Doctor Óscar Carvalho

Professor Doctor Filipe Silva

December, 2023

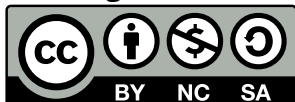
COPYRIGHT AND TERMS OF USE OF THIS WORK BY A THIRD PARTY

This is academic work that can be used by third parties as long as internationally accepted rules and good practices regarding copyright and related rights are respected.

Accordingly, this work may be used under the license provided below.

If the user needs permission to make use of the work under conditions not provided for in the indicated licensing, they should contact the author through the RepositoriUM of Universidade do Minho.

License granted to the users of this work



Creative Commons Attribution-NonCommercial-ShareAlike 4.0 International CC BY-NC-SA 4.0

<https://creativecommons.org/licenses/by-nc-sa/4.0/deed.en>

Acknowledgements

First and foremost, I would like to thank my lead supervisor, Prof. Óscar, for all the guidance, the unconditional friendship, and for the constant flood of sheer knowledge that was so valuable throughout this process. To Prof. Filipe Silva, for giving me the chance of working on this incredible project, supported by Portuguese Foundation of Science and Technology national funds, under the national support to R&D units grant, through the reference projects UIDB/04436/2020 and UIDP/04436/2020, 'HAMaBICo – Hybrid Additive Manufacturing for Bio-Inspired Components', reference NORTE-01-0145-FEDER-000018, LaserMULTICER POCI-01-0145-FEDER-031035, Add.Additive_Manufacturing to Portuguese Industry_POCI-01-0247-FEDER-024533, COMP4TA-Advanced Metal-Diamond Composites for thermal applications POCI-01-0145-FEDER-030416, DILATO NORTE-01-0247-FEDER-047289.

To Paulo Pinto for not only being a stupendous colleague, but a true friend, hearing my constant complaints and providing the assertive advice. To Flávio for the manufacturing tests and for the valuable inputs given. To Joseph Lennox (@lordofthehypens) and the open-source project `Slic3r` for the incredible help in the slicer and path generator development.

To my parents for always pushing me forward and for being the life example of character and sheer determination, a lamp lit on a stormy day. Thank you also for an upbringing full of debates and argumentation, which has undoubtedly contributed for mastering the challenges I took ahead, and sorry for my constant lack of time. To my sister, for always being so supportive and caring, helping out with your immense ingenuity and creativity, a mix between the engineer and the artist.

To my closest friends, Pedro, Guinho, Machado e Raúl for taking me out to dinner and drink, which is exactly what one needs sometimes. For all the support and the true friendship that survives even the end of times. To my newest friends, Chicão, Foguetes, Xabier Xantus, and Alejandro, for all the laughs, the talks, and the craziness. Life wouldn't be same without it. To my beloved dog Pantufa for adopting me nine years ago when I was going crazy with my first MSc thesis and never leaving my side.

STATEMENT OF INTEGRITY

I hereby declare having conducted this academic work with integrity. I confirm that I have not used plagiarism or any form of undue use of information or falsification of results along the process leading to its elaboration.

I further declare that I have fully acknowledged the Code of Ethical Conduct of the Universidade do Minho.

Guimarães, 21/12/2023
(Place) (Date)

(José Miguel Alves Pires)

”

“
'Imagination is more important than knowledge.'
(Einstein)
”

Design funcional e manufatura de estruturas 3D multimaterial através do processo de SLS/SLM

O design funcional é uma abordagem extremamente desejável para otimizar o desempenho de um produto, minimizando o uso de recursos e custos. No entanto, a adoção do design funcional pode exigir o uso de vários materiais ou uma combinação deles, o que é dificultado pelas tecnologias de fabrico atuais. Os implantes biomédicos, como o implante de anca, são um exemplo paradigmático da necessidade de design funcional. Atualmente, apenas alguns equipamentos comerciais são capazes de usar vários materiais [2, 3]. Além disso, exigem um investimento inicial significativo e são adequados apenas para metais, o que limita a gama de aplicações. Consequentemente, a literatura científica centra-se principalmente na modificação de equipamentos mono-material com sistemas de deposição multi-material [4–9], o que infelizmente também requer soluções manuais para configurar a cadeia de manufatura e o equipamento. Isto é agravado pela falta de diretrizes de projeto específicas para o processo **Multi-Material Laser-Powder Bed Fusion (MMLPBF)** e pelo fato de que a maioria dos procedimentos de pré-processamento usar um método manual baseado num formato de dados inadequado [10]. A principal conclusão é que o fabrico via **MMLPBF** é um problema multiobjetivo que requer equipamentos e ferramentas especializadas e design experimental. Assim, o presente trabalho visa reduzir o hiato entre o design e o fabrico de componentes multimaterial, como os implantes de anca, propondo uma abordagem holística para a cadeia de manufatura que possa alavancar o conhecimento do processo e apoiar o design funcional. Foi desenvolvida uma metodologia baseada em modelos para lidar com a elevada complexidade associada ao design e fabrico de componentes multimaterial e colmatar lacunas nesse domínio. O conhecimento adquirido através dos modelos foi usado para a instanciação dum fluxo de trabalho especializado para o processo **MMLPBF** e o desenvolvimento de ferramentas de software de suporte. Em seguida, foi desenvolvido um equipamento personalizado que integra vários lasers de diferentes tipos, que podem ser efetivamente usados para o fabrico de componentes multimaterial usando pós metálicos, poliméricos e/ou cerâmicos. Pela análise efetuada, trata-se do primeiro equipamento **MMLPBF** com esta característica. Adicionalmente, esta metodologia extensível pode ser usada para dar suporte a pós-tratamentos dos componentes, tais como tratamentos térmicos, diretamente da fase de modelação. Foram projetados e fabricados vários componentes multimaterial, seguindo a metodologia desenvolvida. Esses testes validaram todo o ecossistema, demonstrando a sua adequabilidade para o suporte do design funcional de componentes multimaterial usando o processo **MMLPBF**. Por fim, são apresentadas algumas perspectivas para alavancar a base de conhecimento do processo criada, onde ferramentas como a inteligência artificial podem ser usadas para melhorar de forma expedita o processo **MMLPBF**.

Palavras-chave: design funcional, 3D multimaterial, manufatura aditiva baseada em laser, metodologia, software, equipamento

Functional design and manufacturing of 3D Multi-Material structures using SLS/SLM

Functional design is a highly desirable approach to design, optimising the performance of a product while minimising the resources usage and cost. However, the adoption of functional design may dictate the use of multiple materials or a combination of them, which is hindered by the current manufacturing technologies. Biomedical implants, such as hip implants, represent a class of products where functional design is critical. Currently, only a handful of commercial equipments is capable of multi-material fabrication [2, 3]. Moreover, they require a significant initial investment and are only suited for metals, which limits the scope of applications. Consequently, research primarily focuses on upgrading mono-material equipment to add multi-material capabilities [4–9], which undesirably also requires manual workarounds to setup the manufacturing chain and equipments. This is further aggravated by the lack of specific design guidelines for the MMLPBF process and by the fact that most pre-processing procedures use a manual method based on an inadequate data format [10]. problem, requiring specially designed equipments and toolchains, and experimental design. Thus, the present work aims to close the gap between design and fabrication of multi-material components like the aforementioned implants by proposing a holistic approach to the multi-material fabrication of components incorporating metals, polymers, and/or ceramics that can leverage the process knowledge and support functional design. A model-based methodology was devised to address the high complexity associated with the design and manufacturing of multi-material parts and fill the gap in this domain. The knowledge acquired through the relevant models was used for the instantiation of a specialised workflow for the MMLPBF process and the development of a supporting toolchain. Then, a custom equipment was developed that integrates multiple lasers of different types, which can be effectively used for the fabrication of multi-material components using metallic, polymeric and/or ceramic powders. To the best of the author's knowledge, this is the first MMLPBF equipment with this feature. Additionally, this extensible framework can be used to support post-process treatments, such as heat treatments, directly from the modelling stage. Several multi-material components were designed and manufactured following the devised methodology. These tests validated the whole ecosystem, demonstrating its suitability to support the functional design of multi-material components using the MMLPBF process. Lastly, some prospects to leverage the process knowledge database created are presented, where tools like [Artificial Intelligence \(AI\)](#) can be used for straightforward and fast improvement of the MMLPBF process.

Keywords: functional design, 3D multi-material laser powder bed fusion, 3D multi-material fabrication, methodology, software toolchain, low-cost equipment

Contents

List of Figures	xi
List of Tables	xv
List of Listings	xvi
Acronyms	xvii
1 Introduction	1
1.1 Motivation	2
1.2 Main objectives	3
1.3 Thesis organisation	5
2 State of the art	8
2.1 Functional design	8
2.2 Mono-material Laser-Powder Bed Fusion	9
2.3 Multi-material Laser-Powder Bed Fusion	13
2.3.1 Technological Overview	14
2.3.2 Powder delivery systems	16
2.3.3 Manufacturing chain	21
2.4 Applications	27
2.5 Summary	28
3 The problem and its challenges	30
3.1 Proposed Approach – solution	30
3.2 A Global Methodology for 3DMMLPBF processes	31
3.2.1 Motivation	31
3.2.2 Core Principles	31
3.2.3 Concept	32
3.3 Summary	37

4	Development	38
4.1	Project methodologies	38
4.2	Application of the methodology to multi-material 3DMMLPBF	40
4.2.1	Pre-manufacturing: CAD to LCode	41
4.2.2	Manufacturing: LCode to Part	42
4.2.3	Post-Manufacturing: Part to Process	43
4.3	Toolchain	43
4.3.1	Pre-Manufacturer	44
4.3.2	Manufacturer	64
4.3.3	Post-manufacturer	80
4.4	Development of the 3DMMLPBF machine	88
4.4.1	Requirements & Constraints	88
4.4.2	System design	89
4.4.3	Domain specific design & Modelling	94
4.4.4	Implementation: Version 1	107
4.4.5	Implementation: Version 2	109
4.5	Summary	113
5	Tests	118
5.1	Multi-material mono-laser	118
5.1.1	CO ₂ Laser	118
5.1.2	Nd-YAG Laser	123
5.2	Multi-material multi-laser	129
5.2.1	Pre-Manufacturing	130
5.2.2	Manufacturing	131
5.2.3	Post-Manufacturing	135
5.3	3DMMLPBF Improvement	139
5.4	Results	143
5.5	Summary	143
6	Conclusion	145
6.1	Conclusions	145
6.2	Prospect for future work	147
	Bibliography	149
	Appendices	
A	Ezcad API	162
	Annexes	

I	A global methodology for 3D Multi-Material Laser-Powder Bed Fusion (3DMMLPBF) processes	165
II	Graphical Abstract	213

List of Figures

1	3DMMLPBF ecosystem	4
2	Graphical abstract	7
3	Additive manufacturing processes	11
4	LPBF process	12
5	LPBF process and key parameters	13
6	MMLPBF system overview	15
7	Conventional LPBF printer upgraded with a multi-material mechanism	17
8	MMLPBF machine with multiple hoppers	18
9	Vibrating nozzle dispenser system	19
10	Aerosint selective powder deposition system for MMLPBF	20
11	MMLPBF manufacturing chain overview	21
12	MMLPBF Pre-Process software	22
13	Flowchart for data flow for MMLPBF	23
14	Fabricated Voxel file format	24
15	Hip prosthesis and components detail	28
16	Model of the design activity	33
17	Model of pre-manufacturing activity	34
18	Model of manufacturing activity	35
19	Model of post-manufacturing activity	36
20	Workflow 3DMMLPBF-C2P (CAD to Process)	41
21	Workflow for the proposed workflow	43
22	Pre-Manufacturer analysis: use cases	46
23	Pre-Manufacturer analysis: Slicing and path generation overview	47
24	Pre-Manufacturer design: system architecture	47
25	Pre-Manufacturer implementation: 3D models loading and rendering	49
26	Pre-Manufacturer implementation: Slicing and path generation configuration	50
27	Pre-Manufacturer implementation: Manufacturing model generation and visualisation	51

28	Pre-Manufacturer implementation: Slicing and path generation specific configuration	52
29	Manufacturing file is successfully loaded by EzCAD software	52
30	Input <i>.stl</i> models	53
31	Path topologies list and examples	54
32	Fill angle test: 0° to 90°	55
33	Fill density test: 1% to 40%	55
34	Infill extrusion width test: 0.01–0.5 mm	55
35	Shortcomings of 3D Printing paths	55
36	Patches to make 3D printing paths comply with the Laser-Powder Bed Fusion (L-PBF) process	56
37	Pre-Manufacturer test: Cross and Cube input model	57
38	Pre-Manufacturer test: 3 cubes input model	58
39	Pre-Manufacturer test: Cylinder and cross input model	60
40	Pre-Manufacturer test: Cylinder and cross input model with z-offset	61
41	Cylinder and cross input model with z-offset and different slicing parameters	62
42	3DMMLPBF Pre-Manufacturer repository [169]	64
43	Manufacturer analysis: use cases	66
44	Sequence diagram of the LoadGeometryFile use case	67
45	Manufacturer design: system architecture	68
46	Manufacturer design: Manuf thread state-machine diagram	70
47	Manufacturer design: Messaging protocol	71
48	Manufacturer design: High-level class diagram — hierarchy and associations	72
49	Manufacturer implementation — deployment diagram	73
50	Manufacturer implementation: Main window	74
51	Manufacturer implementation: Manage Pen dialog	74
52	3DMMLPBF Manufacturer: Layer visualisation	75
53	Manufacturer implementation: Help dialog	75
54	Manufacturer test: process parameters mapping	76
55	Manufacturer test: materials and height	76
56	Printer log file (excerpt)	77
57	3DMMLPBF Laser connection testing: Master/Slave connection	78
58	3DMMLPBF Laser connection testing: simultaneous connection to multiple slaves	79
59	Manufacturer test: Export data	80
60	3DMMLPBF Manufacturer repository [170]	80
61	3DMMLPBF Post-Manufacturer design: Entity Relationship Diagram (ERD)	83
62	3DMMLPBF Post-Manufacturer design: Deployment diagram	83
63	3DMMLPBF Post-Manufacturer	85
64	3DMMLPBF Post-Manufacturer testing: load output file	86
65	3DMMLPBF Post-Manufacturer testing: Export database	87
66	3DMMLPBF Post-Manufacturer repository [175]	88
67	Working principle of the 3DMMLPBF machine: initial state	90
68	Working principle of the 3DMMLPBF machine: bed drops	91

69	Working principle of the 3DMMLPBF machine: powder recoating	91
70	Working principle of the 3DMMLPBF machine: laser marking	92
71	Working principle of the 3DMMLPBF machine: powder recovery	92
72	Overview of the 3DMMLPBF system	93
73	3D model of the 3DMMLPBF equipment	94
74	Mechanical design: machine 3D model (final version)	95
75	3DMMLPBF mechanical design: deposit and recoating subsystems	96
76	Mechanical design implementation: final result	96
77	Detailed subsystems for MMLPBF subsystem: control loop	97
78	Detailed subsystems for CO ₂ Laser subsystem: control loop	98
79	Overall system schematic wiring	99
80	Axis subsystem schematic wiring	100
81	Temperature subsystem schematic wiring	101
82	Shielding subsystem schematic wiring	101
83	Extraction subsystem schematic wiring	102
84	Electronics development: final result	103
85	Firmware design: system architecture	104
86	Firmware design: LCode Interpreter State-machine diagram	106
87	Firmware design: Messaging protocol	107
88	3DMMLPBF equipment v1.0: Machine, Laser, and Post-Processor and Printer UI	108
89	3DMMLPBF machine v2.0: Recoating system	109
90	3DMMLPBF machine v2.0: Powder recovery system	110
91	3DMMLPBF machine v2.0: Heating system	110
92	3DMMLPBF machine v2.0: Water cooling and atmosphere control systems	111
93	3DMMLPBF machine v2.0 and supporting framework	112
94	Automatic mechanical tests: command protocol	112
95	3DMMLPBF Laser marking testing	114
96	Manufacturing tests: machine's testing dialog	115
97	3DMMLPBF equipment's firmware repository [179]	115
98	3DMMLPBF ecosystem synopsis: Workflow, toolchain and equipment interactions	117
99	CO ₂ laser – bi-material manufacturing test: FreeCAD modelling	119
100	CO ₂ laser – bi-material manufacturing test: Pre-Manufacturing processing	120
101	CO ₂ laser – bi-material manufacturing test: Manufacturing	121
102	CO ₂ laser – bi-material manufacturing test: Produced part	122
103	CO ₂ laser – bi-material manufacturing test: Geometrical measurements using Fiji's SW	122
104	CO ₂ laser – bi-material manufacturing test: SEM analysis	123
105	CO ₂ laser – Post-Manufacturer: Pre-Manufacturer data management	124
106	CO ₂ laser – Post-Manufacturer: Manufacturer data management	125
107	CO ₂ laser – Post-Manufacturer: Mechanical tests manager	126
108	Nd-YAG laser: bi-material manufacturing test – Modelling in EzCAD	126

109	Nd-YAG laser – bi-material manufacturing test: Model preview	127
110	Nd-YAG laser – bi-material manufacturing test: Manufacturing	128
111	Nd-YAG laser – bi-material manufacturing test: Produced part	129
112	Nd-YAG laser – Post-Manufacturer: Manufacturer data management	130
113	Nd-YAG laser – Post-Manufacturer: Mechanical tests manager	131
114	Multi-laser – bi-material manufacturing test: FreeCAD modelling	131
115	Multi-laser – bi-material manufacturing test: Pre-Manufacturing processing	132
116	Multi-laser – bi-material manufacturing test: Lasers’ setup modelling	133
117	Multi-laser – bi-material manufacturing test: Lasers’ setup	134
118	Multi-laser – bi-material manufacturing test: Manufacturing setup	134
119	Multi-laser – bi-material manufacturing test: Manufacturing (network setup)	135
120	Multi-laser – bi-material manufacturing test: Manufacturing (Parameters and lasers setup)	136
121	Multi-laser – bi-material manufacturing test: Manufacturing procedure	137
122	Multi-laser – bi-material manufacturing test: Produced part	138
123	Multi-laser – bi-material manufacturing test: Geometrical measurements using Fiji’s SW	138
124	Multi-laser – bi-material manufacturing test: EM analysis	138
125	Multi-laser – bi-material manufacturing test: SEM analysis (EDS)	139
126	Multi-laser – Post-Manufacturer: Pre-Manufacturer data management	140
127	Multi-laser – Post-Manufacturer: Manufacturer data management	141
128	Multi-laser – Post-Manufacturer: Mechanical tests manager	142
129	AI application for process improvement: Scanning Electron Microscope (SEM) image analysis example	142

List of Tables

1	Overview of the advantages and disadvantages of the various multi-powder deposition systems for L-PBF	20
2	LPBF commercial equipments	25
3	Path topology main fixed parameters	50
4	Layer height tests: 0.025–0.001 mm	63
5	Path benchmarking in terms of computational resources	63
6	Requirements and constraints for the Post-Processor and Printer software packages	65
7	Requirements and constraints for the 3DMMLPBF machine	89
8	Power supply NewStyle 360 W	102
9	Arduino Mega 2560 main specifications	102
10	Microcontroller pin mapping	103
11	Requirements and constraints for the 3DMMLPBF machine's firmware	104
12	3DMMLPBF machine v1.0 specifications	108
13	3DMMLPBF machine v2.0 specifications	110

List of Listings

4.1	SVG syntax example	42
4.2	Custom syntax example	48
4.3	3cubes.svg (excerpt)	56
4.4	Script to create the database: excerpt with the Part entity	84
4.5	Manufacturing output file: Layers	84
4.6	Manufacturing output file: Pens	85
4.7	Database export: Manufacturing model	87
4.8	One layer manufacturing file to test the laser	113
A.1	Ezcad API	162

Acronyms

3DMMLPBF	3D Multi-Material Laser-Powder Bed Fusion (pp. <i>x–xiii, xv, 4–6, 16, 30–32, 37–39, 41, 44, 50, 53, 64, 65, 71, 73, 75, 78, 79, 83, 85–94, 96, 103, 107–112, 114–119, 122, 128, 134, 136, 139, 143, 144, 146, 147, 165</i>)
3MF	3D Manufacturing Format (pp. <i>23, 44</i>)
AI	Artificial Intelligence (pp. <i>vii, 2, 4, 26, 33, 35, 122, 139, 141, 143, 147</i>)
AM	Additive Manufacturing (pp. <i>8–10, 14, 28, 53, 148</i>)
AMF	Additive Manufacturing File (pp. <i>21, 23, 44</i>)
API	Application Programming Interface (pp. <i>5, 68, 82, 89, 162</i>)
CAD	Computer-Aided Design (pp. <i>9, 21, 33, 94, 115, 122, 124, 131, 136</i>)
CAE	Computer-Aided Engineering (pp. <i>33, 40</i>)
CAM	Computer-Aided Manufacturing (pp. <i>22, 23, 25, 34, 37, 40</i>)
CLI	Common Layer Interface (pp. <i>16, 22, 23</i>)
CNC	Computer Numerical Control (pp. <i>8, 9, 22</i>)
CNN	Convolutional Neural Network (pp. <i>139, 141, 144</i>)
DB	Database (p. <i>81</i>)
DBMS	Database Management System (p. <i>81</i>)
DDL	Data Definition Language (p. <i>82</i>)
DED	Direct Energy Deposition (p. <i>10</i>)
DFAM	Design For Additive Manufacturing (p. <i>22</i>)
DFM	Design For Manufacturing (p. <i>22</i>)
DLD	Direct Laser Deposition (pp. <i>10, 14, 28</i>)
DLP	Digital Light Processing (pp. <i>42, 45</i>)
DML	Data Manipulation Language (p. <i>82</i>)
DOE	Design Of Experiments (pp. <i>4, 33, 35, 86</i>)
EBM	Electron Beam Melting (p. <i>10</i>)

EDS	Energy-Dispersive x-ray Spectroscopy (pp. 136, 139)
EM	Electron Microscope (pp. 129, 136)
ER	Entity-Relationship (p. 81)
ERD	Entity Relationship Diagram (pp. xii, 81–83)
FAV	FAbricatable Voxel (pp. 23, 24, 27)
FDM	Fused Deposition Material (pp. 10, 14, 44)
FFF	Fused Filament Fabrication (pp. 4, 44)
FGM	Functionally Graded Material (p. 1)
GUI	Graphical User Interface (pp. 45, 65, 68, 81, 84)
HM	Hybrid Manufacturing (p. 9)
HW	Hardware (p. 82)
I/O	Input/Output (p. 102)
IC	Integrated Circuit (p. 97)
IR	Infra-Red (p. 16)
L-PBF	Laser-Powder Bed Fusion (pp. xii, 1–3, 5, 8, 10, 12–14, 16, 17, 19, 24–26, 28, 30, 31, 40, 51, 53, 56, 59, 90, 145–147)
LMD	Laser Metal Deposition (p. 14)
LOM	Laminated Object Manufacturing (pp. 10, 14)
LSP	Laser Speckle Photometry (pp. 16, 143, 144, 147)
MMAM	Multimaterial Additive Manufacturing (p. 13)
MMFGM	Multimaterial Functionally Graded Material (p. 3)
MMLPBF	Multi-Material Laser-Powder Bed Fusion (pp. vi, vii, xi, 2–5, 8, 14–16, 18, 21–31, 93, 94, 96, 116, 148)
NURBS	Non-Uniform Rational B-Splines (p. 23)
OS	Operating System (pp. 104, 141)
PBF	Powder Bed Fusion (p. 10)
PCB	Printed Circuit Board (pp. 99, 116, 148)
PCI	Peripheral Component Interconnect (p. 73)
PID	Proportional Integrative Derivative (pp. 99, 112)
PLC	Programmable Logic Controller (p. 26)
POV	Persistence Of Vision (p. 44)

PWM	Pulse-Width Modulation (pp. 97, 99, 101)
RDBMS	Relational Database Management System (pp. 81, 82)
SDK	Software Development Kit (pp. 65, 73)
SEM	Scanning Electron Microscope (pp. xiv, 122, 139, 141, 142, 144, 147)
SLA	Stereolithography (p. 53)
SLM	Selective Laser Melting (pp. 1, 10)
SLS	Selective Laser Sintering (pp. 1, 10)
SM	Subtractive Manufacturing (pp. 9, 148)
SQL	Structured Query Language (p. 82)
SSR	Solid-State Relay (pp. 97, 98, 101)
STEP	Standard for The Exchange of Product data (p. 23)
STL	Standard Tessellation Language (pp. 2, 9, 21–23, 25, 27, 33, 44–46, 48, 59, 118, 129, 130, 146)
SVG	Scalable Vector Graphics (pp. 42–45, 53, 64, 115, 146, 148)
SVX	Simple VoXel (p. 23)
SW	Software (pp. 25, 49, 113, 118, 119, 123, 126, 130, 131, 133, 144, 146)
TCP/IP	Transmission Control Protocol/Internet Protocol (pp. 67, 73, 82, 141)
UART	Universal Asynchronous Receiver-Transmitter (pp. 67, 73)
UAV	Unmanned Aerial Vehicles (p. 9)
UI	User Interface (pp. 48, 64, 69, 73, 109, 113, 119, 122)
UML	Unified Modeling Language (pp. 32, 39)
USB	Universal Serial Bus (pp. 45, 133)
VDI	Verein Deutscher Ingenieure (p. 39)
XML	eXtensible Markup Language (pp. 23, 42, 64)

Introduction

Functional design is a highly desirable approach to design, optimising the functional performance of a product while minimising the resources usage and the cost.

However, functional design requires a shift in the manufacturing design paradigm from being process-centered to be function-centered, i.e., product design should focus on the functionality and overall properties of the manufactured component, instead of the technologies required to achieve this.

Furthermore, the adoption of functional design may dictate the use of multiple materials or a combination of them, which is hindered by the current manufacturing methodologies. Conventional manufacturing technologies are mono-material and subtractive, starting from a pre-shape, incurring in wasted material and energy.

Thus, if functional design is the aspiring concept, then additive manufacturing is the vehicle to bring it to life. By adding material only where it is functionally required, the components' properties can be tailored for optimal performance while minimising materials and energy. Intricate geometries can be achieved, which would be otherwise unfeasible by conventional manufacturing technologies.

Nonetheless, the multi-material additive manufacturing is still in its infancy, especially when using metallic and ceramic materials. The current panorama shows that only a handful of commercial equipments can be used for this purpose [2, 3]. However, they require a significant initial investment and are only suited for metals, which limits the scope of applications.

On the other hand, functionally designed components are highly attractive to top-shelf industries like the aeronautical, aerospace and biomedical ones, as they address specific problems in these fields. A paradigmatic example in the biomedical field is the hip implant, whose goal is to mimic the natural behaviour of the bone. As such and not surprisingly, the material composition, properties and structure needs to be varied, as the bone is a great example of an [Functionally Graded Material \(FGM\)](#)'s component.

However, the design and fabrication of these implants are still far from the desired behaviour, as can be proved from the number of forced retreatment surgeries spanning a short period of time (ten to fifteen years after the implantation surgery) [11]. An explanation can be given by the fact that the needed multi-material processing using metals, polymers and ceramics, as well as the respective design methodologies, are still in a premature stage.

[Laser-Powder Bed Fusion \(L-PBF\)](#), a standardisation of all laser powder fusion processes, like [Selective Laser Sintering \(SLS\)](#) and [Selective Laser Melting \(SLM\)](#), is the most promising technology for multi-material fabrication using metallic and composite powders. However, it is extremely complex [10, 12], even in the mono-material scenario. The problem becomes even worst when addressing the controlled combination of multiple metals or

ceramics, as this requires some special form of the material (e.g. powder) and a great amount of energy to produce it (e.g. metals require at least coalescence characteristics to be bonded). In order to successfully produce multi-material components from metals, ceramics, or both, a specific combination of controlled deposition of mass and controlled supply of energy must be achieved, while still managing the interactions with the environment (oxidation, heat transfer, etc.) and among materials (e.g. delamination). This is clearly a multi-physics problem and, as the timing and order of material addition and energy supply is crucial, a topological problem is added up to the stack, indicating why the progress in this field is still fairly limited.

As a result, the research field primarily focuses on upgrading mono-material equipment to add multi-material capabilities [4–9], which undesirably also requires manual workarounds to setup the manufacturing chain and equipments. This is further aggravated by the lack of specific design guidelines for the [Multi-Material Laser-Powder Bed Fusion \(MMLPBF\)](#) process and by the fact that most pre-processing procedures use a manual method based on an inadequate data format [10] [Standard Tessellation Language \(STL\)](#), which is unable to represent accurately holes, discontinuities, and porosity. The main takeaway is that the [MMLPBF](#) fabrication is a multi-objective problem, requiring specially designed equipments and toolchains, and experimental design.

Thus, the present work aims to close the gap between design and fabrication of multi-material components like the aforementioned implants by proposing a holistic approach to the multi-material fabrication using metals, polymers and ceramics that can leverage the process knowledge and support functional design. An appropriate workflow is required to clearly guide end-users and an accompanying toolchain capable of handling the intricacies of the [MMLPBF](#) process. Furthermore, a custom equipment is also required to enable the combination of these materials in the same component, which is not yet addressed by the commercial [L-PBF](#) field. This implies the usage of different types of lasers integrated into a single equipment, which can be further used for procedures such as preheat treatments to alleviate mechanical tensions or to promote better bonding of the materials.

Lastly, and often the most overlooked aspect in any emergent technology, is the process knowledge potential. [AI](#) tools, like deep learning or machine learning, can provide critical insights for the process evolution, mining and leveraging the [MMLPBF](#) process data. A paradigmatic example was reported last year, when Exponential Technologies, in a collaboration with Aerosint, announced a two-fold improvement in component density in a multi-metallic component, within 2 print jobs and 46 samples printed without any prior statistical knowledge, saving time and money [13].

1.1 Motivation

The functional design of components is a complex topic, with a myriad of questions to be answered: what is the function of the component?; what design criteria must be met to fulfil its function?; how will the component be produced, and what data does it require?; how will the component's performance be measured?, among others. The answers are often not clear or simple as they dictate the use of several materials and several manufacturing technologies, increasing severely the complexity of producing such components: how to effectively combine two or more materials into a single component in a synergistic way?

From the designer's perspective it becomes even worst as it must be intimately acquainted with the manufacturing process and apply corrective factors to the design which still might fail due to the complexity of the process, limiting its creativity and the ability to produce functional parts as desired. A good analogy to the multi-material product designer would be of an early programmer: the latter needed to know in full-depth all the intricacies of the

underlying hardware and the moment of its “liberation” was the emergence of the so-called high-level languages; for the former no such liberation is available yet, but will certainly boost the functional design and manufacturing.

The possibility of controlling composition or structure and thus obtain components with desired local properties, as regarding mechanical, tribological, thermal properties, and others are of great interest, as material is only added where it functionally needed, minimising waste and enhancing the overall properties of the component being built. This idea meets its pinnacle with the concept of an **Multimaterial Functionally Graded Material (MMFGM)** – multi-material components with materials gradations in between. High value products would benefit tremendously from this opportunity, namely biomedical implants, like the hip implant, where the outer layers contact directly the living tissue, designing it for osseointegration, but the inner layers act merely as a supporting structure.

The multi-material component’s fabrication from metals and ceramics is still in its infancy, due to the lack of an unresponsive structure that tackles its high complexity, while guiding the end-user. Thus, the present work aims to provide such a supporting structure, building the necessary toolchain, and providing as effective means to materialise the design, by building a proof-of-concept equipment.

1.2 Main objectives

The main goals of the present work is to close the gap between design and fabrication of multi-material components from metallic/polymeric/ceramic materials using the **L-PBF** technology and to provide a sustainable development path for this technology.

To meet these goals, an ecosystem must be developed, based on a holistic approach, that supports functional design and leverages the process knowledge to all manufacturing agents (see Fig. 1), yielding a suitable workflow that guides the user, an integrated toolchain supporting it, and a custom multi-laser equipment capable of producing such multi-material components. The author asserts that this is the most effective way to address the high complexity inherent to this process.

To this end several main objectives have been outlined:

1. Investigate the current panorama of multi-material fabrication using metals, polymers, and ceramics, with special focus on the **L-PBF** technology, and identify its main gaps and shortcomings.
2. Develop a design methodology for multi-material fabrication using these materials via the **L-PBF** technology, using a holistic approach to support functional design and leverage the process knowledge throughout the whole manufacturing chain.
3. Instantiate a practical workflow from the design methodology, taking into account the project constraints and restrictions;
4. Develop an integrated toolchain for the **MMLPBF** process, supporting all stages of the manufacturing chain.
5. Develop and build a proof-of-concept’s equipment for the fabrication of multi-material metallic/polymeric/ceramic components.
6. Test the production of such components using the proposed workflow/toolchain and the equipment built;

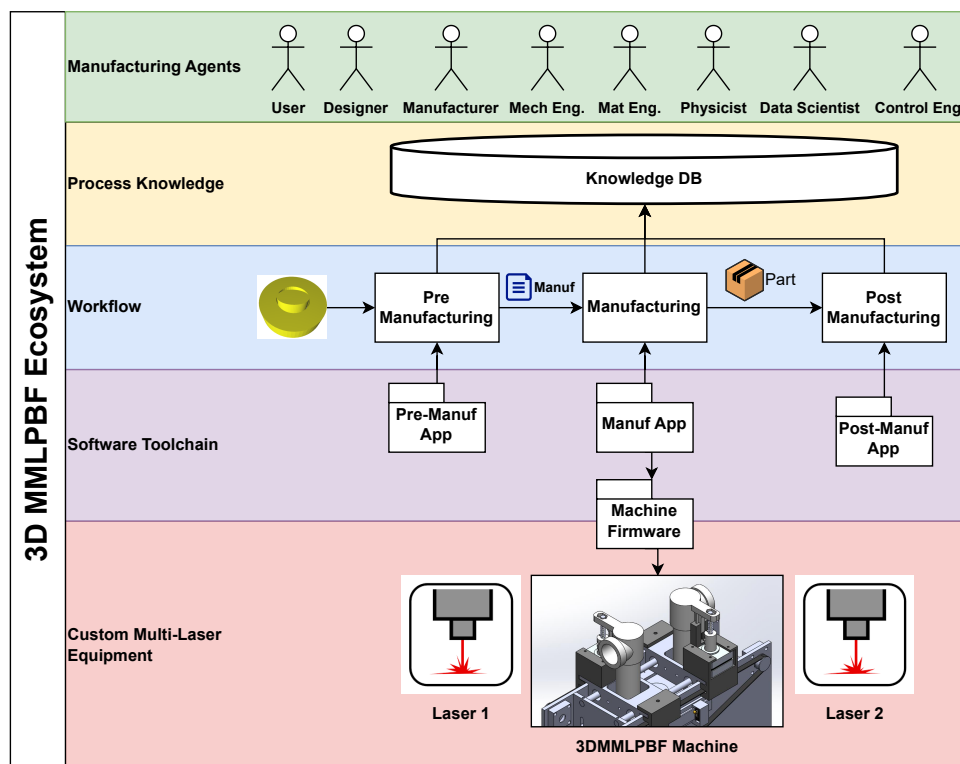


Figure 1: 3DMMLPBF ecosystem

7. Develop a process knowledge database that can be used for process improvement, using tools such as [Design Of Experiments \(DOE\)](#) and AI;
8. Investigate and incorporate mechanisms for process optimisation, namely:
 - Design strategy optimisation;
 - Manufacturing process optimisation: parameters, manufacturing paths, etc;
 - [3DMMLPBF](#) machine optimisation;
 - Data flow optimisation: leverage the knowledge acquired through the process to cascade ‘naturally’ and efficiently to the [MMLPBF](#) process’s optimisation;

The emergence of 3D printing technology provides a paradigmatic example of an ecosystem-based transformation. The concept was first introduced in 1972, when Ciraud [14] proposed a powder process capable of constructing three-dimensional components from a variety of semi-meltable materials. Although Stratasys started to commercialise [Fused Filament Fabrication \(FFF\)](#) printers in the early 1990s, the real boom only occurred in the mid-2000s when RepRap started to release open-source 3D printers [15]. This enabled each user to produce 3D components, but also, and more importantly, to customise, replicate, and enhance their machines. This revolutionised 3D printing, generating multiple projects and emergent companies, which eventually led to the shutdown of RepRap’s business.

The legacy and lesson that RepRap taught us, similar to Prometheus¹, was that knowledge is the most important

¹Titan who stole the fire from the Olympian gods to give it to mankind, condemned for eternity by Zeus to be tied to a rock and have his liver eaten

and expensive asset in any technology, and when knowledge is openly divulged, and every user can effectively make use of it, the hardware and software costs drop massively, and the process evolves greatly from users' tinkering and experience.

The same fundamental principle underlies the philosophy of this project. By developing an ecosystem for multi-material functional design, knowledge from all agents can leverage the process, mimicking natural processes and boosting its evolution. Therefore, knowledge needs to be captured, tracked, and fed back adequately and efficiently to the process by means of a global picture, a design methodology that is applied by instantiating a practical workflow and brought to life by a cost-effective equipment that can fabricate multi-material components embodying this knowledge. A viable technology and a suitable cost-effective manufacturing equipment can be achieved as side effects of this global perspective, serving the greater good of functional design. This can open new prospects in the research field, providing a bootstrapping environment for the [3DMMLPBF](#) process.

1.3 Thesis organisation

This thesis is organised as follows. Chapter 2 provides a comprehensive review of the current state of the art of multi-material fabrication using metals, polymers and ceramics. The functional design approach is introduced, followed by a discussion on the use of laser-based additive manufacturing processes as a viable solution for metallic and composite manufacturing, with particular attention given to the [Laser-Powder Bed Fusion \(L-PBF\)](#) process. To fully support functional design, the [Multi-Material Laser-Powder Bed Fusion \(MMLPBF\)](#) process is introduced, which bridges the gap between [L-PBF](#) processes. An overview of [MMLPBF](#) is presented, including the current panorama, manufacturing chain, challenges, and potential solutions. Finally, the specific applications envisioned in this work are listed.

Chapter 3 presents the multi-material fabrication problem and its challenges using the [L-PBF](#) technology. A methodology devised for multi-material production via [L-PBF](#) technology is introduced to tackle the high complexity of the process and the lack of a supporting methodology, taking into account the key agents of the process and leveraging the process information.

In Chapter 4, the knowledge acquired through the relevant models contained in the proposed methodology is applied to the development of a specialised workflow for the [3DMMLPBF](#)'s process and respective toolchain, contingent of the project's restrictions and resources, and to the development of a machine capable of producing multi-material components from metallic/ceramic powders matching the designed workflow. Based on this workflow, the toolchain was assembled and the missing software components were developed, tested, and validated. Lastly, a custom equipment for the production of multi-material metallic and ceramic components was developed, tested and validated across the mechanical, electronic, and control domains.

In Chapter 5 the multi-material fabrication of metallic/polymeric/ceramic parts is tested, using one or multiple lasers. The complete process, from inception to produced part, is tested as a whole, to ensure the full validation of the designed [3DMMLPBF](#) ecosystem, i.e., methodology, workflow, toolchain, and equipment. Lastly, the prospects for process improvement are outlined, leveraging the process knowledge acquired for systematic and consistent evolution of the [3DMMLPBF](#) manufacturing chain.

The Chapter 6 gives a summary of this thesis as well as prospect for future work.

Lastly, the appendices contain detailed information about the software [Application Programming Interface \(API\)](#), and the annexes contain the paper submitted, stemming out of this work.

Fig. 2 provides a bird's eye view over the present work, addressing the problem and the envisioned solution. The outputs are also highlighted, namely the workflow — from modelling to post-manufacturing — the supporting toolchain, and the custom low budget [3DMMLPBF](#) multi-laser equipment.



Figure 2: Graphical abstract

State of the art

This chapter provides a comprehensive review of the current state of the art of multi-material fabrication for metals and ceramics. The functional design approach is introduced, followed by a discussion on the use of laser-based additive manufacturing processes as a viable solution for metallic and composite manufacturing, with particular attention given to the [Laser-Powder Bed Fusion \(L-PBF\)](#) process. To fully support functional design, the [Multi-Material Laser-Powder Bed Fusion \(MMLPBF\)](#) process is introduced, which bridges the gap between the L-PBF process. An overview of MMLPBF is presented, including the current panorama, manufacturing chain, challenges, and potential solutions. Finally, the specific applications envisioned in this work are listed.

2.1 Functional design

Functional design is a design approach that aims to optimise the functional performance of a product while minimising its cost and complexity. It is a concept that transcends various fields – biomedical [16–18], aerospace [19–21], food [22], chemistry [23], and even clothing [24, 25]. – and is not limited to a specific technology.

Functional design draws inspiration from nature, with its wide spectrum of lightweight and functional structures, such as branched plant shapes, bone tissues, and honeycomb patterns [26]. Historically, humans tried to replicate this design, but simplifications must be made to accommodate manufacturing and assembly constraints. Nonetheless, the fundamental premise is nature-inspired: how to design and manufacture topologically optimised components in a sustainable way with an efficient usage of resources.

Thus, and although the concept of functional design is not new [27], it has become increasingly feasible with the emergence and evolution of technologies such as additive manufacturing [26], enabling designers to create complex structures and functional parts that were previously difficult or impossible to produce using traditional manufacturing techniques. As a result, a paradigm shift in product design and manufacturing is in motion, allowing for the exploration of features, shapes, and geometries to comply with the required functionalities, without being limited by production constraints [28].

[Additive Manufacturing \(AM\)](#) was the main driver for functional design by showcasing how material could be added to specific areas of a component to fulfil a function, which would be otherwise impossible to produce using the traditional subtractive methods, like [Computer Numerical Control \(CNC\)](#) machining. Furthermore, the number and diversity of the AM technologies contributed to functional design in a myriad of ways, and can be primarily categorised into four distinct groups [29]: multi-material, multi-scale, multiform, and multi-functional.

The first category, multi-material, aims to enhance the mechanical properties of an object by depositing multiple dissimilar materials within a single entity. This is required for components with interface with specific properties. For example, in the hip implant, the core material must provide the load bearing capabilities, but the external interface should be composed of bioactive materials to promote osseointegration [30].

The second category, multi-scale, focuses on the design of geometric features in various scales to achieve functional requirements. For example, the wettability of an object is changed from hydrophilic to super-hydrophobic when the surfaces are embedded with micropillars [31].

The third category, multiform, is aimed at designing objects with programmable shape-changing properties after fabrication. This means that the shape of the component will evolve according to an external stimulus, e.g. thermal [32, 33], light [34], or moisture [35].

Lastly, the fourth category, multi-functional, pertains to the design of objects such as multi-functional flexible sensors, and electronics, where the primary focus is on non-structural properties, despite the objects still possessing structural properties. These non-structural properties include sensing [36], thermal [37, 38], hydrodynamic [39], biologic [40], and electric [41, 42].

The limitations of AM must be emphasised, particularly with respect to product quality and productivity, system efficiency, and sustainability. AM processes are constrained by certain manufacturing restrictions, such as the presence of sharp corners, thin geometries requiring support structures, and height errors that result in poor surface finish [43]. In contrast, conventional Subtractive Manufacturing (SM) techniques, such as turning and milling, can yield parts with a superior surface finish but exhibit low throughput in producing highly complex geometries. Consequently, a Hybrid Manufacturing (HM) approach combining AM and SM techniques is advocated as an optimal solution, as it can produce components with intricate geometries and the desired surface finish while minimising both setup time and waste generation [44, 45].

It can easily be recognised that the extra freedom provided by hybrid manufacturing suits better the purpose of functional design. However, this comes at the cost of even greater complexity, especially if multi-material applications are considered. Furthermore, as HM is a superset of AM, it is expected that the improvements on the latter will cascade to the former.

Thus, the present aims to approach functional design through the lens of AM processes. In particular, the investigation centres on the application of multi-material functional design utilising AM technology, which is essential for the development of biomedical implants, such as the hip implant.

2.2 Mono-material Laser-Powder Bed Fusion

The basic concept of additive manufacturing (AM) involves the addition and bonding of material solely in the necessary regions to create the desired component, typically in a layer-by-layer approach through CNC displacement using three-dimensional (3D) model data [12]. As each layer of material is added, the 3D part is incrementally constructed by bonding similar or dissimilar materials. To enable the manufacturing paths to be generated, which dictate the CNC displacement, the 3D models are typically represented in Computer-Aided Design (CAD) form in the STL file format and numerically sliced into numerous virtual layers or cross-sectional data. A wide variety of AM application have been reported namely: aerospace [19, 21, 46], Unmanned Aerial Vehicless (UAVs) [47, 48], houses [49], tooling [50, 51], biomedical implants [52–54], among others.

To accomplish the effective material bonding, the successful combination of material and energy delivery is required, differing with the material and the AM process [12, 55]. The AM processes can be classified by [56]:

- *state of raw material*: liquid, solid sheet or discrete particle;
- *type of material*: metal (layer or direct deposition); polymer (Fused Deposition Material (FDM), stereolithography, polyjet); paper (Laminated Object Manufacturing (LOM)); wood stratoconception).

The ISO 52900 specification standardises the AM processes as follows [57]: material extrusion, material jetting, sheet lamination, vat photopolymerisation, binder jetting, Direct Energy Deposition (DED) and Powder Bed Fusion (PBF). Fig. 3 depicts these seven categories and the related technologies with energy sources, materials used, advantages and drawbacks, and their suitability to produce metallic parts [58]. The processes delimited in red are often used for metallic parts.

The AM started out from being a rapid prototyping tool, enabling fast iteration over design at a reduced cost — reducing the development cycle, and providing resource efficiency [59]. This remained the case for long, due to production times being higher than for conventional methods, and to the generally lower surface quality finishing, so it was commonly cast aside for anything else than as prototyping tool. However, AM provides highly desirable features for the production of high-value products, where time constraints are not so relevant, thus justifying a strong investment in its evolution. This process is traditionally ‘open-loop’ due to its lower complexity and lower cost; however feedback control was introduced to ensure better part quality, in some cases with real-time characteristics [60–62].

When it comes to the additive manufacturing of metallic parts and composites DED and PBF are the most proven and feasible methods [12, 63]. Both processes involve the deposition of powder metal (or less common preforms such as wire) and their simultaneous or subsequent melting, respectively, via a focused thermal energy source, namely an electron beam or a laser beam. In case a laser beam is used the processes can be referred as form of L-PBF, while DED can be further specified as Direct Laser Deposition (DLD) [12]. The usage of an electron beam (Electron Beam Melting (EBM)) makes high scanning speed possible (up to several km/s) due to the lack of moving parts to guide the building spot and requiring less supports [56]; however, the increased complexity and cost does not make it commercially viable yet.

Besides being easier to use, laser sources are attractive for numerous other reasons [64]: small spot diameter, minimising the molten pool and the surrounding area (heat-affected zone); high energy density; accurate control of the energy flow. Thus, they are widely used in AM processes, especially concerning metallic materials with high melting points [65].

Comparing both laser-based technologies, L-PBF offers the following advantages over DLD: smaller spot diameter, providing better processing accuracy and a smaller melt pool, thus yielding smaller surface roughness and greater geometric resolution. For the opposite reasons, DLD can process larger parts, providing the range of deposition head is large enough [66]. This can be extended to the multi-material domain, with L-PBF being better suited to process high-precision small and medium-size multi-metal parts [66]. Thus, the L-PBF process arises as the current bet for commercial and industrial applications for the fabrication of high-precision multi-material parts using metals and ceramics [67–72].

L-PBF uses a focused laser beam to selectively melt (SLM) or sinter (SLS) metallic or composite powders, layer-by-layer, to build 3D components. As shown in Fig. 4, the powder is fed and uniformly distributed on the powder bed

¹Used with permission from Springer: licence nr. 5296320585850

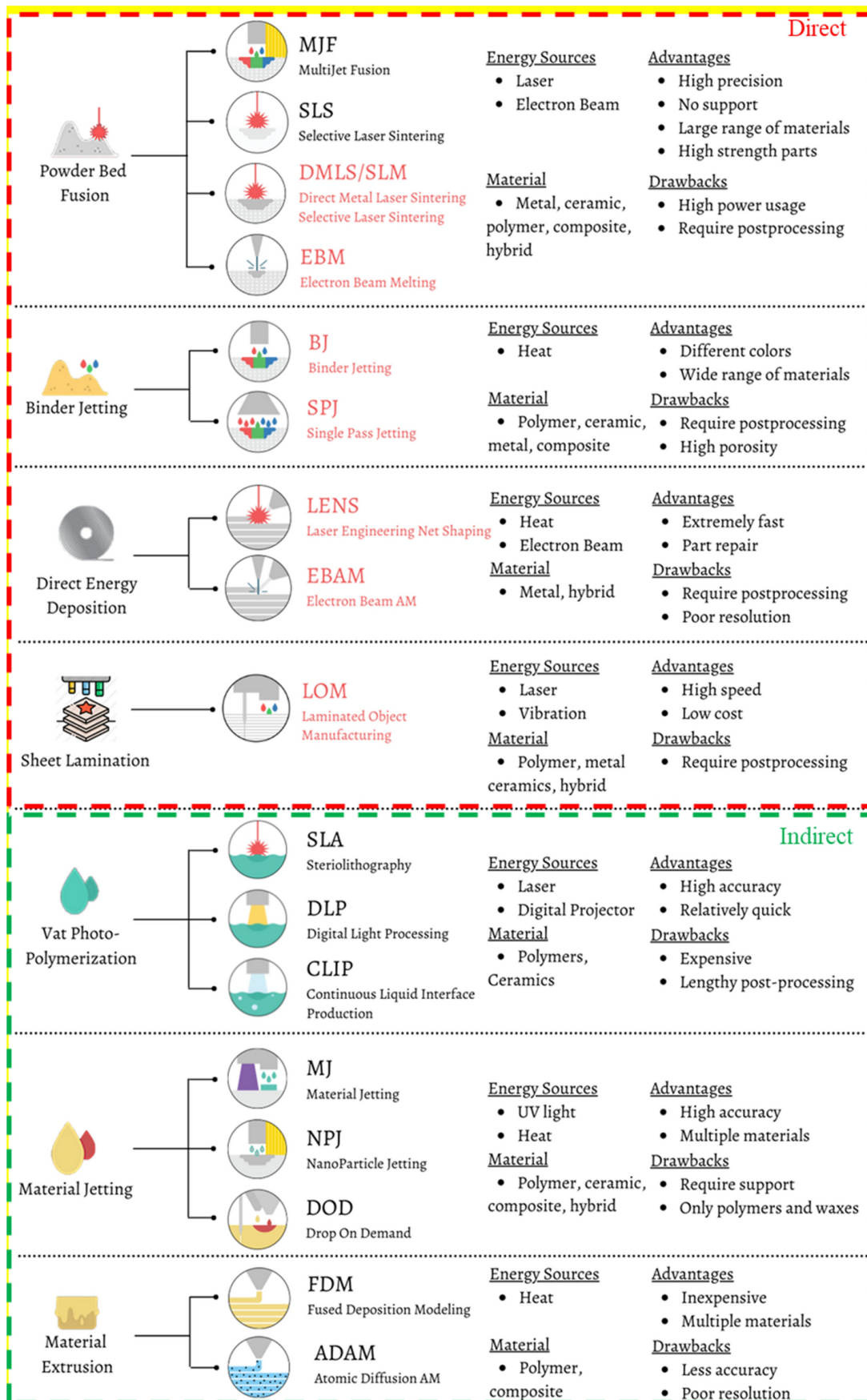


Figure 3: AM processes (withdrawn from [58])¹

using a spreading mechanism, like a roller. The laser beam melts specific areas of the powder bed, accordingly to the laser scanning pattern. After a layer is completed, the powder bed lowers by the height of the deposited layer, a new layer is deposited on the powder bed and the process is repeated. Depending on the energy density of the laser beam and the materials used, the material can be fully melted rather than sintered, allowing different properties (crystal structure, porosity, etc.)

This repetitive process results in unmelted excess metal, providing structural support and additional protection from oxidation and thermal stress, ideal for overhanging structures. Thus, the the powder bed is also usually heated to diminish temperature gradients which can weaken the part, leading to its collapse or fracture [12].

The metallic powders are highly susceptible to oxidation, which is further aggravated by the high thermal gradients induced by laser operation and the powder bed heating. Thus, to minimise this effect, an enclosing and controlled shielding system with an inert gas, typically argon or nitrogen, is used.

The part is generally built upon a substrate plate to prevent powder bed platform damage, which must be removed to obtain the finished part upon process completion.

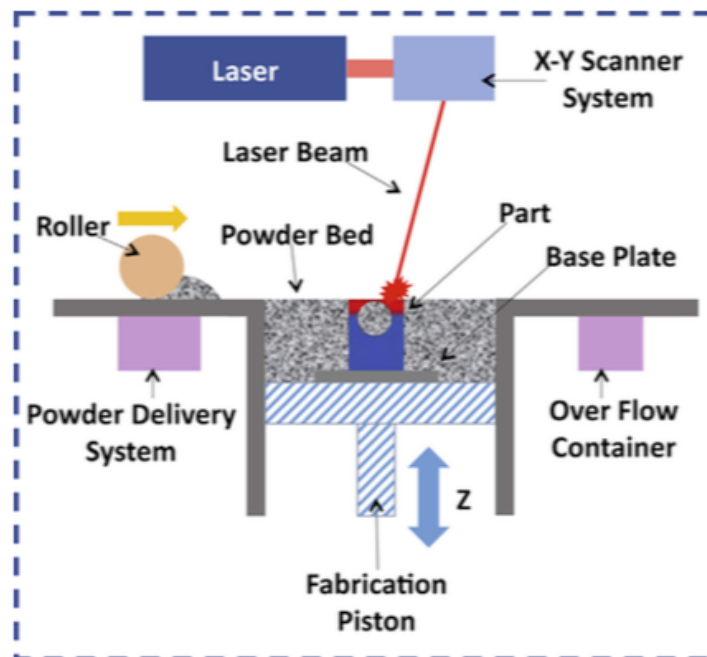


Figure 4: L-PBF process (withdrawn from [12])²

Figure 5 delineates the key processing parameters for the L-PBF process. The thermal history, residual stress, and microstructure of a fabricated part are profoundly influenced by the laser processing parameters, ultimately impacting its quality [73]. Laser power, laser scanning speed, hatch distance constitute the most notable parameters, contributing to the energy density affecting the part, which influences the geometry of melt pools, thermal gradients, and cooling rates. The energy density is the primary driver of melting and can be achieved through various combinations of the aforementioned parameters [74]. This makes the process of determining optimal parameters a multi-objective optimization problem. Scanning strategy is the primary driver of energy density and can be leveraged to optimise surface roughness, refine microstructure, and reduce porosity [75, 76], while mitigating residual stresses, thermal deformation, and defects [77–79].

²Used with permission from Elsevier: licence nr. 5296180869039

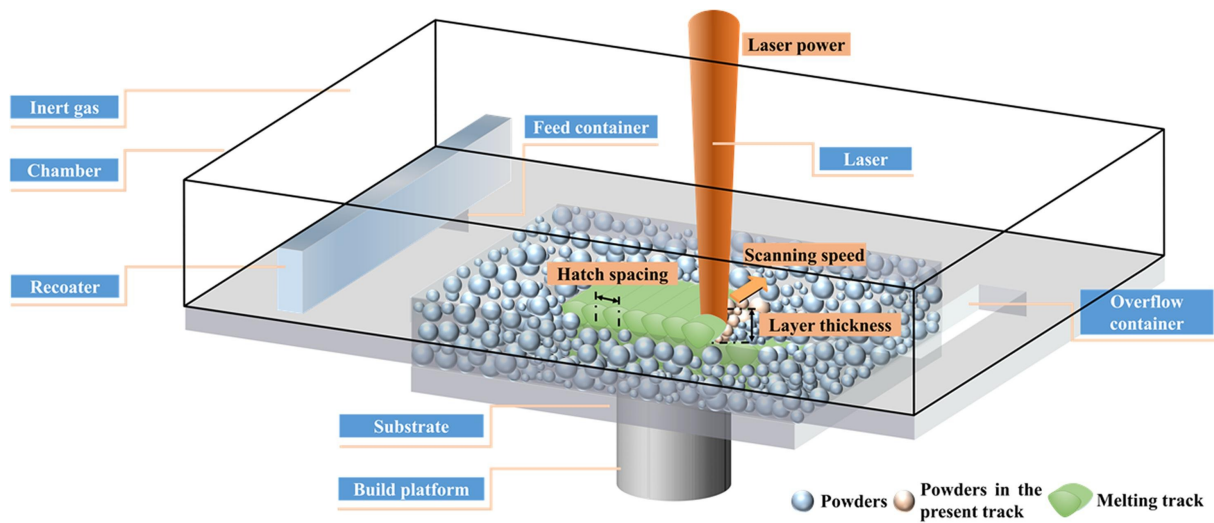


Figure 5: L-PBF process and key parameters³: white fonts indicate machine components while the black fonts illustrate the key processing parameters (withdrawn from [80])

Zou et al. conducted a numerical simulation to analyse the scanning strategy of single and multi-laser scanning for residual stress[76]. They discovered that due to higher energy heat input, the residual stress of a sample increases with the number of lasers used, but careful planning of scanning sequence and direction can mitigate this. Moreover, they found that the two-scanning strategy can reduce residual stresses by more than 10% when compared to the single-scanning strategy. This re-melting can improve surface roughness and porosity [75].

2.3 Multi-material Laser-Powder Bed Fusion

The capability to fabricate multiple material parts is highly desirable as it allows for the accurate placement of material according to its functionality, providing custom-tailored parts for specific applications with enhancement of its mechanical properties and behaviour in service. However, the existing 3D printing techniques are mainly for mono-material part fabrication [66]. The emerging [Multimaterial Additive Manufacturing \(MMAM\)](#) technology can enhance the AM parts performance by varying compositions or type within layers, unachievable by conventional manufacturing processes [63], without the need for complex manufacturing process and expensive tooling [81, 82].

The range of applications are vast and pivotal. In the biomedical engineering field, [MMAM](#) enabled the production of 3D engineered tissue (3D spinal cord [83]), biomedical devices such as microneedle arrays [84] and diagnostic devices [85], multi-material cellular structures targeting orthopaedic implants [52], and 3D artificial models for preclinical or preoperative surgical training [86, 87], among others. In the soft robotics field, where flexibility is key for complex actuations and motions, [MMAM](#) enabled the production of pneumatically driven elastomeric actuators [35] and direct integration of functional components required for it (e.g., a silver-nanoparticle ink acting as a resistive heating element [88]). In electronics [MMAM](#) is critical for direct manufacturing of 3D electronic devices where electrically dissimilar materials including conductors, semiconductors, and dielectrics are integrated together [81]. Some examples are a 3D magnetic sensor with integrated electronics components and conductive

³Used with permission from Elsevier: licence nr. 5296470787752

paths [89], stretchable strain or pressure sensors [90] and a highly stretchable electronic LED board [91], yielding high potential for wearable electronics, and even a fully 3D printed and package Li-ion battery [92].

To achieve this superior performance over AM, different materials or chemicals need to be physically delivered to any point in the 3D space during the additive manufacturing. In some processes, like direct 3D printing in Objet, FDM, this is relatively straight-forward to achieve as the materials are deposited in the platform dot-by-dot or line-by-line via nozzles; to incorporate multi-material fabrication multiple nozzles can be added [63].

For multi-material fabrication of metals, a similar result could be achieved through the use of LENS process or DLD, as they can use multiple nozzles/hoppers in the part fabrication. For example, multi-material components manufactured by Laser Metal Deposition (LMD) has been demonstrated in literature [93, 94]. However, in other processes, like L-PBF, and LOM, this is not trivial, as the materials are delivered as whole layer by a scraper or as a solid sheet, requiring new material delivery systems to be first developed [63].

Nonetheless, L-PBF provides higher precision, smaller feature size and the ability to produce lightweight structures based on lattices, such as turbine blades, which cannot be easily achieved by LMD [95, 96]. On top of that, DLD is a more difficult process to master due to added complexity of deposition control, on top of the melt-pool control, which can cause variations in the laser spot due to local increase of part's height as a result of the deposition [97].

Thus, L-PBF is the most well-suited option for the manufacturing of multi-material components using metals and ceramics, which was further demonstrated by several works [7, 8, 98, 99].

2.3.1 Technological Overview

This section presents the technological challenges and the possible solutions to tackle MMLPBF current drawbacks.

Fig. 6 illustrates the overview of a MMLPBF system based on the commercial equipments available and the scientific literature [67–72, 100]. The dashed components are optional. Upon careful examination of Fig. 6, numerous resemblances with the traditional L-PBF procedure portrayed in Fig. 4 can be observed. Such parallels should be expected since the most straightforward technique for manufacturing multi-material components using L-PBF involves modifying the powder delivery system of a pre-existing commercial equipment [4–7, 9, 101].

The MMLPBF system comprises:

- Powder bed: reciprocating platform, moving along the z-axis, where the component is built.
- Powder delivery system: mechanism by which powder is fed and delivered to the building platform. The precise and dependable placement of materials within the powder bed is contingent upon the proper functioning of this paramount system, rendering it indispensable to the process of multi-material fabrication. It must be carefully designed to limit cross contamination. Several technologies were applied to this pivotal system, namely, conventional recoating [102, 103], patterning drums [104], powder spreading with removal by suction [4, 5, 19, 52], vibrating nozzle [105–107], hopper powder feeding [71, 98], alternating powder deposition [108], and electrophotographic powder deposition [109–112].
- Powder recovery/recycling system: another very common issue associated with the combination of multiple materials is powder contamination, which is an inevitable consequence of material joining and powder removal, unmelted areas of powder in the vicinity of the melt pool, and oxidation. The reuse of this material is, therefore, even more challenging, which is aggravated by its high cost. Powder recovery/recycling systems

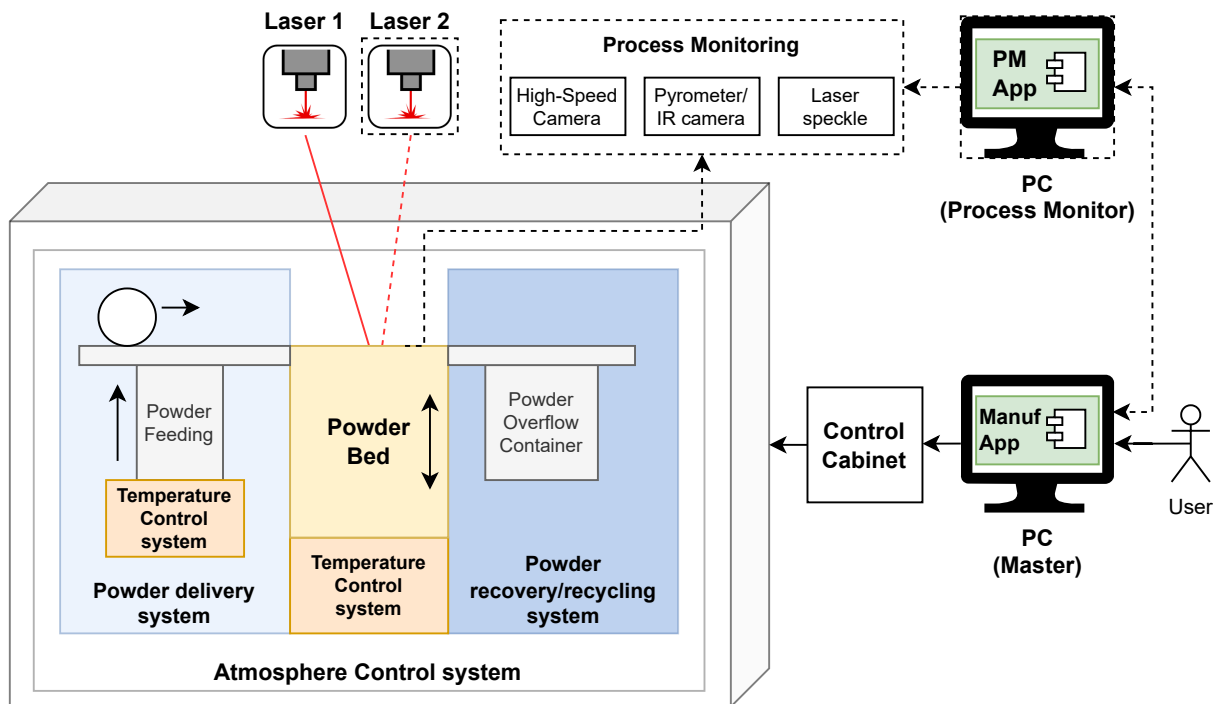


Figure 6: MMLPBF system overview

are applied to mitigate this issue partially achieved by using the variation of different physical properties between powders, such as particle size distribution (sieving) [113], magnetism [114], wettability [115], and particle inertia induced by different powder densities [116]. Efforts should be made to recuperate the surplus powder conveyed by the powder delivery system with the aim of minimising powder contamination and facilitating its intimation, thereby achieving optimal levels of recyclability and contributing for overall process sustainability and cost-effectiveness [117].

- Temperature control system: powder materials should be preheated to facilitate fusion or coalescence induced by the laser paths and to diminish temperature gradients which can weaken the part, leading to its collapse or fracture [12]. It is mandatory on the powder bed, and typically also included in the powder reservoirs.
- Atmosphere control system: for powder materials, particularly metallic ones, it is essential to maintain a controlled atmosphere to prevent oxidation. This is particularly crucial when considering the elevated thermal gradients induced by laser operation and the heating of the powder bed. To mitigate this effect, an enclosing and controlled shielding system, which utilises an inert gas, typically argon or nitrogen, is employed [12].
- Laser: the laser's systems are responsible for the generation of the beam (beam generation) and focusing it in the powder bed accordingly to the provided 2D coordinates (galvo scanning), inducing the melting of the powder materials. Optionally, additional lasers can be used. Firstly, to increase productivity. In this case, lasers are used with materials of the same type (e.g., metal alloys) and, thus, are usually just a duplicate with the same wavelength. Hence, they can be combined through a single set of mirrors and focusing lens, and used simultaneously, moving along a X-Y gantry [6]. Secondly, if different types of materials are used,

e.g., metals and ceramics, lasers of different wavelengths are required, due to the variation in the spectrum of radiation absorption and spot size.

- Control system: controls the manufacturing process, commanded by an application. The User manages the process interacting with this application to provide the topological data and process parameters. The topological data (slices and paths information) is typically conveyed in the *.SLI format – proprietary, used in the EOS and 3D Systems systems frameworks [118] – or [Common Layer Interface \(CLI\)](#) or *.ILT formats – open source, used, e.g., in the Aconity or Renishaw frameworks [67, 100]. Aurora Labs equipments, on the other hand, require the machine instructions to be provided directly (G-Code) [6]. The application will then generate the appropriate machine instructions, if required, and dispatch them.
- Process Monitoring: the [L-PBF](#) process benefits greatly of a closed-loop and adaptative control. This becomes even more true for [MMLPBF](#) due to its increased complexity. The melt pool is monitored using [Infra-Red \(IR\)](#) cameras, pyrometers, or laser speckles. The first two sensors are used to analyse the temperature evolution of the component, and allow to assess the stability of the process, but not on the material condition. On the other hand, [Laser Speckle Photometry \(LSP\)](#) analyses the change in the interference patterns of the laser (speckles) to identify inhomogeneities in 3D printing and even “invisible” defects [119]. The high-speed camera is used to capture the melting process only for qualitative assessment of the build process and powder distribution [117]. Obviously, this requires a significant investment and resources, but could greatly benefit the manufacturing quality.

Next, the main [MMLPBF](#) topics are analysed and discussed, namely, the powder delivery system, the manufacturing chain and equipments, and the manufacturing methodologies.

2.3.2 Powder delivery systems

One of most crucial parts of [MMLPBF](#) fabrication is the correct and adequate placement of the different materials in the building area, while minimising the cross contamination between them. Thus, there are significant efforts in the research and commercial domains to pursue more effective powder delivery systems [72, 104].

The simplest powder deposition system relies on the adaptation of [3DMMLPBF](#) process to use the conventional [L-PBF](#) system [102, 103]: (1) the build process is halted at the layer where the material transition is desired, (2) the powder is changed, (3) the building is resumed. This imposes several limitations. First, only a single material can be used at a time. Second, the material transitions occur in a layer-wise manner [72], and the abrupt changes in the physical properties of the materials’ interfaces leads to defects and, consequently, stress concentrations, which can induce fracture of the components [120]. Furthermore, powder compaction and bed levelling require several passages of the recoating unit, and the laser procedure should be repeated on the transition layer 2–3 times to ensure better fusion between materials [102].

The next improvement step is ensuring that cross contamination is minimised through the use of a proper removal method between materials’ depositions. Thus, the same limitations of the conventional method apply. The simplest method to remove the powder is resorting to a vacuum suction system [5], which ideally should be dedicated to each material [52] to avoid cross contamination. Bareth et al. [4] upgraded a commercial unit of a AconityONE printer with a multi-material mobile plug-in module to feed a second material to the building chamber

(Fig. 7). However, the same suction system is used for both materials. Marques et al. [19], on the other hand, utilised a dedicated powder removal system.

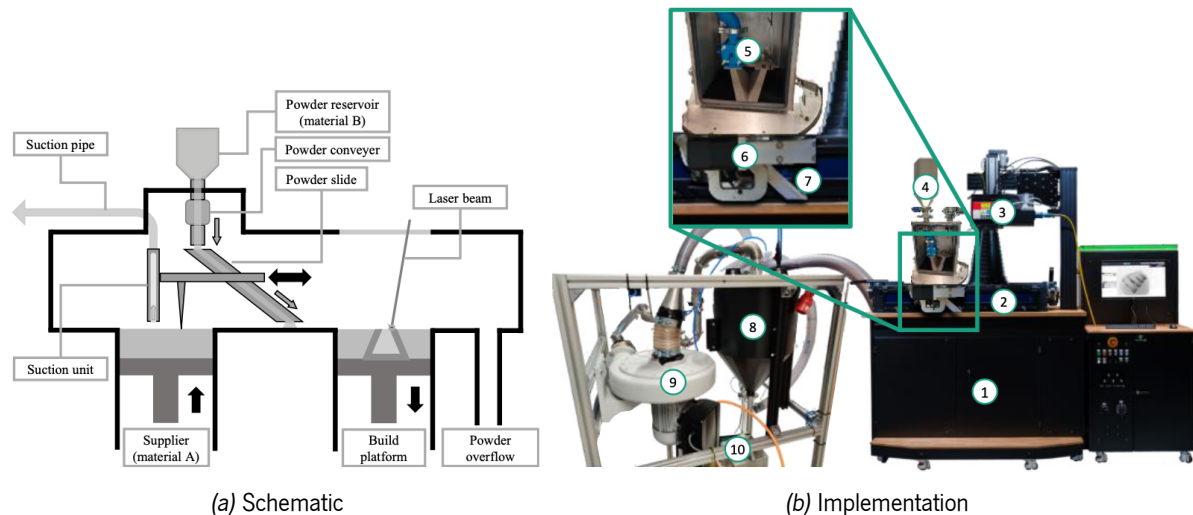


Figure 7: Conventional LPBF printer upgraded with a multi-material mechanism – 1: AconityONE; 2: process chamber; 3: scan head; 4: powder deposit (material B); 5: powder conveyor; 6: recoater and suction unit; 7: powder slide; 8: cyclone separator; 9: vacuum pump; 10: electronic control unit (withdrawn from [4])⁴

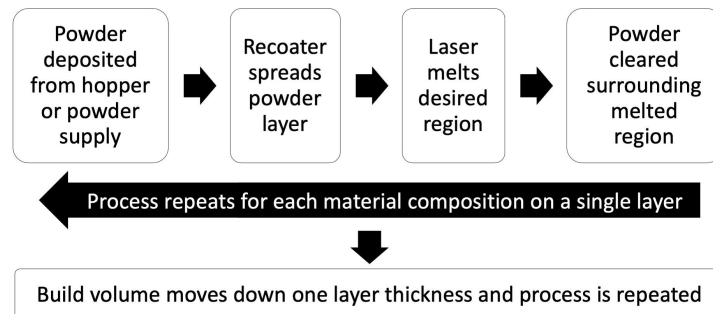
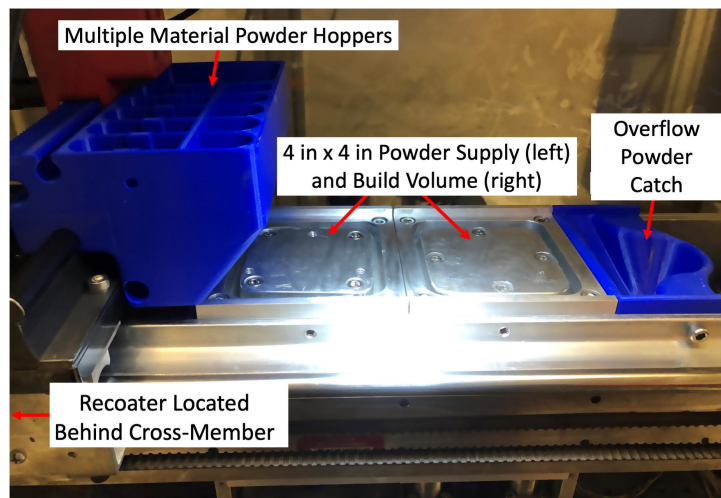
Another variation of the spreading principle is used by alternating powder deposition systems. These systems utilise two opposing recoaters, whether aligned [121] or perpendicular [122] to each other, to spread two materials and obtain an inter-layer material variation.

Powder hoppers provide separate housing for delivering powders to the building chamber, sectioning the build area. They can be employed for mono-material processing or for blending multiple powders simultaneously to obtain a specific composition. They are typically placed externally and above the processing chamber, and operated with piezoelectric transducers and solenoid valves to regulate the unloading of powder [108, 123], which is then spread onto the powder bed by a recoating system, such as a coating blade [108]. This system allows, not only layer-wise material transitions, but also discrete and gradient material transition along the build direction [107]. Very recently, Walker et al. [98] installed a powder hopper system into a L-PBF machine for graded alloy processing, with the capability to deposit specific powder of varying material composition in any 3-dimensional location (see Fig. 8). The composition mixtures are created prior to processing and separated into individual hoppers or the powder supply, for multi-material processing.

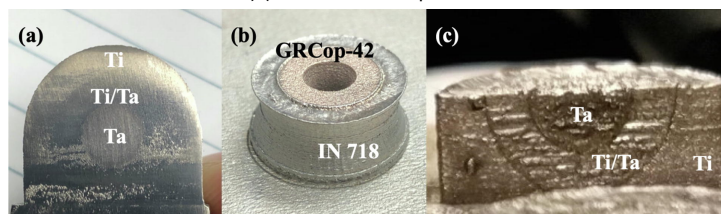
The ultrasonic vibration-assisted powder delivery system with a vortex suction nozzle is currently the most researched approach for multiple powder delivery [72]. The powders are selectively deposited by means of nozzles with small orifices [124] regulated by controlling the electrical pulses to the piezoelectric transducers [105, 106, 125]. This allows for more precise control of the powder flow rates. Wei et al. [106] developed a vibrating nozzle system capable of depositing up to six discrete powder materials within one layer. Demir and Previtali [107] used a mixed approach and developed a double hopper powder delivery system based on piezoelectric transducers which enabled the manufacturing of a Fe/Al-12Si specimen, with an intermixed region between the two materials (Fig. 9).

⁴Used under the terms of the [Creative Commons BY-NC-ND 4.0 licence](https://creativecommons.org/licenses/by-nc-nd/4.0/).

⁵Used with permission from Elsevier: licence nr. 5296470140711



(a) Structure and process



(b) Components produced: (a) concentric circles of Ti to Ta on the vertical plane; (b) IN 718 to GRCop-42 in the horizontal plane and (c) Ti to Ta in both the vertical and horizontal planes

Figure 8: MMLPBF machine with multiple hoppers (withdrawn from [98])⁵

Kumar et al. [126] used glass pipettes as ‘hopper-nozzles’ to spread powder, by means of gas pressure or vibration feed, allowing a precise powder delivery, without the need to vacuuming the excess [126].

Next, we shall discuss the most disruptive technologies. The electrophotographic technology is used to build patterned layers composed of multiple powders using metal powder transfer. The working principle relies on the electrical charge of the powders, similarly to common paper toner printers xerographic process [127]. First, a photoreceptor is uniformly charged using an electrical corona to a specified charge density [128]. Following this, laser exposure is used to selectively discharge the photoreceptor according to layer data, resulting in an electrostatic image containing powder data of the component for a given layer [109, 129]. The photoreceptor is then brought close to the powder supplier, causing powder particles to attach to the appropriate charged areas of the photoreceptor. The developed powder image is then transferred onto the charged build substrate via electrostatic

⁵Used with permission from Elsevier: licence nr. 5536180654674

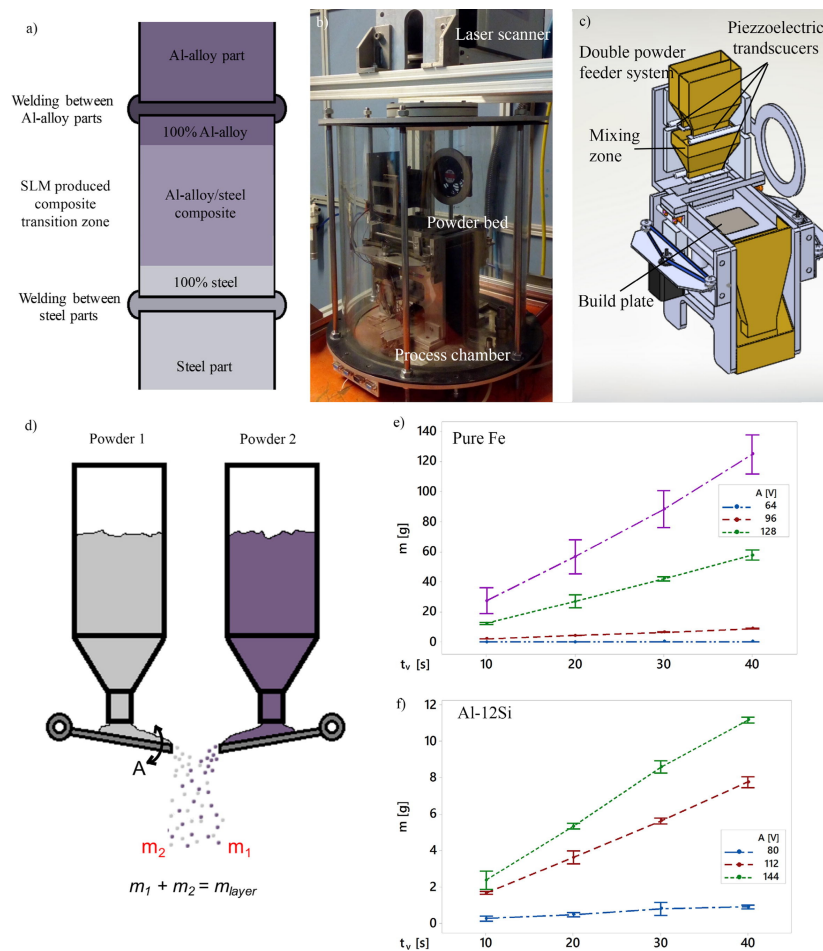


Figure 9: Vibrating nozzle dispenser system: a) Concept of using multi-material transition zone for assembling Al-alloys with steel. b) In-house built prototype SLM system with multi-material processing capability. c) Design of the powder feeder system. d) Working principle of the powder feeder for mixing powders. e) Calibration curves of the delivered powder mass (m) of pure Fe and f) Al-12Si as a function of applied voltage (A) and vibration time (t_v). Error bars depict 95% confidence interval for the mean. (withdrawn from [107])⁶

attraction force [130]. In the final step, the photoreceptor is cleaned with a blade to remove residual particles and discharged with a second laser exposure before the start of the next powder deposition cycle [111].

In 2019, Aerosint used the electrophotographic principle [131] to develop a novel selective powder deposition technology that enables the deposition of dry powder particles, such as polymer, metal, or ceramic, to form a single layer containing at least two materials with low waste [104] (Fig. 10). The technology employs rotating patterning drums, where each drum deposits one material. This process selectively deposits a volume pixel (voxel) of powder in a layer-by-layer fashion, with speeds up to 200 mm/s, and is less sensitive to powder characteristics than conventional systems [132]. Currently, Aerosint selective powder deposition system is used only in Aconity machines – AconityMIDI+ and AconityMICRO L-PBF printers – to enable multi-material fabrication [133].

Mussatto [72] classified the powder deposition systems technologies accordingly to the type of powder material used, the cross contamination level, material transition between layers, the gradative powder deposition within one layer, the discrete powder deposition within one layer, and the time to form a powder bed (Table 1). The results show that the level of productivity is low for all technologies except conventional and alternating spreading. Furthermore, powder spreading with suction is overall the most well performing. It can be used with all types of powder materials,

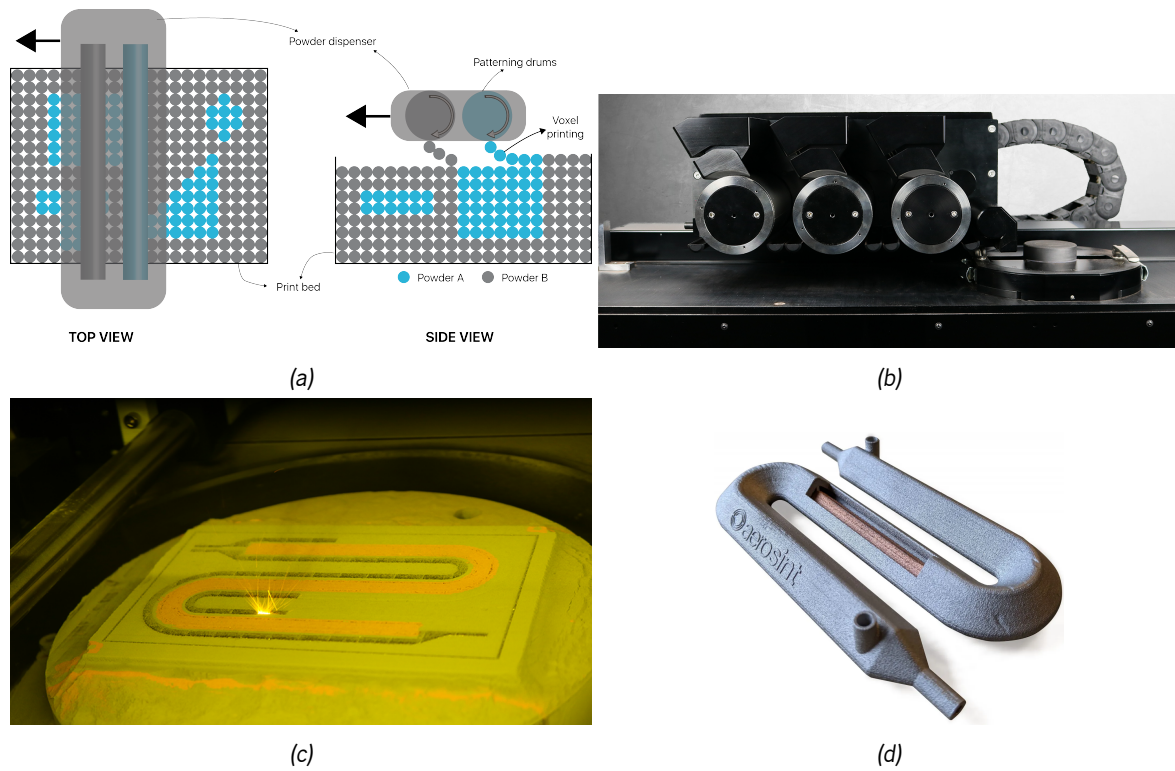


Figure 10: Aerosint selective powder deposition system for MMLPBF: (a) Process [104]; (b) Dual powder recoater [133]; (c) CuCrZr-316L Heat Exchangers part printing on Aconity MIDI+ LPBF printer powered with Aerosint’s multi-material recoater [134]; (d) printed part [133]. Reproduced with permission, copyright Aerosint SA

and has the lowest cross contamination, although with the significant shortcoming of not allowing gradient powder deposition.

Table 1: Overview of the advantages and disadvantages of the various multi-powder deposition systems for L-PBF (adapted from [72])⁷

System	SP	PB	MP	PP	MEP	CP	PPPCCL	OPPLLT	GPDWOL	DPDWOL	LPTFPB
Conventional spreading	✓	✓		✓	✓	✓	L	✓			T
Patterning Drums	✓		✓		✓	✓	H	✓		✓	S
Spreading + suction	✓	✓	✓	✓	✓	✓	L	✓		✓	VS
Vibrating Nozzle	✓	✓	✓		✓	✓	M	✓	✓	✓	VS
Hopper feeding	✓	✓	✓		✓	✓	H	✓	✓	✓	S
Alternating	✓	✓	✓	✓	✓	✓	M	✓			T
Electrophotographic	✓		✓		✓	✓	H	✓		✓	VS

SP = Single Powder; PB = Powder blends; MP = Multi powder

PP = polymeric powders; MEP = Metallic Powders; CP = Ceramic Powders

PPPCCL = Post Printing Powder Cross Contamination Level; L = Low; M = Medium; H = High;

OPPLLT = One Powder Per Layer (Material Transition Between Layers)

GPDWOL = Gradient Powder Deposition Within One Layer

DPDWOL = Discrete Powder Deposition Within One Layer

LPTFPB = Level of Productivity (Time to Form a Powder)

The author further concluded that despite many significant advances in the multi-material processing over the

⁷Used under the terms of the [Creative Commons BY-NC-ND 4.0 licence](https://creativecommons.org/licenses/by-nc-nd/4.0/).

last few years, the issue of powder cross-contamination remains a serious problem that needs to be addressed. Furthermore, there is an urgent need for an in-depth analysis of the **MMLPBF** process so that the knowledge generated can be used to optimise and improve the process to specific needs.

2.3.3 Manufacturing chain

Fig. 11 illustrates the **MMLPBF** manufacturing chain based on the scientific literature [135] and the commercial equipment panorama [67–71, 100]. The manufacturing chain is divided into three stages: pre-process, in-process, and post-process.

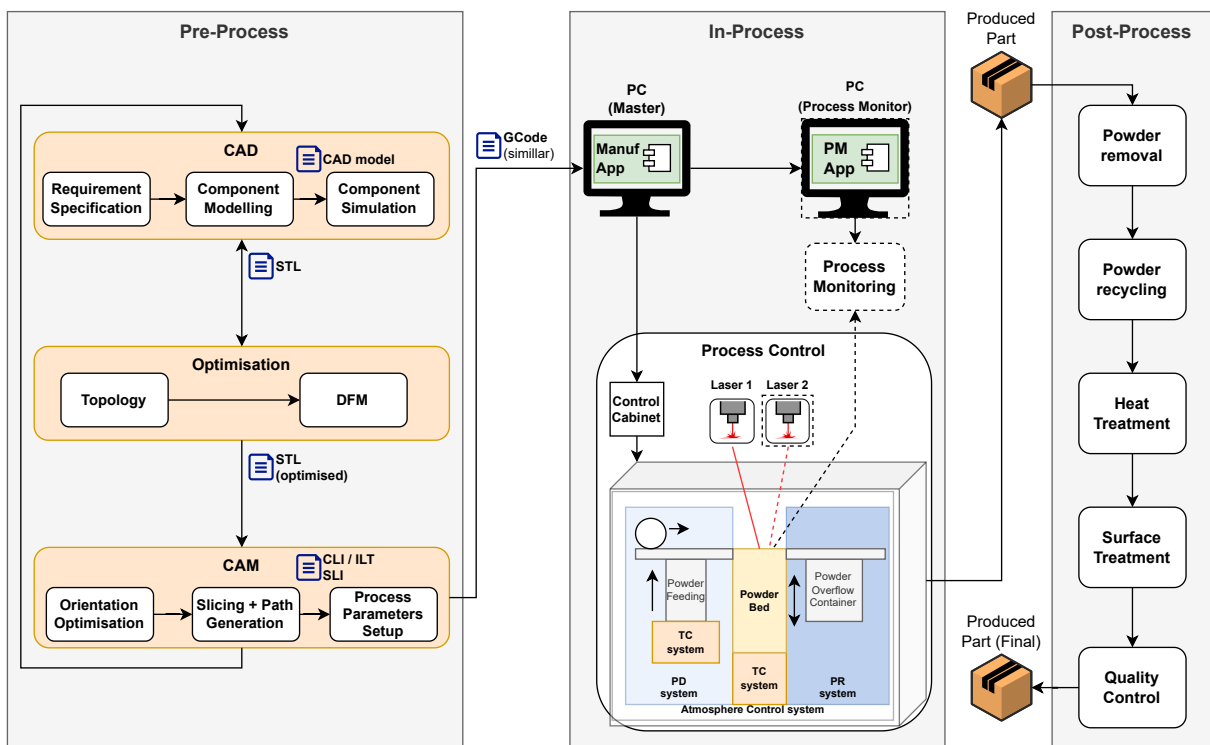


Figure 11: **MMLPBF** manufacturing chain overview

2.3.3.1 Pre-Process

In the pre-process stage, the component is designed as an assembly of multiple individual **CAD** models corresponding to each material, and the transition between them, according to the requirements specifications [136, 137]. This is a result of the limitation of most of the mainstream commercial software to express material information, which hinders multi-material design [131]. On the other side of the spectrum one has specialised software for the generation of graded material transitions in volumetric models, like **GrMMaCAD** (Graded Multi-Material CAD), which supports the assignment of locally varying material properties within a 3D model [138].

The model is then simulated both at a material scale and integrated (assembled) scale. The geometry of each model is exported independently, usually in the **STL** format, **OBJ** (Object file format), **Additive Manufacturing File (AMF)**, and **PLY** (polygon file format) [139]. A sanity check is performed on the geometry file (and repaired) and the

topology is optimised. The **Design For Manufacturing (DFM)** or **Design For Additive Manufacturing (DFAM)** imposes constraints on the topology taking into consideration the manufacturing process.

Then, in the **Computer-Aided Manufacturing (CAM)** phase, the model is virtually placed into the building platform, and the orientation is optimised, and, if required, supports are generated for the component to ensure adequate printing. Each material model is then sliced, and the paths are generated, yielding the layer information typically in the open-source formats (CLI, ILT – Aconity [67], Reinshaw [100]), or the proprietary SLI (EOS, 3D Systems) [118]. Each material model is then merged in the manufacturing model. The topological data is mapped to the process parameters, accordingly to each material, yielding the manufacturing instructions for the equipment, typically in a G-Code similar format [6].

Fig. 12 shows an extensive list of some of the many software applications for the **MMLPBF** pre-processing compiled by Moreno et al. [140]. The vast majority of these applications are closed-source and released under commercial licences.



Figure 12: MMLPBF Pre-process software (withdrawn from [140]⁸)

The pre-processing procedure is time and effort consuming and it involves the generation of large amounts of data [10, 131, 141]. Nonetheless, the available software suite does not provide the automation required for the process. Fig. 13 shows one example of a custom manual data pre-processing procedure devised by Wei et al. [92] to surpass the lack of software tools for the **MMLPBF** process. The parts were modelled and assembled, and individual material geometry converted into the **STL** format. Then, each material is sliced and hatched using a proprietary **CNC** CAM tool to generate the toolpaths and G-Code for the powder dispensing system. Furthermore, the process is complex and does not scale well to industrial applications [131].

⁸Used under the terms of the [Creative Commons BY-NC-ND 4.0 licence](https://creativecommons.org/licenses/by-nc-nd/4.0/).

⁹Used with permission from Elsevier: licence nr. 5296410224943

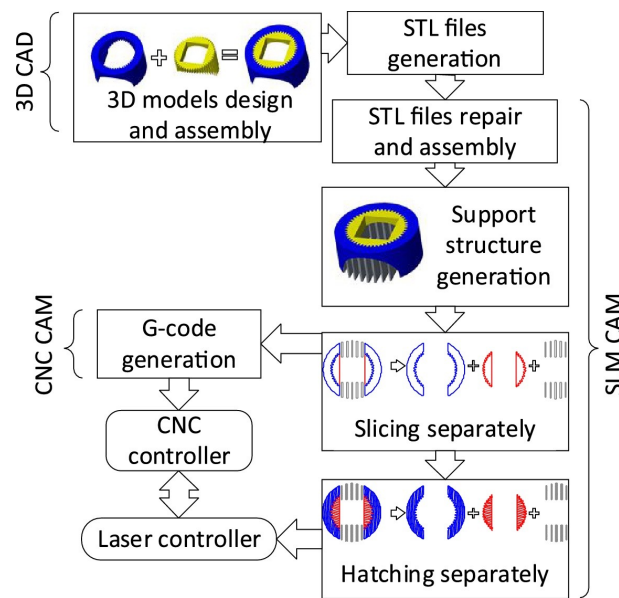


Figure 13: Flowchart for data flow for MMLPBF (withdrawn from [92])⁹

Thus, several methods have been proposed to address the shortcomings of the current pre-processing procedure for the MMLPBF process. Firstly, there is the need for a data interface file that can convey both geometrical and material information [131]. STL files are a tessellation of facets and the corresponding normals without any material data. Furthermore, it is unable to accurately represent holes, porosity and discontinuities. As a result, back in 2009, Hiller and Lipson have proposed STL 2.0 to combine geometric and material information [142], but it never gained traction [131]. The OBJ file can store colour information, but not material one [131]. On the other hand, the AMF file conveys geometric and material information, but occupies a large storage space and is not yet mature [143, 144]. The PLY file can express texture and colour, but not when a part contains different material properties [145].

Hence, other file formats were developed for MMLPBF fabrication, namely FABricatable VoXel (FAV), Simple VoXel (SVX), and 3D Manufacturing Format (3MF), which can convey information about the material gradient and micro-scale physical properties [139]. The first two are based in volume discretisation using volume pixels (voxels): FAV incorporates colours, materials, and connection strength information (Fig. 14); SVX comprises material allocation, density, and colour information [131]. The 3MF is a open source standard file format based on the eXtensible Markup Language (XML) specification to describe the intrinsic and extrinsic information of a model. However, it does not support higher-order representations such as Non-Uniform Rational B-Splines (NURBS) (used by GraMMaCAD [138]) and Standard for The Exchange of Product data (STEP) [131].

Secondly, comes the slicing and path generation procedure. As aforementioned (see Section 2.2) the energy density is the primary driver of melting and can be regulated through a combination of scanning strategy (type, hatching distance, angle) and process parameters (laser power, laser scanning speed). Several scanning strategies were tried out, namely simple, alternate, stripes, island, sinusoidal, and chessboard [117, 131]. Mussatto et al. [146] used Solidworks to 3D model the specimens which were then sliced by the commercial slicing tool Netfabb Autodesk. In the same work, the authors needed to generate the 3D models of the specimens using a sine function and Excel Macro and the JavaScript programming language to generate the sinusoidal hatching and export it to the CLI format. Thus, the commercial CAM tools available are not able to produce custom paths in a straightforward

and flexible manner.

Lastly, we have the manufacturing file generation. Most commercial L-PBF equipments are only available for mono-material fabrication [72] and, as aforementioned, they require upgrading for multi-material fabrication. For example, Nadimpali et al. [6] upgraded an Aurora Labs S-Titanium PRO to use two 150 W CO₂ lasers simultaneously, but they needed to modify directly the G-Code instructions to operate the machine. This defeats the purpose of pre-processing, as it requires specialised staff to do the on-line programming of the machine with explicit manufacturing instructions that would otherwise been generated by the pre-processing procedure.

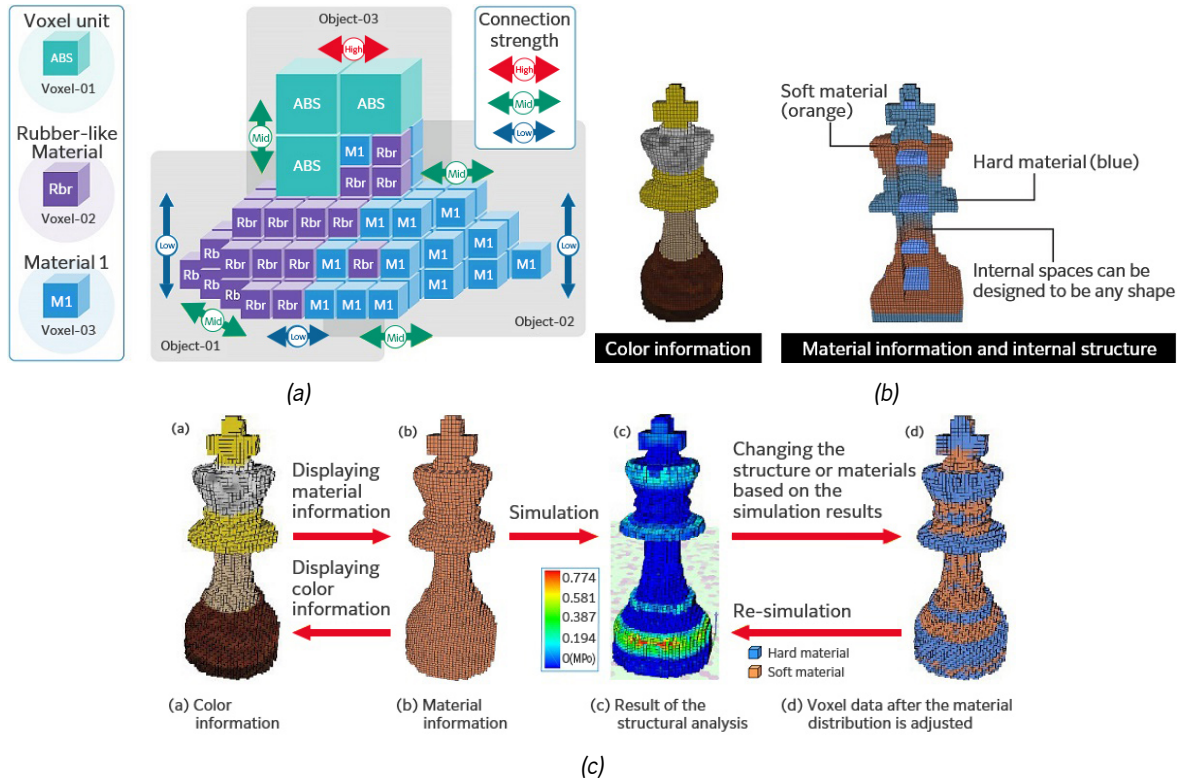


Figure 14: FAV file format [147]: (a) Conceptual diagram showing voxels arranged three-dimensionally; (b) the FAV format can retain information on internal structure, colour, and material; (c) Simulations can be performed on voxel data as-is, and designs can be modified to reflect simulation results. Reproduced with permission, copyright FUJIFILM Business Innovation Japan Corp.

2.3.3.2 In-Process

In the In-Process stage, the manufacturing instructions are used to control the MMLPBF building cycle. Process monitoring and closed-loop control are optional, but strongly recommended, to ensure optimal manufacturing quality.

The most significant challenge in the MMLPBF process is to guarantee the accurate and effective delivery of the different materials to the building chamber. However, only few commercial systems can be used for multi-material fabrication out of the box [3, 67, 104]. Thus, in this section, we explore further the panorama of available solutions, both in the commercial and research fields.

Table 2 shows a list of most relevant L-PBF commercial equipments, based on a survey over product specifications [2, 3, 69, 100, 148–150]. The prices were obtained from quotations provided directly by the manufacturers,

and do not include taxes. From this list, all equipments use a feedstock of metallic powder, but only the AconityMIDI+ [2] and the SLM 280 2.0 [3] can be used for multi-material fabrication. The [Software \(SW\)](#) stack for these two equipments includes commercial proprietary software for pre-process or in-process management. The entry-level product for Aconity – AconityMINI – starts at 228 K €, thus it is expected that AconityMIDI+ surpasses this. On the other hand, the SLM 280 2.0 starts at 500 K €. This clearly demonstrates that the initial investment in a [MMLPBF](#) equipment is significantly high. Furthermore, in the current setup, these equipments can only be used with metallic powders, which limits the scope of applications.

Table 2: L-PBF commercial equipments [2, 3, 69, 100, 148–150]

Equipment	Build Volume	Materials	LT (μm)	MM	# Lasers	PH ($^{\circ}\text{C}$)	PM	SW Stack	NW (kg)	Cost (€)
AconityMINI	$\varnothing 250 \times 250$ mm	metals	10 (min)	No	1 (Fiber)	800 (max)	Optional	Autodesk Fabb Premium AconityStudio	850	228 K
AconityMIDI+	$\varnothing 150 \times 150$ mm	metals	10 (min)	Yes	4 (Fiber)	1000 (max)	Optional	Autodesk Fabb Premium AconityStudio	1600	N.D.
TruPrint3000	$\varnothing 300 \times 400$ mm	metals	20	No	4 (Fiber)	200 (max)	Optional	Proprietary Tool Suite	4300	950 K
SLM 280 2.0	280 x 280 x 280 mm	metals	20 (min)	Yes	2 (Fiber)	550	Included	Proprietary Tool Suite	1300	500 K
RenAM 500Q/S	250 x 250 x 350 mm	metals	30 (min)	No	4 (Fiber)	N.D.	Included	QuantAM RenAMP InfiniAM	1960	N.D.
EOS M300-4	300 x 300 x 400 mm	metals	N.D.	No	4 (Fiber)	N.D.	Included	EOSPRINT2 EOS ParameterEditor EOSTATE Monitoring Suite EOSCONNECT Core EOSCONNECT Core EOSCONNECT MachinePark Materialise Magics Metal Packages and modules	5500	1300 K

LT: Layer Thickness; MM: Multi-material; PH: Preheating; PM: Process Monitoring; SW: Software; NW: Net weight

As a result of the lack of commercial solutions for [MMLPBF](#) and/or their cost, researchers tried to upgrade some of these equipments. Liu et al. [9] and Sing et al. [8] upgraded a powder feeder of a conventional L-PBF system – SLS 250 HL from SLM Solutions – equipped with a 400 W fiber laser to store and deliver two metallic powder materials separately. C18400 copper have been successfully deposited on top of 316L stainless steel and AlSi10Mg, although the transition zone between the two materials could not be controlled, which is the most critical in a multi-material part. Anstaett et al. [7] also upgraded a SLS 250 HL L-PBF system to deposit two metallic powders, combining a Cu-alloy and a tool steel to produce a multi-material component [7].

More recently, Nadimpali et al. [6] upgraded an Aurora Lavs S-Titanium Pro L-PBF equipment, due to its multiple hopper dispenser, to combine 150 W CO₂ lasers simultaneously, with an average maximum power output of 255 W. The two beams pass separately through a set of optics before entering into the focus lens resulting in a single spot with approximately 150 μm in diameter in the processing plane. The powders are mixed thanks to the powder dispensation and sweeping mechanisms. However, the authors required to explicitly modify the G-Code to operate the machine. In 2022, Schneck et al. [5] also upgraded a SLM 250 HL L-PBF equipment with a powder dispensing system consisting of a suction module and blade coater to manufacture a prototype injection nozzle for an internal combustion engine using metallic powders. The pre-processing was manual, with each material of the 3D component modelled independently and exported as STL file, which was then sliced and converted to the proprietary SLM file format using AutoFab [CAM SW](#).

Lastly, Bareth et al. [4] upgraded an Aconity MINI L-PBF equipment with a multi-material mobile plug-in module to feed a second material to the building chamber (Fig. 7). However, the same suction system is used for

both materials, which increases the cross contamination and diminishes the powder recyclability rate. The multi-material module was connected to the machine's [Programmable Logic Controller \(PLC\)](#), which made it possible to be controlled directly from the software by modifying the custom G-Code.

2.3.3.3 Post-Process

The [L-PBF](#) and [MMLPBF](#) post-processing are identical and involve several fundamental steps and challenges such as powder removal and recycling, part separation, in-situ process monitoring, post-processing treatments and quality control. However, there are currently no specific guidelines available for the mechanical and thermal post-processing of multi-material parts [10].

Separation of mixed powders represents an additional challenge, which requires the removal of various powder materials from each other as well as the elimination of process-related impurities.

The current state of the art in material separation proves to be challenging and has not been implemented in practice [141, 151]. Seidel [135] evaluated the different working principles for powder recyclability, such as, particle size, ferromagnetism, density, mass, electrical conductivity and surface wettability. The author concluded that ferromagnetic separation and sieving are the most promising technologies.

When validating the part, it is important to investigate mechanical and thermal parameters and microstructural analyses in the joining zone. Several investigations have been conducted to characterise the joining zone of 2D specimens using optical methods such as optical and scanning electron microscope (SEM) images to analyse the microstructure, strength, and defects [7, 19, 52, 106, 152].

The last fundamental problem is related to process knowledge. It is critical to understand the process thoroughly to obtain good quality parts [153–155].

2.3.3.4 Prospects for improvement

The main takeaway is that the [MMLPBF](#) fabrication is a multi-objective problem, requiring specially designed equipments and toolchains, and experimental design.

Back in 2012, Gu et al. [156] highlighted the need to create a process knowledge database to handle the inherent complexity of the process and support its evolution. Yet, ten years later Mussatto [72] reports the gap was still not addressed and there is an urgent need for an in-depth analysis of the [MMLPBF](#) process to ensure sustainable process improvement.

It is essential to develop a multi-material simulation software tool or an [AI](#) prediction method of the optimal process parameters beforehand to narrow the actual experimental range [66]. Last year, Exponential Technologies, in a collaboration with Aerosint, reported the two-fold improvement in component density within 2 print jobs and 46 samples printed without any prior statistical knowledge. This yielded a reliable parameter set for printing Stainless Steel 316L and Inconel 625 combinations, saving time and money [13].

Furthermore, machine learning can be used as a means for automated evaluation and classification of sensor data to assist in process monitoring and closed-loop control of the [MMLPBF](#) equipment. However, the research is still in a developing stage [55, 157].

Only a handful of commercial [L-PBF](#) equipments support multi-material fabrication out of the box, and all of them, use metallic powders, limiting the scope of applications and, inherently, functional design. This may be a limitation of some powder deposition systems, but it most linked to the fact that only fiber lasers are used for the

printing. Moreover, the significant initial investment may be an obstacle, especially in the research field, further hindering the process evolution.

The manufacturing chain is complex and the toolchain varies greatly among manufacturers, specially within the pre-process stage. Specific guidelines for **MMLPBF** were not identified and most pre-processing procedures use a manual method based on inadequate data format (**STL**) [10]. Further research is required to assemble a coherent and straightforward pre-processing tool to enable multi-material functional design, simulation, and optimisation. The most promising approaches are based on volume discretisation (voxels), like the **FAV** format and the **GraMMaCAD** software. In the post-processing, further research is required for the surface and heat treatments involving multi-material components [10].

2.4 Applications

After introducing the theoretical foundations for multi-material fabrication, it's important to highlight the possible applications, as they usually drive any given methodology, and they certainly should drive the functional design, providing a more clear view of what is being accomplished and how.

The main application for functional design through the use of multiple materials in the scope of this PhD project is in the biomedical field – the hip implant. This aims to address several issues encountered in the current hip implants that lead to a short lifespan of these prosthetic implants, with forced revision surgeries spanning a short period of time (ten to fifteen years after the implantation surgery) [11].

The goal of the hip implant is to mimic the natural behaviour of the bone to serve as its suitable replacement; as such, and not surprisingly, the material composition, properties and structure needs to be varied. Fig. 15 illustrates the hip implant constitution. The artificial acetabular cup and femoral head replace the damaged natural articulation [158]. Thus, here allocated materials must have low friction and withstand wear and mechanical loads. The femoral head is anchored in the femur by the stem. The acetabular cup is anchored in the pelvis and is composed of a shell in which a liner is inserted that provided the load bearing articulating surface. On other hand, shell and stem have to provide good bone integration [159]. Furthermore, the leaching of toxic metallic ions, the tribocorrosion effect, and stress shielding, imposes significant challenges on the design [160]. This requires different materials and varying compositions to achieve the desired individual component's function; however, the most important design goal is the overall function of the hip implant, requiring especial attention to the interfaces between components, but maintaining good properties for the individual components also.

According to a recent review article [160], crosslinked polyethylene, titanium alloys, CoCr alloys, stainless steel, zirconium-niobium alloy, tantalum, ceramics, and composite combinations are among the commonly used materials for prosthesis fabrication. In particular, bioceramics coatings such as DLC and TiN have demonstrated promising results in enhancing osseointegration. However, due to the significant disparity in mechanical properties among the current implant materials, the lifespan of hip implants may be considerably reduced.

The multi-material additive manufacturing, and more specifically **MMLPBF**, can mitigate this problem by allowing some of the assembled components to be merged in a single component, where the characteristics of the interfaces are custom-tailored to obtain the desired local properties, obviously through careful design.

¹⁰Used under the terms of the [Creative Commons BY-NC 3.0 licence](https://creativecommons.org/licenses/by-nc/3.0/).

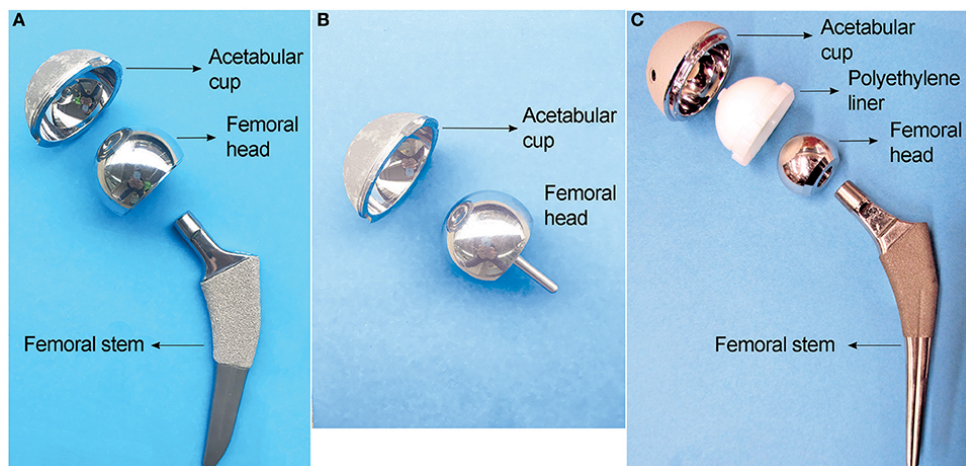


Figure 15: Three main types of hip implants showing ball-and-socket joint regions: (A) Large head metal-on-metal (MoM) total hip implant. (B) MoM hip resurfacing. (C) Metal-on-polyethylene (MoP) total hip implant. (withdrawn from [159]¹⁰)

2.5 Summary

This chapter provides an overview of the current state of the art in the realm of multi-material fabrication of metals and composites and its contribution to functional design. AM processes were examined and categorized, with a particular focus on their usefulness in rapid prototyping and the manufacture of high-value parts by facilitating material addition only where needed, thereby achieving functional design objectives. Hybrid processes were briefly mentioned as a better, but more complex, match for functional design. Therefore, the focus in this work is limited to AM processes.

Laser sources are an attractive option for AM processes due to their small spot diameter, high energy density, and precise energy control, making them well-suited for fabricating metallic parts with high melting points and thin details. L-PBF and DLD represent the two dominant approaches in this field, with L-PBF being best-suited for small and medium-sized multi-metal parts with high resolution and DLD being preferable for larger parts and lower resolution. Given the additional complexity of DLD, L-PBF processes currently represent the best commercial and industrial option for fabricating high-precision multi-material parts.

The L-PBF process was examined in detail, along with its requirements and working principle. Multi-material additive manufacturing (MMAM) was introduced as a highly desirable technology, facilitating the precise placement of material based on its functionality, thereby yielding custom-tailored parts for specific applications with improved mechanical properties and behavior in service beyond what is achievable by conventional methods. The potential applications of MMAM are wide-ranging and critical, particularly in the fields of biomedical engineering, soft robotics, and electronics.

Subsequently, the current panorama for the MMLPBF process was presented, highlighting the subsystems that make up the MMLPBF equipment, with particular emphasis on the powder delivery system, which is critical for multi-material fabrication. Several working principles and available technologies for this system were discussed, with the powder spreading with suction being the most mature technology, while the most promising one is based on the electrophotographic principle, the patterning drum.

The manufacturing chain was examined, focusing on the most significant challenges, including material variation across several directions in the powder-deposit system, joining dissimilar materials, powder contamination,

numerous process parameters affecting the quality of the produced part, lack of design guidelines, manual pre-processing, and the lack of post-processing treatment research. The most relevant commercial equipment capable of multi-material fabrication was presented, with only a handful of these able to handle metallic powders, limiting their scope of application. Furthermore, the initial investment required for these machines is considerably high, which may explain why the majority of research literature focuses on upgrading mono-material LPBF equipment with multi-material powder delivery mechanisms, despite the need for manual pre-processing and manual programming of the equipment.

The prospects for improvement across the manufacturing chain were outlined. Tools for designing and simulating multi-material components manufacturable by the [MMLPBF](#) process are required, and machine learning could have a significant impact on the process, by mining process data to provide sets of parameters and build strategies for producing components with better mechanical properties in a cost-effective manner.

Finally, the specific applications of interest to this work were presented, with the hip implant being a notable example. There is high demand for improved quality implants due to their high replacement rate and invasive procedures. They require multiple materials, including metals and composites, to perform effectively in various regions of the body, making them a perfect showcase for [MMLPBF](#).

In conclusion, [MMLPBF](#) fabrication presents a multi-objective problem requiring a specialized equipment and toolchain, as well as experimental design. The present state of [MMLPBF](#) pre-processing techniques is primarily focused on addressing specific issues within the multi-material processing domain, and lacks a holistic approach that could enhance knowledge transfer throughout the manufacturing process. Additionally, these techniques are closely connected with proprietary solutions that hinder customisation and impede the evolution of the process. Therefore, there is a need for a comprehensive methodology to produce multi-material metallic and composite components that can handle the inherent complexity of the [MMLPBF](#) process and leverage its knowledge. This entails establishing a [MMLPBF](#) process database, as suggested by Gu et al.[156] and Mussatto[72], that is accessible to all relevant parties in the manufacturing chain.

The problem and its challenges

The fabrication of multi-material parts using L-PBF is a complex and challenging topic. Most commercially available L-PBF systems are designed for mono-material fabrication, lacking the flexibility and processing capability for multi-material processing [72]. The L-PBF systems that allow multi-material fabrication only use metallic powders, limiting their scope of applications and hindering functional design.

Moreover, the MMLPBF process presents a multi-objective problem, requiring specialized equipment, toolchain, and experimental design. However, the current status of the manufacturing chain forces users to search for workarounds to handle specific problems, as a global infrastructure is not established. This shifts the focus from functional design to the manufacturing process, defeating the intended purpose.

Thus, there is a need for a comprehensive methodology to produce multi-material metallic and composite components that can handle the inherent complexity of the MMLPBF process and leverage its knowledge throughout the manufacturing chain to all relevant agents.

This chapter lays the foundation for such infrastructure, devising a global methodology for the MMLPBF process. This methodology adopts a holistic model-based approach to problem-solving, serving as a supporting framework for the establishment of a suitable workflow and the development of an appropriate toolchain that can be used to design and manufacture multi-material metallic and composite components.

3.1 Proposed Approach – solution

A model-driven approach was adopted to address the complexity associated with the fabrication of multi-material parts using the L-PBF process. A model is an abstract representation of a system that can be used to answer questions about it [161], and it forms the foundation of the proposed global methodology for the MMLPBF process. Modelling has also been shown to be an effective tool for prototyping, developing, and testing mechatronics systems, which aligns with the proposed methodology and aims to improve the quality of the solution while minimizing time, costs, and errors.

The proposed solution includes a global methodology for L-PBF processes that can leverage the process's knowledge throughout the manufacturing chain, making it more accessible while reducing the overall complexity to a manageable level. Additionally, a specific 3DMMLPBF workflow that considers project constraints and resources is proposed. The necessary toolchain for the entire process is assembled, and the 3DMMLPBF machine is developed, tested, and integrated with the process's framework. Finally, the process data is systematically collected and fed

back to the relevant manufacturing agents to improve the process.

3.2 A Global Methodology for 3DMMLPBF processes

The global methodology for 3DMMLPBF processes is described next.

3.2.1 Motivation

The proposed methodology aims to address the shortcomings of available pre-processing methodologies and is based on three fundamental aspects. Firstly, there is a lack of a comprehensive methodology that encompasses the MMLPBF process as a whole, which considers all the key agents and leverages the existing knowledge. Secondly, there is a need to develop customisable equipment that can fabricate multi-material metallic and composite components, as currently available processing technology does not provide the desired level of freedom and customisation. Finally, there is a need for an efficient way to handle the inherent complexity of the MMLPBF process.

Additionally, the high cost and lack of customisation of current commercial equipment limits its potential, as the end-user has limited access to the machine and process parameters. This is particularly critical in research environments, as it reduces research opportunities, increases inequality in the field, and hinders the evolution of the MMLPBF process.

The underlying philosophy of the proposed methodology is reminiscent of open-source principles, which emphasize transparency and bootstrapping capabilities. This approach applies to both software and hardware tools.

3.2.2 Core Principles

Knowledge, the theoretical or practical understanding of a subject, is the most important human asset. However, knowledge acquisition is a nonlinear process, as a single piece of additional data can invalidate complete models [161]. Still, MMLPBF knowledge is scattered around its agents without an apparent connection. Moreover, some techniques used in L-PBF processes are based on empirical evidence [12], requiring the capture of contextual and rationale information behind such decisions. To address these challenges, it is imperative to capture the relevant knowledge and context and deliver it to the appropriate agents, thereby facilitating the efficient usage of knowledge throughout the MMLPBF process.

The MMLPBF methodology is based on several core principles, which include:

- Abstraction: The provision of layer(s) to abstract from the internal specifics of the process, while maintaining tractable interfaces.
- Modularity: The ability to replace every component of the process with another of identical functionality.
- Independence: The agnosticism of the process regarding inputs, as long as the valid interfaces are respected.
- Flexibility: The capability to handle different inputs/components, allowing for the inclusion of new parameters or the conjunction of their effects, thereby supporting different materials, machines modules, slicing strategies, among others.
- Extensibility: The ability to add new components to the process without compromising it.

- High Customisation: Both software and hardware-based components should allow for a high degree of customisation of their operation.
- Capability of managing different information flows: The ability to collect and deliver pre-manufacturing, manufacturing, and post-manufacturing data to its handler in a convenient way.
- Evolution: The acquisition of knowledge should be used to improve the process continually.
- Guidance to end-users: The acquired knowledge should enable the creation of guidelines and heuristics to aid the end-user.
- Maximisation of process control: An open developing environment enhances the end-users' capability to control the process, allowing normal users to evolve into power users, as opposed to closed environments.

3.2.3 Concept

The objective is to gain a comprehensive understanding of the 3DMMLPBF manufacturing chain from a first-principles perspective using models to represent the system with manageable complexity and to provide insights into the system [161]. The Unified Modeling Language (UML) was chosen to create the relevant models due to its flexibility in modelling a wide range of artefacts, including software systems, processes, and work products [161].

Initially, the actors involved in the process were identified as the key agents interacting with the system and classified as either internal, those that take effective action in the process, or external, those that benefit from or induce actions in the process.

The internal actors include:

- **Designer**: ideates a concept and translates it to a virtual 3D representation (CAD model).
- **Manufacturer**: utilises the appropriate materials, techniques and tools to convert the virtual 3D model into a physical object.

The external actors include:

- **Physicist**: studies all physical phenomena in the process and contributes to greater knowledge of the process by providing physics models and parameters, enabling better control strategies, better materials properties, and faster processes.
- **Materials/Mechanical Engineer**: contributes to the process by studying all materials/mechanical properties of the produced part in service and usually provides empirical knowledge in the form of a set of rules that improve the part's properties and performance.
- **Control Engineer**: studies the process control, which is an effective means of achieving system goals in a regulated and bounded way, and generates the control strategies to be used in the process [97].
- **Mathematician**: studies the manufacturing path topology, the geometric and interchange data representation of the 3D virtual model for machine execution.

- **Data Scientist:** studies all process-generated data using data-driven models, leveraging the immense quantity of data available to identify patterns to produce more efficient and accurate empirical knowledge. This information can be used to design better experiments, using **DOE**, and to control the process more effectively, using **AI** techniques [72, 97].

Subsequently, the manufacturing chain was decomposed into four models that will be detailed next, namely: design model, pre-manufacturing model, manufacturing model and post-manufacturing model.

3.2.3.1 Design Model

Figure 16 depicts the design model of the manufacturing chain in detail. The design process starts with the identification of the object's function or application by the designer. Subsequently, a comprehensive requirements analysis is conducted, and design criteria are established based on the obtained results. Following this, the object is modeled in a **CAD** software, which yields a 3D **CAD** model of the object. Ideally, this model should undergo an optimisation stage where it is converted into a parametric **Computer-Aided Engineering (CAE)** model and then passed to a **CAE** optimiser. This optimiser determines the optimal material distribution as a function of the design criteria. If the optimal configuration is not achieved, the designer should optimize the 3D **CAD** model. Finally, for both optimised and non-optimised 3D **CAD** models, a data file representing the object's geometry is generated, with the most common being an **STL** file.

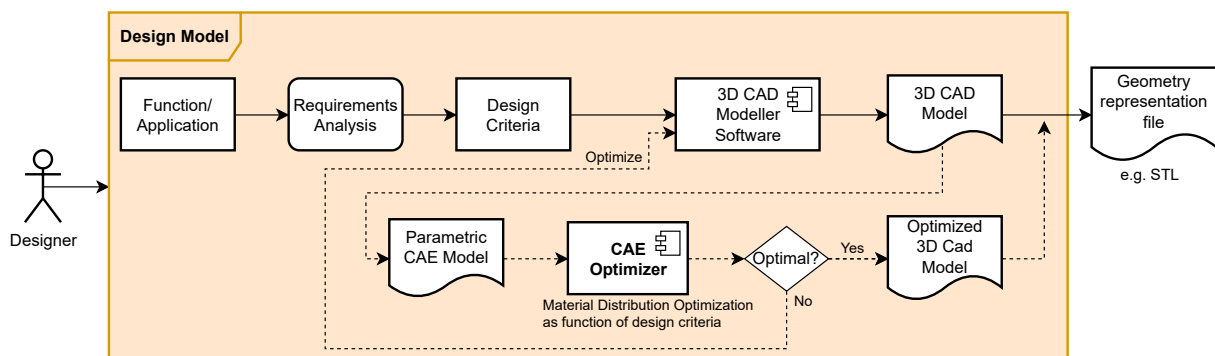


Figure 16: Model of the design activity

3.2.3.2 Pre-Manufacturing Model

Fig. 17 illustrates the pre-manufacturing phase. The dashed components are included to optimise the process, while the solid-lined ones represent the conventional setup.

In the conventional workflow, the **Manufacturer** transfers the 3D geometry file to the **Slicer**, which, in turn, slices it into 2D layers by using cross xy planes. However, issues may arise in this phase, particularly when the geometry representation file is a surface tessellation (**STL**), which is unable to accurately represent holes, porosity and discontinuities. This challenge will be addressed in greater detail later.

The **Slicer** merges these 2D layers, derived from several materials, into a single layer for each layer height, and then the **Post-Processor** maps the process parameters to them. Moreover, the **Post-Processor** generates the manufacturing file, which contains the corresponding machine instructions, such as the `.lcode` file.

The *Post-Processor* requires the development of a grammar that the machine can comprehend, thereby compiling a standard code that the machine can interpret, such as modified G-code. Consequently, this standard code comprises language tokens based on the machine, process, and material tokens, and generates manufacturing instruction tokens that are leveraged by the compiler to generate machine-compliant instruction code. The interpreter is constructed based on these tokens and adds to the firmware.

The *CAM optimiser* and *Adviser* are optional components that can be used to refine the manufacturing process. The *CAM optimiser* optimises the topology based on the manufacturing technology, employing structured knowledge derived from machine, process, and material data. The *Adviser*, in contrast, provides convenient part orientation, file data sanity check, and conformity to standards, based on empirical knowledge originating from machine, process, and material data. Although both of these optional components can be employed to optimise the 3D CAD model from the design stage, the *CAM optimizer* relies on structured knowledge and should issue recommendations as errors or warnings, thereby halting the process. Conversely, the *Adviser* is guided by heuristics and guidelines and should offer suggestions.

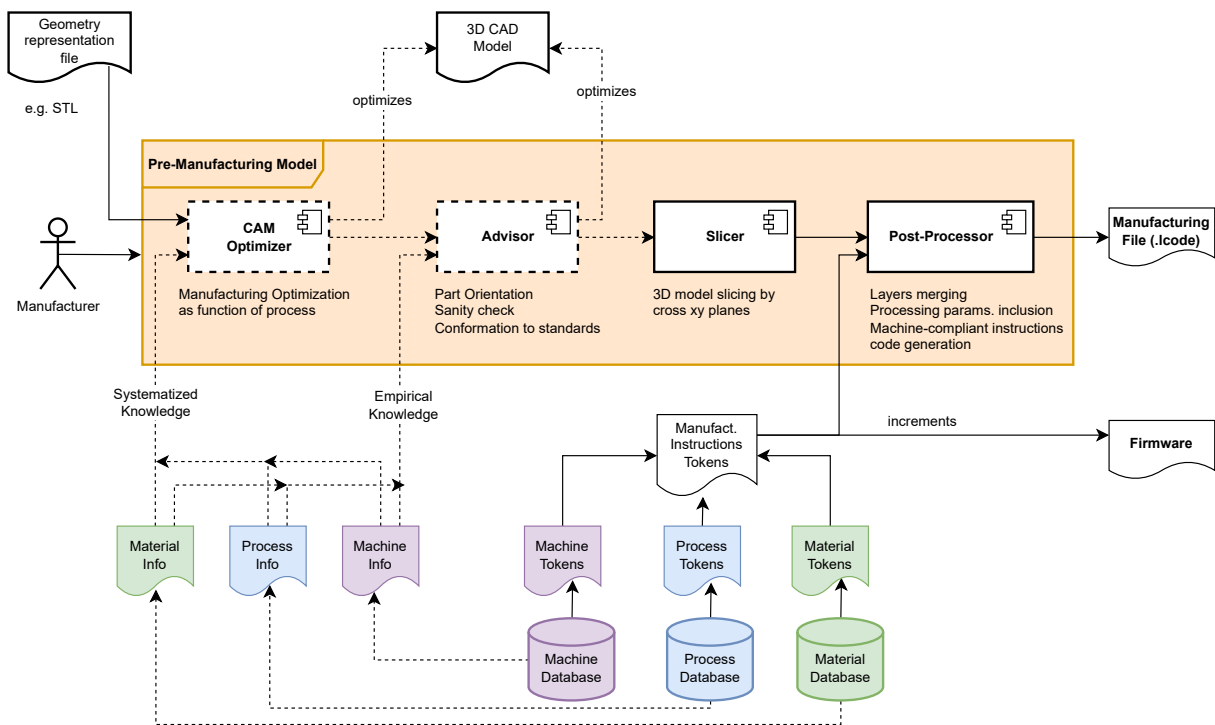


Figure 17: Model of pre-manufacturing activity

3.2.3.3 Manufacturing Model

The manufacturing model includes the control model and the manufacturing process model (Fig. 18) tightly coupled together.

The *Manufacturer* supplies the manufacturing instruction file, containing the manufacturing process relevant data for the part fabrication, to the interpreter – a software module of the machine’s firmware. The interpreter then reads, parses and interprets the *.lcode* instructions. While the End-of-File (EOF) has not been reached, the *Firmware* issues commands sequentially to the control chain: the control board and the controlled parts like motors, the laser,

the heating elements, etc. This yields an effect on the manipulated variable (e.g., mean voltage of a heating resistor) which affects the manufacturing process, represented as a transfer function, different for each process variable.

The result of the control action will be a variation in the controlled variable state (e.g., temperature, laser speed, etc.), affecting the manufactured part, which is measured by a sensor (e.g. encoder, thermocouple, pyrometer, etc.) and fed back to the control board for comparison with the desired values for the process variables, with the control action being adjusted accordingly.

Additionally, the process variables are registered by another software component – the logger – which reads, converts, and logs the relevant parameters as a process info data file to be stored in the process trials database. When the manufacturing file reaches the end, the part is produced and ready for the next stage – the post-manufacturing phase.

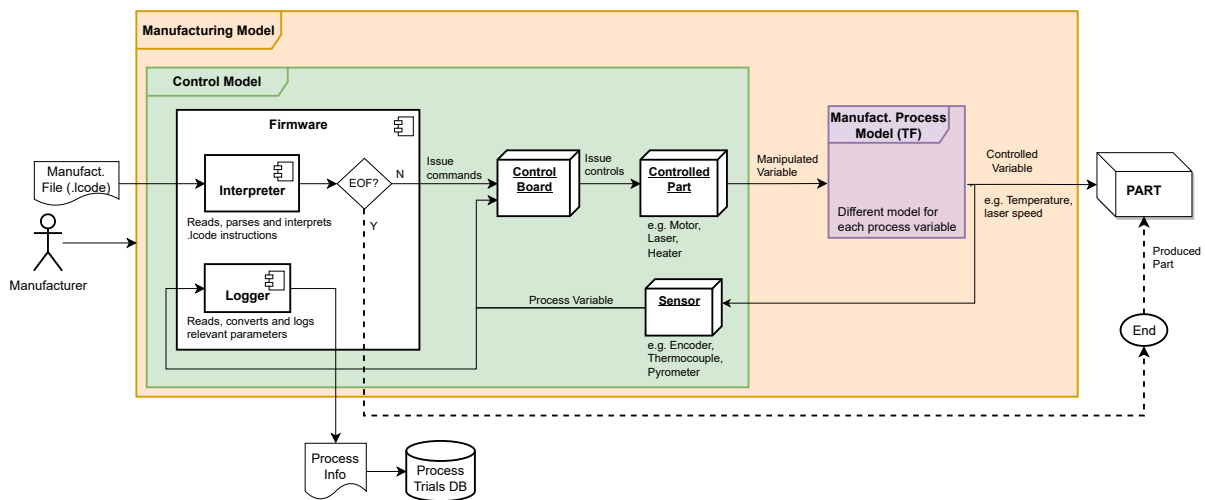


Figure 18: Model of manufacturing activity

3.2.3.4 Post-Manufacturing Model

The post-manufacturing stage (fig. 19) is arguably the most crucial phase in the manufacturing chain, yet often the most overlooked, as the quality analysis of the process and of the produced part are conducted in this phase, with the relevant outputs cascading to the preceding stages.

For instance, material and mechanical engineers can respectively perform the material analysis and mechanical behavior analysis of the produced parts, thereby increasing the material and mechanical properties databases.

The mechanical properties and material information aid the physicist in performing the physical analysis through simulation or modeling techniques, resulting in physical models that ultimately generate physical laws or theories, predicting what happens or proposing why it happens.

Another often neglected role in the manufacturing chain is that of the data scientist, who conducts process data analysis through one of two methods: [Design Of Experiments \(DOE\)](#) or [Artificial Intelligence \(AI\)](#). Analysing process data history via [DOE](#) enables the design of more effective and statistically relevant experiments, resulting in another iteration of the manufacturing phase; analysing via [AI](#) enables the recognition of data patterns, leading to empirical models that can generate empirical laws or theories, producing heuristics and guidelines that update the [Adviser](#) software component.

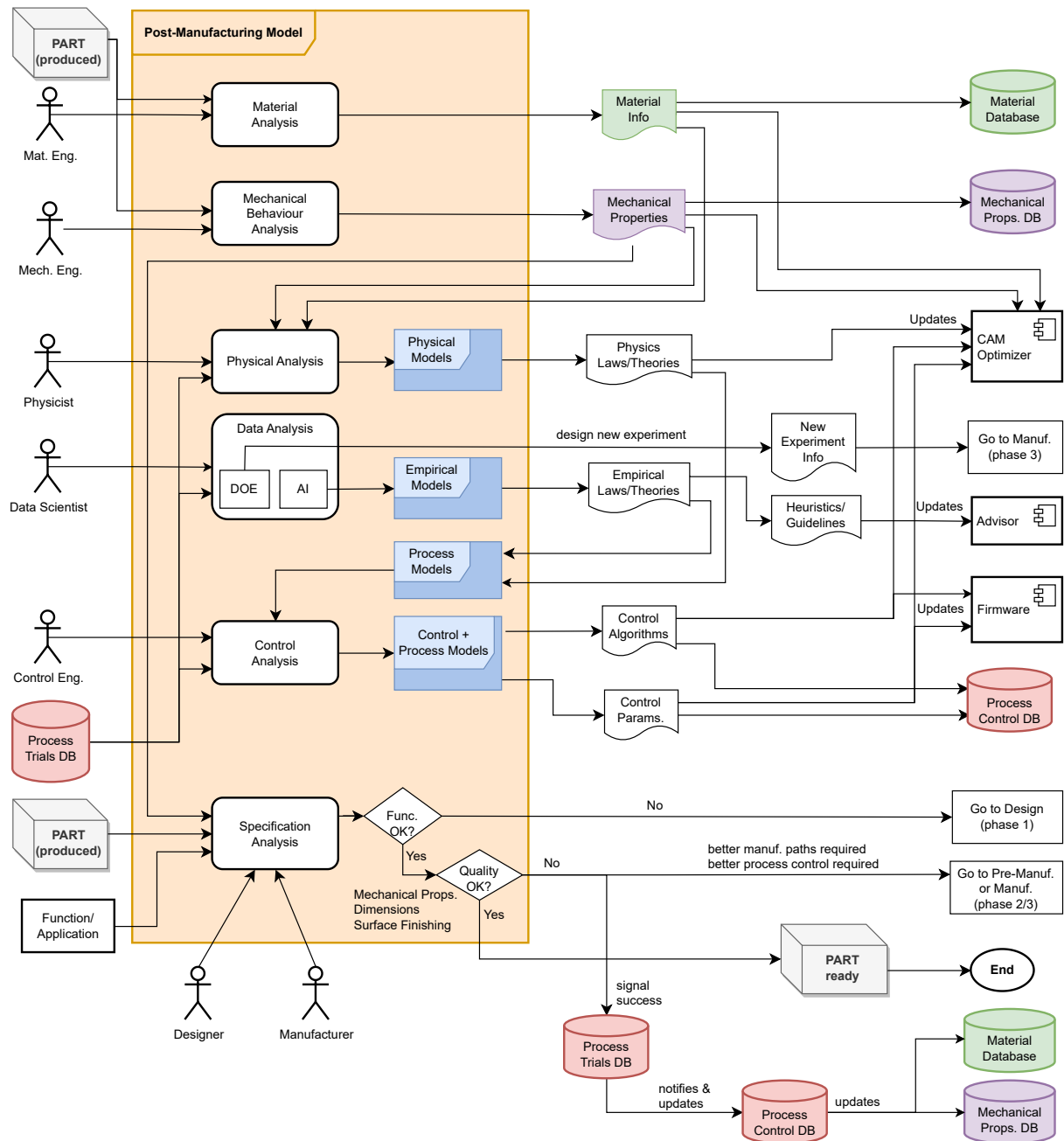


Figure 19: Model of post-manufacturing activity

The process models will then be generated from both physical and empirical laws/theories that together form the process trials data information, allowing the control engineer to conduct the control analysis. From this analysis stems an integrated model of the *control + process* combination, which yields control algorithms and parameters. Both these outputs are used to update the machine's firmware and are stored in the process control database. Additionally, they are also used, along with the material information, the mechanical properties, and physical laws/theories, to update the *CAM optimiser*.

Lastly, the designer and the manufacturer conduct the specification analysis, taking into account the compliance of the produced part and its mechanical properties with the function/application in question. If the function/application is not fulfilled, the design should be repeated. If the quality of the produced part, namely mechanical properties, dimensions, surface finishing, etc., is not obtained, better manufacturing paths or better process control may be required, leading to a new iteration starting at the pre-manufacturing or manufacturing phases.

This information should be properly debugged to be conveniently and correctly delivered to the appropriate agent: if the former is verified, this information should be conveyed to the mathematician for topology optimization; if the latter is true, the relevant information should be conveyed to all the agents responsible, directly or indirectly for the control, such as the physicist, data scientist, and control engineer. If the quality is according to the specifications, the result will be a produced part that is ready for service, and this trial should be signalled as successful, with the relevant information cascading to all databases for further improvement of all involved models.

The post-manufacturing model developed highlights the untapped potential in the manufacturing chain of 3DMMLPBF components. The structured data stemming from this model could be used to train the current cutting-edge neural networks in the search of better heuristics. This improvement can be particularly significant for the control models employed, given the highly intricate nature of the multi-physics problem. Moreover, with an adequate amount of data, notable advancements can be made without adding noticeable complexity.

3.3 Summary

The inherent complexity of multi-material fabrication drives away most commercial solutions, specially in the metallic and composite panorama due to the multi-physics problem associated to the project, the vast number of process parameters, and the lack of a global structure that supports the multi-material procesing development, worsened by its closed nature, hindering the technological advances in this area.

To address these challenges, this section proposes a global methodology for the 3DMMLPBF process. This methodology leverages the knowledge of the manufacturing process throughout the production chain, using a model-based approach to reduce the overall complexity to a more manageable level.

Further, the proposed methodology facilitates the derivation of a customized workflow that aligns with the project's constraints and resources, and supports the assembling of the necessary toolchain for the overall process. Additionally, it empowers the development of a low-cost 3DMMLPBF machine, allowing for subsequent testing and integration with the process's framework.

Development

In this chapter, the knowledge acquired through the relevant models contained in the proposed methodology is applied to the development of a specialised workflow for the 3DMMLPBF's process and respective toolchain, contingent of the project's restrictions and resources, and to the development of a machine capable of producing multi-material components from metallic/ceramic powders matching the designed workflow. The toolchain is assembled and the missing software components are developed, tested, and validated. Lastly, a custom equipment for the production of multi-material metallic and ceramic components was developed, tested and validated across the mechanical, electronic, and control domains.

4.1 Project methodologies

A foreword is required for the development methodologies and the sequence of development steps: for the software development – toolchain, machine's control and user interface – the waterfall methodology was used; for the mechanical and electronics development and integration the V's cycle was used as both systems' development needs to be done side-by-side.

Waterfall model The waterfall model is a simple and convenient method for the software development. It envisions the optimal method as a linear sequence of phases, starting from requirement elicitation to system testing and product shipment [162] with the process flowing from the top to the bottom, like a cascading waterfall.

In general, the phase sequence is as follows: analysis, design, implementation, verification and maintenance.

1. Firstly, the project requirements are elicited, identifying the key requirements and constraints the system being developed must meet from the end-user perspective, captured in natural language in a product requirements document.
2. In the analysis phase, the developer should convert the application level knowledge, enlisted as requirements, to the solution domain knowledge resulting in analysis models, schema and business rules.
3. In the design phase, a thorough specification is written allowing the transition to the implementation phase, yielding the decomposition in subsystems and the software architecture of the system.
4. In the implementation stage, the system is developed, following the specification, resulting in the source code.

5. Next, after system assembly and integration, a verification phase occurs and system tests are performed, with the systematic discovery and debugging of defects.
6. Lastly, the system becomes a product and, after deployment, the maintenance phase start, during the product life time.

While this cycle occurs, several transitions between multiple phases might happen, since an incomplete specification or new knowledge about the system, might result in the need to rethink the document.

Unified Modelling Language (UML) The [Unified Modeling Language \(UML\)](#) is a standard notation, widely used in the software industry, with high expressiveness, i.e., conveying complex ideas succinctly and precisely [161].

The goal of [UML](#) is to provide a standard notation with constructs for a broad range of systems and activities (e.g., distributed systems, analysis, system design, deployment). This means [UML](#) is not restricted to the software's world, but can also be used to model processes in other areas. For example, [UML](#) was used previously to develop the [3DMMLPBF](#) methodology's models.

System development focuses on three different models of the system [161]:

1. **The functional model:** represented in UML with use case diagrams, describes the functionality of the system from the user's point of view.
2. **The object model:** represented in UML with class diagrams, describes the structure of the system in terms of objects, attributes, associations, and operations.
3. **The dynamic model:** represented in UML with interaction diagrams, state-machine diagrams, and activity diagrams, describes the internal behaviour of the system.

Development methodology of mechatronics' systems – VDI 2206 The [Verein Deutscher Ingenieure \(VDI\)](#) ("German Engineers Association") 2206 guideline is a flexible procedural methodology for the development of mechatronics' systems. It aims to leverage the cross-domain synergy, characterised by two levels of design support [163]: micro-level, with a general problem-solving cycle; macro-level with a V-model cycle.

The V-model is useful for mechatronics' systems development, because it combines the top-down (system design) and bottom-up (system integration) approaches, and it enforces the need of permanent verification/validation between the requirements and the actual (virtual and/or real) system [163].

The V-model consists of the following stages: [163]:

- **Requirements:** Defined characteristics/features for the individual design task, representing at the same time the starting point in the design and the measure for the evaluation of the later product;
- **System design:** Definition of a cross-domain solution concept describing the essential features of the future product. The overall function of a system is divided into sub-functions with suitable working principles and/or solution elements assigned to them and the performance of the functions is evaluated in the overall system context.

- **Domain-specific design:** The solution concept — developed conjointly by the involved domains — is now detailed separately in the those domains, as specialised design and calculations are required to guarantee the functional performance, especially with the critical functions.
- **System integration:** The results from the specific domains are integrated synergistically to form the overall system.
- **Verification/Validation:** The solution concept is compared to the requirements to assure the actual system characteristics are verified (the product matches the specifications) and validated (the product is suitable for its intended use).
- **Modelling and model analysis:** The described phases are flanked by the modelling and analysis of the system characteristics by modelling and simulating its behaviour using computer-aided tools.
- **Product:** Result of a successful macro-cycle. This does not mean its the final product, but the ongoing concretion of the future product (product maturity).

A complex mechatronic product will typically not be finished within one macro-cycle, requiring several iterations.

4.2 Application of the methodology to multi-material 3DMMLPBF

The proposed methodology is complex and extensive, and therefore needs to be implemented by stages, where only the most essential features are considered in each development phase, being intensively tested before the integration in the framework. Furthermore, the manufacturing process chosen for the multi-material fabrication of tridimensional metallic and composite parts is the [L-PBF](#).

Thus, a simplified workflow for this process is proposed (Fig. 20) as a means to: produce customised 3D multi-material parts with freedom of shape and process control; test the proposed methodology; increase the process's knowledge; quickly iterate over the manufacturing chain with different part's design and different processing solutions, as will be detailed further ahead. This workflow, together with the methodology proposed, paved the way for the correct development and deployment of both software and hardware (mechanical/electronic) components.

The workflow — named *3DMMLPBF-C2P (CAD to Process)* — integrates the design model, pre-manufacturing model without the [CAE](#) and [CAM](#) optimisation steps, manufacturing model and post-manufacturing model, respectively. The workflow is divided in three phases:

- **Pre-manufacturing:** component design and manufacturing file's generation;
- **Manufacturing:** manufacturing file processing and process monitoring and logging;
- **Post-manufacturing:** collection of pre-manufacturing, manufacturing and post-manufacturing data, concerning the 3D and manufacturing models, the process information, materials, and mechanical tests performed for future analysis, process improvement, and bootstrapping.

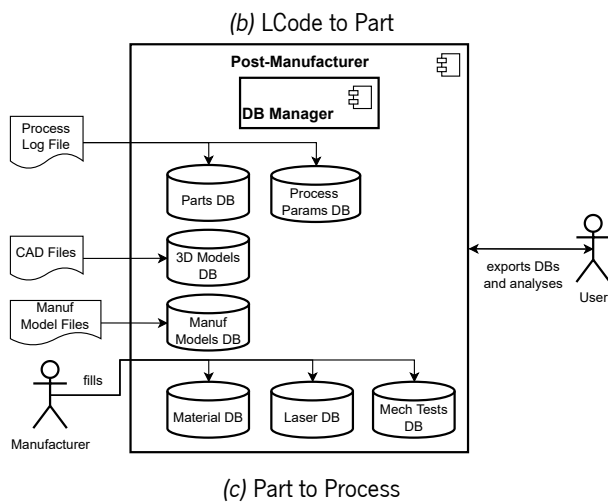
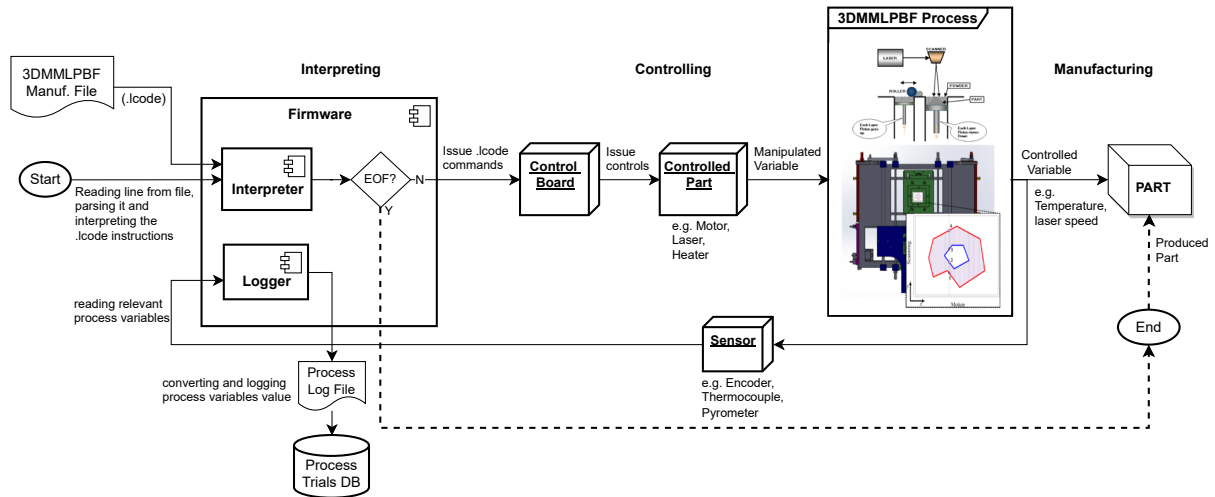
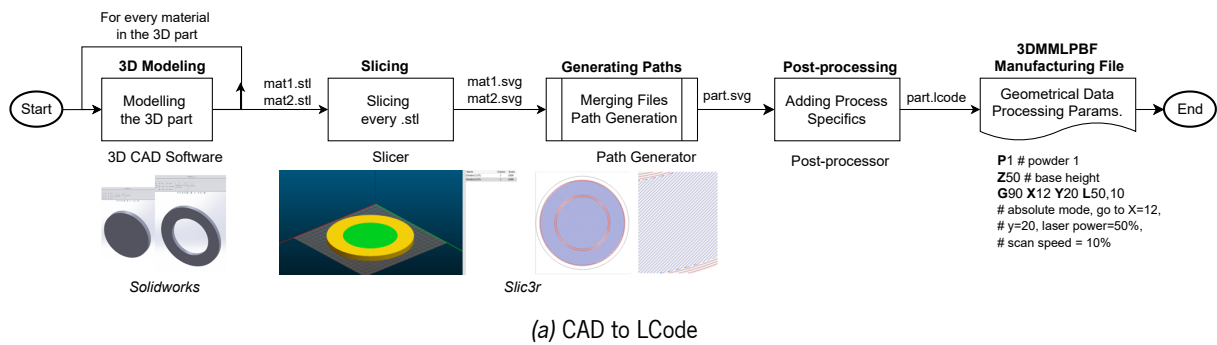


Figure 20: Workflow 3DMMLPBF-C2P (CAD to Process)

4.2.1 Pre-manufacturing: CAD to LCode

Fig. 20a illustrates the pre-manufacturing stage, whose goal is the generation of the file containing the manufacturing instructions. Each material of the 3D model is modelled individually, in a common 3D CAD modelling software (e.g. SolidWorks), and a tessellation file of the surface is produced, containing the geometric information. In this initial stage, the 3D model is considered to have no holes, porosity or discontinuities, as this would invalidate the usage of the surface tessellation, i.e., the multi-material modelled parts are considered to be completely filled in.

The next phases – *Slicing and Path Generation* – consists in the cross-sectioning of the 3D model and the path

generation (infilling) of each cross-section. The output of these phases is a [Scalable Vector Graphics \(SVG\)](#) file; the choice of this file format is due to the use of markup language, namely [XML](#), for describing two-dimensional vector and mixed vector/raster graphics [164]. This allows the conveying of extra information besides the geometry, that can be packed in a structure node, for example line colour attribute to represent different materials, addressing the multi-material representation ambiguity. This strategy is already applied to other types of 3D printers which require each layer to be represented as image, for example [Digital Light Processing \(DLP\)](#) resin or powder-bed printers [165]. Additionally, because [SVG](#) is a vector format, any scaling transformation is simple. Listing 4.1 illustrates an example of the `.svg` syntax.

Regarding the pre-manufacturing's logic, each material is sliced in layers and output as a [SVG](#) file. Then the files are combined for each layer and the scan paths are generated, yielding a complete [SVG](#) file of the part.

Listing 4.1: SVG syntax example

```

1 <svg width="200" height="200" xmlns="http://www.w3.org/2000/svg">
2   <path d="M10 10"/>
3   <circle cx="10" cy="10" r="2" fill="red"/>
4 </svg>

```

This file, containing the geometry information pertaining to the scan paths, will be post-processed to add the process relevant parameters, like material and process parameters with the former being pulled from the material database and the latter being defined by the end-user. The result will be a file (`.lcode`) containing the manufacturing instructions for the 3DMMLPBF process with the geometrical data and process parameters. An extract sample is provided in 20, illustrating the tokens used:

- P1: Powder 1
- Z50: base height
- G90 X12 Y20 L50,10: absolute mode, go to X=12, Y=20, with laser power at 50% and scan speed at 10%.

4.2.2 Manufacturing: LCode to Part

Fig. 20b illustrates the manufacturing stage, whose goal is the processing of the file containing the manufacturing instructions. This file will be read line-by-line, parsed and interpreted, issuing commands to the control board based on the `lcode` instructions of the file. The remainder of the operation – controlling and manufacturing – is similar to the one described in the manufacturing model (Section 3.2.3.4), with the controlled part inducing an effect in the 3DMMLPBF process and the controlled variable that affects the manufactured part being measured and logged by the logger software component to a process log file, which is stored in the process trials database. When the *End-of-File* is reached, the process terminates and the part is manufactured.

This workflow represents the typical one for the 3DMMLPBF manufacturing process. However, due to the closed nature of the proprietary software of the available CO₂, Nd-YAG and fiber lasers, the workflow cannot be directly implemented. In the future, the control software for the lasers will be implemented and integrated in the 3DMMLPBF machine, but for now a workaround was used.

This workaround consists in separating the geometric data from the process data at the post-processing stage and assigning it, respectively, to the laser and the 3DMMLPBF machine. The processing parameters of the laser

are encoded in the SVG file as line attributes that the laser software is able to recognise and use for the scan paths marking.

Fig. 21 illustrates the architecture of this solution with the representation of the data streams, the software components that use those streams, the hardware nodes where the software components are assigned and the protocols under which they communicate, namely serial communication for laser and 3DMMLPBF machine synchronisation.

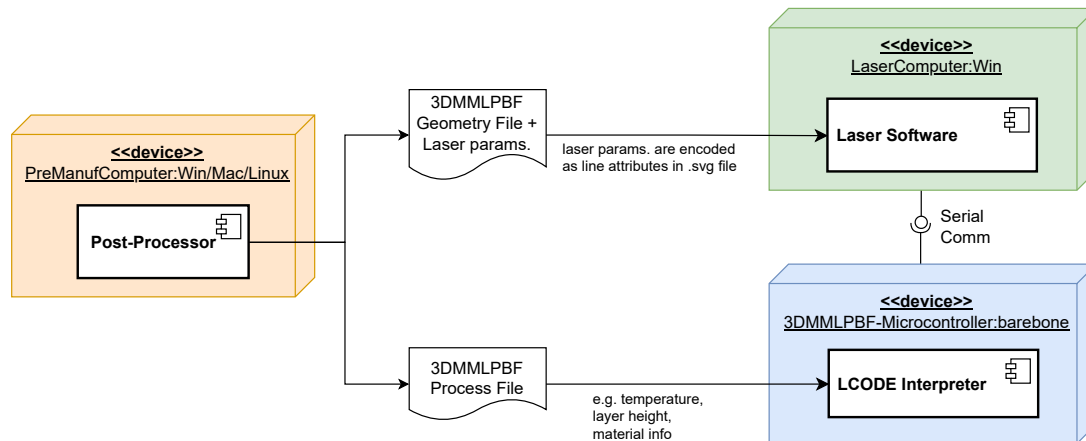


Figure 21: Workaround for the proposed workflow: two separate data files — geometry and process — are used by the laser software and LCODE interpreter for scanning paths marking and process related tasks, respectively

4.2.3 Post-Manufacturing: Part to Process

Fig. 20c illustrates the post-manufacturing stage, whose goal is the collection of all of the data relevant to the overall process, for future analysis, and process improvement and bootstrapping.

The data collection is semi-automatic: several files can be imported by the Post-Manufacturer software; other data must be filled in by the Manufacturer, namely materials, laser information (manufacturer, power, etc.), and the mechanical tests performed. The process log file will add information to the Parts and Process Params databases, the CAD files to the 3D Models database, and the manufacturing files to the Manuf Files database.

The Post-Manufacturer contains a database manager, responsible for storage and retrieval of all the data. The User represents all of the manufacturing agents and should be able to export the database and analyse the desired data, whether it is a small part or all of it.

4.3 Toolchain

The toolchain development comprises the following components from the 3DMMLPBF-C2P workflow:

- **Pre-Manufacturer:** Slicer + Path generator
- **Manufacturer:** Post-processor + Printer
- **Post-Manufacturer**

4.3.1 Pre-Manufacturer

The *Pre-Manufacturer* term is loosely used here as it doesn't contemplate the 3D modelling stage. Instead, it uses the 3D models for each material as inputs, yielding the geometric and topological data required for manufacturing, i.e., the scanning paths with custom annotations.

4.3.1.1 Requirements & Constraints

The main requirements for the *Pre-Manufacturer* software are:

- Loading and visualization of 3D models geometry of each material
- Configuration of the main slicing and path generation parameters, most notably: layer height, path type, path width, path density, and path angle. Also, the `User` should be able to configure different path attributes for each of the model being processed, or generically to all models.
- Slicing and path generation
- Visualisation of slicing and path generation results
- Generation of the manufacturing file

On the hand, the main constraints are:

- Only `STL` files are supported as input
- Only `SVG` files are supported as output
- Limited time: developing a slicer and path generator from scratch is a labour-intensive task

4.3.1.2 Analysis

For the first iteration of the *Pre-Manufacturer*, *Slic3r* was used as a starting point to bootstrap the development. *Slic3r* [165] was created in 2011 within the RepRap community by Alessandro Ranellucci and consists mainly of an open-source toolpath generator for 3D printers with high configurability: it reads 3D models (`STL`, `OBJ`, `AMF`, `3MF`) and it converts them into G-Code instructions for 3D printers. It served as a platform for experimenting several new ideas that later became technology standards, such as multiple extruders, brim, variable-height layers, per-object settings, modifiers, post-processing scripts, G-code macros, etc. [166].

One pivotal idea around the choice of *Slic3r* is that the slicing and path generation used for 3D printers should be similar to the ones used for `3DMMLPBF` manufacturing, with adequate tweaking of the processing parameters.

Its main features are [166]:

- G-code generation for `FFF/FDM` printers;
- conversion between `STL`, `OBJ`, `AMF`, `3MF` and `Persistence Of Vision (POV)` formats;
- auto-repair of non-manifold meshes (and ability to re-export them);
- `SVG` export of slices;

- built-in [Universal Serial Bus \(USB\)](#)/serial host controller, supporting multiple simultaneous printers each one with a spool queue;
- OctoPrint integration (send to printer);
- built-in projector and host for [DLP](#) printers;

The core parts of *Slic3r* are written in C++11, with multithreading with two main code base paths:

- *C++11 + Perl*: includes the core (C++11) and a high-layer abstraction to support the [Graphical User Interface \(GUI\)](#), with *WxWidgets* support.
- *C++11 only*: includes the core (C++11) and a Command Line Interface written in C++11 also, with a fairly small subset of the functionalities.

Some notes are in place:

- The main features provided correspond to the *C++ + Perl* path, with most of these being available in the command line interface.
- *Slic3r*, by default, only allows SVG export of slices, and not of the toolpaths.
- Model merging and arrangement in the building plate is supported only in the *C++ + perl* path, which is strongly discouraged for new developments.

Thus, the C++ path was chosen, but it requires the implementation of new functionalities, namely the [SVG](#) export of the toolpaths after slicing with model merging (corresponding to different materials), and the ability to generate custom tags as required by the workflow.

Next, the *Pre-Manufacturer's* use cases were outlined to specify the required functionalities in more detail (Fig. 22), and categorized:

- **Inputs:** The *User* can add, remove or manipulate the rendered [STL](#) 3D model in the canvas. Additionally, the *User* should be able to check if the resulting 3D model is contained within the machine-specific manufacturing bounding volume, i.e., if its dimensions do not exceed the manufacturing capabilities.
- **Processing:** The *User* can load and save the configuration file, used to setup the slicer and path generation parameters, such as: layer height, path type, path width, path angle, and path density. The *User* must be able to process the [STLs](#) models, i.e., slice them, generate the manufacturing paths, and merge them into a single manufacturing model.
- **Outputs:** The *User* can generate the manufacturing model — [SVG](#) file — and visualise it in the canvas to validate the processing.
- **Miscellaneous:** The *User* can obtain help on the interface usage, and on the slicer and path generation configuration.

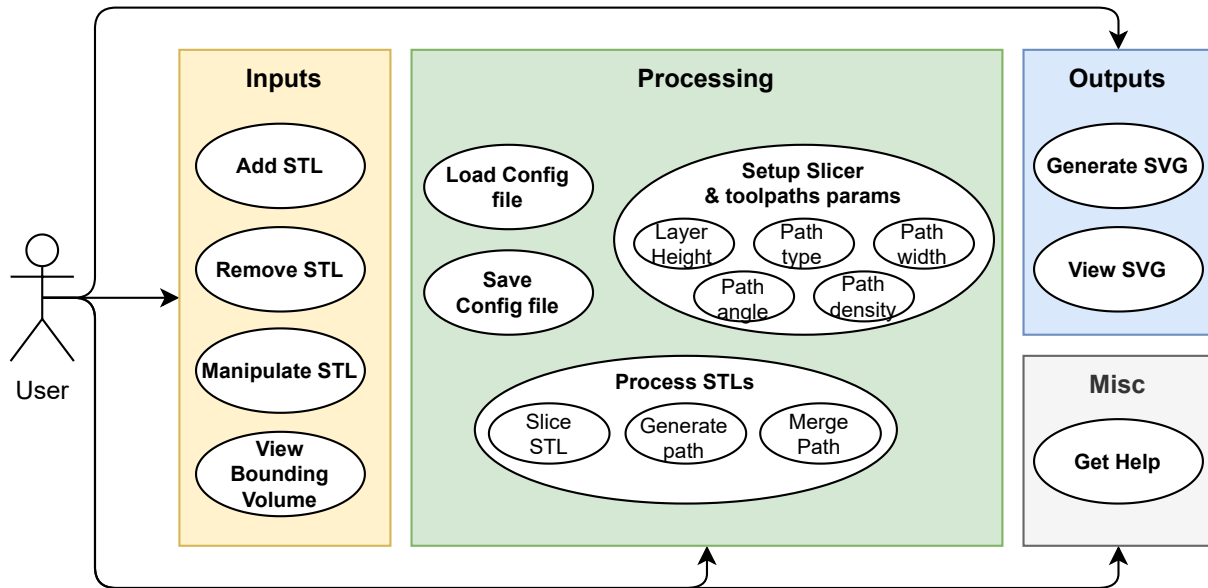


Figure 22: Pre-Manufacturer analysis: use cases

The slicing and path generation is critical for the pre-manufacturing stage, especially for multi-material fabrication, thus, it was analysed in more depth (see Fig. 23). The *STL* models are loaded into canvas, retaining their relative positions, and processed in parallel. In this split phase, the slices coordinates are calculated individually for each model, and then the slices are checked to see if they intersect other models, which then appends them to the other models' slices. The slicing and the path generation utilise the *User* defined parameters for each model. In the slicing, the *STL* model is cross-sectioned in a predefined direction (z-axis, in this case), yielding the intersection contours. This is possible because the *STL* model contains the tessellation information as triplets of points and the facet normal which indicates the surface orientation (inwards or outwards). Then, the contours are filled according to a given rule which determines how points from the contours are connected between them, i.e., the tool path is generated. Lastly, the filled sections of each model are combined together, sorting them by z-coordinate to produce a complete multi-material manufacturing model.

4.3.1.3 Design

After refining the use cases and exploring the flow of events through them, the system architecture was devised, illustrated in Fig. 24:

- **User interface:** This outer layer constitutes the front-end of the application and is responsible for handling all user interaction through the *UI Engine*.
- **Inputs:** Two software components are required to handle the inputs – the *STL Reader* and the *STL Renderer*. The former parses and loads the *STL* model into the memory, and the latter renders it on screen.
- **Processing:** In this layer the *User* configures and runs the processing, which can be enabled at a specific-level (model-based) or generically (applied to all models). The slicing and path generation is provided by

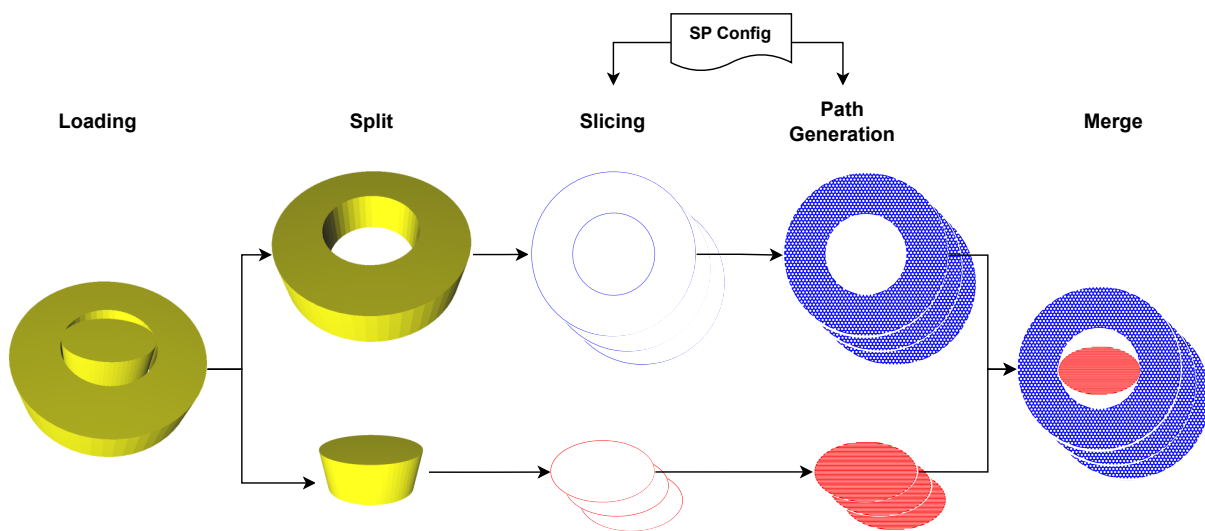


Figure 23: Pre-Manufacturer analysis: Slicing and path generation overview

the core `Slic3r` which is then wrapped as a library (for runtime execution) or as a package (to add new functionalities, like a new path type). The configuration is managed by the `SP Config` component. After slicing and generating the paths, these are merged into a single model by the `Path Merger` component through tag annotation.

- **Outputs:** The `SVG Exporter` and `SVG Renderer`, respectively, export and render the manufacturing model into the screen.

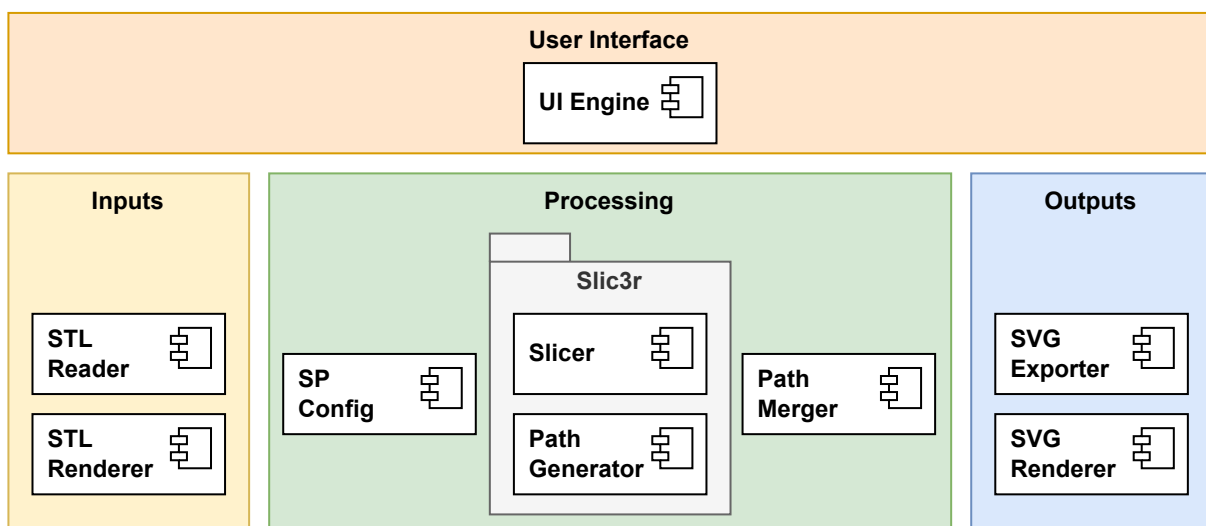


Figure 24: Pre-Manufacturer design: system architecture

Following the devised system architecture, the sequence diagrams were designed to capture the flow of events throughout the software execution as a response to an use case triggering. Then, the class diagrams were devised, constituting the blueprints for implementation.

4.3.1.4 Implementation

The *Pre-Manufacturer* was implemented in C++11 using the Qt framework for the [User Interface \(UI\)](#) development.

Firstly, a bug was fixed and patched in the slicing algorithm of Slic3r, namely `infill extrusion width` was ill-defined, causing the minimum filling spacing to be 0, yielding program crashes and floating-point exceptions thrown. A bug report, together with a pull-request for a fix, was issued to the upstream repository — Slic3r — and successfully merged.

The merging of the models was implemented by pushing them into a container after slicing and sorting the layers by z value. Furthermore, the exporting was subdivided in header, footer and body, with the former being performed for the largest, and the latter all layers consecutively.

The preservation of models' coordinates was accomplished in the similar manner, calculating the models' coordinates as relative to the one with the largest bounding box.

For the toolpaths export and custom tagging, a new function was created, which builds the toolpaths from polylines tags, as a replacement for the previous implementation, which used `<path d= M ... z>` and specific tokens to start and close the path, namely M and z[167].

Also, for custom tagging it were included the following tags to specify important information both to *EzCAD* software and for post-processor, namely:

- `id`: based on the following naming structure — `l#_m#_h#`, where `l`, `m`, and `h`, represent the layer's ID, material and height, respectively;
- `slic3r:z`: layer's z-value (absolute)
- `slic3r:slice-z`: layer's slicing z-value — height where the slicing is performed.
- `slic3r:mat`: material index
- `slic3r:layer-height`: layer's height
- `polyline points`: path trajectory points
- `style`: contains the meta information about the path's filling, such as colour, width, and type.

An example of the syntax of the `.svg` output file is presented in listing 4.2.

Listing 4.2: Custom syntax example

```

1 <g id="l0_m1_h350" slic3r:z="0.3500" slic3r:slice-z="0.1750" slic3r:layer-height="0.3500" slic3r:mat=
  "1">
2 <polyline points= "... " style="fill: none; stroke: white; stroke-width: 0.1; fill-type: evenodd"
  slic3r:type="internal-infill" />

```

Fig. 25 through Fig. 27 illustrate the *Pre-Manufacturer* application's implementation outcome. The STLs models are successfully added, loaded and rendered in the canvas, with the enclosing bounding volume represented in black (Fig. 25). The slicing and path configuration can be used generically — same parameters for all models — or specifically — different parameters for each model (Fig. 26). This is also an improvement over the Slic3r's existing codebase. Lastly, it can be asserted that the manufacturing file is successfully generated and rendered in the canvas (Fig. 27). Additionally, the geometry and statistics of each layer can be visualised.

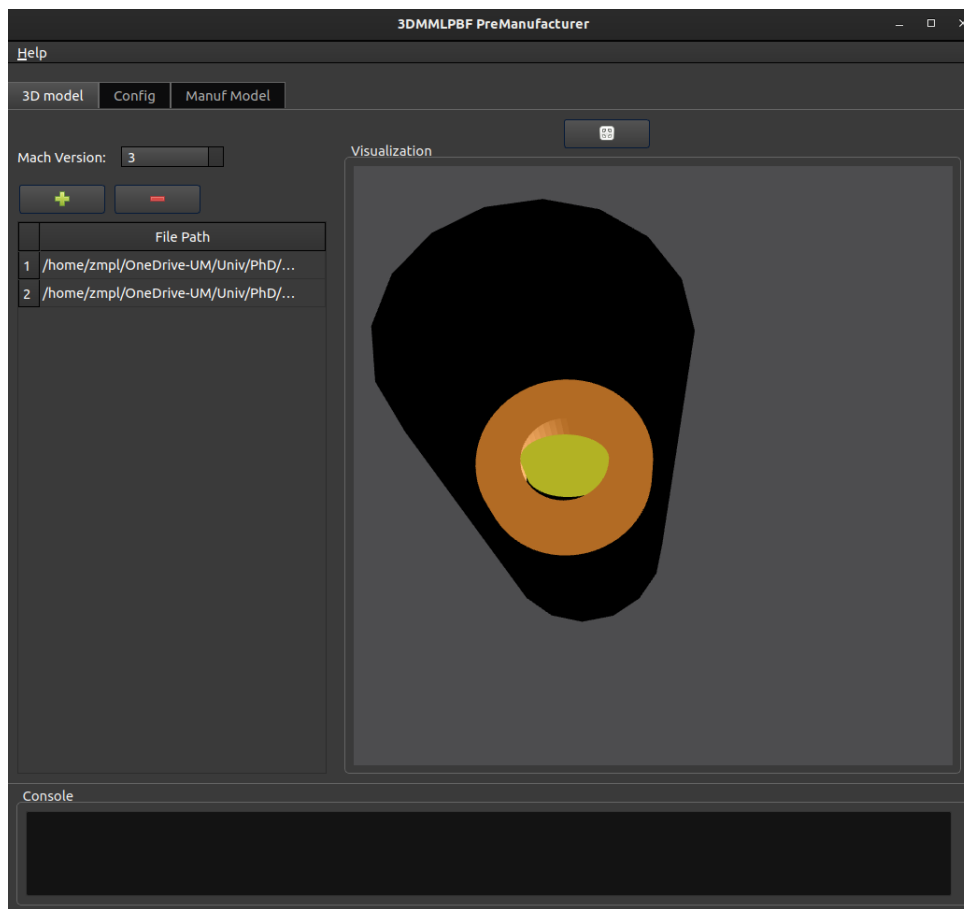


Figure 25: Pre-Manufacturer implementation: 3D models loading and rendering

Looking into the configuration modes in more depth, the User can select between a generic configuration (Fig. 26) — provided by the configuration file — or a specific configuration — supporting different path attributes for each of the model being processed (Fig. 28). Fig. 28a shows the slicing and path generation parameters for each of the models, namely, different fill angles, fill densities, fill patterns and infill extrusion widths. The results are shown in Fig. 28b and Fig. 28c, where it can be clearly seen that the different parameters were applied individually to each input model.

4.3.1.5 Testing and Validation

The required features were successfully implemented. However, further testing and analysis is required to validate the Premanufacturer's SW application, namely, regarding compatibility with the workflow, the suitability of the path topologies generated, its behaviour with different input models, and the computational resources used.

Compatibility between manufacturing file and workflow To validate the compatibility of the manufacturing file with the downstream workflow, the output file was imported to the EzCAD software — the native software for laser engraving and marking (Fig. 29). It can be seen that now layers contain the toolpath information with preservation of coordinates and that this file can be successfully imported by EzCAD preserving the layer naming scheme and geometrical data.

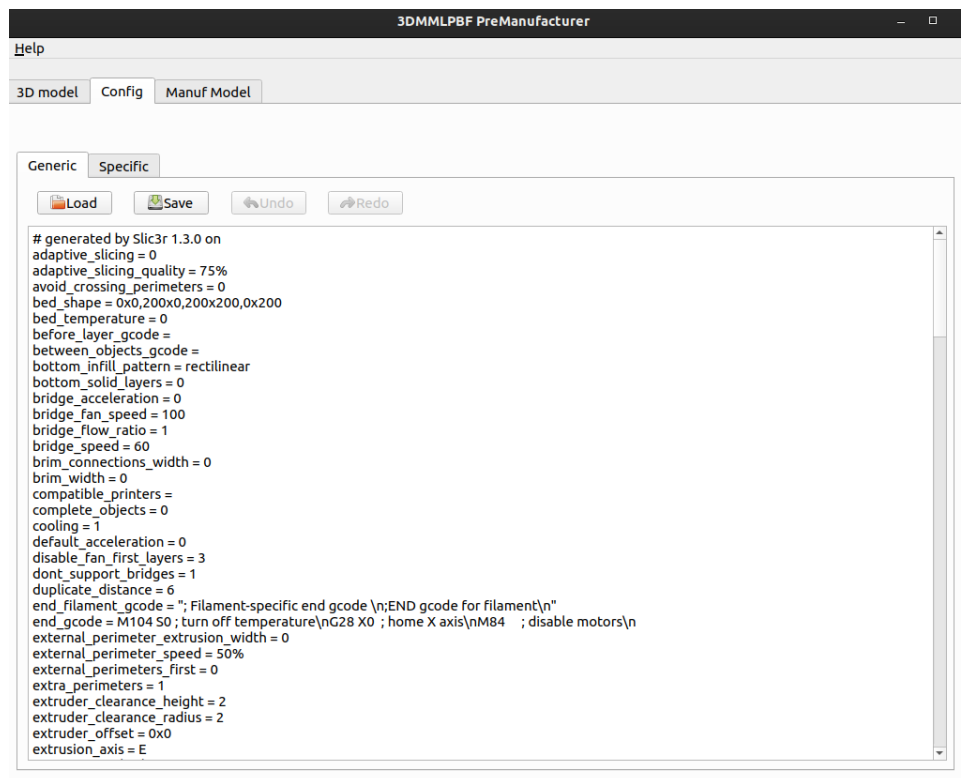


Figure 26: Pre-Manufacturer implementation: Slicing and path generation configuration

Suitability of the path topologies As aforementioned, the slicer and path generator library used is based on 3D printing. Thus, it is necessary to understand if the paths generated can be applied to the 3DMMLPBF process.

The slicer supports different path topologies, namely:

- **Rectilinear:** rectilinear, aligned rectilinear, grid, triangles, stars, and cubic;
- **Planar:** archimedean chords, Hilbert curve, and octagram spiral;
- **Honeycomb:** honeycomb, and 3D honeycomb;
- **Others:** concentric, and gyroid

The `.stl` input models used for the testing were: `mod1.stl` – a torus, simply called a *ring*; `mod2.stl` – a disk (see fig. 30). These models aim to represent two different materials and the simplest of the cases of multi-material processing: filled and unfilled regions without overlapping, but close enough that the bonding can occur via welding.

As a common denominator between the tests, the following main parameters were fixed (see Table 3): fill angle, fill density and infill extrusion width. Fig. 31 lists the different topologies, showcasing that the slicer + path generator is able to generate the different topologies for multi-material components.

Table 3: Path topology main fixed parameters

fill angle	fill density	infill extrusion width
45°	15 %	0.1 mm

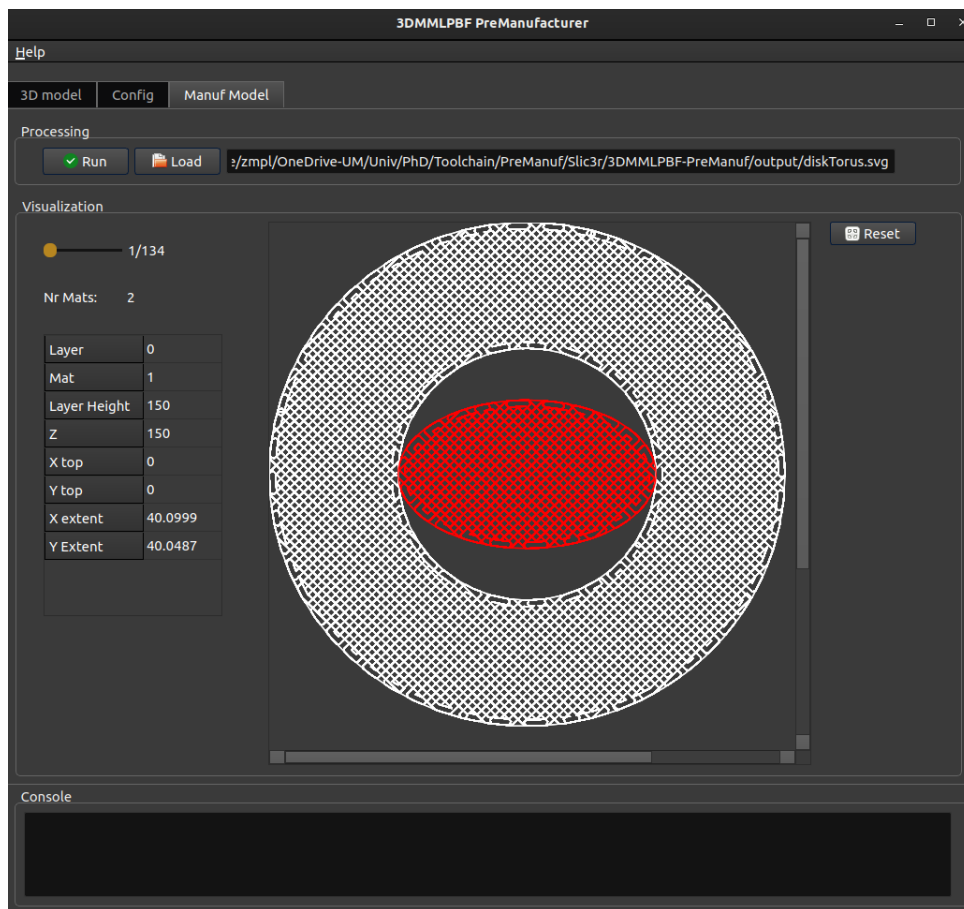


Figure 27: Pre-Manufacturer implementation: Manufacturing model generation and visualisation

To test the path generation parameters the same 3D models were used and the path topology selected was the rectilinear one. Only one material is shown, as the slicing and path generation for multi material was previously validated. The following parameters were varied: fill angle, fill density, infill extrusion width.

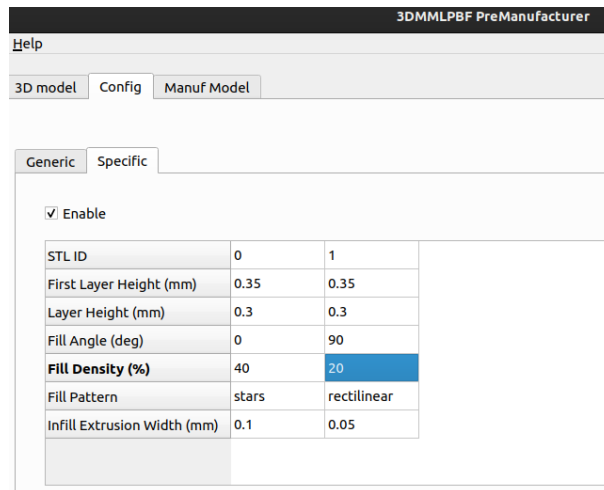
Fig. 32 shows the successful variation of the fill angle from 0 to 90 degrees, which can be used to target different thermal affected regions of the component.

Fig. 33 illustrates the fill density's variation from 1% to 40%. For very low fill densities, e.g. 1–5%, the slice is only partially filled; increasing the fill density from 20 to 40%, the slice is almost completely filled. These higher fill densities (40% for the models in analysis) can be helpful in enabling the porting of the 3D printing path topologies to L-PBF ones, as the reduced distance between fillings (fill spacing) helps to promote powder melting in small gaps.

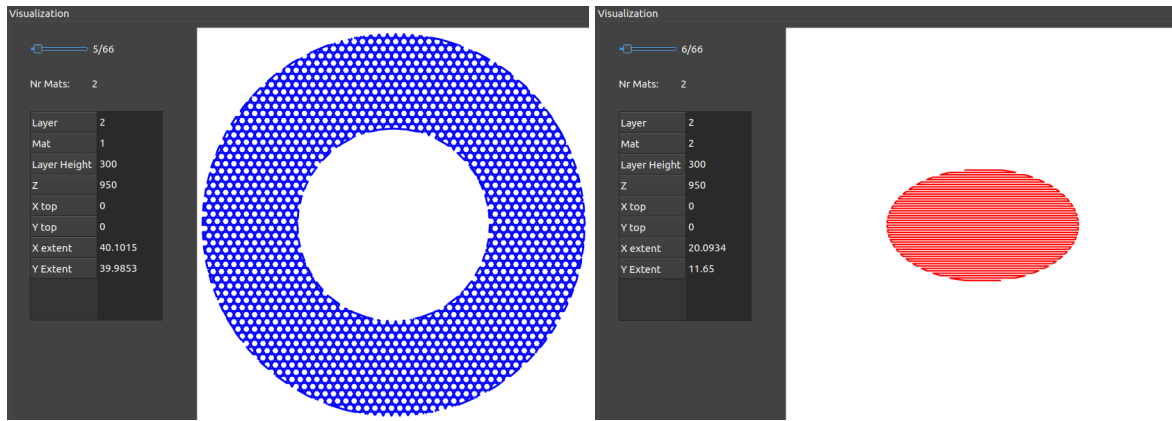
Fig. 34 illustrates the variation of the infill extrusion width from 0.01 to 0.5 millimetres. For very low extrusion widths, e.g. 0.01–0.02 mm, the slice is almost completely filled, which can be beneficial for L-PBF paths. For higher infill extrusions widths, e.g. 0.5 mm, the part is only partially filled.

Although related, fill density and infill extrusion width are conceptually different: infill extrusion width is the filling width, which can be lowered to mimic the laser marking path width; fill density is the amount of filling paths per slice's area.

After the assessment and analysis of the path topologies for 3D printing and its main parameters, one must address its shortcomings when applied to the L-PBF process:



(a) Slicing and path generation configuration for each model



(b) Model 1

(c) Model 2

Figure 28: Pre-Manufacturer implementation: Slicing and path generation specific configuration

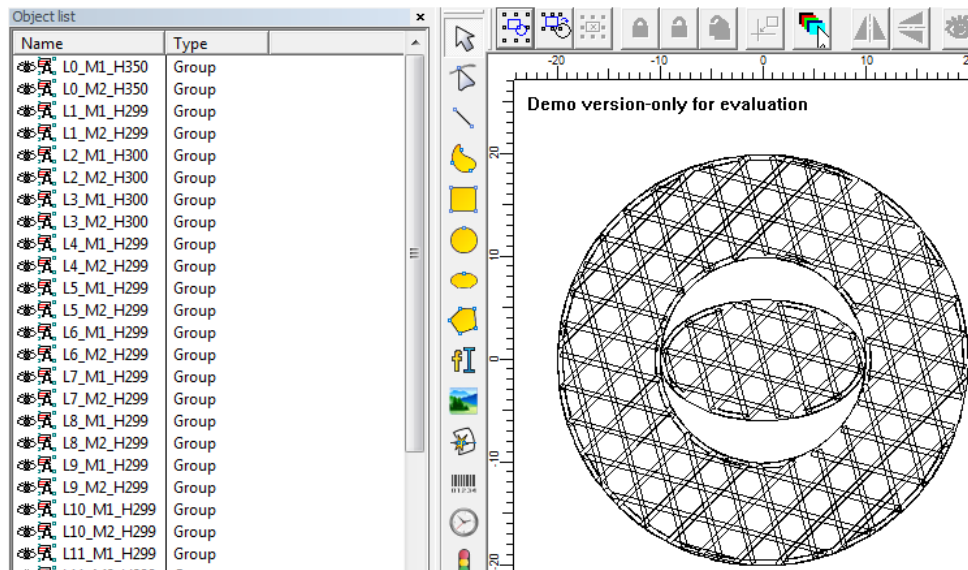


Figure 29: Manufacturing file is successfully loaded by EzCAD software

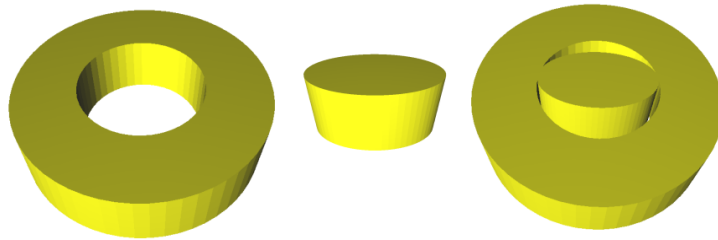


Figure 30: Input .stl models: mod1.stl (left); mod2.stl (centre); assembled (right)

1. The path generation with SVG export is based on the Stereolithography (SLA) technology. Thus, the bottom and top layers are not filled – only contours show up (see Fig. 35a). Also, intermediate layers only have filling – they lack perimeters (see Fig. 35b). Both these aspects are critical for L-PBF trajectories.
2. The filling has bridges between endpoints, i.e., the trajectory is fully connected (see Fig. 35b). However, common laser paths are not connected.
3. Filling has width (internal extrusion width) (see Fig. 35b). This causes the laser paths to be doubled, because it uses the external perimeters of the infill to set the trajectory.
4. 3D printing filling paths aim to minimise the travel distance of the extruder, while the laser paths may require a different manufacturing order: e.g., paths always starting from the leftmost intersection points and reaching the rightmost ones.

Some patches were applied to solve these issues (see Fig. 36). A configuration option was added to allow the User to choose between connected and disjoint paths (Fig. 36a). The results are yielded in Fig. 36b and Fig. 36c. It can be seen that the top layer is now filled with a disjoint path and for other material with a connected path and with perimeters. Furthermore, because the paths can be disjoint, they can be used with a specific orientation in mind, i.e., systematically starting from left and going to right. Finally, and although not optimal, the filling width can be reduced to match the manufacturing requirements. Hence, the modified path topologies can be applied to the 3DMMLPBF's process.

Input models It is important to assess the *Pre-Manufacturer's* behaviour when processing different input models:

- *Cross and cube*: a bi-material component with an internal cavity belonging to one material and the external component to another; this is a good example of a multi-material component that is only feasible via additive manufacturing (Fig. 37a);
- *3 cubes*: a three material component, with each cube being enclosed by an outer one. Once again, this a typical example of a component only feasible using AM (Fig. 38a).

Furthermore, the integrity of the .stl file format produced and the agnostic behaviour of the slicer and path generator in respect of the inputs was tested by using a different 3D CAD modelling tool – FreeCAD – an open source 3D parametric modeller [168], as well as Solidworks.

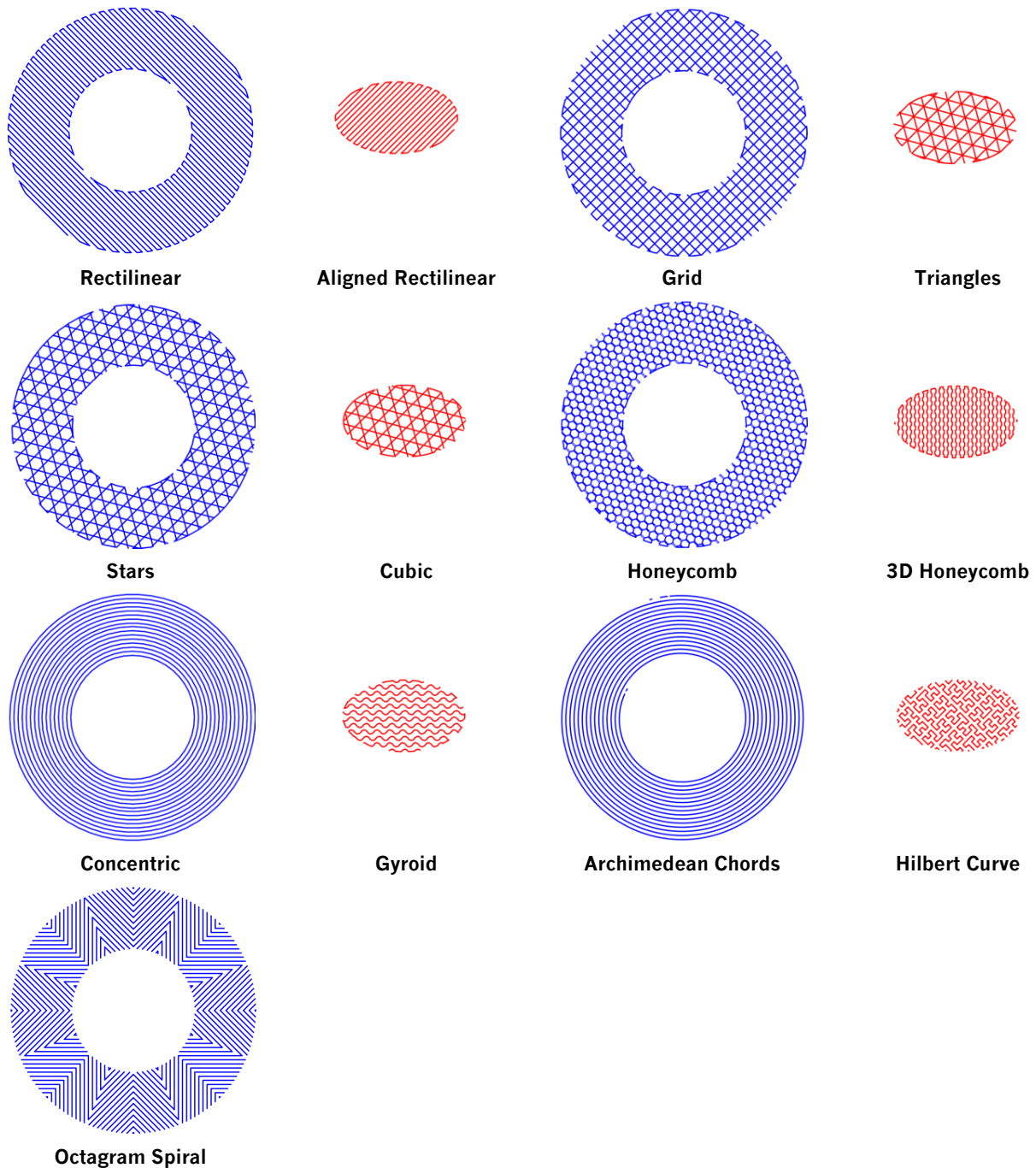


Figure 31: Path topologies list and examples

Cross and Cube Fig. 37a illustrates the cross and cube 3D model. The component was exported as two .stl files corresponding to each material and loaded into the Pre-Manufacturer, for slicing and path generation, using the default values (see Fig. 37b). Fig. 37 shows the results, with both sub-components being sliced and filled with the rectilinear pattern in consecutive layers and for different materials (Fig. 37d and Fig. 37e). Thus, the slicer and path generator performs well with a different input model and is agnostic about the origin of the .stl input files.

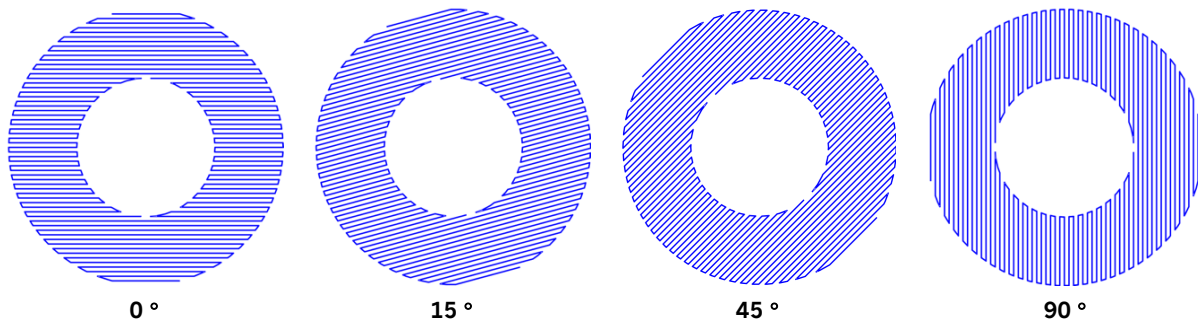


Figure 32: Fill angle test: 0° to 90°

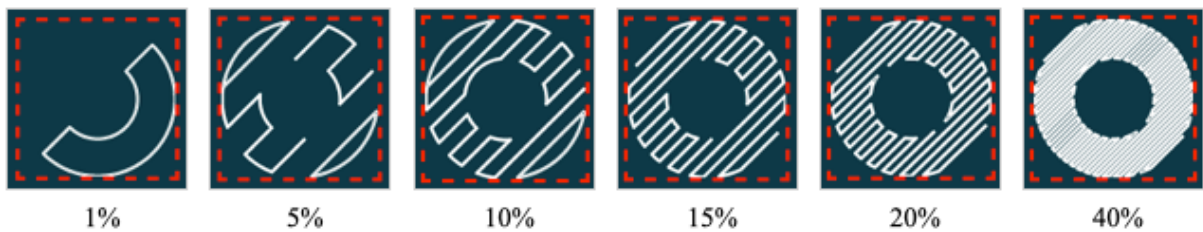


Figure 33: Fill density test: 1% to 40%

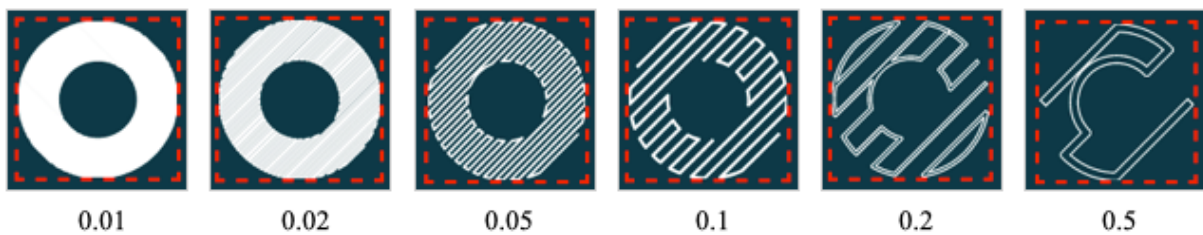
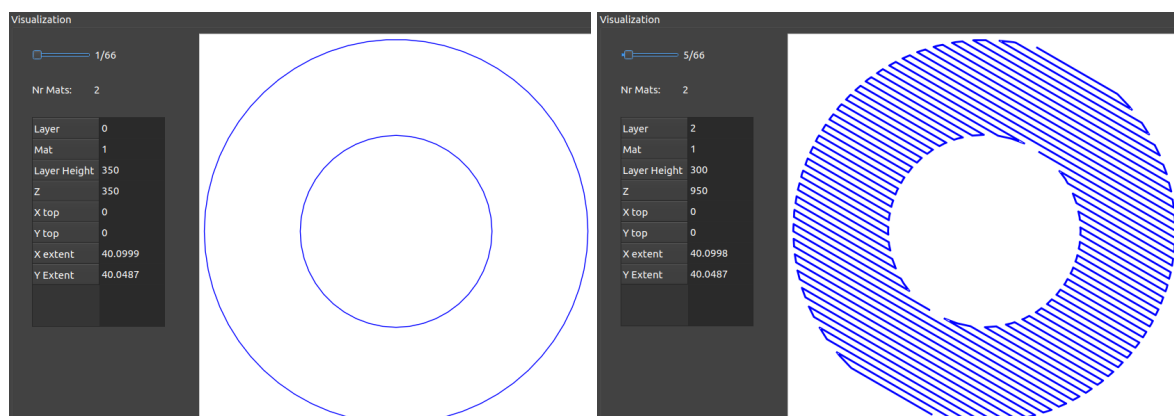


Figure 34: Infill extrusion width test: 0.01–0.5 mm



(a) Top layer is not filled

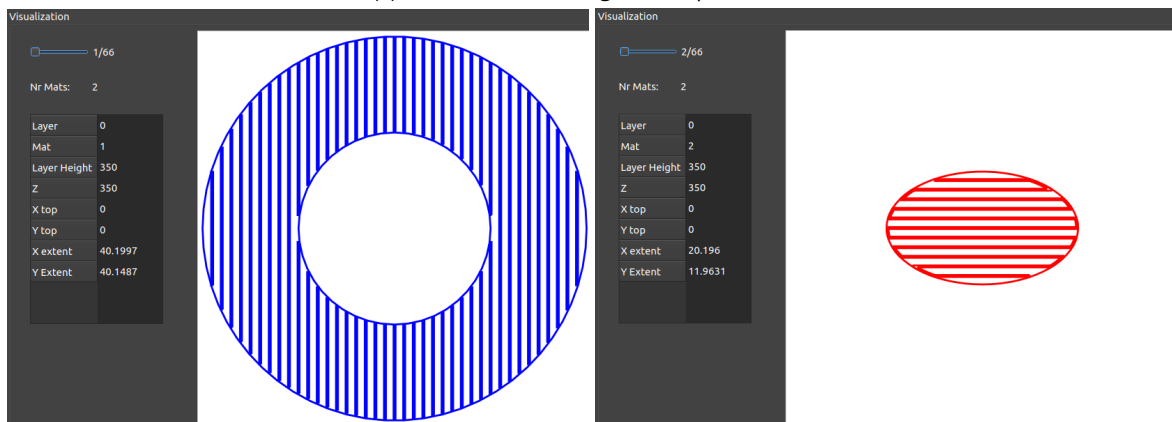
(b) Intermediate layers lack perimeters, they are fully connected and have width

Figure 35: Shortcomings of 3D Printing paths

3 Cubes Fig. 38a illustrates the *3 cubes* 3D model. The component was exported as three *.stl* files corresponding to each material and loaded into the *Pre-Manufacturer* for slicing and path generation (see Fig 38b). Fig.38 shows the results, with all sub-components being sliced and filled with the rectilinear pattern in

Generic		Specific
<input checked="" type="checkbox"/> Enable		
STL ID	0	1
First Layer Height (mm)	0.35	0.35
Layer Height (mm)	0.3	0.3
Fill Angle (deg)	0	90
Fill Density (%)	20	20
Fill Pattern	rectilinear	rectilinear
Infill Extrusion Width (mm)	0.2	0.2
Connect Paths	0	1

(a) Connect Paths configuration option added



(b) Top layer is filled with a disjoint path with exterior perimeters

(c) Intermediate layer is filled with a connected path with exterior perimeters

Figure 36: Patches to make 3D printing paths comply with the L-PBF process

consecutive layers corresponding to the three materials.

Listing 4.3 shows an excerpt of the generated .svg file, where it can be seen that the slicing and path generation occurred for all three materials.

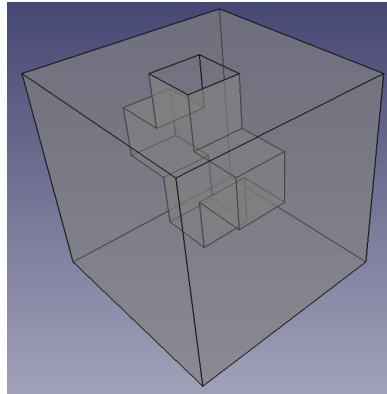
Once again, the slicer and path generator performs well with a different input model and is agnostic about the origin of the .stl input files. Furthermore, it is capable of handling models with more than two materials.

Listing 4.3: 3cubes.svg (excerpt)

```

1 <g id="LO_M1_H350" slic3r:z="0.3500" slic3r:slice -z="0.1750" slic3r:layer -height="0.3500" slic3r:mat="1">
2 <polyline points="19.9854,0.115674 19.8843,0.014645 19.8136,0.085356 19.9146,0.186385
   19.9854,0.115674" style="fill: none; stroke: blue; stroke-width: 0.1; fill-type: evenodd"
   slic3r:type="internal-infill" />
3 <polyline points="..." style="fill: none; stroke: blue; stroke-width: 0.1; fill-type: evenodd"
   slic3r:type="internal-infill" />
4 <polyline points="20,0 0,0 0,20 20,20 20,0" style="fill: none; stroke: blue; stroke-width: 0.1;
   fill-type: evenodd" slic3r:type="" />
5 </g>
6 <g id="LO_M2_H350" slic3r:z="0.3500" slic3r:slice -z="0.1750" slic3r:layer -height="0.3500" slic3r:mat="2">
7 <polyline points="14.9854,5.77252 14.2275,5.01464 14.1568,5.08536 14.9146,5.84323 14.9854,5.77252"
   style="fill: none; stroke: red; stroke-width: 0.1; fill-type: evenodd" slic3r:type="internal-infill" />

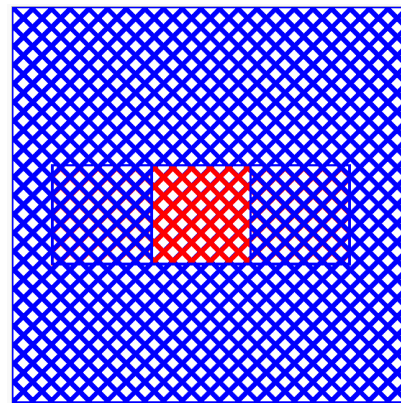
```



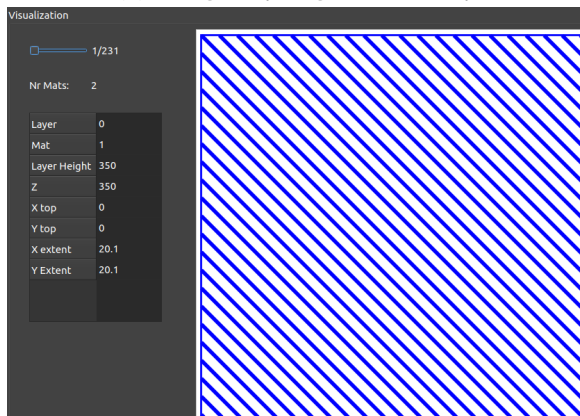
(a) Cross and Cube 3D model

Generic		Specific
<input checked="" type="checkbox"/> Enable		
STL ID	0	1
First Layer Height (mm)	0.35	0.35
Layer Height (mm)	0.15	0.15
Fill Angle (deg)	45	45
Fill Density (%)	15	15
Fill Pattern	rectilinear	rectilinear
Infill Extrusion Width (mm)	0.1	0.1
Connect Paths	0	0

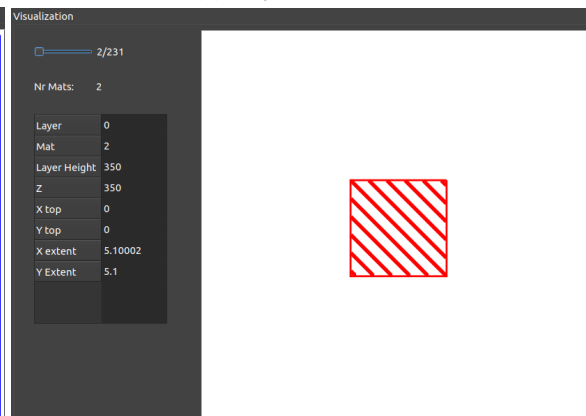
(b) Slicing and path generation setup



(c) Output: main view

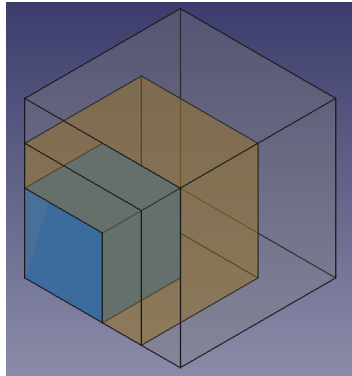


(d) Output: material 1



(e) Output: material 2

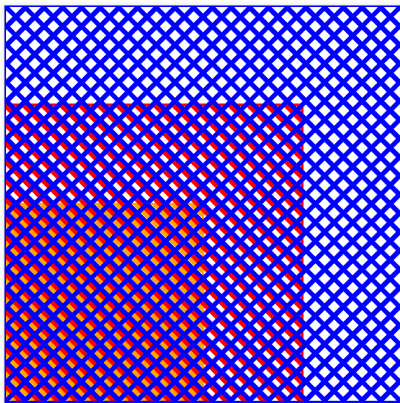
Figure 37: Pre-Manufacturer test: Cross and Cube input model



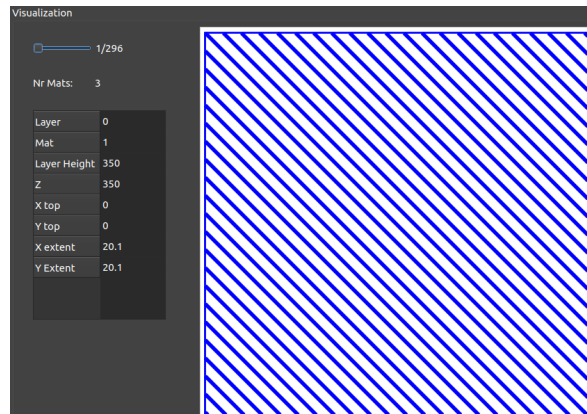
(a) 3 cubes 3D model

Generic		Specific		
<input checked="" type="checkbox"/> Enable				
STL ID	0	1	2	
First Layer Height (mm)	0.35	0.35	0.35	
Layer Height (mm)	0.15	0.15	0.15	
Fill Angle (deg)	45	45	45	
Fill Density (%)	15	15	15	
Fill Pattern	rectilinear	rectilinear	rectilinear	
Infill Extrusion Width (mm)	0.1	0.1	0.1	
Connect Paths	0	0	0	

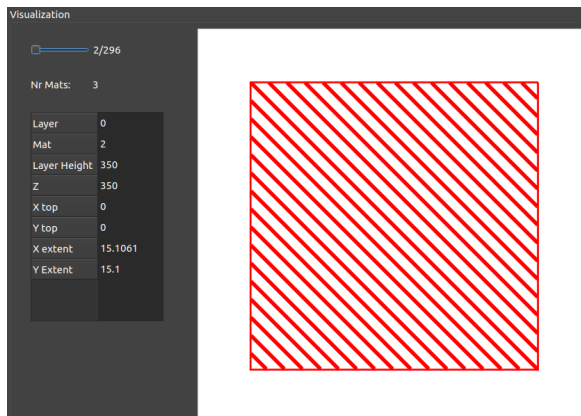
(b) Slicing and path generation setup



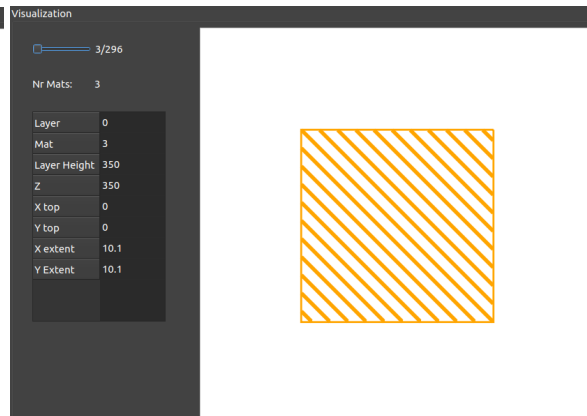
(c) Output: main view



(d) Output: material 1



(e) Output: material 2



(f) Output: material 3

Figure 38: Pre-Manufacturer test: 3 cubes input model

```

8 <polyline points= "... " style="fill: none; stroke: red; stroke-width: 0.1; fill-type: evenodd"
   slic3r:type="internal-infill" />
9 <polyline points= "15,5 0,5 0,20 15,20 15,5 " style="fill: none; stroke: red; stroke-width: 0.1; fill
  -type: evenodd" slic3r:type="" />
10 </g>
11 <g id="L0_M3_H350" slic3r:z="0.3500" slic3r:slice -z="0.1750" slic3r:layer-height="0.3500" slic3r:mat=
  "3">
12 <polyline points= "9.98535,10.4866 9.51344,10.0146 9.44272,10.0854 9.91464,10.5573 9.98535,10.4866 "
   style="fill: none; stroke: orange; stroke-width: 0.1; fill-type: evenodd" slic3r:type="internal-
   infill" />
13 <polyline points= "... " style="fill: none; stroke: orange; stroke-width: 0.1; fill-type: evenodd"
   slic3r:type="internal-infill" />
14 <polyline points= "10,10 0,10 0,20 10,20 10,10 " style="fill: none; stroke: orange; stroke-width:
   0.1; fill-type: evenodd" slic3r:type="" />
15 </g>

```

Models' coordinates and different slicing parameters Models' merging uses the z-coordinate for sorting the slices to be filled, and must obey the absolute coordinates conveyed by each STL model. This means the models' coordinates must be preserved relatively to each other, while placing the largest bounding volume model at the bed's level ($z = 0$).

Moreover, different slicing parameters can be applied individually for each model, such as first layer height and layer height, which can result in additional slices for each model. The rule is simple: if a slice from one model has a different z-coordinate from the other models, and this slice intersects them, then, this slice z-coordinate is added to the set of slices of these models. However, the slice added to the other models must meet their layer height requirements, i.e., the slice is bounded between $slice_z \leq z \leq slice_z + lh/2$, where $slice_z$ is the z-coordinate of the originating model's slice, and lh is the layer height of the destiny model's slice.

One might think that the slices are purely bi-dimensional, as they in fact are, but the thickness (z-coordinate) is required for the 3D printing paths, for example to calculate raft layers. They are maintained here for the L-PBF's process, because they convey the layer height to be manufactured, which is expected to be different from model to model, as each model represent a distinct material, and different materials have different "penetration" heights, i.e., different wavelength absorption rates.

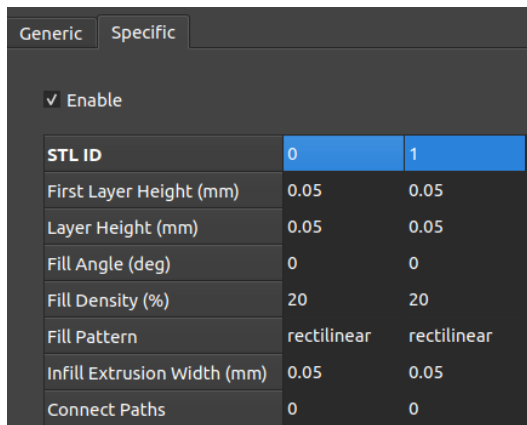
To test this, a cylinder and cross 3D model was sliced with different models coordinates and different slicing parameters. Fig. 39a shows the cylinder and cross model, with the same minimum z-coordinate ($z = -2.50 \text{ mm}$) across materials. This model was then processed in the Pre-Manufacturer in accordance to the configuration shown in Fig. 39b, and the results are displayed in Fig. 39. Thus, the referencing of the models to the same z-coordinate, and the same slicing parameters used across both materials, yielded 700 layers (Fig. 39c), with layers combining both materials at the same z-coordinate ($z = 50 \mu\text{m}$), as illustrated by Fig. 39d and Fig. 39e.

Next, the same multi-material 3D model was used, but with a slight offset in Z of $+20 \mu\text{m}$ in the cross model (Fig. 40a). This model was then processed in the Pre-Manufacturer using the same configuration (Fig. 40b), and the results are displayed in Fig. 40. Now, the manufacturing model contains almost 1300 layers (Fig. 40c), nearly double. Layer 0 is set at $z = 50 \mu\text{m}$ (Fig. 40d) and layer 1 at $z = 70 \mu\text{m}$, due to the $+20 \mu\text{m}$ offset, for both materials (Fig. 40e and Fig. 40f), even though the material 1 is not explicitly configured to be sliced at this z-coordinate.

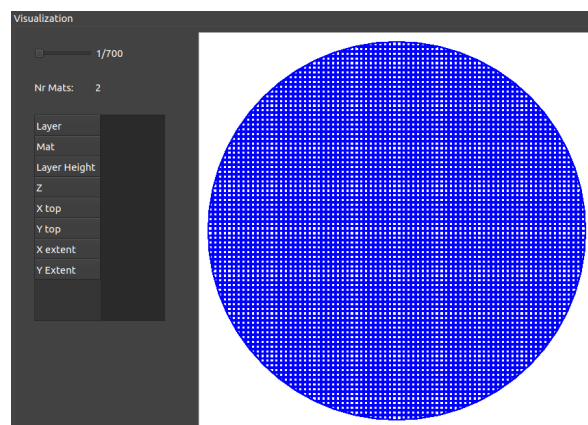
Lastly, the multi-material 3D model with a slight offset (Fig. 40a) was processed in the Pre-Manufacturer using different slicing parameters for each material (Fig. 41a), and the results are displayed in Fig. 41. Now, the manufacturing model contains almost 1100 layers (Fig. 41b). Layer 1 is set at $z = 70 \mu\text{m}$ (Fig. 41c and Fig. 41d),



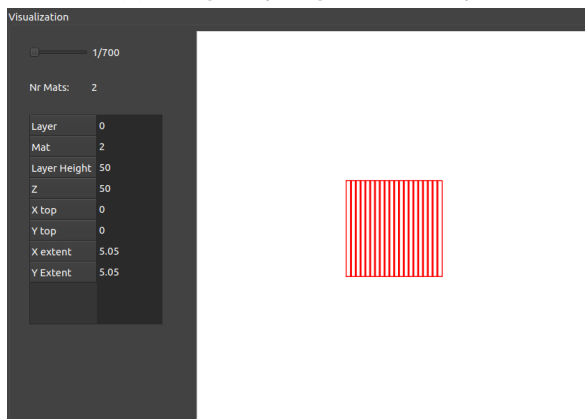
(a) FreeCAD preview



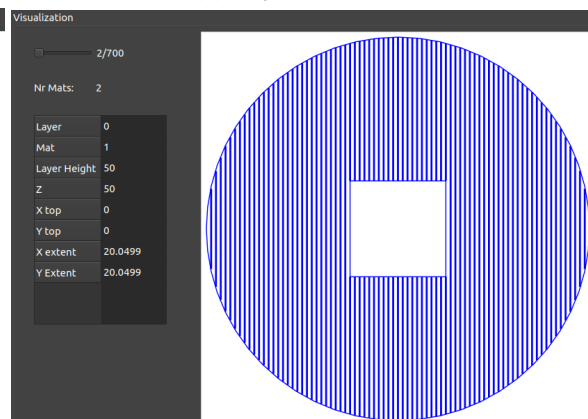
(b) Slicing and path generation setup



(c) Output: main view

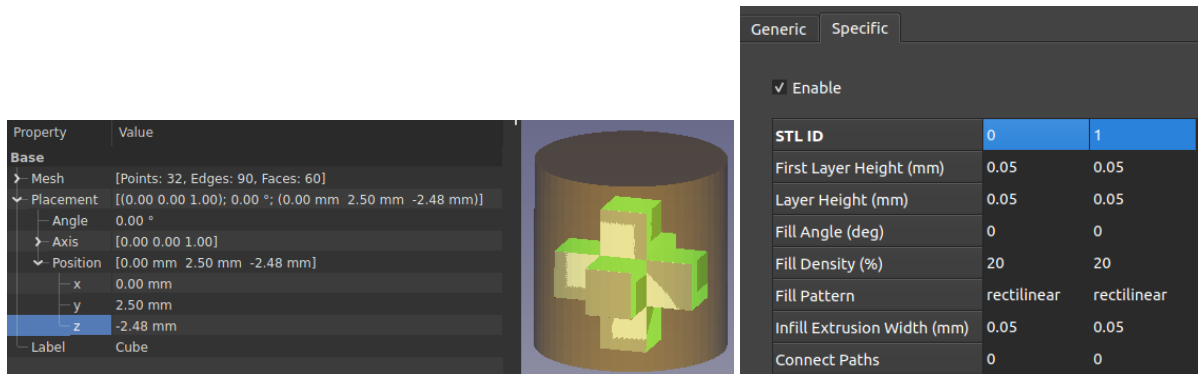


(d) Output: Layer 0 – material 1



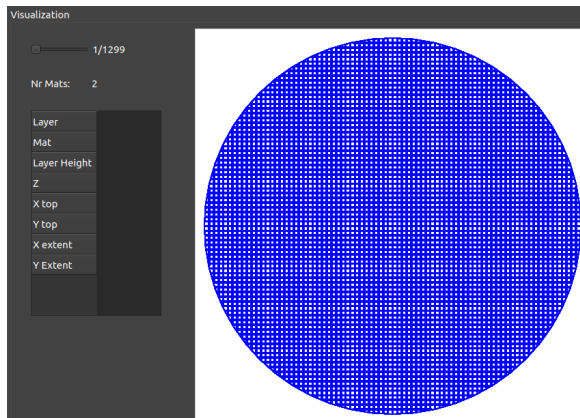
(e) Output: Layer 0 – material 2

Figure 39: Pre-Manufacturer test: Cylinder and cross input model

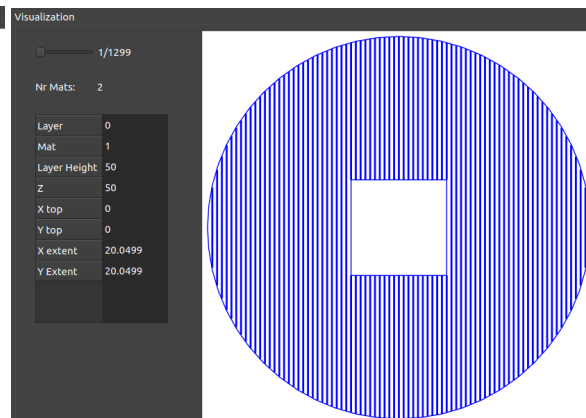


(a) FreeCAD preview

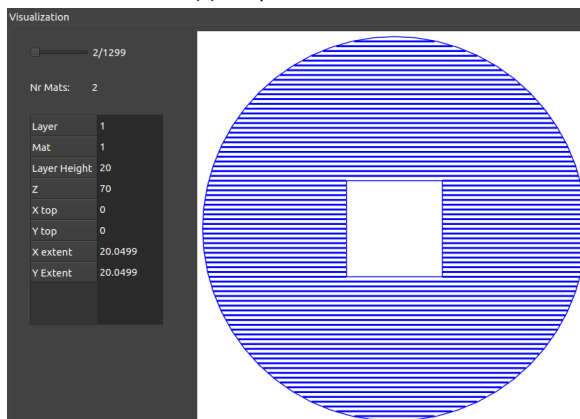
(b) Slicing and path generation setup



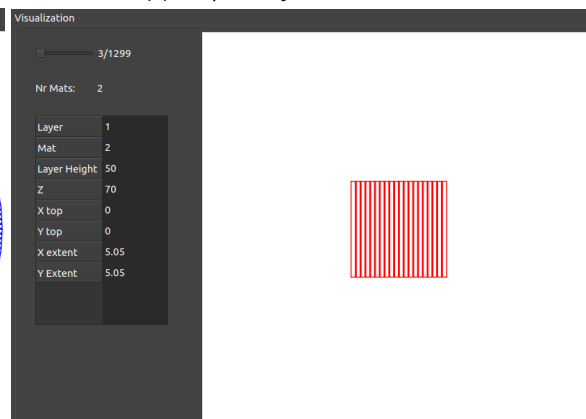
(c) Output: main view



(d) Output: Layer 0 – material 1



(e) Output: Layer 1 – material 1



(f) Output: Layer 1 – material 2

Figure 40: Pre-Manufacturer test: Cylinder and cross input model with z-offset

but different layers heights, respectively 50 and 100 μm , because it is the second layer of material 1 (*layer height* applies) and the first layer of material 2 (*first layer height* applies). For layer 3, located at $z = 150 \mu\text{m}$, the layer height also differs, but it now corresponds to the layer height of each material, as illustrated in Fig. 41e and Fig. 41f.

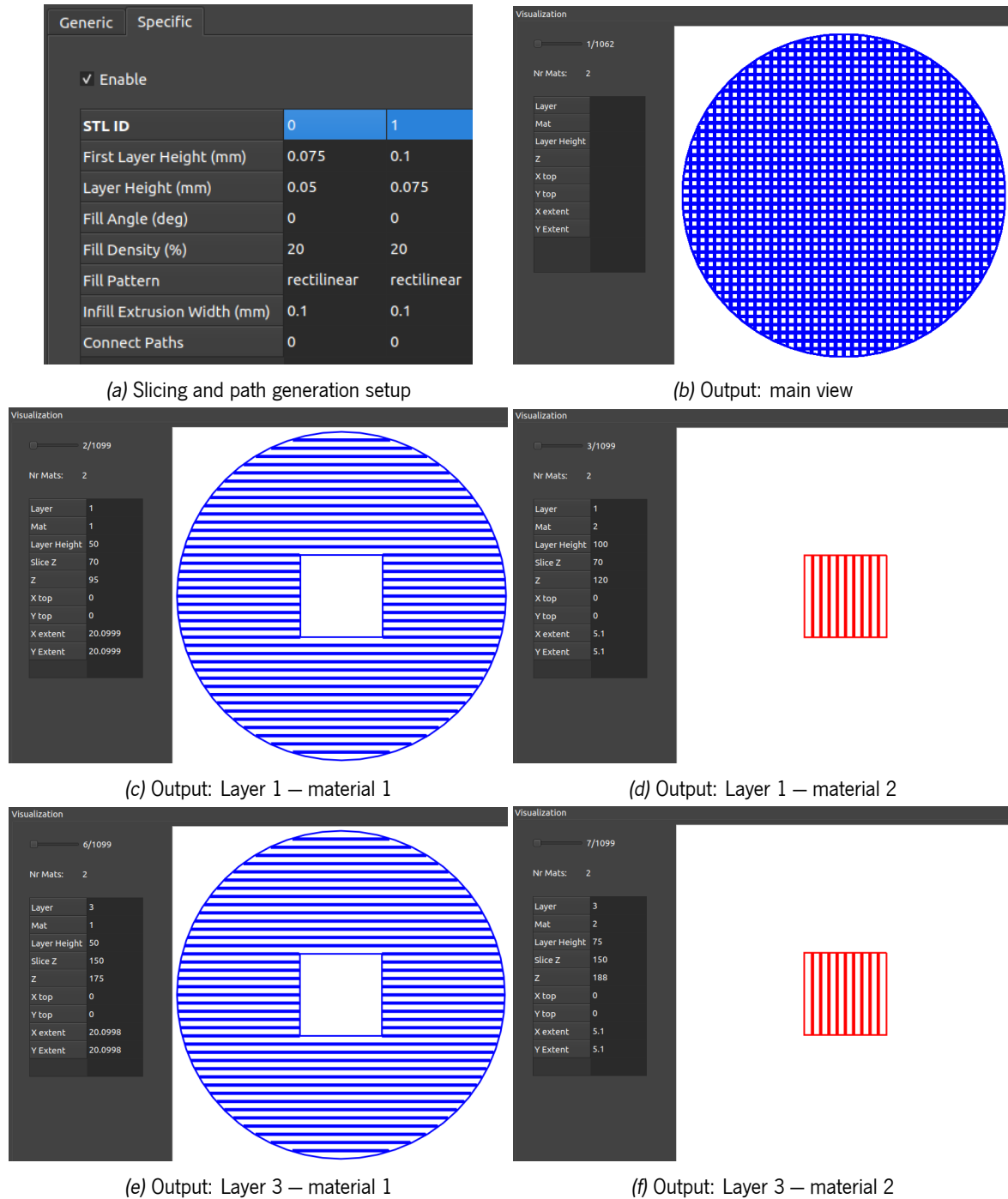


Figure 41: Pre-Manufacturer test: Cylinder and cross input model with z-offset and different slicing parameters

Computational resources To analyse the slicer performance, the path generation parameters were maintained (see Table 3) and the layer height was varied from 0.025 to 0.001 millimetres, and the number of layers, execution

time, and file size were registered in table 4. As can be seen, for 25 micrometers, the number of layers is 120, taking 2.86 seconds to compute and yielding a file size of 1.3 MB. Decreasing the layer height, increases the number of layers as expected, as well as the computation time and file size. Even more interesting is that the slicer is capable of slicing layers with 1 micrometer height within a reasonable amount of time (79.4 seconds), which excels the fabrication requirements. However, the file size is penalised as expected, yet, is still tolerable.

Table 4: Layer height tests: 0.025–0.001 mm

Layer height [mm]	Nr. of layers	Computation time [s]	File Size [kB]
0.025	120	2.86	1300
0.020	150	3.84	1600
0.015	198	5.52	2100
0.010	298	7.12	3100
0.005	592	14.50	6200
0.001	1456	79.39	29400

Also, it is important to understand the impact of using different path topologies in terms of computational resources, namely file size and execution time. For that purpose, the disk and torus model was processed with a layer height of 0.15 mm and with the same remaining path topology parameters (see Table 3). The fill pattern was also kept the same for all materials and with disjoint paths, except for *3D Honeycomb* and *Gyroid*, where this is not possible. Furthermore, several trials were performed and the relevant parameters averaged.

Table 5 shows the benchmarking results. The rectilinear paths have roughly the same order of magnitude for execution time and file size, being the fastest and most compact paths. The planar paths present a high disparity in execution time, with the *Archimedean Chords* being the slowest of all paths. The file size also varies from low (4 MB) to medium (14 MB). The honeycomb paths take roughly the same time to execute (medium) and have the highest file sizes (almost 30 MB for the *3D Honeycomb*). Lastly, the *Concentric* path is fast to execute but medium in size, whereas the *Gyroid* has a medium execution time but a high file size.

Table 5: Path benchmarking in terms of computational resources

Path Class	Path Type	Time Avg [ms]	File Size Avg [MB]	Connected
Rectilinear	Rectilinear	1011	2.5	0
	Aligned Rectilinear	554	2.4	0
	Grid	569	2.5	0
	Triangles	1100	2.4	0
	Stars	1025	2.4	0
	Cubic	1194	2.4	0
Planar	Archimedean Chords	14158	14.4	0
	Hilbert Curve	5130	14.7	0
	Octagram Spiral	1714	4.0	0
Honeycomb	Honeycomb	7243	22.8	0
	3D Honeycomb	8545	29.9	1
Others	Concentric	3283	9.4	0
	Gyroid	6897	22.5	1

Since the processing is done offline, i.e., without connection to the actual manufacturing, the values displayed

here are not critical. The execution time is fairly low, except for the *Archimedean Chords*. The file size, on other hand, varies greatly (2 to 30 MB), and is a result of the output format used — *SVG* is an *XML*-based file, with focus on user readability, rather than on compactness. This is a trade-off that must be assessed in the future to clarify if a new file format is required. Nonetheless, the impact of the file size is minimised, because it is an intermediate representation, i.e., it is not sent directly to the machine.

Validation Thus, from the implemented *Pre-Manufacturer* software component is now possible to produce toolpaths from multiple 3D models (corresponding to multiple materials) into a single file, encoding geometrical and material info, that can be readily used from the laser software and the *Manufacturer's* software. The software is available online [169] (see Fig. 42) and released under the AGPL v3 licence.

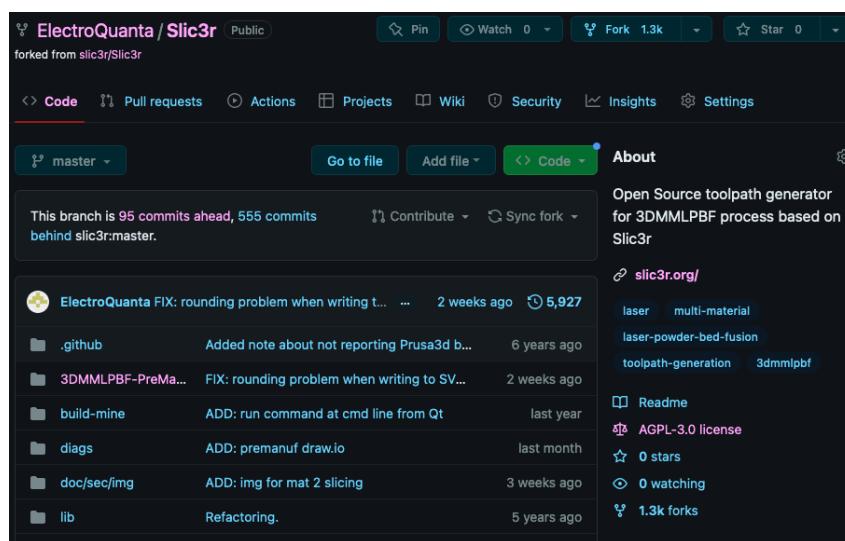


Figure 42: 3DMMLPBF Pre-Manufacturer repository [169]

4.3.2 Manufacturer

The *Manufacturer* software is divided into the **Post-Processor** and **Printer** software packages.

The *Post-Processor's* goal is the mapping of the relevant process parameters, like material and manufacturing ones, to the geometrical information pertaining to the scan paths, adding the process specifics into the manufacturing workflow to obtain produced parts with the required characteristics. The relevant manufacturing parameters should be pulled from the respective database, namely *material* and *process*. However, in the initial stage, their goal is to serve as a guideline with the end-user being the ultimate responsible for their assignment.

The *Printer* commands the 3DMMLPBF machine and manages the communications required to perform the actual manufacturing.

Both packages are wrapped into a single **UI**, thus, for the sake of simplicity, they will be addressed simultaneously, following the waterfall methodology.

4.3.2.1 Requirements & constraints

Table 6 lists the requirements and constraints for the *Post-Processor* and the *Printer*.

The main requirements for the *Post-Processor* are: loading the manufacturing model and render it; map the manufacturing paths to process parameters (e.g., through a pen) and provide the visual feedback (e.g., changing the colour associated to the pen); and sort layers by different criteria, e.g., layer's ID, layer's number, material, and pen. On the other hand, process mapping is bounded by the *EzCAD Software Development Kit (SDK)*.

Regarding the *Printer*, its main requirements are: commanding the *3DMMLPBF* machine, supporting the calibration, powder filling, laser testing and marking, and the actual manufacturing; managing all communications required for manufacturing; ensuring safety mechanisms to protect the *User*. As a constraint, laser control is also bounded by the *EzCAD SDK*.

Table 6: Requirements and constraints for the Post-Processor and Printer software packages

	Post-Processor	Printer
Requirements	<ul style="list-style-type: none"> - Load manufacturing model and render it - Map the manufacturing paths to process parameters - Provide visual feedback of the mapping - Sort layers by different criteria: ID, number, material, pen 	<ul style="list-style-type: none"> - Command the 3DMMLPBF machine: calibration, powder filling, laser testing and marking, printing - Manage all communications required for manufacturing - Ensure safety mechanisms to protect the User
Constraints	<ul style="list-style-type: none"> - Process mapping is bounded to the EzCAD SDK - Limited time 	<ul style="list-style-type: none"> - Laser control is bounded to the EzCAD SDK - Limited time

4.3.2.2 Analysis

Fig. 43 illustrates the *Manufacturer's* use cases, specifying the required high-level functionalities for the two software packages — *Post-Processor* and *Printer*. There are three actors interfacing the system: *User*, *3DMMLPBF machine*, and *Laser*.

In the *Post-Processor*, the *User* can load and render the geometry file (manufacturing model), view the part's and layers' statistics, sort layers by criteria, setup the manufacturing parameters, and map the manufacturing parameters to the geometry.

In the *Printer*, the *User* can manage the communications and the manufacturing. The communications management comprise the machine and lasers' network. The *User* can select the communication port, connect or disconnect the machine. On the other hand, the *User* can also add other lasers, besides the current one, to the network, enabling multi-material fabrication using multiple lasers. Regarding the manufacturing, the *User* can: calibrate the machine, i.e., calibrate each axis individually and setup the machine parameters; manage the laser actuation — configure the laser parameters, and preview, test, and stop marking; manage (run, pause, stop) the actual manufacturing. Additionally, the *User* can export data for the subsequent analysis and import by the *Post-Manufacturer*, namely the manufacturing information and a log file with process's control information.

Next, the interactions between objects were defined and use cases were mapped to objects with sequence diagrams to describe the internal behaviour of the system, for each use case.

Fig. 44 illustrates, as an example, the sequence diagram for the *LoadGeometryFile* use case. The *User* presses the *Geometry file button*, which is captured by its control, triggering the creation of the *Select Geometry File Dialog*. A file list is presented to the *User*, which selects a geometry file. The file is loaded and the dialog is *destroyed*. Then, the filename is displayed in the *GUI*, indicating to the *User* the success of the operation. Lastly, the relevant

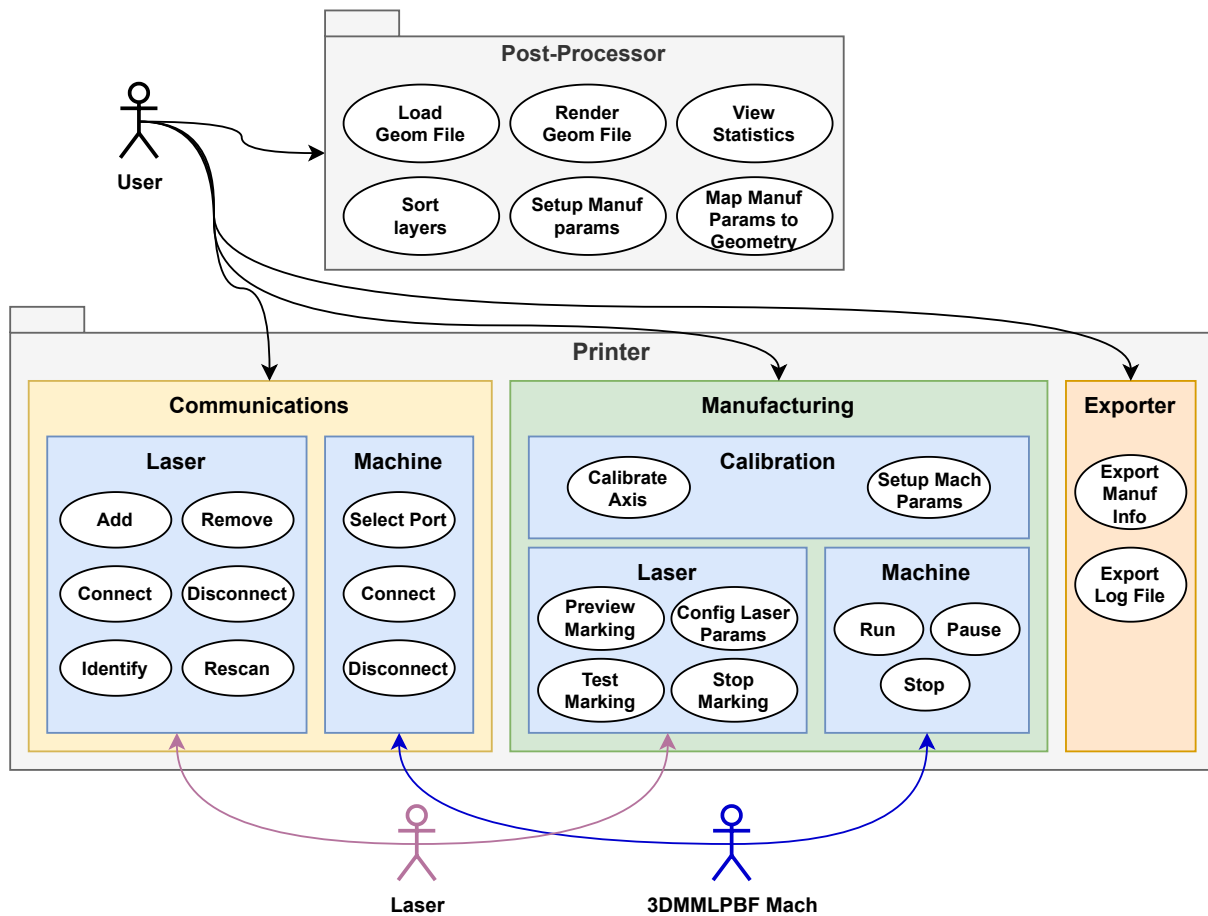


Figure 43: Manufacturer analysis: use cases

information are presented to the user namely: filename, layer count, material count and layers list and the graphical preview of the file is displayed.

4.3.2.3 Design

Fig. 45 depicts the *Manufacturer's* system architecture:

- **User interface:** this outer layer constitutes the front-end of the application and is responsible for handling all user interaction through the UI Engine.
- **Inputs:** the inputs are handled by the *Post-Processor* to read and render the manufacturing geometry (Geom Reader and Geom Render) and also to manipulate it (Layer Manager). The Pen Manager manages the available pens, which are used as an abstraction to map the process parameters to the geometry.
- **Manufacturing:** The Laser Manager handles the laser configuration (Param Manager) and all laser requests to preview (Preview Entity) and mark an entity (Mark Entity) or multiple entities (Mark Entity Queue Manager). The distinction between the marking components is required due to the fact that these entities can be manufactured by different lasers, which demands a paralleled architecture (multithreaded). The Calib Manager handles the machine calibration and the Output Exporter is responsible for logging the manufacturing information for further analysis into a file. The Manuf Manager

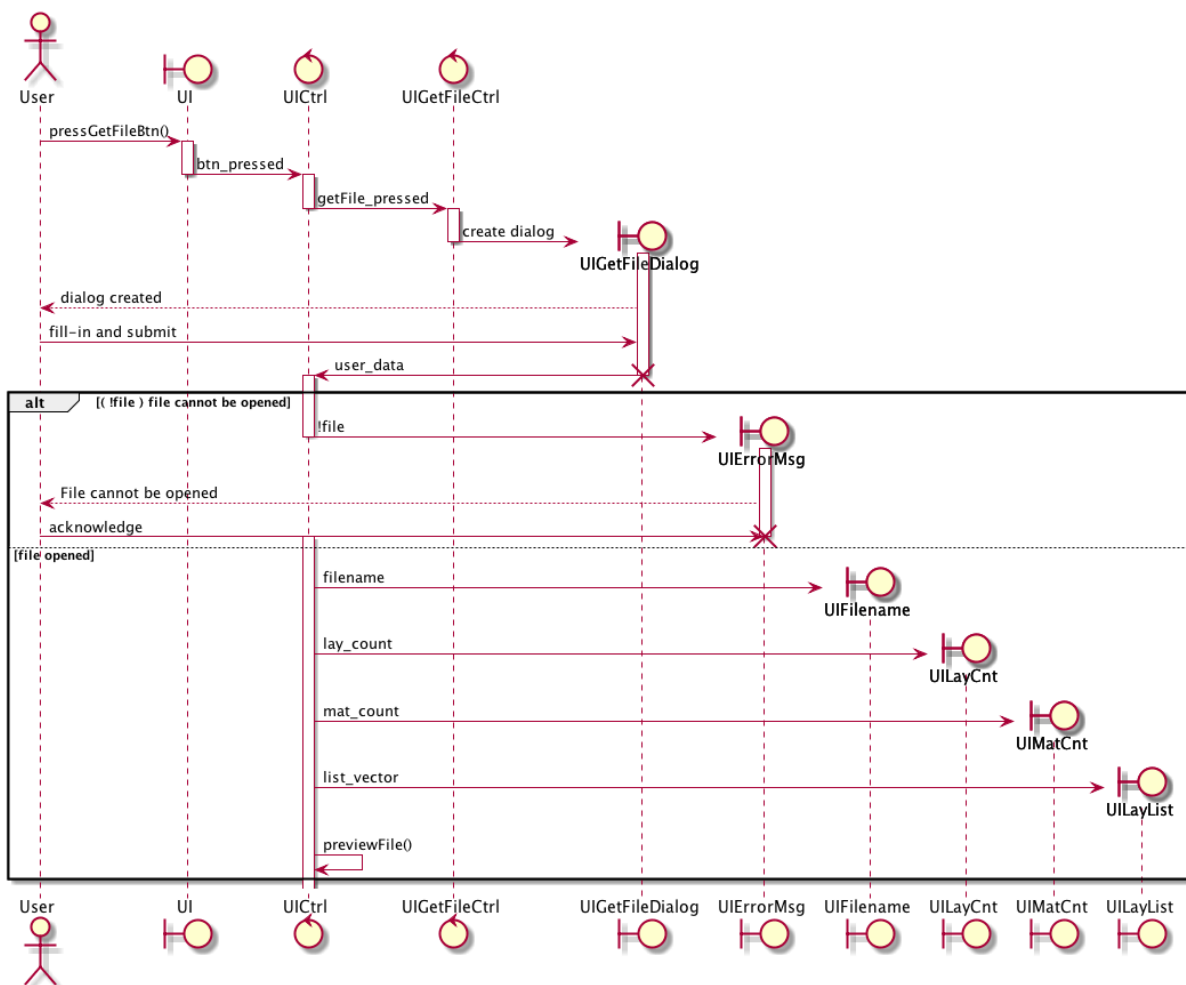


Figure 44: Sequence diagram of the LoadGeometryFile use case

handles the manufacturing procedure, issuing the commands for the machine and laser actuation for each layer until the end-of-file is reached or the procedure is halted (*User* pauses/stops the process or an error occurs).

- Communication:** The *Manufacturer* application communicates with the machine (*Mach Comm Manager*) and the laser(s) (*Laser Comm Manager*). The *Manufacturer–Machine* communication is point-to-point, thus, a serial link was adopted using the RS232/RS485 protocol ([Universal Asynchronous Receiver-Transmitter \(UART\)](#)). The communication between the *Manufacturer* and the lasers is multi-point, thus, a client-server model was established using the [Transmission Control Protocol/Internet Protocol \(TCP/IP\)](#) protocol for delivery guarantees: the master laser, connected to the machine and one laser, requests (client) entity marking from another laser (server). Additionally, a fixed-size message protocol was devised to guarantee determinism and ease parsing, comprised of the command, arguments, payload and a validation (ACK). This protocol is generic and was applied on top of both communications (laser and machine).

Next, the sequence diagrams and its flow of events were analysed, yielding a viable solution – through algorithmic design – and a static architecture – a class diagram.

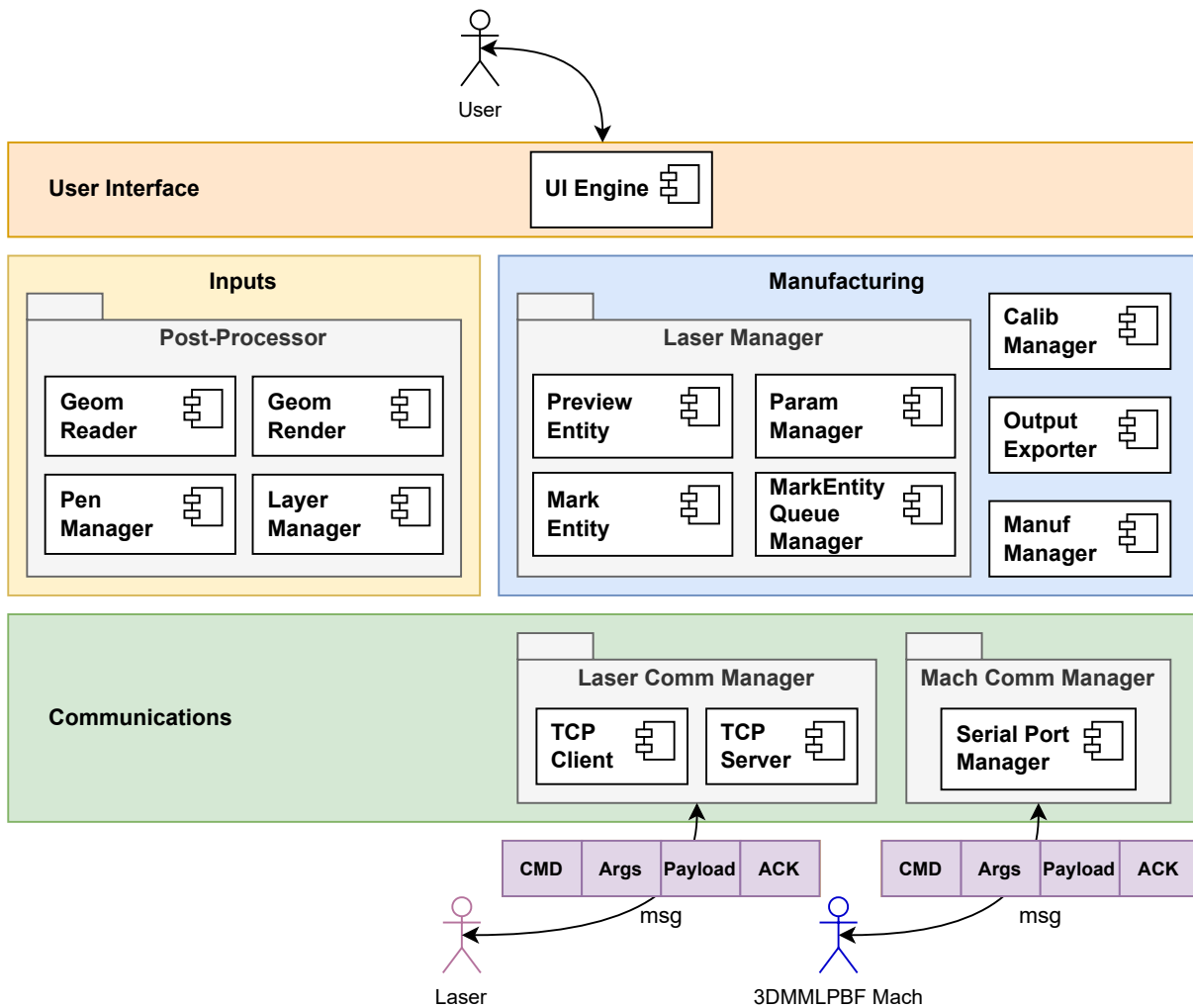


Figure 45: Manufacturer design: system architecture

For the algorithm design, two main tools were used: pseudocode and state machine diagrams for threads design.

Algorithm 1 depicts the pseudocode for the *Choose File* use case. In short, a dialog is presented to the *User* to select an *EzCAD* file. If the file is successfully open, it is loaded. Then, the layers are *filled in* and its relevant attributes retrieved. Lastly, the *GUI* refresh is done and the *pens* are generated based on the layer's material.

The design process – i.e., the pseudocode elaboration – was repeated to all of the aforementioned use cases.

The state-machine diagrams are useful to represent deterministic behaviour in software, which is fundamental to increase its robustness. As aforementioned, the *Manufacturer* application is event-driven and multithreaded, mainly for the following reasons: communications' transactions are executed asynchronously, i.e., there is no prediction of when the next packet of data will arrive; the laser management relies on the *EzCAD API* which is implicitly asynchronous, e.g., if an entity is being currently marked, the *User* must be able to stop it immediately if something goes wrong; the actual manufacturing consumes data from communication sources and produces new data to run the laser and the machine, and, as both are asynchronous, requires it to operate in the same manner.

Fig. 46 illustrates the state-machine diagram for the *Manuf* thread. It consists of nine main states:

Algorithm 1 Choose File**Input:** User pressed the Choose File button

```

1: procedure OnSelectFile()
2:   variables declaration
3:     dlg: FileDialog
4:     fname: string
5:     err, layerCount: integer
6:     layer: Layer
7:     layers: vector of Layer
8:   end variables declaration
9:   dlg ← FileDialog('EzCAD File')
10:  if dlg = NULL then
11:    PRINT('Could not create dialog')
12:    exit
13:  end if
14:  fname ← dlg.getPathName()
15:  err ← loadFile()
16:  if err ≠ SUCCESS then
17:    PRINT('Unable to open file')
18:    exit
19:  end if
20:  layerCount ← getLayerCount()
21:  for all layer in layers do
22:    getLayerInfo(layer)           ▷ get layer's info: name, dimensions
23:    layers[] ← layer
24:  end for
25:  PaintCanvas(layers[0])           ▷ Draw first layer to screen
26:  FillTable()                       ▷ Fill Table with layers' info
27:  FillCountBar()                   ▷ Fill Bar with layers and material count
28:  updatePosBar()                   ▷ Update Bar with first layer position and dimensions
29:  generatePens()                   ▷ generate pens based on layer's material
30: end procedure

```

- **Init:** this is the initial state. The *EzCAD* library handler is configured, and if everything works well, it transits to the *Idle* state, otherwise it goes to the *Error* state.
- **Idle:** this is default state where the thread waits for incoming requests.
- **ManufLayer:** if a *newID* event is posted, then this state is triggered. If the last layer ID was manufactured, then request the machine to perform the cleanup (recover powders). Otherwise, the *UI* is updated with new layer ID's information. If the previous layer's ID material is the same as the new one, then the bed does not need to descend, otherwise yes. Then, the command for layer processing is issued for the machine (via the communications layer).
- **RunLaserEntity:** After recoating is complete, a request is issued to mark the current layer's ID, which will be handled by the *Mark Entity Queue*'s thread and dispatched for marking by the *Mark Entity*

thread. When the current layer's ID is complete, the `newID` event will be posted and `Manuf Layer` will take over and continue to drive the manufacturing.

- **RequestStop:** If the `User` pressed the `Stop` button, a request must be submitted to the `Mark Entity Queue's` thread to stop the laser, and another one must be submitted to the machine by issuing the stop command, dispatched by the communications layer.
- **Stop:** After the machine and the laser acknowledged everything was stopped, we wait for the `restarted` event to go to `Idle`.
- **Cleanup:** After completing the manufacturing of the last layer, the cleanup procedure is triggering by issuing the command `Aspirate` to the machine, containing the material number to collect.
- **End:** After cleanup is performed, manufacturing is completed, so we wait for the `restarted` event to start a new manufacturing procedure.
- **Error:** If an error occurs, this state is triggered, and the message will be dispatched to the UI.

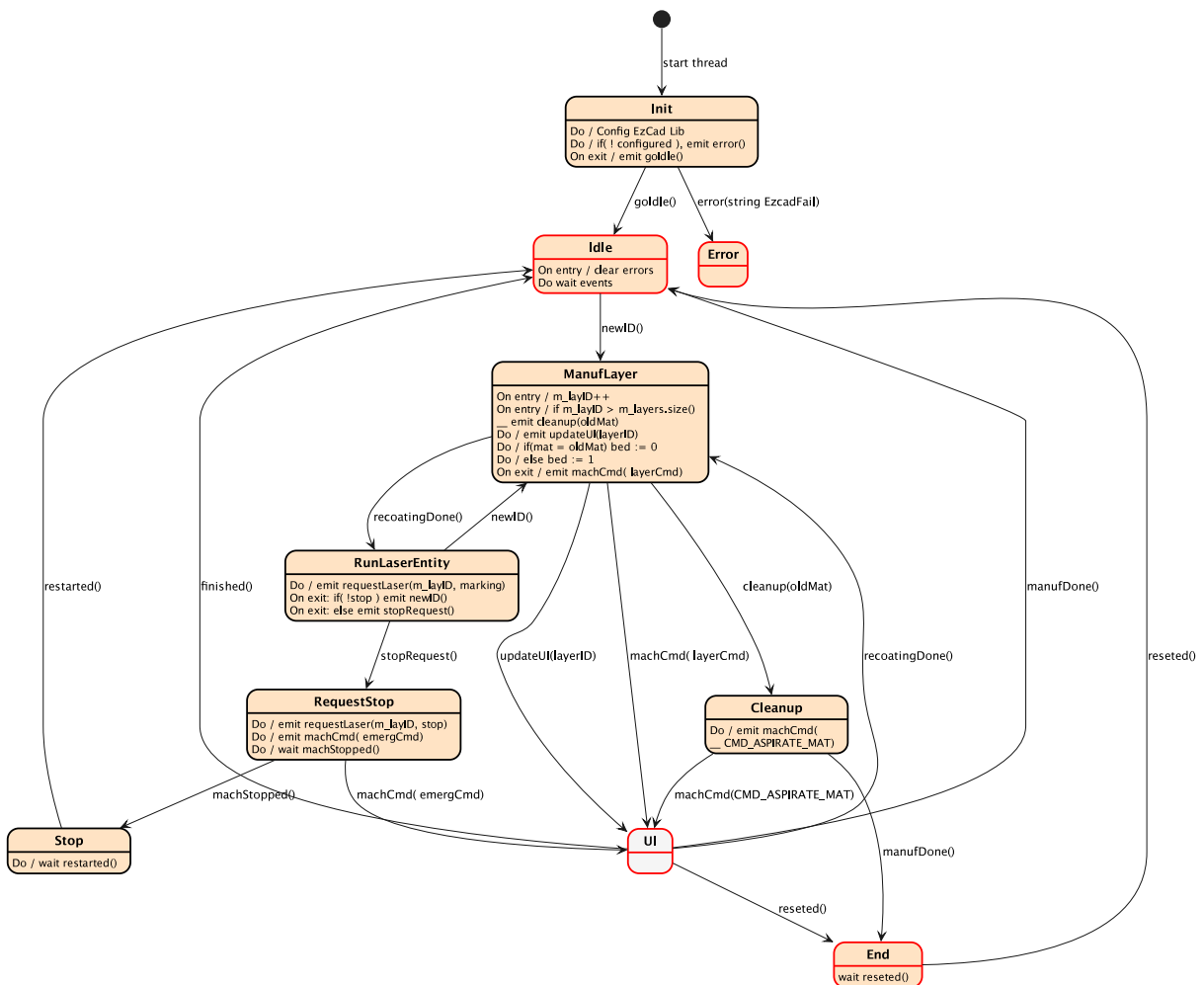


Figure 46: Manufacturer design: Manuf thread state-machine diagram

The `Manufacturer` must talk a common language with the `3DMMLPBF`'s machine and with the slave computers. Fig. 87 specifies this common language – the messaging protocol – with the following structure:

1. **CMD**: command exchanged between the `Manufacturer` and the machine or slave lasers. The commands highlighted in green represent the commands exchanged solely with the slave lasers (the machine's messaging protocol will be addressed later). The several command types are listed, alongside with the command's grammar. For example, the `LASER_MARK_ENTITY` command requires the laser's ID, the entity's ID to mark, the corresponding pen's ID, and the actuation's delay.
2. **args**: represents the command's arguments. For example, `LASER_MARK_ENTITY`'s laser ID, entityID, and penID goes into arguments 0, 1–2, and 3, respectively.
3. **payload**: represents an additional command's attribute, such as, laser's actuation delay, distance, layer height or parameter's value. For example, the `LASER_MARK_ENTITY`'s delay is defined here.
4. **ACK**: represent's the acknowledgment signal, used to validate a message.

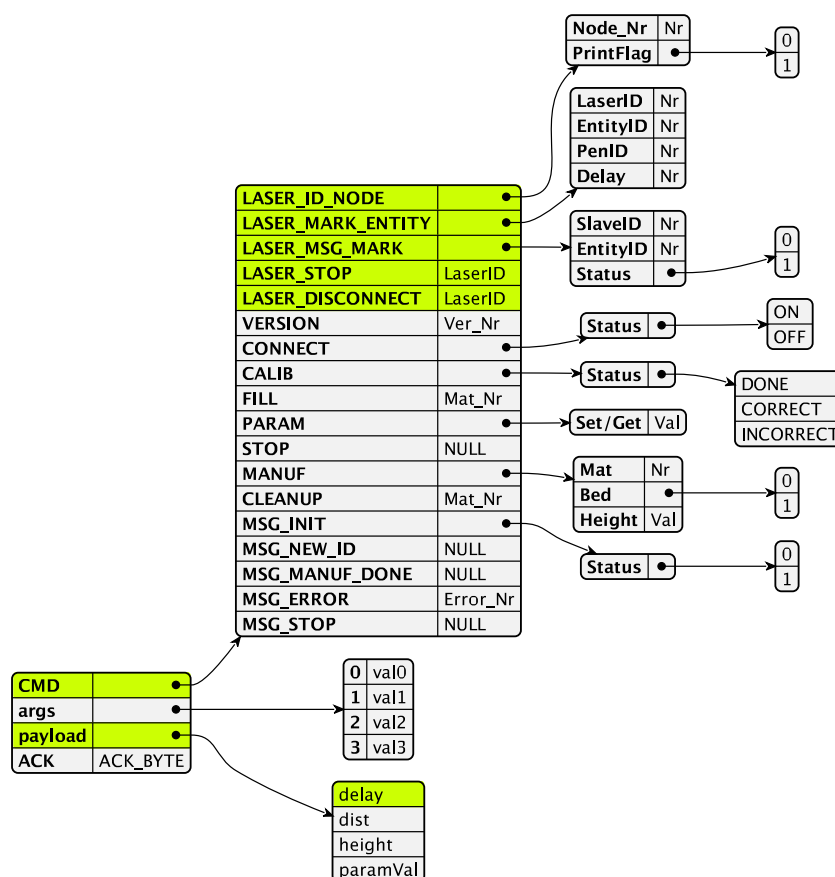


Figure 47: Manufacturer design: Messaging protocol

The static architecture was then devised using class diagrams, which allow to represent the interdependency between objects, using associations and attributes. An association represents a relation between two or more classes with several properties: name, role and multiplicity. An attribute is a property of an individual object with a name and a type.

Fig. 48 illustrates the Manufacturer's class hierarchy and respective associations. Four dialog classes were created to interface the user — `MainDialog`, `ManagePenDialog`, `InputDialog`, and `MessageBox` — which inherit from an *abstract class* `Dialog`. The `InputDialog` and `MessageBox` are simple `Dialogs` to validate user input and feedback relevant information to the user. `ManagePenDialog` is the user interface to pen management and is composed by a set of `Pens`, which, in turn, contain an associated color.

`MainDialog` is the main user interface to the Manufacturer's application and is composed by:

- **Pen:** a set of `Pens` is used to map the manufacturing parameters to the geometry.
- **Layer:** a set of `Layers` combines the geometry and process information required for the manufacturing.
- **Laser:** a set of `Laser` manages the laser's information in the network and is strongly linked with the number of `TCPClients`.
- **TCPClient:** a set of `TCPClients` is stored to manage the available and ongoing connections to other lasers in the network.
- **TCPServer:** a `TCPServer` is binded to the Manufacturer's application to listen and serve requests incoming from other lasers in the network.
- **SerialPort:** manages the serial communication with the machine.
- **InReader:** handles the loading of input files to the *Post-Processor*.
- **OutWriter:** handles the export of output files containing the manufacturing history.
- **Worker:** the `Worker` is the base class for thread management from which derive the `PreviewLaser`, `MarkEntity`, `MarkEntityQueue`, and `Manuf` thread classes.

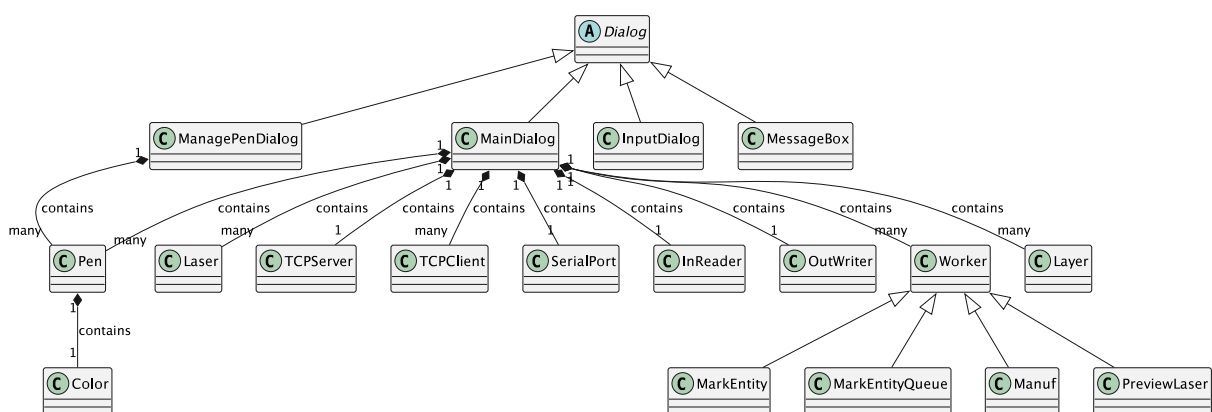


Figure 48: Manufacturer design: High-level class diagram — hierarchy and associations

4.3.2.4 Implementation

Fig. 49 illustrates the deployment diagram for the Manufacturer's software, assigning software artifacts to the hardware nodes where they are executed. The Manufacturer's application can be deployed in any computer

connected to a laser that uses *EzCAD SDK*-compatible control boards, managed through a [Peripheral Component Interconnect \(PCI\)](#) interface. Lasers' computers can be connected together to form an array using the [TCP/IP](#) protocol and any supporting interface (e.g., Ethernet). Only one laser's computer is connected to the *3DMMLPBF* machine (via serial [UART](#) interface), becoming the *Master* in the network. This computer exchanges transactions with the *Firmware* to control and obtain feedback about the manufacturing procedure. There is no limitation in the software to the amount of slave lasers, besides the [TCP/IP](#) imposed one of 65535 ports. However, there is a physical limitation of how to arrange those lasers over the building platform.

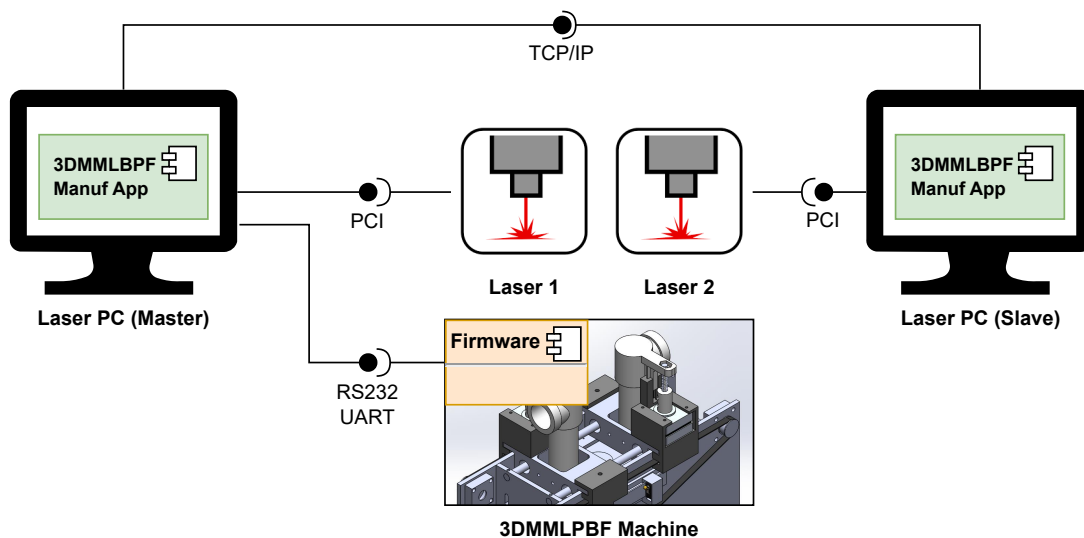


Figure 49: Manufacturer implementation – deployment diagram

Next, the *Manufacturer's* application was implemented in C++11 using the Qt framework for the UI development, taking into account its class diagram, and the designed algorithms and state machines. It uses the *EzCAD API* (see Appendix A) to manage laser related operation. Fig. 50 through Fig. 53 illustrate the *Manufacturer's* UI implementation outcome.

Fig. 50 displays the main window of the application. The **Communications** section handles the laser network and machine communications. In the **Configuration** section, the *User* loads the geometry, with the bounding box view being rendered on canvas and the statistics displayed. Additionally, the *Layers'* table is filled, where, besides the geometry data are also the process parameters (mapping to a *Pen*) and the laser marking information (lasers' list and delay between markings). The **Calibration** enables the *User* to calibrate each machine axis and set the machine parameters. In the **Processing** section the *User* selects the output file, and manages the laser actuation and manufacturing execution. Lastly, a console is added to provide user feedback.

Fig. 51 shows the *Pen Manager* dialog, where the *User* manages the manufacturing pens.

Fig. 52 illustrates the visualization of each layer with a different pen, signalled to the *User* by a different color. Furthermore, it is possible to modify the lasers performing the marking and the delay between each of those (see Fig. 52a).

Lastly, Fig. 53 shows the help dialog, providing relevant assistance to the *User*.

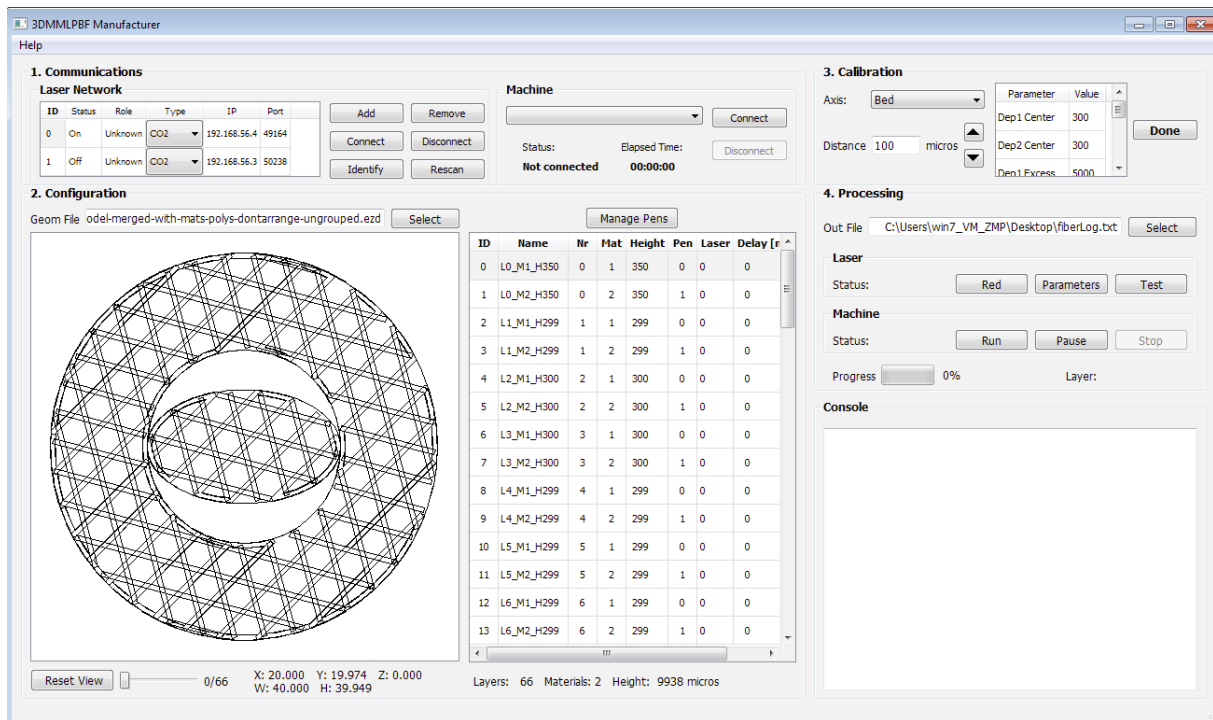


Figure 50: Manufacturer implementation: Main window

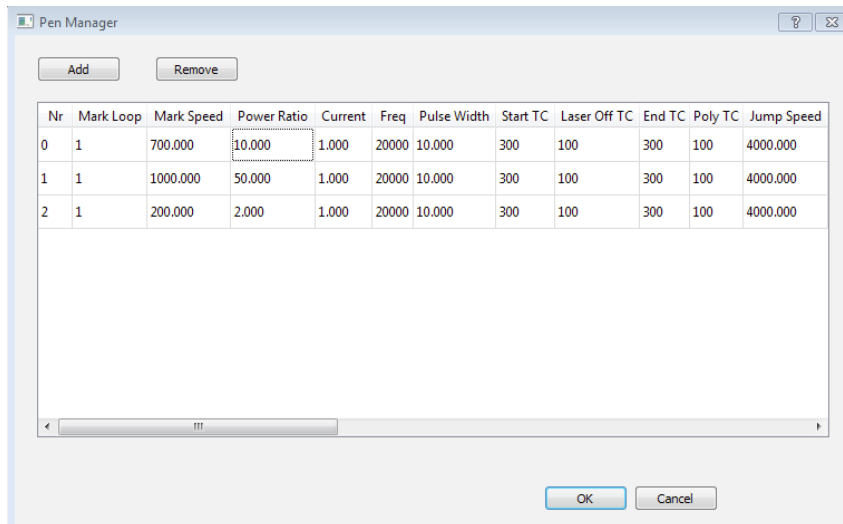


Figure 51: Manufacturer implementation: Manage Pen dialog

4.3.2.5 Testing and Validation

In this section, the Manufacturer's software is tested and validated, concerning the post-processor and printer components, as well as the laser connection.

Post-Processor For the post-processor, the .svg file parsing and rendering was tested, as well as the laser parameters mapping to each material. Fig. 52 shows that both expected behaviours are achieved.

Fig. 54 illustrates the mapping of the process parameters to the geometry, using a pen. By default, the Post-Processor assigns pens to each material (see Fig. 54b, and Fig. 54c), but the User can add news pens and associate

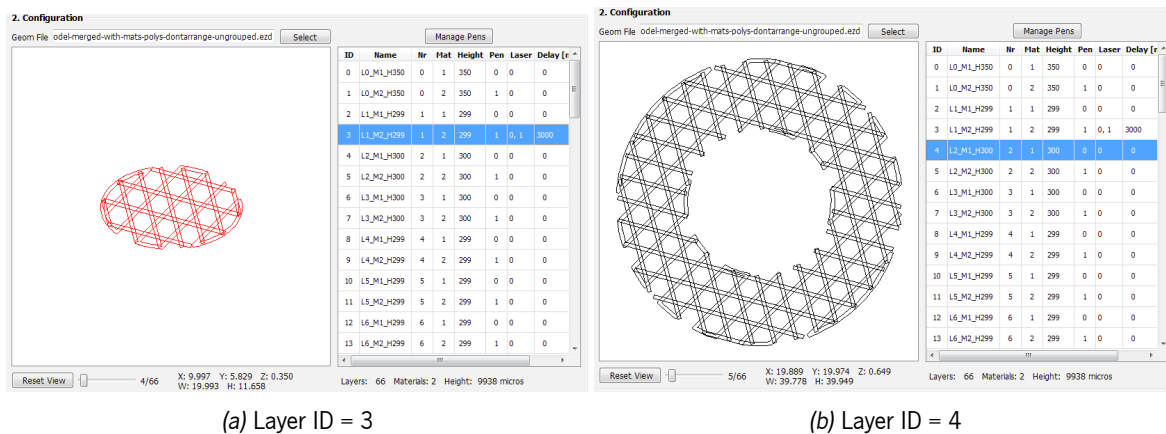


Figure 52: 3DMLPBF Manufacturer: Layer visualisation

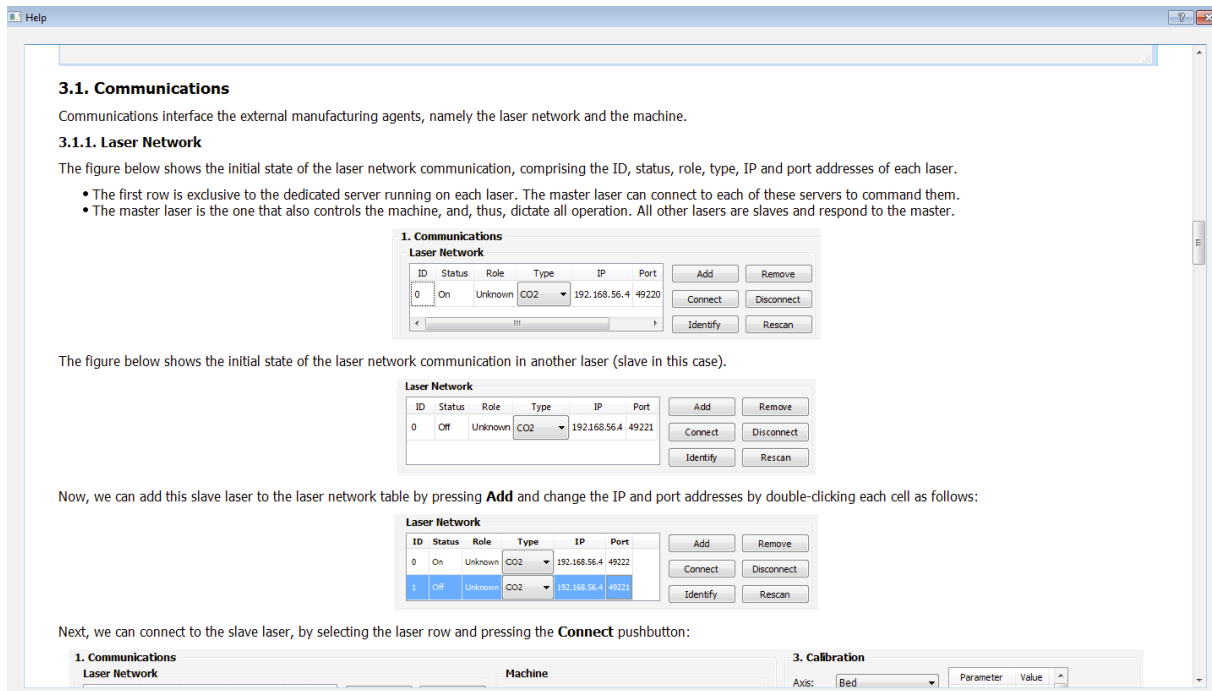


Figure 53: Manufacturer implementation: Help dialog

them to any desired layer (see Fig. 54d). Thus, layers can be mapped independently to different pens, corresponding to different processing parameters, without any correlation to a material or layer number.

Fig. 55 shows the outcome of out-of-range materials or height. Fig. 55a illustrates the 3 cubes model loading, whereas Fig. 55b illustrates the cross and cube model loading. The loading fails, not due to the post-processor inability to process the manufacturing file, but due to printer restrictions: the 3DMLPBF machine can only handle two materials at the moment, and within the available manufacturing volume.

This is a result of the tight coupling between these two software components — post-processor and printer — in an attempt to aid the user from an early stage, as it becomes very frustrating to prepare the component for printing to then see it fail in the printing operation due to materials excess. However, nothing prevents the post-processor and the printer to accommodate more materials or more volumous components, if the 3DMLPBF machine is

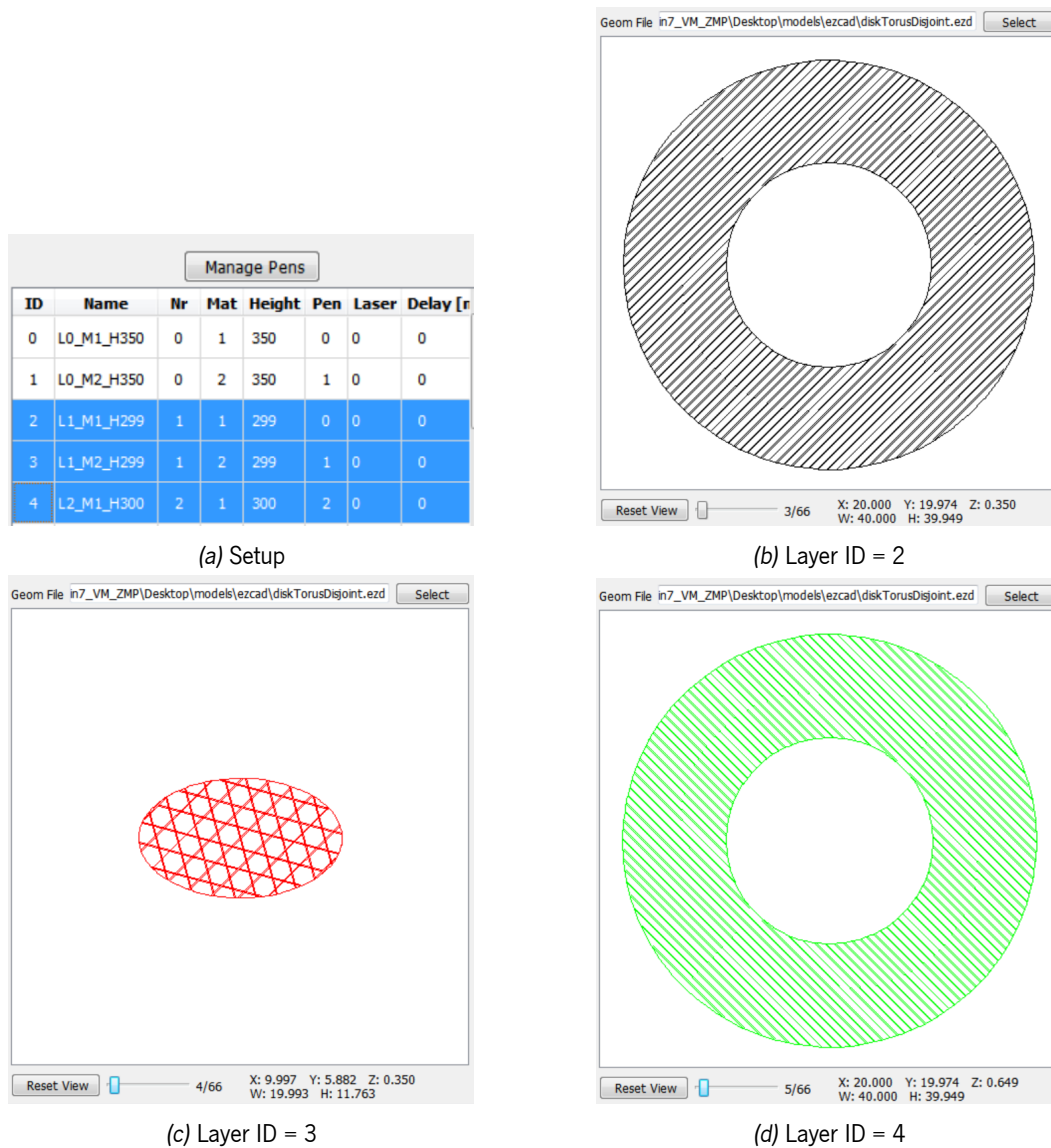


Figure 54: Manufacturer test: process parameters mapping

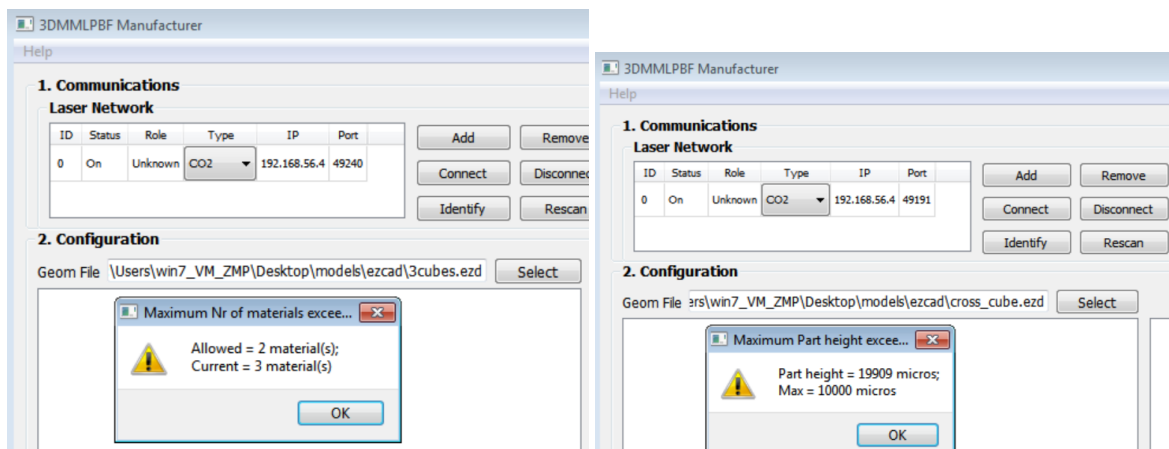
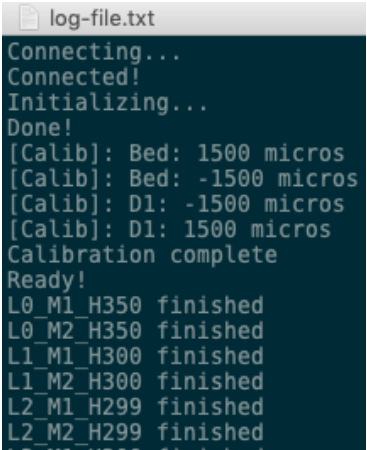


Figure 55: Manufacturer test: materials and height

extended.

Printer The Printer was tested by performing the dry-running of the machine execution in offline mode, i.e., without connecting the microcontroller to the plant (machine), and logging the outcome to file. Stepper motor movement and mechanical endstops triggering are simulated by an appropriate estimated time and laser actuation is signalled to the log file directly. This enabled the quick debug of several models printing, testing: communication protocol, message passing, thread execution and program's logic. An excerpt of a log file is presented in Fig. 56.



```

log-file.txt
Connecting...
Connected!
Initializing...
Done!
[Calib]: Bed: 1500 micros
[Calib]: Bed: -1500 micros
[Calib]: D1: -1500 micros
[Calib]: D1: 1500 micros
Calibration complete
Ready!
L0_M1_H350 finished
L0_M2_H350 finished
L1_M1_H300 finished
L1_M2_H300 finished
L2_M1_H299 finished
L2_M2_H299 finished

```

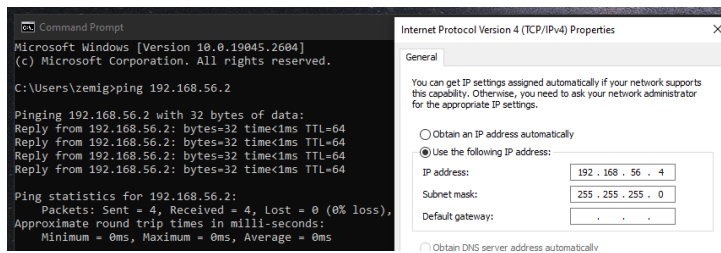
Figure 56: Printer log file (excerpt)

Laser connection The master – slave connection was tested for one slave (Fig. 57) or multiple slaves simultaneously (Fig. 58). Fig. 57 illustrates the connection procedure: first the network needs to be configured; then the Master tries to connect to the slave laser; if the connection is accepted by the slave, then both nodes print to the console informative messages. Additionally, the Master system reminds the User that the same geometry file needs to be uploaded to the slave system and the pens need to be configured accordingly, although they don't need to match the Master's system pens. In fact, if the laser type is different, it is usually recommended to modify its marking parameters (pens).

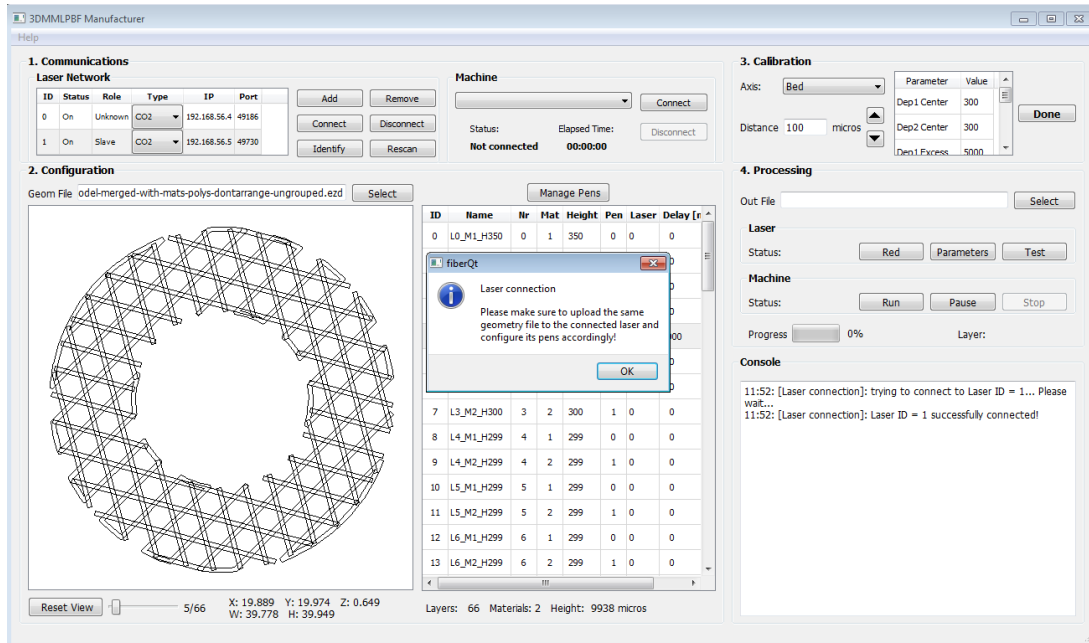
Fig. 58 shows that the Master system can connect to multiple slave lasers simultaneously. Thus, the technical obstacle is not from the software, but from the spatial arrangement of the lasers over the printing bed, which is specially true for the lasers with bulky scanning heads.

Exporting Data Fig. 59 illustrates the Manufacturer's data export options and an example. The User can export the layers, pens, or all manufacturing information (Fig. 59a). A text file will be generated containing the respective data (Fig. 59b). Comments start with the % character and are used to provide additional context to the User. Fig. 59b shows the manufacturing information's generated file, containing all the layers and pens used for manufacturing, which can be later imported by the Post-Manufacturer's software.

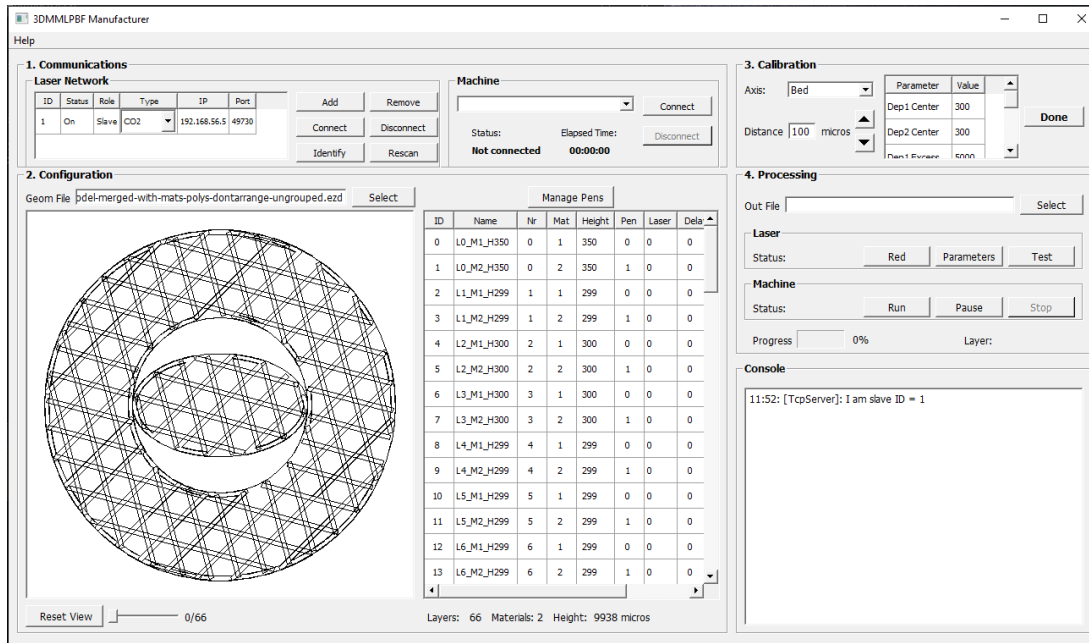
Validation The tests performed validated the Manufacturer's application in compliance with the defined requirements. The Post-Processor maps the geometrical and topological data to process parameters using pens. The Printer handles the actual manufacturing: manages communications, drives the process, and allows



(a) Network configuration

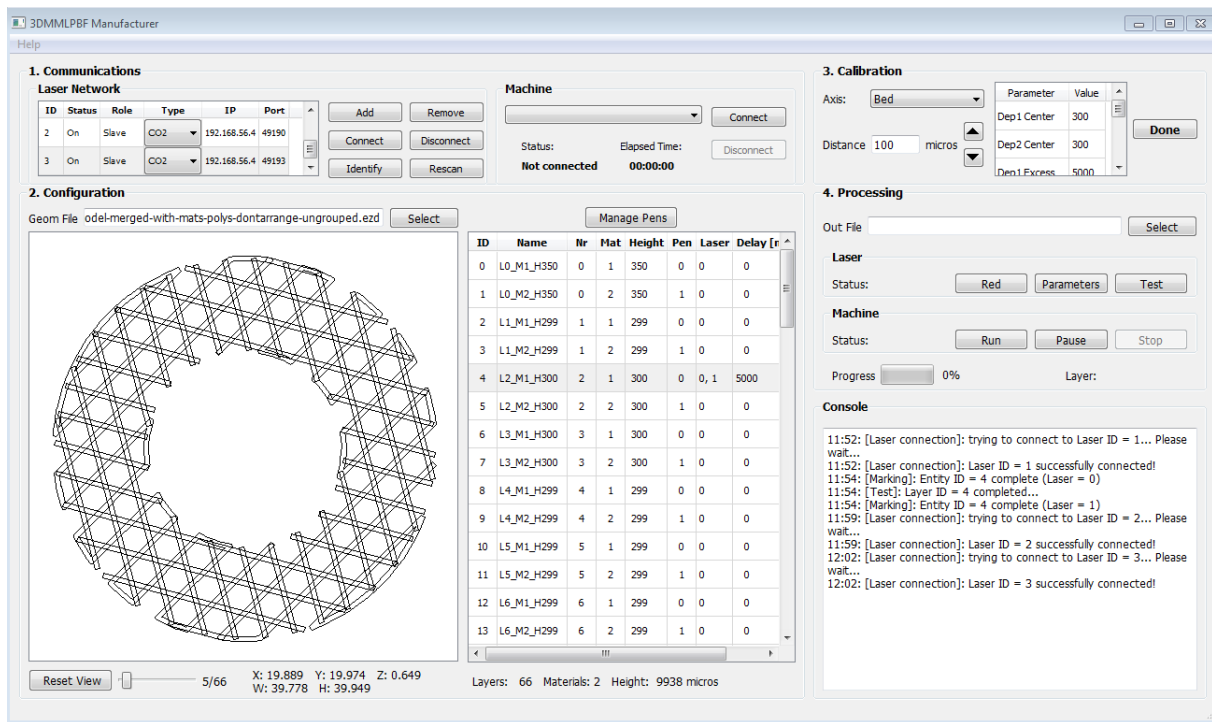


(b) Master tries to connect to slave

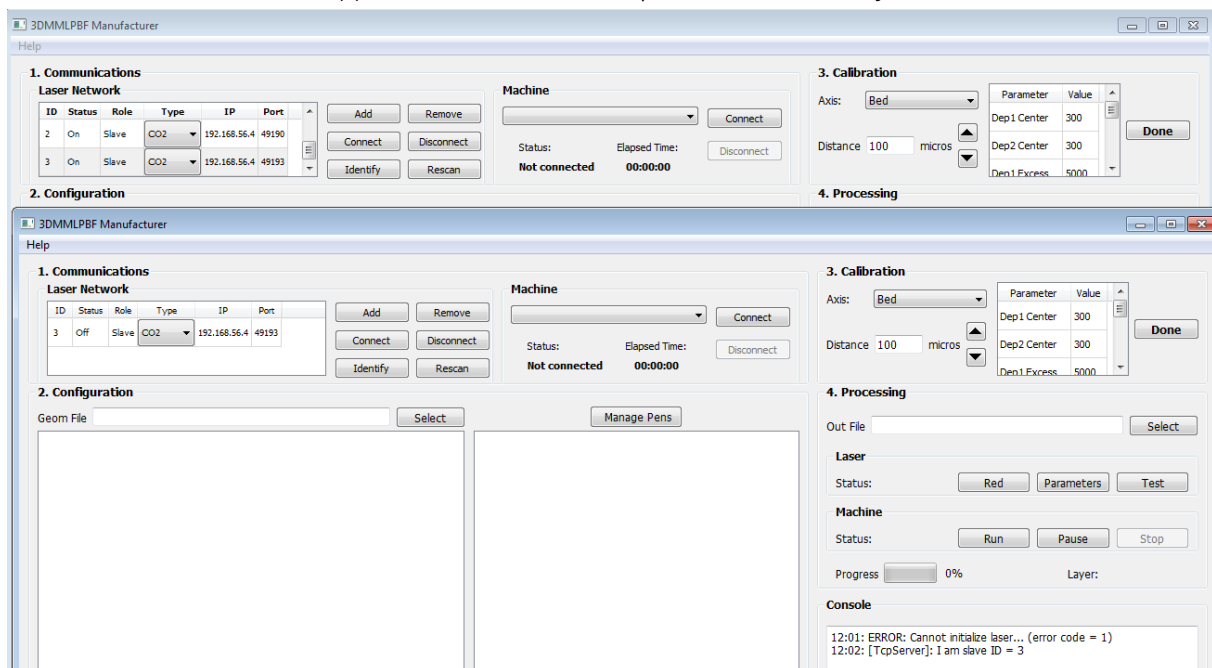


(c) Slave accepts connection

Figure 57: 3DMMLPBF Laser connection testing: Master/Slave connection



(a) Master can connect to multiple slaves simultaneously



(b) Slave accepts connection

Figure 58: 3DMMLPBF Laser connection testing: simultaneous connection to multiple slaves

the data export for posterior analysis. Furthermore, the multi-material concept is materialized at the processing level, via the Post-Processor, and at the manufacturing level by the equipment and the multiple lasers that can be coordinated by the Printer. The software is available online [170] (see Fig. 60) and released under the AGPL v3 licence.

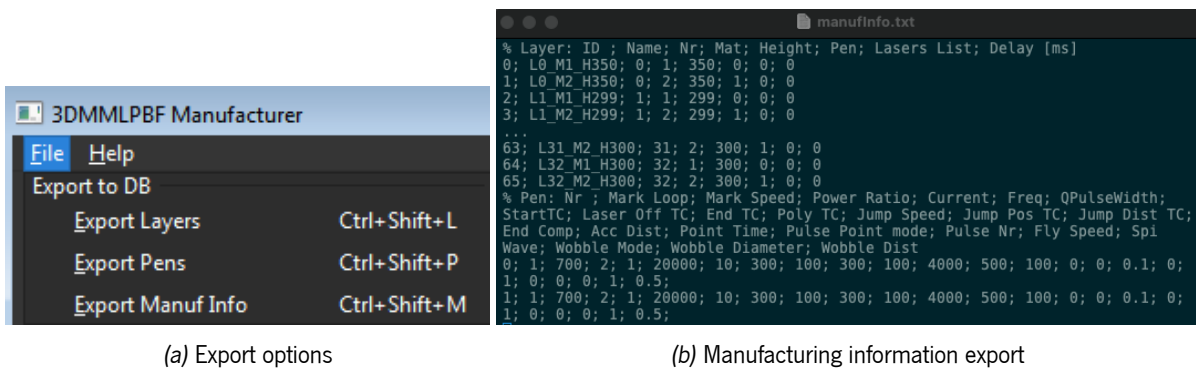


Figure 59: Manufacturer test: Export data

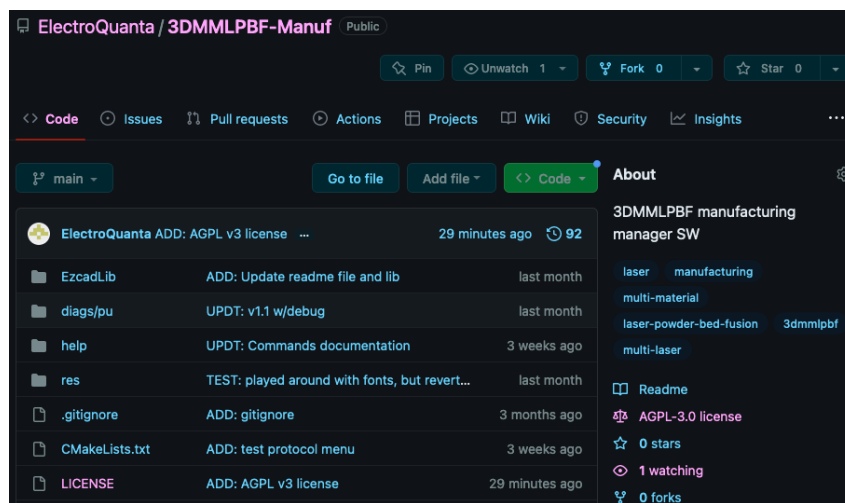


Figure 60: 3DMMLPBF Manufacturer repository [170]

4.3.3 Post-manufacturer

The post-manufacturer goal is to feedback the relevant information to all agents in the manufacturing field, such as, process, material, manufacturing paths, mechanical tests performed and mechanical properties, among others.

As aforementioned, this information can be used to optimize the manufacturing chain, increasing the manufactured part quality through the test and analysis of process's behaviour using design of experiments, the formulation of heuristics and guidelines, and toolchain and equipment improvements.

The post-manufacturer software development is described next.

4.3.3.1 Requirements & Constraints

The main **requirements** identified for the post-manufacturer software and their priority are as follows:

- *High priority*: Store and retrieve information about the relevant manufacturing chain entities in the form of a process knowledge database.
- *High priority*: Add, edit and remove the entities' related information.
- *Medium priority*: Ease the information feedforward and feedback, providing import and export options of process files and databases.

- *Low priority:* Display models information in a straightforward way

The main **constraints** identified and their priority are as follows:

- *High priority:* Open-source solution.
- *High priority:* Ease of use through an **GUI** (not only power users will use this).
- *Medium priority:* Scalable solution.
- *Medium priority:* Cross-platform.

4.3.3.2 Analysis

As established by the requirements, a manufacturing chain database must be implemented and managed. A **Database Management System (DBMS)** is a software designed to assist in maintaining and utilizing large collections of data. A **Relational Database Management System (RDBMS)** is a subset of **DBMS** with relationship between tables (entities) and rows (entities' attributes). The tables are related to each other using primary and foreign keys. It is the most used database model widely used by enterprises and developers for storing complex and huge amounts of data [171]. Some examples of **RDBMSs** are Oracle Database, MySQL, IBM DB2, SQLite, PostgreSQL, and MariaDB.

Entity-Relationship model The **Entity-Relationship (ER)** data model enables the description of the data involved in a real-world enterprise in terms of entities and their relationships and is widely used to develop an initial database design. The key concepts for this database design modeling tool are [171]: the entity — an object in the real world; the entity set — a collection of entities; the attributes describing an entity; the domain — the set of values for each attribute; the relationship — association between two entities; and the key — minimal set of attributes whose values uniquely identify an entity in a set. Keys can be further divided into primary — if they identify an entity in the table they belong — and foreign — if they are used to identify entities in another table.

The **ERDs** use a graphical conventional to quickly and clearly depict the entities involved and how they relate to each other. In a **ERD** entities are represented by rectangles, attributes by ellipses, and the relationships as lines between entities. In the rectangles and ellipses are placed the names of the different entities and attributes. The relationships have cardinalities — 1 : 1 (one-to-one), 1 : M (one-to-many), and M : N (many-to-many) — and may be mandatory or optional.

Selection of the RDBMS The most relevant **RDBMSs** are [172] Oracle Database, Microsoft SQL Server, MySQL, SQLite. The first two, although very advanced, are proprietary and costly solutions, and, thus, were excluded. MySQL is a free, open-source RDBMS solution that Oracle owns and manages. Even though it's freeware, MySQL benefits from frequent security and features updates. Large enterprises can upgrade to paid versions of MySQL to benefit from additional features and user support. SQLite is a C-language library that implements a small, fast, self-contained SQL database engine — an embedded **Database (DB)** — which means the **DB** engine runs as a part of the app. Despite all these advantages, SQLite is not easily scalable and cannot be customized, lacking user management and security features. Thus, MySQL became the obvious **RDBMS's** solution.

Structured Query Language (SQL) Ideally, a database language allows the creation of a database and table structures, the execution of basic data management tasks (add, delete, and modify), and the execution of complex queries designed to transform the raw data into useful information. Moreover, it must provide a clear and easy syntax, it must be portable and conform to some basic standard. [Structured Query Language \(SQL\)](#) complies well to these requirements [173].

SQL functions fit into two broad categories [173]:

1. *Data Definition Language (DDL)*: it includes commands to create database objects such as tables, indexes, and views, as well as commands to define access rights to those database objects.
2. *Data Manipulation Language (DML)*: it includes commands to insert, update, delete, and retrieve data within the database tables

MySQL Interfaces MySQL works under the client–server paradigm. It has several client interfaces that can interact with the server, through connectors and [APIs](#), i.e., the drivers and libraries that one can use to connect applications in different programming languages to MySQL database servers. The application and database server can be on the same machine, or communicate across the network [174]. The following interfaces are available: Java, Python, JavaScript, C++, C, C#, PHP, ODBC, NBD Cluster, MySQL Shell, and X DevAPI.

From the list of available interfaces, the most well suited to interface the [RDBMS](#) are the [C API](#) and the [C++ connector](#), as they are they provide better performance. The [C++ connector](#) was chosen for compatibility with the toolchain devised. It is licenced under the GPL with the FLOSS License Exception.

4.3.3.3 Design

The first step of the databases' design is the identification of the database entities, following the relational database model and the entity-relationship design model. Fig. 61 shows the resulting [ERD](#), containing the most relevant entities and the relationships between them, namely: manufactured parts and models, the original 3D models, mechanical tests performed, mechanical properties of the manufactured part, process paths and parameters (pen), material, layers and laser information. For example, a `Part` can be manufactured by different lasers, it has only a `3DModel` (containing multiple `STL` files) and only a `ManufModel` (with only a `SVG` file), and can have multiple mechanical tests performed over it.

Then, following the analysis phase's considerations, the software architecture was devised. Fig. 62 illustrates the deployment diagram with the software components and the interactions between them, mapped to the target [Hardware \(HW\)](#) node. The `User` interacts with `AppManager` through the `UI` which handles user requests and updates the `UI` accordingly. Database requests are managed through `DB Manager`, querying the [RDBMS](#) (`DB server`) and handling database responses. This follows a client-server architecture with the communications performed through the [TCP/IP](#) protocol using a known socket, running on the same device (host device). Thanks to this distributed architecture, the server, which only handles database requests, can be implemented as a daemon, minimising resources usage. Furthermore, this enables quick deployment of local databases, without the hassle of setting up remote storage. As a drawback, it limits the scalability and availability of the database, although a centralised local database can be set up.

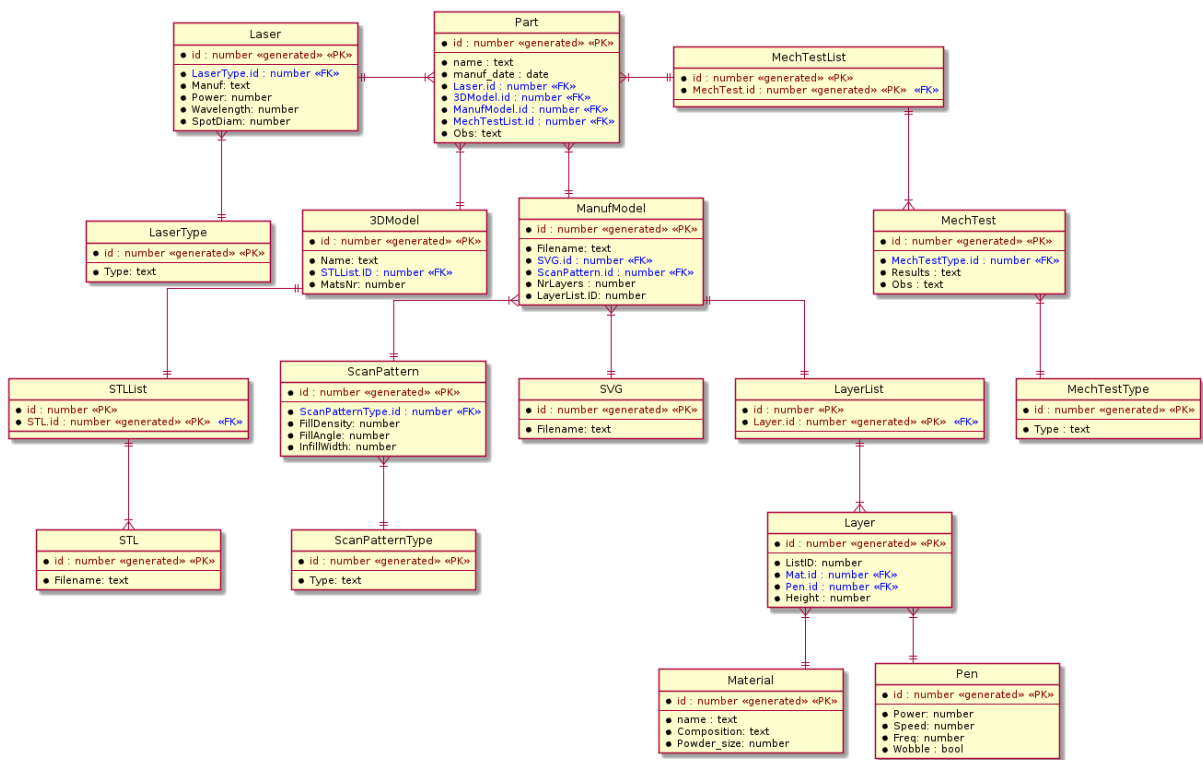


Figure 61: 3DMMLPBF Post-Manufacturer design: ERD

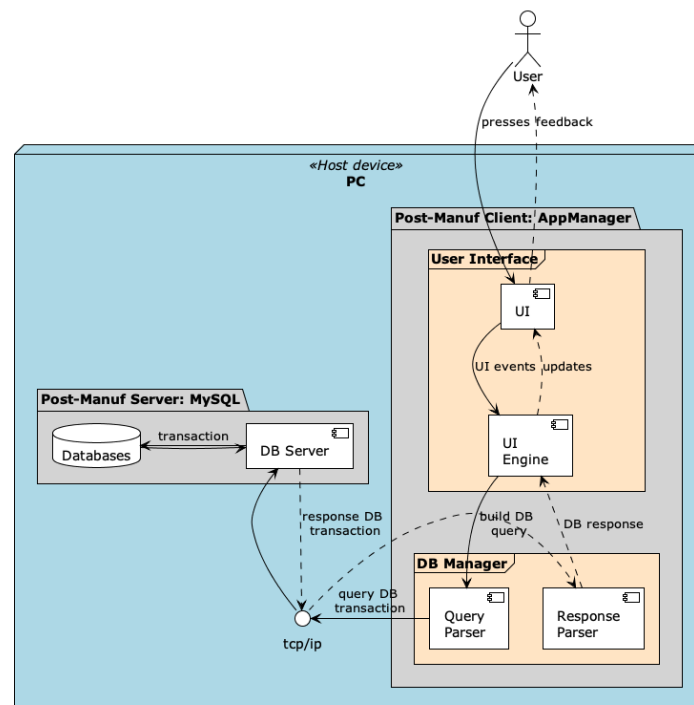


Figure 62: 3DMMLPBF Post-Manufacturer design: Deployment diagram

4.3.3.4 Implementation

Following the deployment diagram (Fig. 62), the post-manufacturer was implemented in a cross-platform framework with an open-source licence — Qt, using the C++ connector interface aforementioned to manage database transactions.

The database was created using a script. An excerpt of the database script initialisation is illustrated in Listing 4.4 for the Part entity.

Listing 4.4: Script to create the database: excerpt with the Part entity

```

1  /*PART */
2  CREATE TABLE Part(
3  id int AUTO_INCREMENT,
4  name varchar(100),
5  manif_date date,
6  Laser_id int,
7  model3D_id int,
8  manifModel_id int,
9  mechTestList_id int,
10 obs varchar(100),
11 PRIMARY KEY(id),
12 FOREIGN KEY(Laser_id) REFERENCES Laser(id) ON DELETE CASCADE,
13 FOREIGN KEY(model3D_id) REFERENCES model3D(id) ON DELETE CASCADE,
14 FOREIGN KEY(manifModel_id) REFERENCES manifModel(id) ON DELETE CASCADE,
15 FOREIGN KEY(mechTestList_id) REFERENCES mechTestList(id) ON DELETE CASCADE);

```

Fig. 63 illustrates the Post-Manufacturer GUI for the Part and Manufacturing model views. The top-level entities are shown as the top tabs, namely part, 3D model, manufacturing model, laser, and mechanical tests. In the former the User can visualise Part related information, manage database entries, update or export the database. The latter, comprises the model, the scan pattern, its layers and the associated materials and pens. The manufacturing model can be loaded and previewed, alongside with the manufacturing output file (the output from the equipment). All databases can be exported separately for appropriate handling by each process' agent.

4.3.3.5 Testing and validation

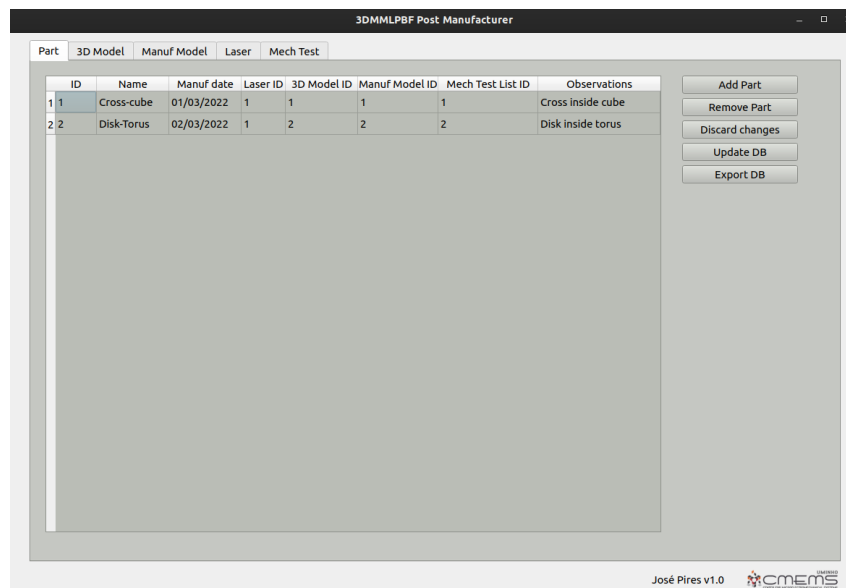
After each successful manufacturing run, the Printer writes the relevant process information to log files, namely layers and pens. These files can then be imported by the Post-Manufacturer for quick and error-prone database filling. Listing 4.5 and Listing 4.6 illustrate the manufacturing output files for layers and pens, respectively. The first line contains a comment, indicating the correspondence between tags and values. The remaining of the file consists of a comma-separated list of values, with each database entry belonging to an individual line.

Listing 4.5: Manufacturing output file: Layers

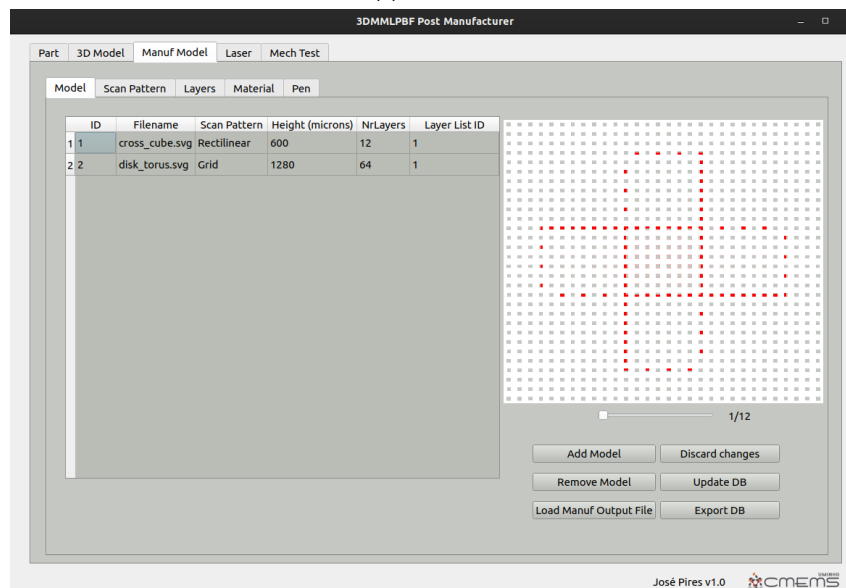
```

1  % Layer, Material, Height, Pen
2  0, 1, 50, 0
3  0, 2, 50, 1
4  1, 1, 50, 2
5  1, 2, 50, 3
6  2, 1, 50, 2
7  2, 2, 50, 3

```



(a) Part view



(b) Manufacturing model view

Figure 63: 3DMMLPBF Post-Manufacturer

```

8 3, 1, 50, 2
9 3, 2, 50, 3
10 4, 1, 50, 2
11 4, 2, 50, 3
12 5, 1, 50, 0
13 5, 2, 50, 1

```

Listing 4.6: Manufacturing output file: Pens

```

1 % Nr, Mark Loop, Freq, Speed, Power Ratio, Wobble Mode
2 0, 1, 20000, 1200, 50, 0
3 1, 1, 20000, 1400, 30, 0

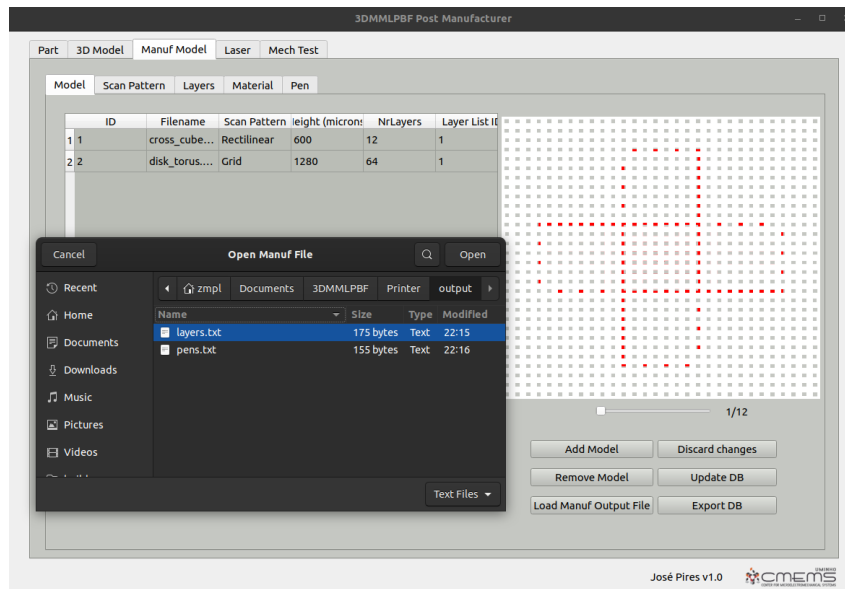
```

```

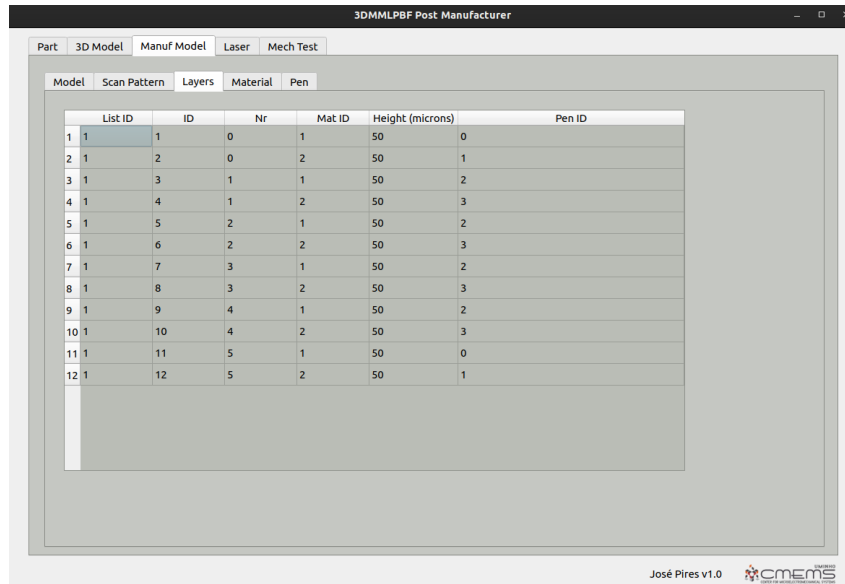
4 | 2, 1, 20000, 850, 45, 0
5 | 3, 1, 20000, 1000, 25, 0

```

Fig. 64 showcases a manufacturing output file import, namely layers, although both could be loaded simultaneously. After selecting the file and acknowledging it, the file is successfully loaded and fills the Layers view, which can be saved to the database by the User.



(a) Select files to load



(b) result example: layers loaded

Figure 64: 3DMMLPBF Post-Manufacturer testing: load output file

The same principle applies for the 3D models (.stl) and manufacturing (.svg) files. However, for this case, the User must fill in the information manually. This software component is also capable of previewing models' geometry, as illustrated in Fig 63, for the manufacturing model.

Lastly, an User may wish to export the database for data mining, analysis, DOE or to share it other users.

Thus, this functionality was tested by selecting the Export DB pushbutton (Fig. 65) with the result being shown in Listing 4.7. As expected, the database can be successfully exported.

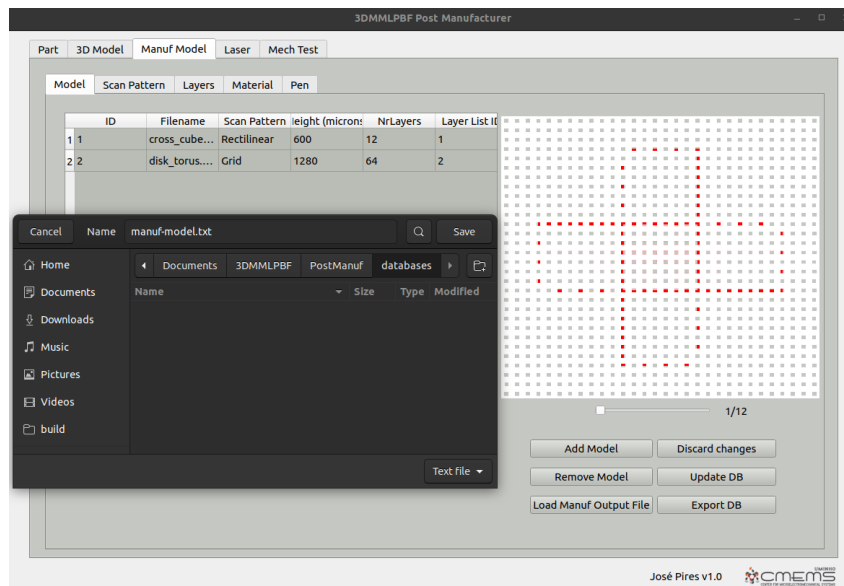


Figure 65: 3DMMLPBF Post-Manufacturer testing: Export database

Listing 4.7: Database export: Manufacturing model

```

1  % Manuf Model
2  # Model
3  1, cross_cube.svg, 2, 600, 12, 1
4  2, disk_torus.svg, 4, 1280, 64, 2
5  # Layer
6  1, 1, 0, 1, 50, 0
7  1, 2, 0, 2, 50, 1
8  1, 3, 1, 1, 50, 2
9  1, 4, 1, 2, 50, 2
10 1, 5, 2, 1, 50, 2
11 1, 6, 2, 2, 50, 3
12 1, 7, 3, 1, 50, 2
13 1, 8, 3, 2, 50, 3
14 1, 9, 4, 1, 50, 2
15 1, 10, 4, 2, 50, 3
16 1, 11, 5, 1, 50, 0
17 1, 12, 5, 2, 50, 1
18 # Pen
19 0, 1, 20000, 1200, 50, 0
20 1, 1, 20000, 1400, 30, 0
21 2, 1, 20000, 850, 45, 0
22 3, 1, 20000, 1000, 25, 0
23 # Material
24 1, matA, Al20Cu80, 50
25 2, matB, Cu20Al80, 50
26 # Scan Pattern
27 1, 2, 50, 45, 50
28 2, 4, 50, 45, 50
29 # Scan Pattern Type

```

```

30 1, Aligned Rectilinear
31 2, Rectilinear
32 3, Honeycomb
33 4, Grid

```

Validation The Post-Manufacturer software is able to manage the different information flow stemming from the whole manufacturing chain in a convenient and efficient manner. The software is available online [175] (see Fig. 66) and released under the AGPL v3 licence.

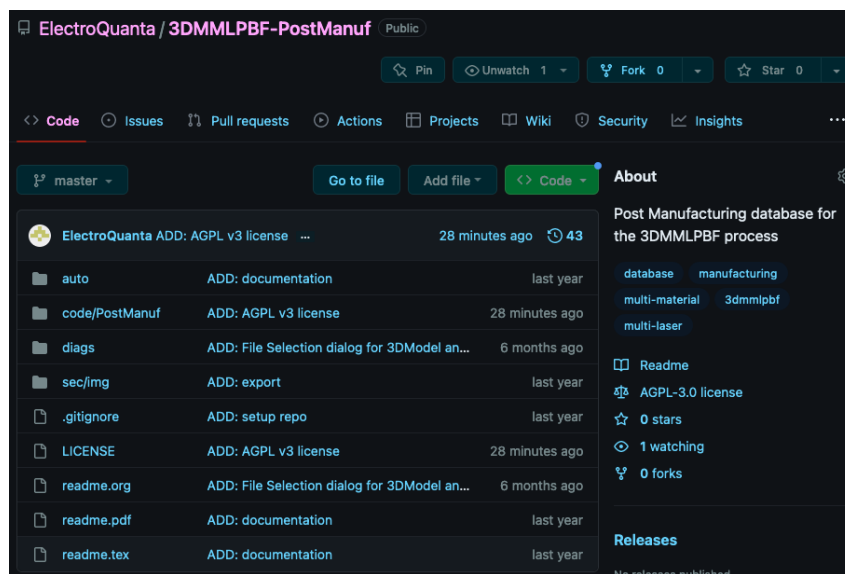


Figure 66: 3DMMLPBF Post-Manufacturer repository [175]

4.4 Development of the 3DMMLPBF machine

The development of the 3DMMLPBF machine is based on the VDI-2206 guideline, more specifically the V-model macro cycle, comprising the following phases: requirements elicitation, system design, domain-specific design, system integration, verification/validation and modeling and model analysis.

4.4.1 Requirements & Constraints

Table 7 lists the overall system requirements and constraints for the 3DMMLPBF machine. The requirements are divided into functional ones — directly related to the machine’s functionalities — and non-functional ones — describing the properties of the system. On the other hand, the constraints are divided into technical and non-technical ones.

The requirements are as follows:

- **Manufacturing of 3D multi-material parts according to the specifications:** the machine must correctly interpret the manufacturing instructions and actuate accordingly;
- **Laser control:** the laser motion must be accurately managed to produce the indicated manufactured trajectories with the designated process parameters;

Table 7: Requirements and constraints for the 3DMMLPBF machine

	Functional/Technical	Non-Functional/Non-technical
Requirements	<ul style="list-style-type: none"> - Production of 3D multi-material parts according to the specifications - Control of laser trajectories with appropriate parameters - Control of all machine's movements - Material feeding and recovery management - Temperature's control - Atmosphere's control 	<ul style="list-style-type: none"> - Robust structure - Safe - Friendly UI
Constraints	<ul style="list-style-type: none"> - The EzCAD API is required for laser control - The Windows development platform is required for compliance with the EzCAD API 	<ul style="list-style-type: none"> - Limited budget - Limited time - Limited manpower

- **Motion control:** the positioning and motion of the moving elements of the machine must be properly handled for accurate part production and minimisation of induced efforts on mechanical components;
- **Material feeding and recovery management:** the powder needs to be delivered in a evenly and controlled way to the building area. Furthermore, the powder from one material needs to be recovered and handled properly, before introducing powder from a new material;
- **Temperature control:** the temperature of the materials' powders in the reservoirs and in the building area must remain within acceptable range;
- **Atmosphere control:** The equipment must provide an inert shielding to prevent oxidation reactions at the part's surface;
- **Robust structure:** the machine should sustain the imposed efforts and the surrounding environment;
- **Safety:** in case of an equipment's failure, the manufacturing process must stop immediately and communicate it to the user. Additionally, protective enclosure for laser radiation should be installed;
- **Friendly user interface:** the interface between the user and the machine should provide meaningful information for machine operation and guidance in case of errors.

The constraints are as follows:

- **Laser control:** the proprietary software for laser control must be used, through its [API](#));
- **Software development platform:** for compliance with the laser control [API](#), the *Windows* platform was considered for the development of machine's control and interface software components.
- **Limited resources:** budget, time, and manpower are very limited.

4.4.2 System design

The 3DMMLPBF system was designed by identifying the overall function of the system and dividing it into sub-functions with suitable working principles. Thus, a working principle for the machine was defined, similar to the

one of the typical L-PBF machines, but it includes some tweaks for multi-material processing, as supported by the proposed 3DMMLPBF methodology. Fig. 67 illustrates the machine initial state, with the Master system controlling the machine and one laser, and issuing commands to the Slave system that controls the other laser. The working principle is as follows:

1. the printing bed lowers by layer height (Fig. 68);
2. the powder deposit goes up by layer height and the powder is spread by the recoating system to the printing bed; the machine signals the laser that it is ready for laser marking (Fig. 69);
3. each laser marks the scanning paths, and when it finishes, it stops and signals to the Master system the current layer's ID has been completed. When all lasers finished marking, the Master system issues the next 1code instruction (Fig. 70);
4. the machine proceeds with the 1code instructions processing: if a new material is needed, the powder is recovered via powder recovery system (Fig. 71) and a new material is fetched from the respective reservoir and fed to the printing bed; the machine signals the laser that is ready for marking;
5. the process is repeated for each new layer and for each new material in a layer until the *End-of-File* is reached.

Additionally, the temperature and the shielding must be controlled for adequate manufacturing.

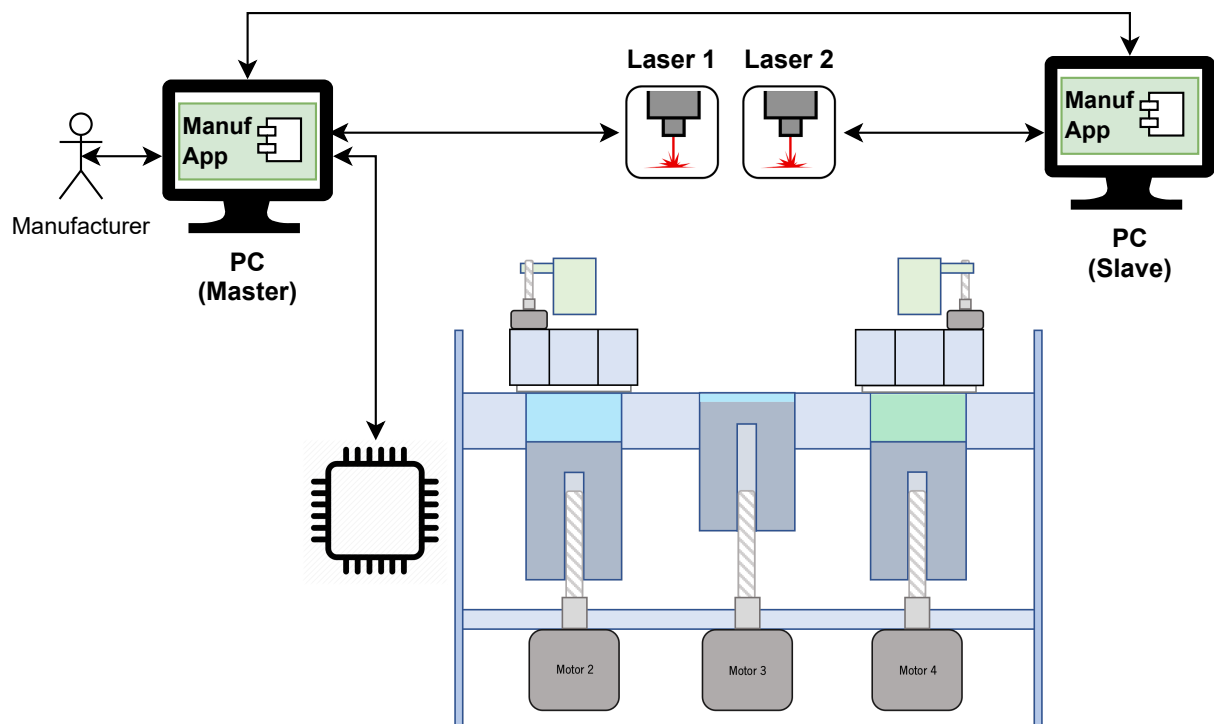


Figure 67: Working principle of the 3DMMLPBF machine: initial state

After defining the working principle, it is possible to identify the main subsystems responsible for the corresponding sub-functions:

- **Axis subsystem:** responsible for controlling the movement of the moving axes;

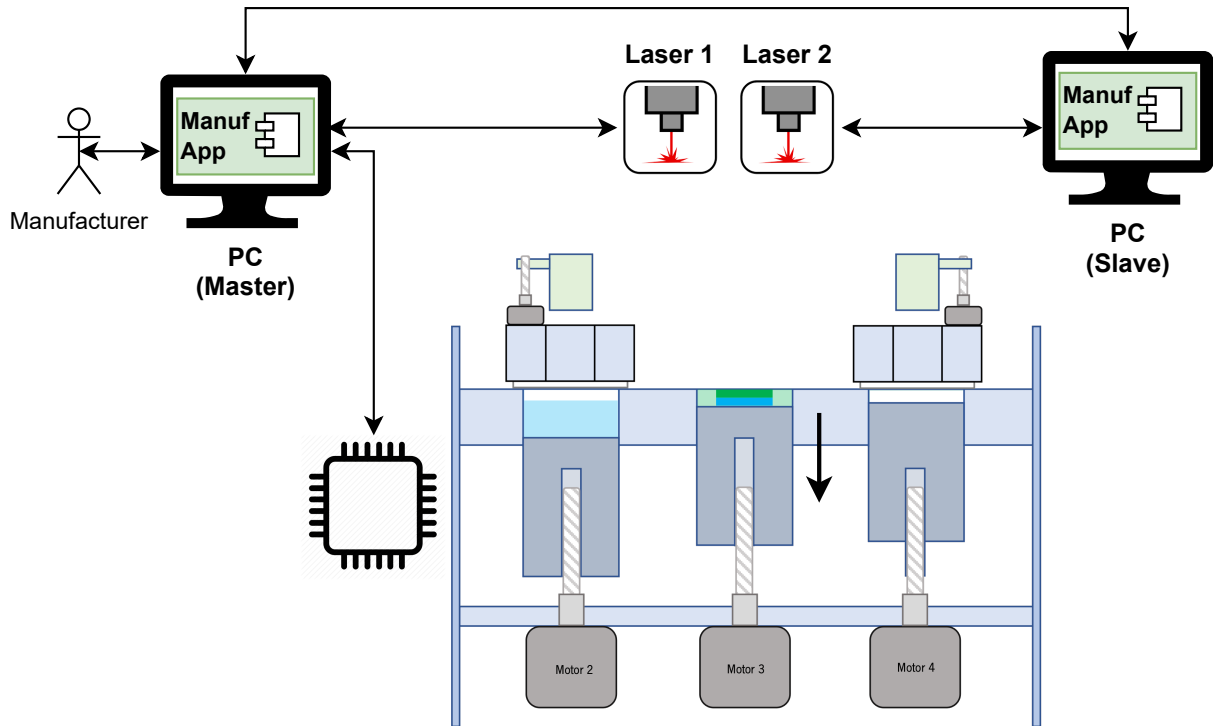


Figure 68: Working principle of the 3DMMLPBF machine: bed drops

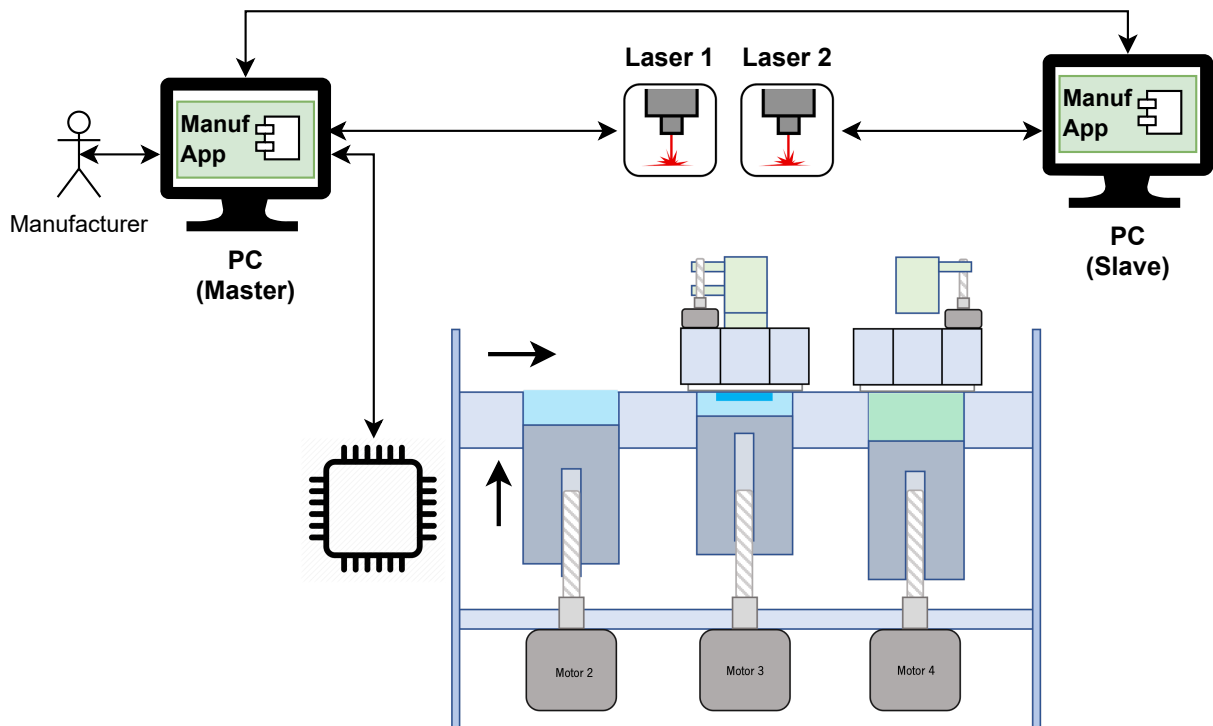


Figure 69: Working principle of the 3DMMLPBF machine: powder recoating

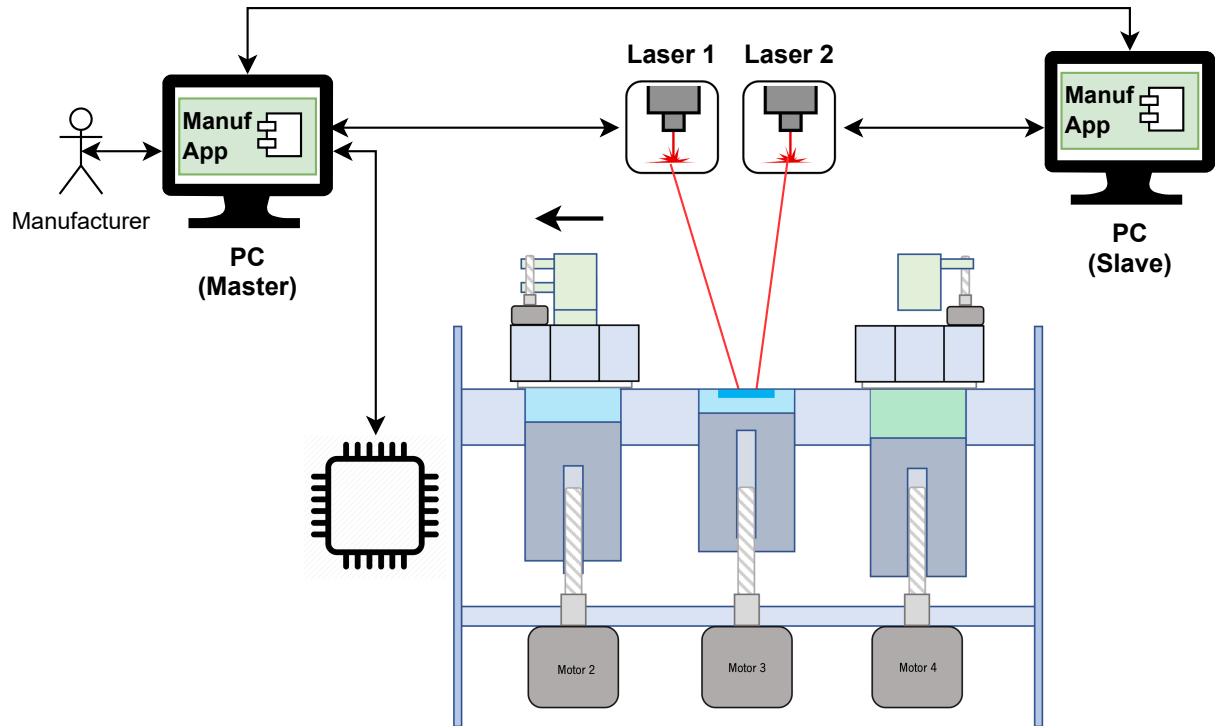


Figure 70: Working principle of the 3DMMLPBF machine: laser marking

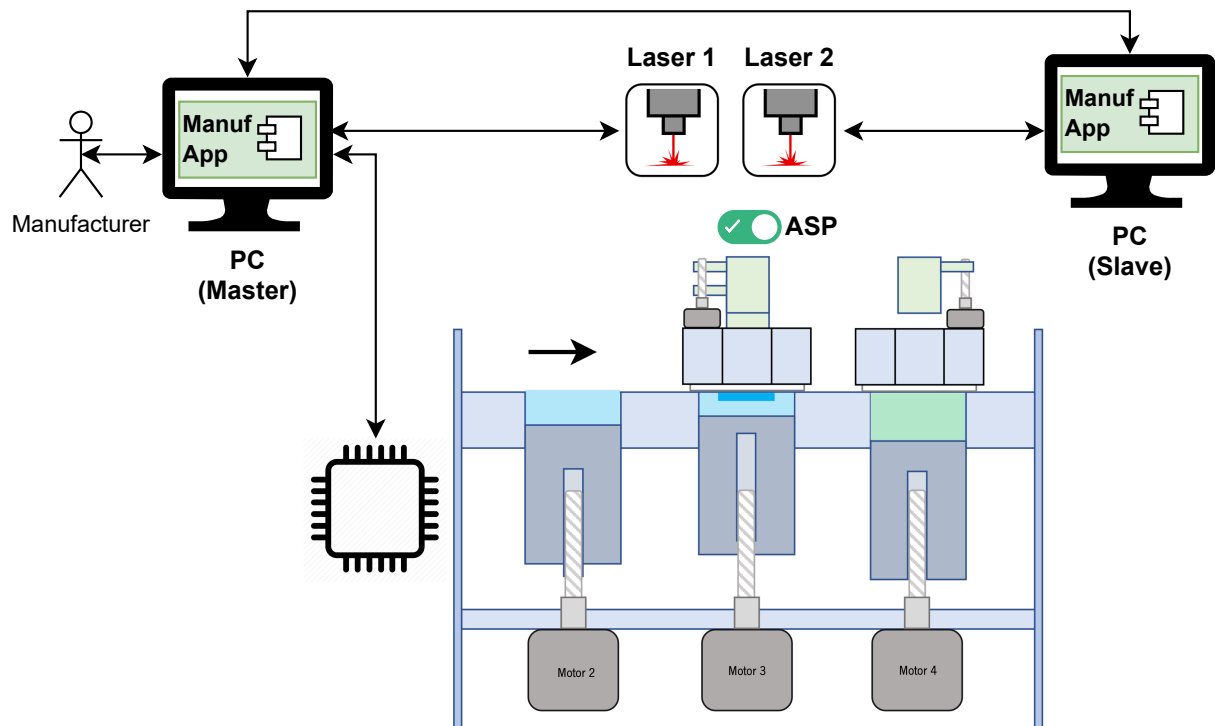


Figure 71: Working principle of the 3DMMLPBF machine: powder recovery

- **Heating subsystem:** responsible for heating the printing bed and the powder reservoirs;
- **Shielding control subsystem:** responsible for controlling the machine's internal shielding;
- **Powder recovery subsystem:** responsible for proper recovery of the materials' powders;

Likewise, although no hardware is necessary to be designed, as the laser is controlled directly by software, it is possible to identify the main laser subsystems to be controlled, namely:

- **Beam generator subsystem:** responsible for laser beam generation with the appropriate parameters;
- **Scanning subsystem:** responsible the laser scanning paths, by proper alignment and focusing of the laser beam in the provided locations;
- **Wobble subsystem:** responsible for the fast oscillation of the laser beam for improved 'welding' properties;

These subsystems can then be instantiated to form the global system as indicated in Fig. 72. In fact, by identifying general functions/behaviour enclosed in general subsystems, it is possible to abstract these subsystems and model and simulate them independently, and then cascade the results to the instantiated subsystems. Peek [176] calls this an object-oriented approach to machine design, combining the similar approach available for software development to another one for hardware development, attaining the advantages of such approach on building better, faster, easier, and more flexible, modular machines.

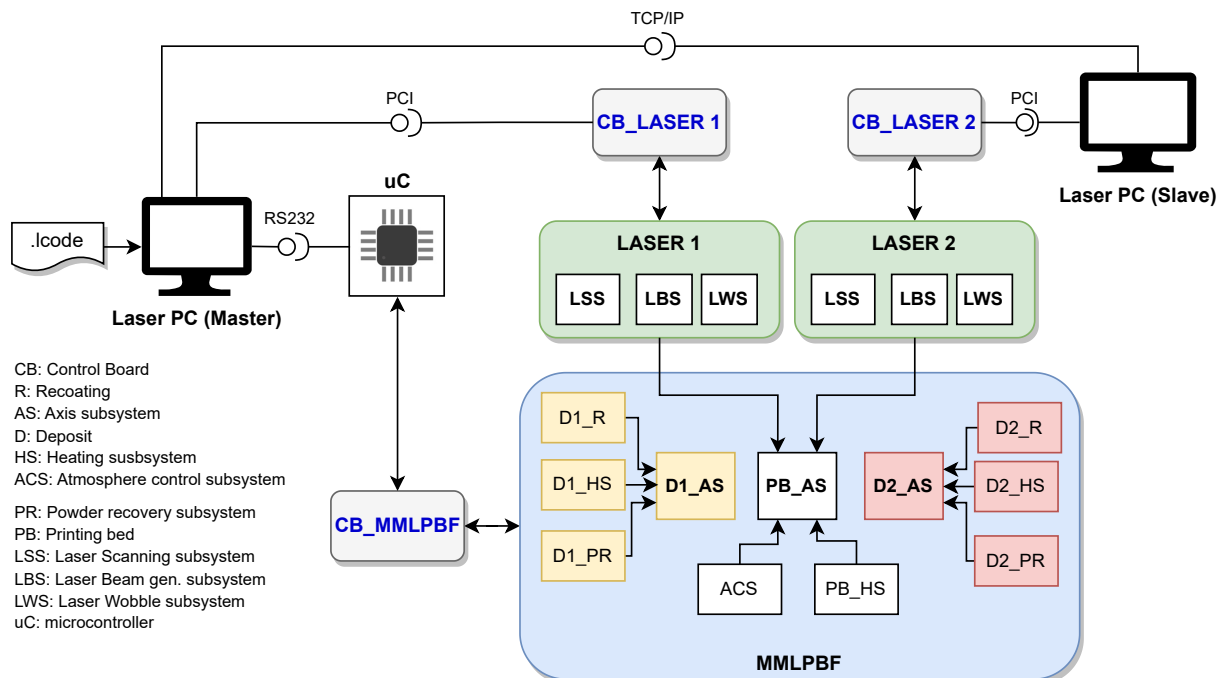


Figure 72: Overview of the 3DMMLPBF system

Fig. 72 illustrates a overview of the 3DMMLPBF system which can be mainly decomposed into the MMLPBF subsystem (in blue) and the Lasers' subsystems (in green). The former is responsible for the multi-material processing in the z-axis, and the latter for the selective laser procedure in the x-y plane. As aforementioned, the lasers can

form a network, and operate independently to handle different materials and achieve different mechanical properties of the produced part.

Also, as previously illustrated in Fig. 49, the master system drives the manufacturing, reading the .1code and issuing commands for its own laser and the 3DMMLPBF machine, as well as for all lasers in the network. The firmware, running on the microcontroller, will be responsible for handling the master system's requests and controlling the equipment.

The MMLPBF subsystem contains three main subsystems, corresponding to the deposits and the powder bed. All these subsystems have individual heating control. The deposits include also recoating and powder recovery subsystems. The powder bed includes also the atmosphere control subsystem.

The Laser subsystem is comprised of a scanning subsystem (LSS), the laser beam generator (LBS) and the wobble subsystems (LWS).

Based on the working principle and the overview of the global system, the machine was 3D modelled in a CAD software namely, Solidworks® (see Fig. 73). This allowed to test the design, by simulating the motions required for the machine to operate and the placement of all the components in an optimised way. The equipment includes: the *powder recoating system* (blue); the *printing bed and powder reservoirs*(green); the *heating elements* (not visible) for bed and reservoirs heating; *powder recovery system* (not depicted) consisting of a vacuum suction system with granulometric sieve; *atmosphere control system* (not depicted) consisting of a pressurised circulation system *actuators*, like motors (in brown); and *sensors* (not depicted) for positioning and temperature measurements.

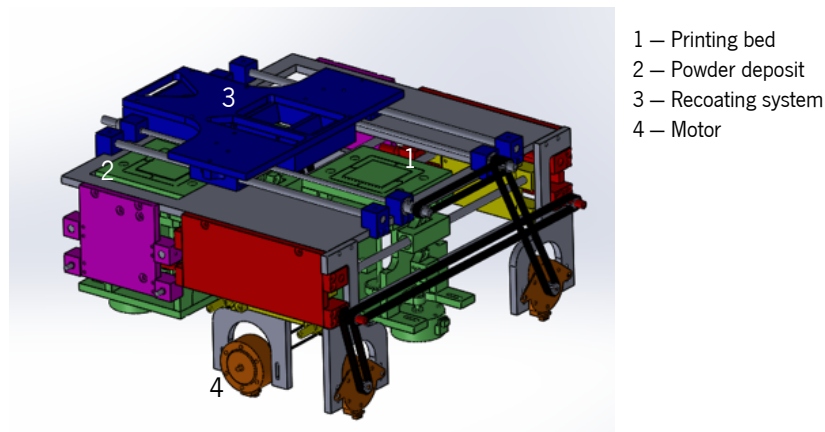


Figure 73: 3D model of the 3DMMLPBF equipment

4.4.3 Domain specific design & Modelling

After finding a viable general solution to the problem, with the architecture of the global system in both mechanical and control terms, the solution concept – developed conjointly in the involved domains – is now detailed separately in those domains, as specialised design and calculations are required to guarantee the functional performance, especially with the critical functions.

4.4.3.1 Mechanical design

The mechanical design was performed by another laboratory staff element, as part of a multidisciplinary project. Here are presented and described the main machine elements for comprehension purposes.

Machine The machine 3D model is illustrated in Fig. 74, with the following dimensions (length x width x height): 560 x 450 x 280 millimeters. There are three deposits: bed — where the part is built; deposits 1 and 2 for the respective materials. The bed default movement direction is down, while the deposits is up. The recoating promotes the powder spreading on the bed in an even and homogeneous fashion thanks to the swipers (see also Fig. 75b). The deposit commutator is responsible for aligning the deposit with the bed for powder feeding from the two available materials. The axes use screws with a thread pitch of 1 millimeter and with anti backlash system to further improve resolution.

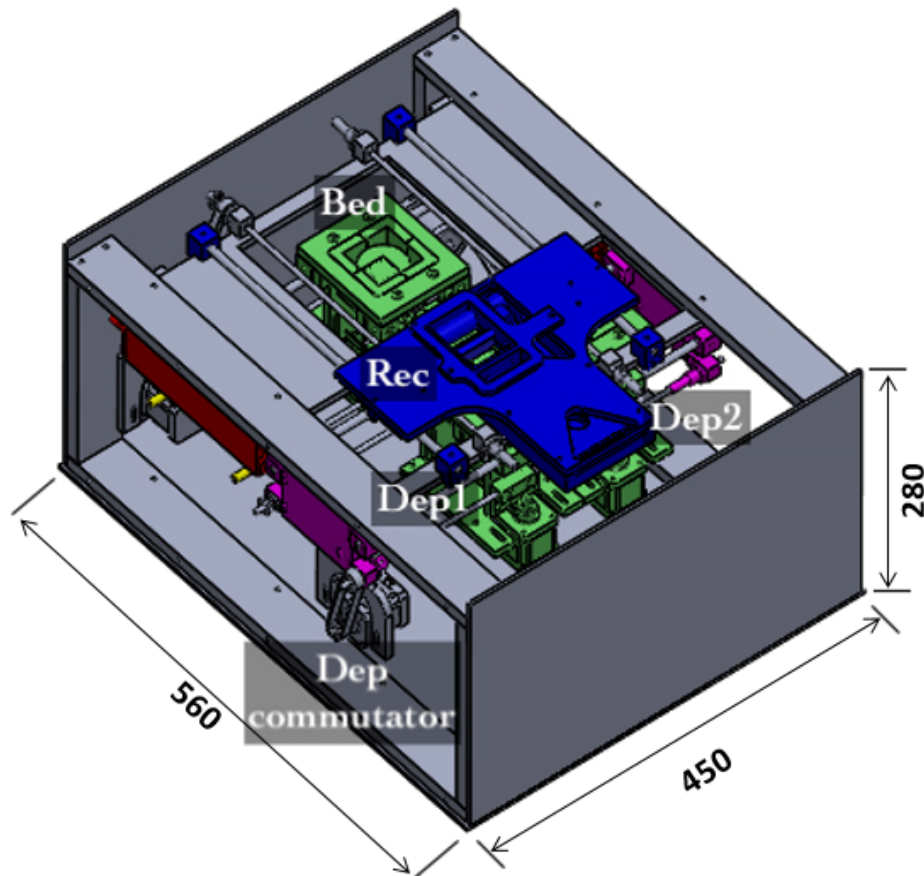


Figure 74: Mechanical design: machine 3D model (final version)

Deposit The deposit 3D model is illustrated in Fig. 75a. The stepper motor drives the transmission belt coupled to the axis, moving it in the defined direction. The powder platform is where the powder effectively lies. Thus, this corresponds to the initial position of the bed deposit and the ultimate final position on the deposits 1 and 2.

Recoating The recoating 3D model is illustrated in Fig. 75b. It uses silicone swipers to spread the powder homogeneously in the bed. It also includes an extraction cyclone for proper connection to the extraction system, adequately removing the material being currently processed if a new one must be added.

Final result After designing, dimensioning and manufacturing the mechanical components indicated in the mechanical design, the subsystems were assembled and integrated in the main system. The final result is presented

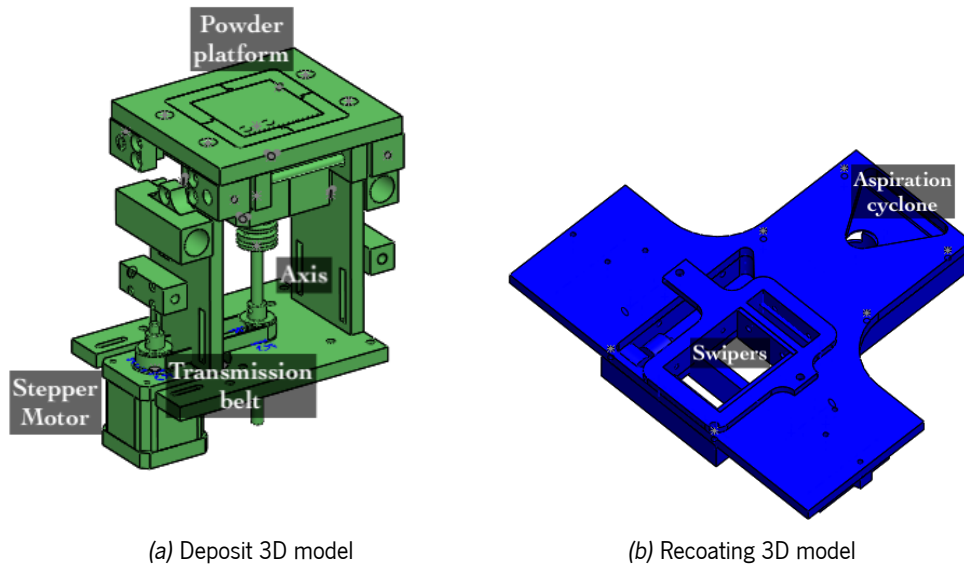


Figure 75: 3DMMLPBF mechanical design: deposit and recoating subsystems

in Fig. 76.

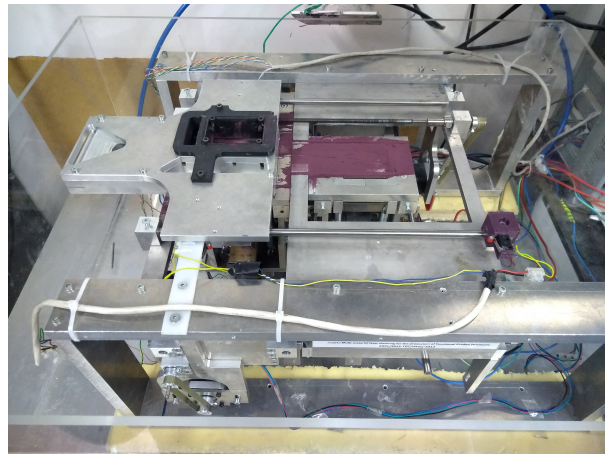


Figure 76: Mechanical design implementation: final result

4.4.3.2 Control design

For the control design, the subsystems were further detailed, represented in terms of the control loop (open or closed-loop), for both main subsystems – MMLPBF and laser – depicted respectively in figs. 77 and 78.

For the MMLPBF subsystem, it can be seen that the axis, heating and shielding control subsystems work in closed loop (although the last one is implicit, i.e., it does not depend on the external signal applied) and the powder recovery system works in open loop, via timed control action.

- In the axis subsystem, the microcontroller sends the desired position to the control board, which compares it to the actual position and updates the position based on the error, issuing a command signal to the stepper motor driver which, in turn, commands the stepper motor that applies torque on the respective axis. The

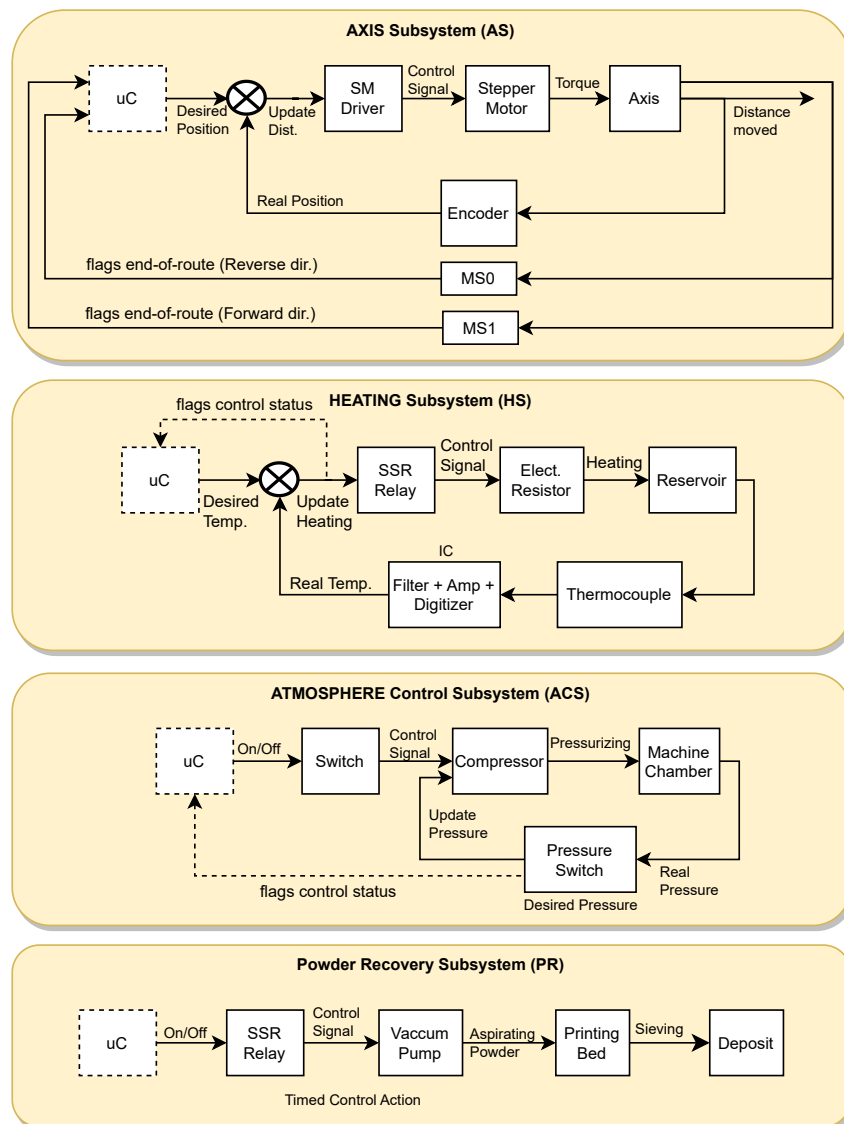
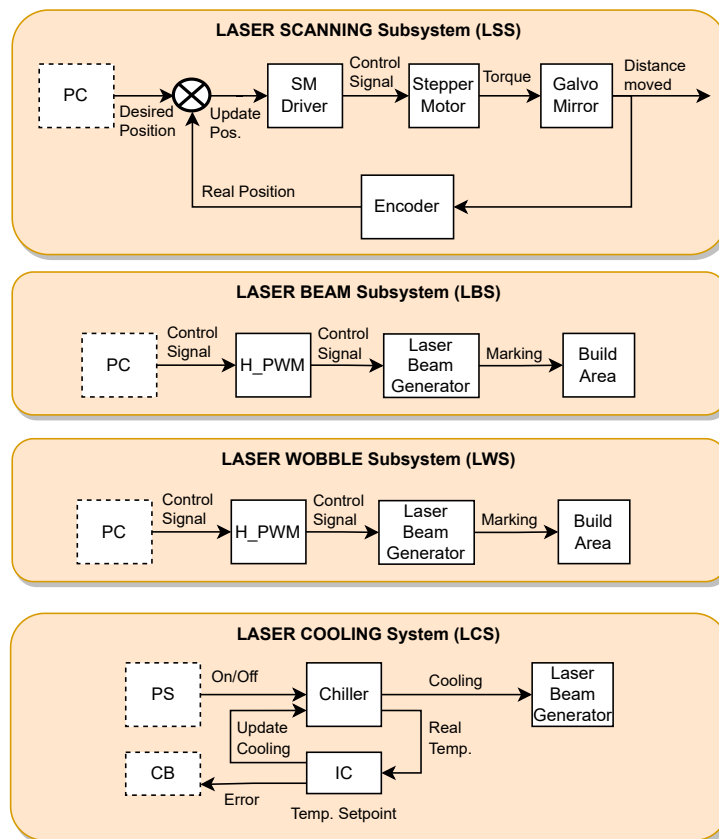


Figure 77: Detailed subsystems for MMLPBF subsystem: control loop

position is monitored by an encoder, which feeds back the converted signal to the control board. The two micro-switches are both a redundant safety measure – to prevent motor overruns – and a reference position for the axis when machine is initialised.

- In the powder heating subsystem, the operation is similar, but for a different finality – temperature control. The microcontroller sends the desired temperature to the control board, which compares it to the actual temperature and updates the ‘heating’ based on the error, issuing a **Pulse-Width Modulation (PWM)** signal to the **Solid-State Relay (SSR)** which modulates the current passing through the electrical resistor that dissipates heat by *Joule effect*, heating the reservoir. The temperature is measured by a thermocouple, that in conjunction with an **Integrated Circuit (IC)** for cold-junction compensation, filtering, amplification and digitisation, feeds-back the signal corresponding to the actual temperature. A control status flag should be used to signal to the microcontroller that the process is out-of-control (bit comes to 1), which the latter should use to stop ‘immediately’ and wait for the process to be controlled again (bit comes to 0).

Figure 78: Detailed subsystems for CO₂ Laser subsystem: control loop

- In the shielding control subsystem, the microcontroller simply activates a power switch at machine's startup, to start the compressor which pressurises the machine chamber with inert gas, namely Argon (*Ar*). The machine chamber's pressure is measured with a pressure switch (with the desired pressure set manually) that the compressor uses for controlling the pressure. The pressure switch should also set the out-of-control flag to off (the process initialises out-of-control), signalling to the microcontroller that the normal procedure can occur.
- Lastly, for the powder recovery subsystem the conceived solution comprises the extraction of powder from the printing bed and delivery to the correct deposit via granulometric sieving. Thus, the microcontroller activates the vacuum pump when required via an [SSR](#), shutting it down after a designated amount of time.

Although the Laser subsystem is not object of hardware design, and the control is performed via software, it is still important to understand the general panorama of the laser control.

- The laser scanning subsystem is similar to the axis one, but instead of the stepper motor moving an axis, it actuates the galvanometric mirrors to scan the building area and the controlling order comes from the computer, as opposed to the microcontroller.
- In the laser beam and laser wobble subsystems the operation is basically the same, changing the observed effect: generating the laser beam or fast-oscillate it after its generation. For this purpose, the computer

issues the order and the hardware PWM takes care of modulating the signal according to the appropriate laser parameters.

It is important now to address some design decisions, namely the use of stepper motors in conjunction with encoders for feedback, and the type of controller used in the feedback loop. For the former, the main reason is related to availability and budget restrictions: there was a surplus of these type of motors available and, alongside with the servomotors' higher unit cost, it became the evident choice for the project.

For the latter, the type of controller chosen was the **Proportional Integrative Derivative (PID)**, due to its high versatility and configuration easiness: the PID controllers are agnostic about the characteristics of the plant (process) to control and as there are several different control loops to manage, it also became obvious what type to use, despite in the modelling phase some parameters can be null, yielding different versions of the general PID controller (P, PI, PD).

4.4.3.3 Electronics design

The subsystems are now analysed in respect of their electronic constituents, selecting and designing the necessary parts. Multisim was used to simulate the circuits behaviour and Autodesk Eagle to design the circuits towards the production of a **Printed Circuit Board (PCB)**. Additionally, Eagle enables hierarchical modelling, supporting modular and iterative design. The main wiring schematic is depicted below in Fig. 79, showing the wiring between all subsystems. In thick lines can be seen the logical buses, merely to group logical signals by subsystems.

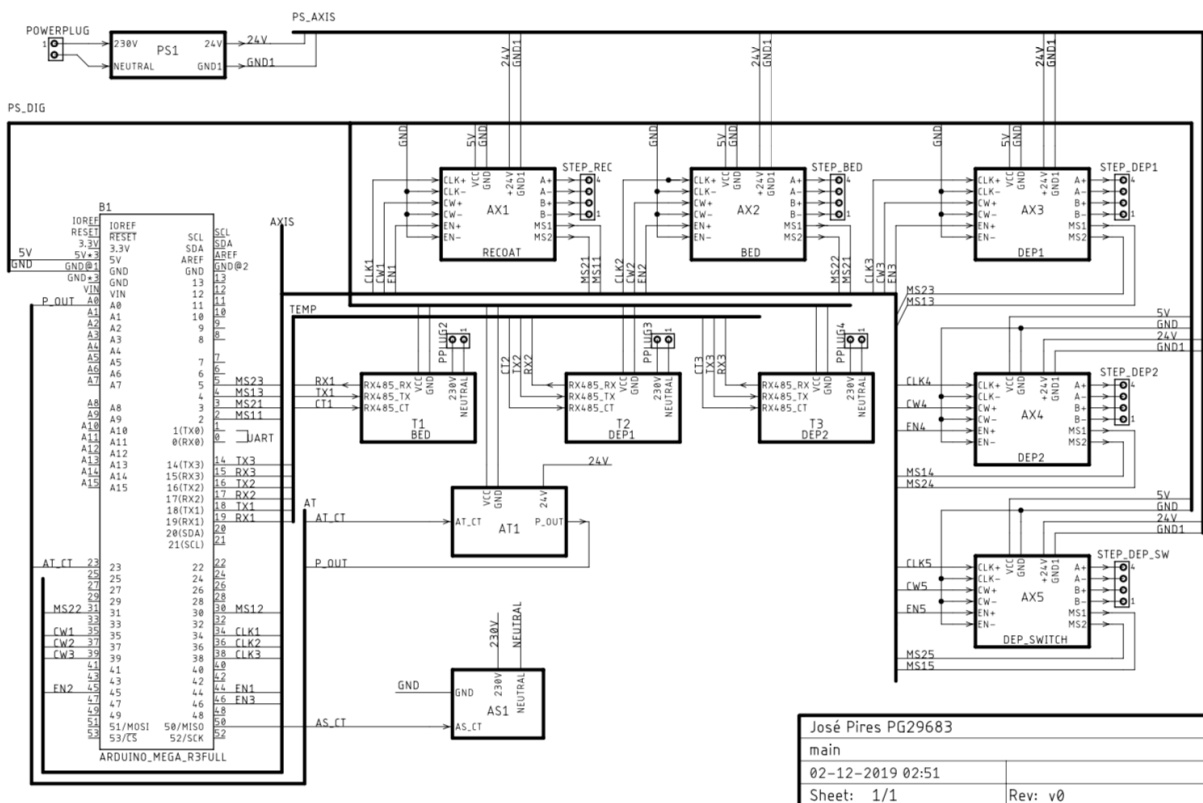


Figure 79: Overall system schematic wiring

Axis subsystem Fig. 80 illustrates the wiring diagram for the *Axis* subsystem and is comprised of a stepper motor, a stepper motor driver, and microswitches. The encoder may be included in future versions if open-loop control is not accurate enough.

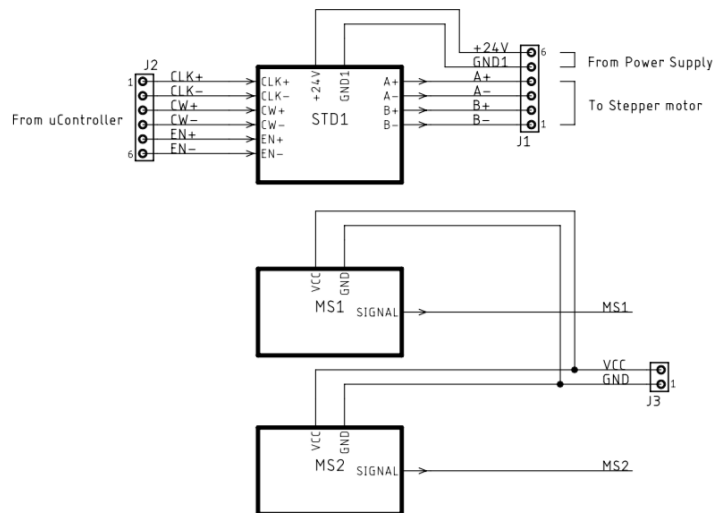


Figure 80: Axis subsystem schematic wiring

The stepper motor is responsible for producing the necessary torque to move the loads across the axis. The bipolar stepper motor NEMA 17 was selected with adjustable step resolution of up to 1/32. This stepper motor has a 1.8° step angle, corresponding to 200 steps per revolution, a step accuracy of 5%, a rated current of 2.5 A, and a detent torque of 280 g-cm.

The stepper motor driver is required for adequate control and timing of the stepper motor. The desired requirements for the driver are: microstepping functionality up to 1/16 (minimum); selectable up to 3 A of rated current; output voltage of 12 V (min) and 24 V (desired) as steppers motors perform better at higher voltages; high commutation frequency for higher operating speeds; passive cooling, if possible. For these reasons, the 31306-MS driver board was selected which uses the TOSHIBA IC TB6560AHQ, known for its performance at a low price.

Endstops are used to detect and prevent motor overrun past limit positions. Mechanical endstops were chosen because they are inexpensive and simple to control, requiring only a pull-up resistor and watching out for induced noise from motors which can cause false triggering by using screened cable.

Temperature subsystem As depicted in Fig. 77, the *Temperature* subsystem is comprised of: temperature controller; solid-state relay for output; heating element; and thermocouple. The wiring diagram is depicted in Fig. 81. The temperature controller chosen includes output signal via solid-state relay. The RS485-TTL converter will be implemented in a future version, for data exchange between temperature controller and microcontroller, enabling temperature reading and parameter setting and monitoring on-the-fly.

Shielding control subsystem As depicted in Fig. 77, the *shielding* subsystem is comprised of: electronic switch (mosfet) and solenoid valve; pressure sensor. The wiring diagram is depicted in Fig. 82.

An inert gas is used to prevent the oxidation of the metallic powders, phenomenon that is severely aggravated by the temperature increase. The selected gas was argon, due to its availability in the laboratory, despite its cost,

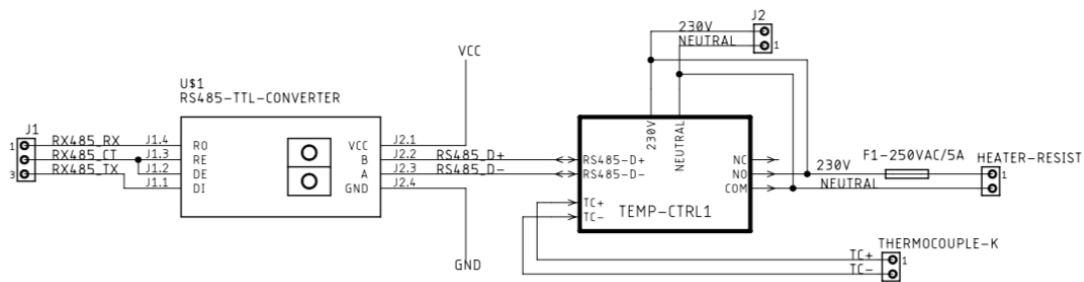


Figure 81: Temperature subsystem schematic wiring

when compared, for instance with nitrogen. The argon supply occurs in two stages: first a vacuum of about 100 Pa; and then filling to a pressure of 0.5 bar which reduces the initial oxygen amount to 0.04% as reported by Wang et al. [177].

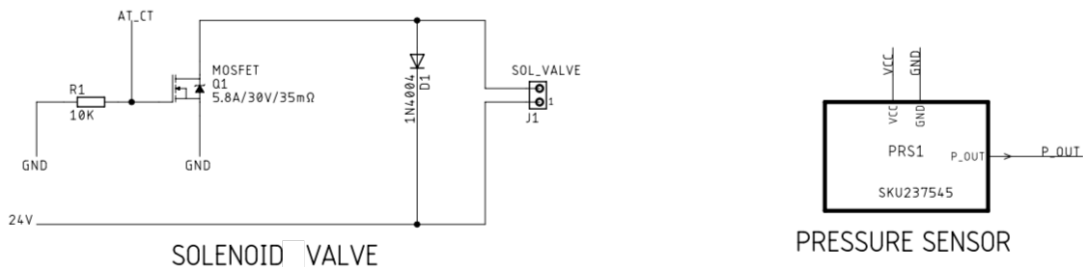


Figure 82: Shielding subsystem schematic wiring

To control the proportional solenoid valve, the circuitry presented in 82 is used. A MOSFET is used to drive the solenoid, via a control signal received from the microcontroller acting on the MOSFET's gate – AT_CT. By using a PWM technique on the gate of the MOSFET, the timing of the valve can be controlled, allowing more or less fluid to flow, actively controlling the pressure in the chamber. A note is entitled here: PWM operation is only advisable in proportional solenoid valves, as they are specially made for this effect; otherwise, premature wear would occur and unstable oscillation behaviour associated.

A pull-down resistor is used to prevent pin floating, which could false triggering of the solenoid valve. The fly-back diode is used to protect the output pin from the current peak occurring when the solenoid valve coil is powered off (inductive load).

The pressure sensor is used to measure the pressure in the chamber for adequate control.

Extraction subsystem Fig. 83 illustrates the wiring diagram for the extraction subsystem comprised of an SSR and a vacuum pump. When a high level signal (5V) is fed to the SSR's input (AS_CT), the photo-diode will conduct and the optocoupler will be triggered, activating the vacuum pump; when a low signal is fed, the vacuum pump will be turned off.

Power supply The power supply is responsible for supplying the DC current required by the stepper motors, which should be operated at 24 VDC, for improved performance. In fact, the higher the voltage, the better the performance; however, as the stepper motor driver voltage rating is 24 V, this was selected. Considering the worst case scenario, i.e., if all motors were driven simultaneously, the total current supplied is 12.5 A (2.5 A per motor).

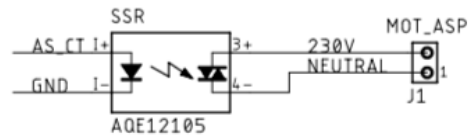


Figure 83: Extraction subsystem schematic wiring

Thus, the power supply minimum requirements are: 24 VDC / 12.5 A. The power supply selected has an output current of 15 A at 24 V, yielding 360 W of power output. The power supply is switch regulated for increased performance. Table 8 lists the power supply's main specifications.

Table 8: Power supply NewStyle 360 W

Input Voltage	Output Voltage	Power	Output current	Type
115/230 VAC	24 VDC	360 W	0 ~15 A	Switch regulated

Microcontroller The microcontroller manages all system tasks, by monitoring the inputs and generating the outputs in the accurate timing, triggered by internal state changes (temperature, pressure, etc.) or external events (user requests/commands; gcode processing, etc.). The main requirements for the microcontroller unit are:

- widely available: for increased wide-spreading and adoption;
- high abstraction: programming microcontrollers can be intimidating, especially if dealing with all the low-level details; an abstraction layer can ease the learning curve, as suggested by the 3DMMLPBF-C2P methodology.
- ease of use;
- cost-effective;

For the above mentioned reasons the Arduino platform was chosen, more specifically the Arduino Mega 2560, due to the amount of [Input/Output \(I/O\)](#) pins required. Table 9 lists its main specifications.

Table 10 lists the pin mapping, mapping the microcontroller pins to the functionality required as indicated in the main schematic wiring (Fig. 79).

Table 9: Arduino Mega 2560 main specifications

Operating voltage	5 V
Digital I/O pins	54 (15 provide PWM output)
Analog Input Pins	16
DC Current per I/O pin	20 mA
Flash memory	256 KB (8 KB are used by the bootloader)
SRAM	8 KB
EEPROM	4 KB
Clock speed	16 MHz

Final result After designing, dimensioning and acquiring the electronic components indicated in the electronic design, the subsystems were assembled and integrated in the main system. The final result is illustrated in Fig. 84: at the top the power supply; in the middle the microcontroller, the stepper-driver boards and mechanical endstops circuitry; at the bottom the temperature controllers for each powder deposit.

Table 10: Microcontroller pin mapping

Subsystem	Signal	Function	Pin	I/O
Axis	EN+	Enable	[32, 35, 38, 41, 44]	Output
	CW+	Direction	[33, 36, 39, 42, 45]	Output
	CLK+	Step	[34, 37, 40, 43, 46]	Output
	MS1	Home microswitch	[2, 4, 5, 6, 7]	Input
	MS2	Default microswitch	[3, -, -, -, 8]	Input
Comm	RX	Serial reception	0	Input
	TX	Serial transmission	1	Output
Thermo	RX485_RX	RS485 reception	[19, 17, 15]	Input
	RX485_TX	RS485 transmission	[18, 16, 14]	Output
	RX485_CT	RS485 control	[47, 49, 51]	Output
Shielding	AT_CT	Shielding control	23	Output (PWM)
	P_OUT	Pressure sensing	25	Input
Extraction	AS_CT	Extraction control	27	Output (PWM)



Figure 84: Electronics development: final result

4.4.3.4 Software

The software specific design for the 3DMMLPBF machine regards the development of the *lcode* interpreter (vide Section 4.2.2) and related control components, constituting what is commonly known as the machine's firmware.

Requirements and Constraints Table 11 lists the requirements and constraints for the 3DMMLPBF machine's firmware. The main requirements are: provide support for the manufacturing tasks; communicate with the `Manufacturer` application to obtain the manufacturing instructions and to provide feedback; interpret `lcode` instructions to execute the manufacturing; and enforce safety mechanisms to protect the *User*.

On the other hand, the main constraints are technical: the target platform has low memory, so the firmware must have a low memory footprint; the firmware runs the system’s most critical tasks and, thus, must have low latency and high responsiveness.

Table 11: Requirements and constraints for the 3DMMLPBF machine’s firmware

Requirements	<ul style="list-style-type: none"> - Provide support for the manufacturing tasks (axis motion, recoating, powder recovery, temperature control, shielding control) - Communicate with the Manufacturer application - Interpret lcode to run the manufacturing - Enforce safety mechanisms to protect the User
Constraints	<ul style="list-style-type: none"> - Low memory footprint - Low latency: soft real-time or real-time deadlines

Design Fig. 85 shows the firmware’s architecture. In the lowest layer, we have the actual electronics hardware executing the manufacturing. Above that, we have the device-drivers that abstract the hardware’s operation, providing the basic low-level services required to interface the hardware (**Hardware Abstraction Layer**). The **Operating System (OS) layer** provides services at the system level, abstracting and managing the system’s resources and supporting the application’s modules. For example, the OS layer is responsible for the scheduling and synchronisation of concurrent tasks in the system, like serial port management and axis controller management. The **Communications layer** manages the communications with the outside world, namely the Manufacturer, via the Serial Port Manager. As aforementioned, a fixed-size protocol built on top of RS232/RS485 protocol is used for transaction exchanging. Lastly, the **Application layer** provides the system’s high-level functionalities, such as: communication handling, i.e., assessing if a valid message has arrived; lcode interpretation of valid instructions; axis, temperature and shielding controlling. The Application layer’s modules interact with the Communications layer and the OS layer to request their services or to get notified of a relevant event.

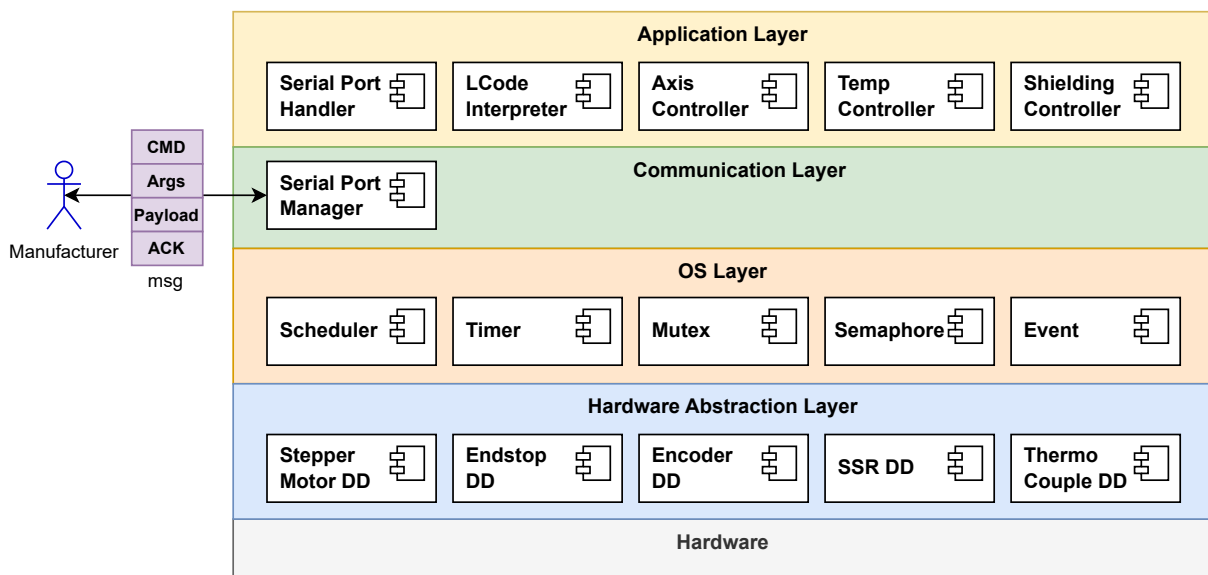


Figure 85: Firmware design: system architecture

Now, we turn our focus into each application's module/task. Fig. 86 illustrates the state machine diagram for the `LCode Interpreter`, the main system's task:

1. **Init**: after power on, the machine is initialised: loading previous settings, configuring motors, starting other system's tasks (heating and shielding control), initialising serial communication, and homing all axes. If the homing procedure fails, an error event is triggered and the state machine transits to the `Error` state.
2. **Idle**: this is the default state and where the `LCode Interpreter` state-machine really starts. It handles the event-loop of the interpreter. On entry, it turns off the suction system and the motors. It also checks if the other system's tasks, like the `TempController` or the `Shielding Controller`, emitted any error. If so, the system's goes to the `Error` state. If a valid serial message has arrived, it is parsed, and dispatched to the appropriate handler, triggering the transition to the corresponding state, namely: `Calib`, `Fill`, `Manuf`, `Cleanup`, or `Stop`.
3. **Stop**: eventually, during the material processing, the user may issue an emergency stop. If this happens, the machine is halted, stopping all motors and sending to the *Master system* the `MSG_STOP` message.
4. **Calib**: if a calibration message is received, we check its status, and if it is done, we check the manufacturing height available and compare to the part's height to enable the manufacturing. In either case, a message is issued to the *Master system* with the calibration status. Otherwise, if the calibration is ongoing, the motor, distance, and motion's direction are retrieved and dispatched to the `MoveMotor` external thread (here represented as a state for simplification purposes). Then, we wait for the motor's motion to finish or for a timeout, signalling an error.
5. **Fill**: in this state, we check for a valid material, and if so, the recoating systems' are homed, and then the material's recoater is brought to its center position, aligning itself with the deposit to allow the deposit's filling with the powder. After successful alignment, it transits to `Idle` and waits for more commands.
6. **Manuf**: this is the manufacturing handler state. The material, the bed flag, and the layer's height are retrieved. If a new material is to be added, the old one is removed. If a new layer is issued, then the bed drops also by layer's height. Then, powder is inserted and spread across the printing bed. The recoating procedure is repeated for the number of recoating passages defined in the `Manufacturer's` application. If everything works well, the message `MSG_NEW_ID` is sent back to the `Manufacturer`, signalling it is ready for further processing.
7. **Cleanup**: in this state, we check for a valid material, and if so, the material's recoater is brought to its centre position, aligning itself with the deposit to allow the powder recovery. After the timer elapses, the powder recovery system is turned off again, and the `MANUF_DONE` message is sent back to the `Manufacturer`, signalling the manufacturing procedure is completed.
8. **Error**: this a terminal state. The error is emitted back to the `Manufacturer` and we wait for the `restarted` signal to be posted.
9. **MoveMotor**: this state is actually an external thread, but as most states request its services, it was added to the diagram to facilitate the comprehension. The motor, distance, and motion's direction are retrieved

and used to move the motor. If a timeout occurs, an error happened. Otherwise, the `motorDone` signal is emitted with the corresponding motor's index.

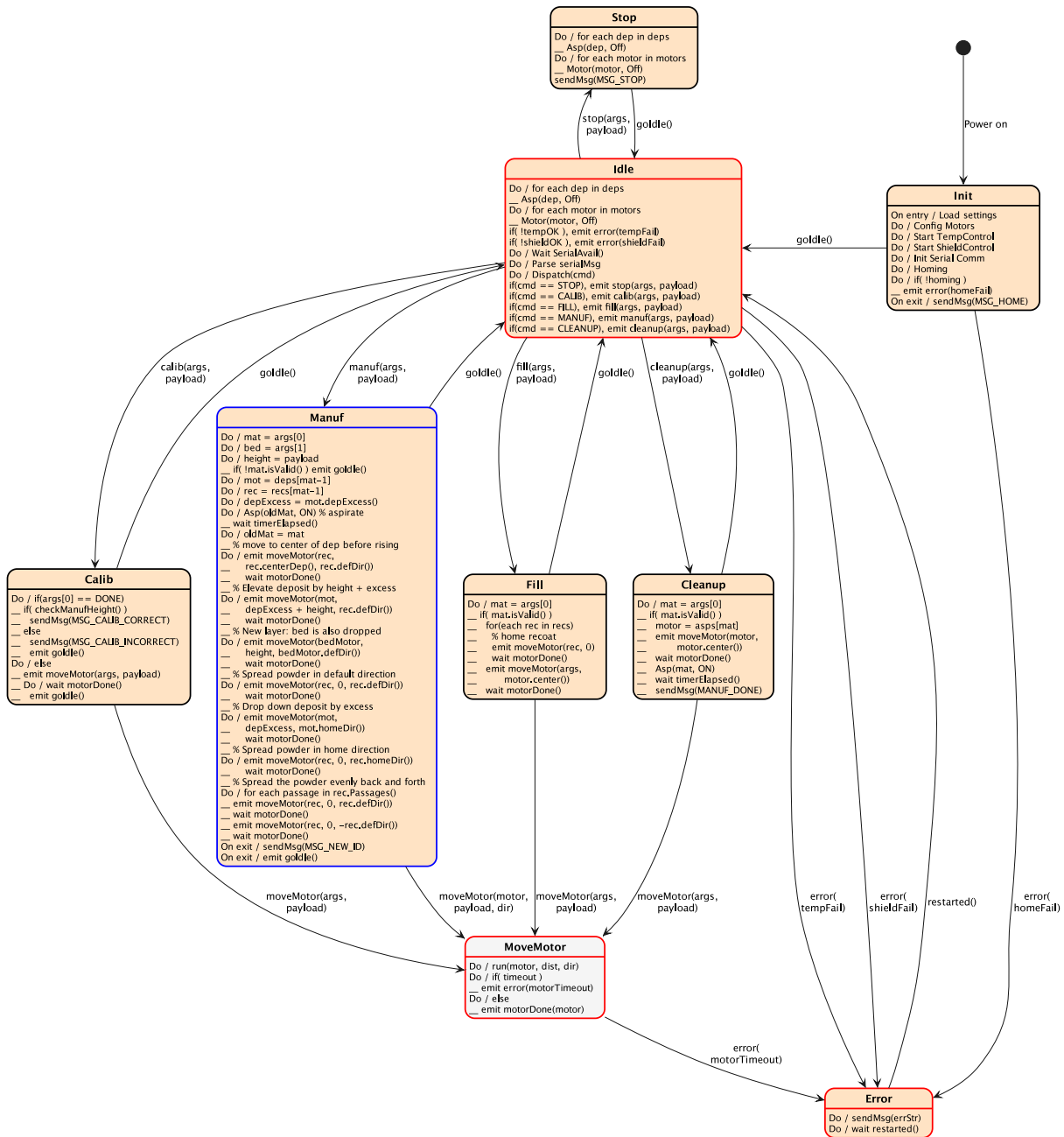


Figure 86: Firmware design: LCode Interpreter State-machine diagram

Lastly, Fig. 87 specifies the messaging protocol as a subset of the Manufacturer's messaging protocol, with the following structure:

1. **CMD**: command exchanged between the Manufacturer and the machine — `MSG_` represent commands sent back to the Manufacturer, while the other ones are sent by the Manufacturer. The several command types are listed, alongside with the command's grammar. For example, the `MANUF` command requires the material, the bed flag, and the height to be bundled in the message.

2. **args**: represents the command's arguments. For example, MANUF's material and bed goes into arguments 0 and 1, respectively.
3. **payload**: represents an additional command's attribute, such as, laser's actuation delay, distance, layer height or parameter's value. For example, the MANUF's height is defined here.
4. **ACK**: represents the acknowledgement signal, used to validate a message.

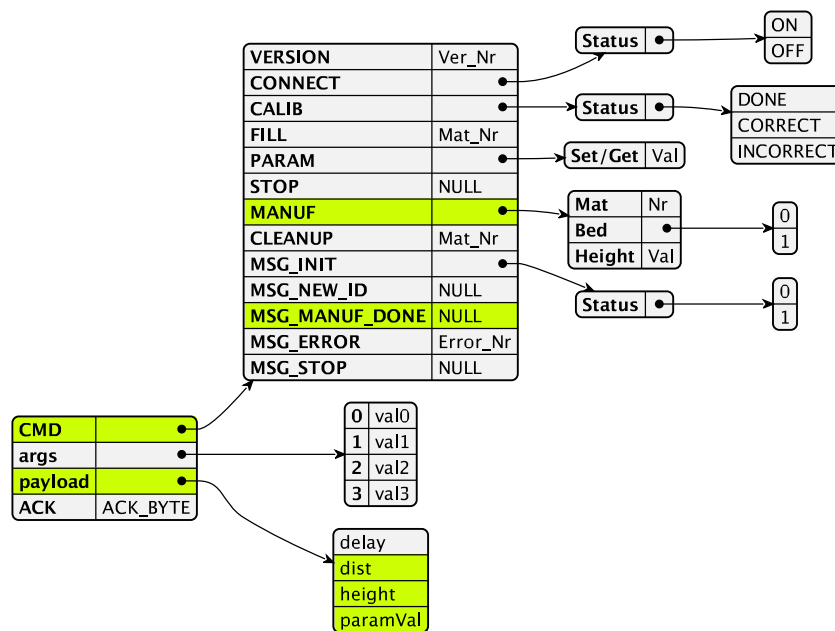


Figure 87: Firmware design: Messaging protocol

Implementation The firmware was implemented by stages using the C/C++ programming language for the Arduino platform. The hardware abstraction layer was firstly implemented and tested to guarantee the hardware's control was fully operational. Then, the Serial Port Manager was implemented, alongside with the fixed-size messaging protocol and tested to ensure data's integrity. Lastly, all applications modules/threads were implemented to support the message validation and dispatching, the `lcode` interpretation, and the control of the axes, temperature and shielding.

4.4.4 Implementation: Version 1

The completion of the first full development cycle of the V-model methodology used yielded the version 1.0 of the 3DMMLPBF equipment. Fig. 88 shows the first version of the 3DMMLPBF equipment comprised of three systems (see also Fig. 49 and Fig. 72): 3DMMLPBF system – machine, control circuitry and microcontroller; laser system – CO_2 laser in this case; master system – Manufacturer's UI controlling the 3DMMLPBF and laser systems. It is important to note that the visible electronics are protected from user manipulation by an enclosing frame; for illustration purposes this cover was removed. Table 12 lists the 3DMMLPBF machine v1.0 specifications.

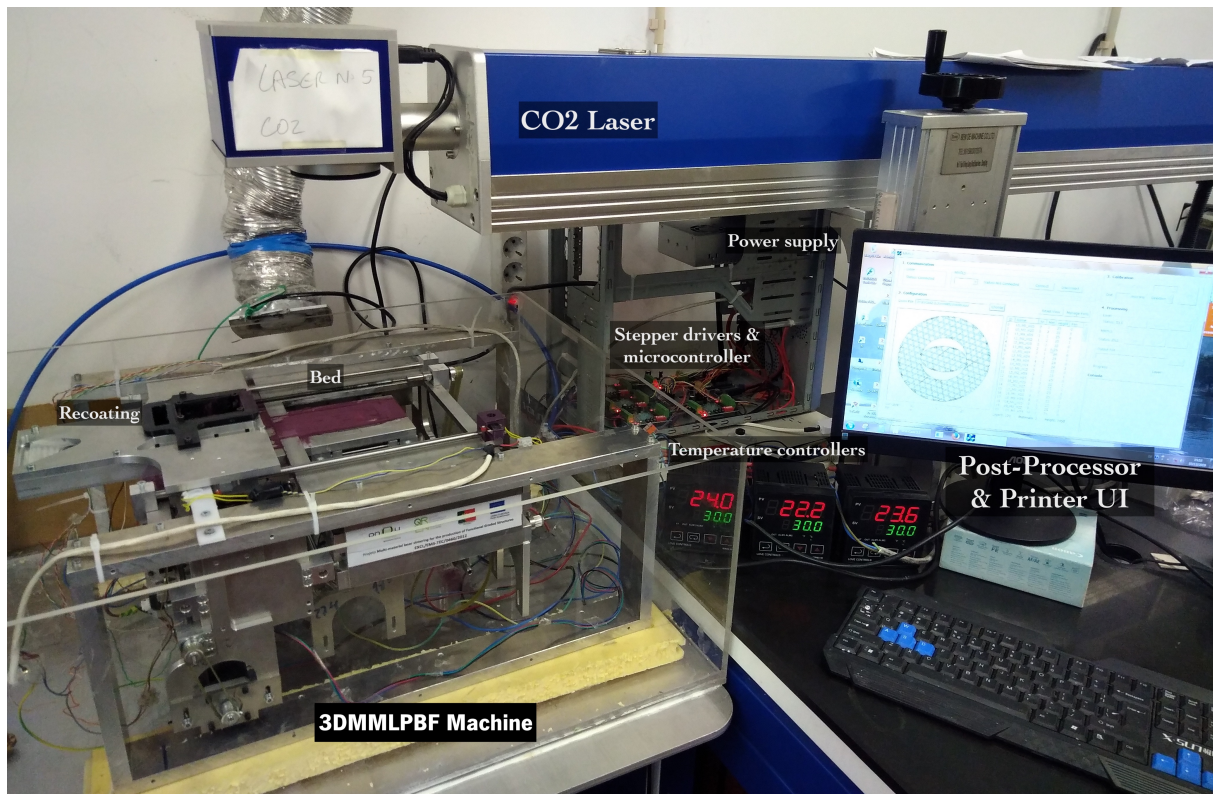


Figure 88: 3DMMLPBF equipment v1.0: Machine, Laser, and Post-Processor and Printer UI

Table 12: 3DMMLPBF machine v1.0 specifications

Dimensions (l x w x h)[mm]	560 x 450 x 280
Power supply	Laser: 400 VAC, 10 A Machine: 24 V, 15 A
Build dimensions [mm]	50 x 50 x 50
Nr. of materials	2
Temperature	Tested up to 250°C (higher temperatures can be used) Type: CO ₂
Laser	Power: 30 W Spot size: 50 μm
Resolution [μm]	Full-step (all axes, except bed): 5 ± 0.25 1/16-step (bed): 0.32 ± 0.016
Estimated cost [€]	Laser: 7500 Machine: 1500 Total: 9000

The equipment axes' have micrometric resolution, it can support up to 250°C (at least), but the feature that stands out the most is its low cost (circa 1500 €). Adding up to the laser cost, the total costs is under 10 k€, making it affordable which can act as starting point for greater adherence of people.

However, the first version of the 3DMMLPBF equipment is bulky, resulting in higher resource consumption, namely powder and energy (heat dissipation), which, in its present form, can make the operational costs unfeasible. Also, the powder recoating system was not very effective, making room for improvements.

Thus, this triggered another development cycle, leading to the second version of the 3DMMLPBF system.

4.4.5 Implementation: Version 2

The 3DMMLPBF equipment v2.0 is a more compact version of the previous one, optimising powder consumption and recovery, and manufacturing efficiency, with relevant improvements in the powder delivery, heating, cooling, and powder removal systems. The major modifications were in the mechanical domain, as the electronics and the software suffered only minor ones. The development of this equipment's version is partially documented by Figueiredo [178], when developing a better recoating system for the 3DMMLPBF.

Fig. 89 illustrates the new recoating system developed by Figueiredo as an improvement over the previous version. It consists of two carts moved by a belt and pulley system powered by a stepper motor. Each cart moves from the periphery to the bed dragging each material contained in the deposit, and back. Each cart contains a scraper made of high-temperature silicone to seal the cart opening and deliver a smooth and uniform layer of powder to the bed area.

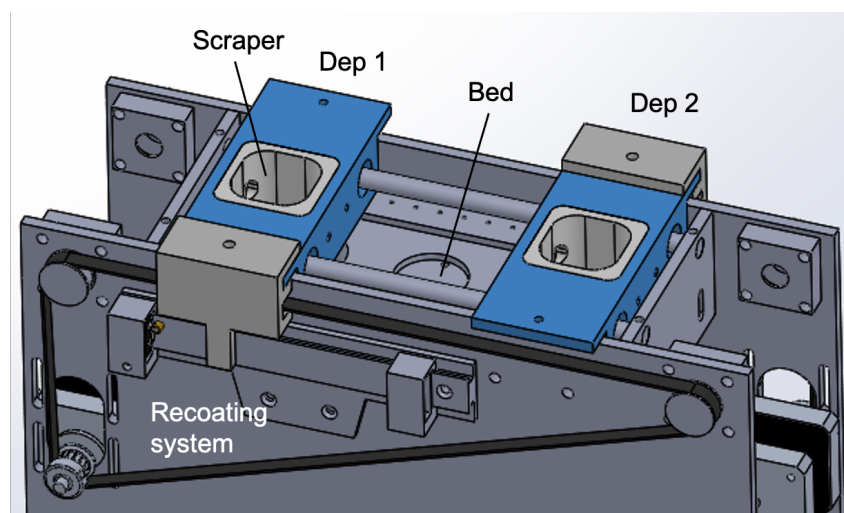


Figure 89: 3DMMLPBF machine v2.0: Recoating system (adapted from [178])

Fig. 90 illustrates the powder recovery system consisting of two connecting tubes to the end of which are connected hoses leading to a vacuum system, responsible for the powder removal. The tubes sit on top of the powder deposits and are actuated by a stepper motor via an endless screw, ensuring the distance to the deposit is minimal for optimal powder removal. The vacuum systems are independent, minimising powder contamination.

Fig. 91 illustrates the heating system used to preheat the powders closer to the temperature of the focused laser beam over the powder bed. It aims to minimise thermal shocks which induces mechanical stress on the produced parts. It consists of an array of heating cartridge elements distributed over evenly along the deposits and bed areas.

Fig. 92 illustrates the water cooling and atmosphere control systems, with inlet and outlet flows ensuring proper fluid circulation to ensure adequate temperature control and maintenance of reducing atmosphere.

Fig. 93 illustrates the 3DMMLPBF equipment v2.0 and the supporting framework – Laser, Post-processor and Printer UI. It is clearly visible the size reduction and the vacuum suction inclusion.

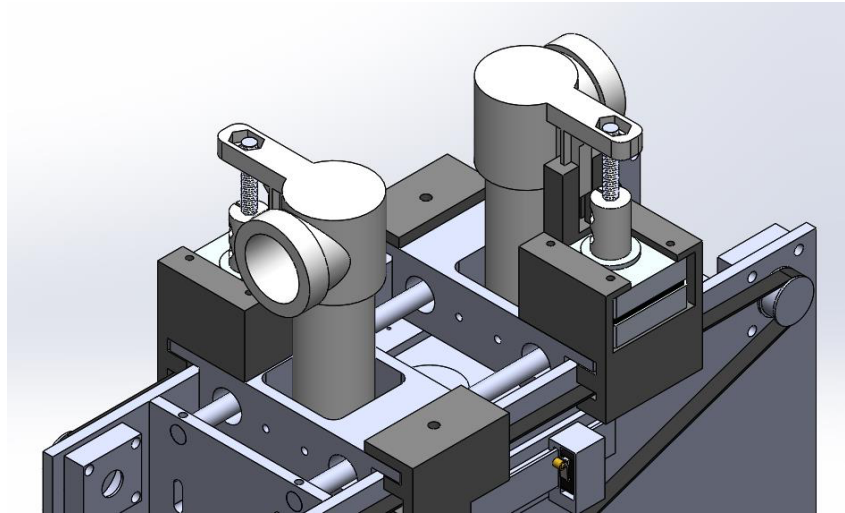


Figure 90: 3DMMLPBF machine v2.0: Powder recovery system (withdrawn from [178])

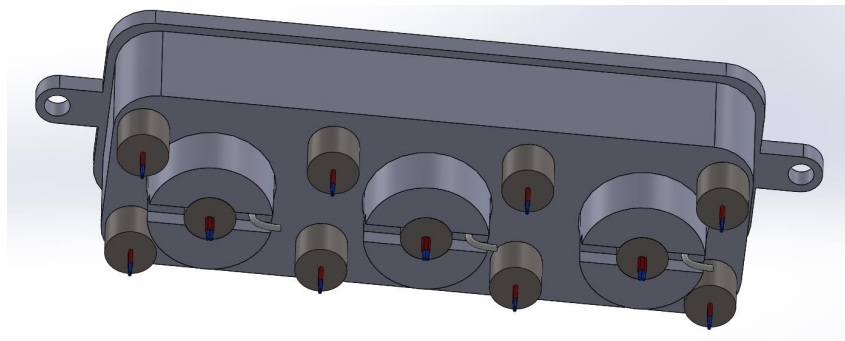


Figure 91: 3DMMLPBF machine v2.0: Heating system (withdrawn from [178])

Table 13 lists the 3DMMLPBF machine specifications. The equipment can now integrate two lasers of different types to enable the multi-material fabrication of metallic and ceramic materials. Furthermore, its estimated cost is 10 to 20 times less of the commercial multi-material equipments.

Table 13: 3DMMLPBF machine v2.0 specifications

Dimensions (l x w x h)[mm]	320 x 100 x 400
Power supply	Laser: 400 VAC, 10 A
	Machine: 24 V, 15 A
Build dimensions [mm]	25 \varnothing x 100
Nr. of materials	2
Temperature	Tested up to 250°C (higher temperatures can be used)
Lasers	Type: CO ₂ ; Power: 200 W; Spot Size: 50 μ m
	Type: Nd-YAG; Power: 300 W; Spot size: 200 μ m
Resolution [μ m]	Full-step (all axes, except bed): 5 \pm 0.25
	1/16-step (bed): 0.32 \pm 0.016
Estimated cost [€]	Lasers: 12000
	Machine: 1200
	Total: 13200

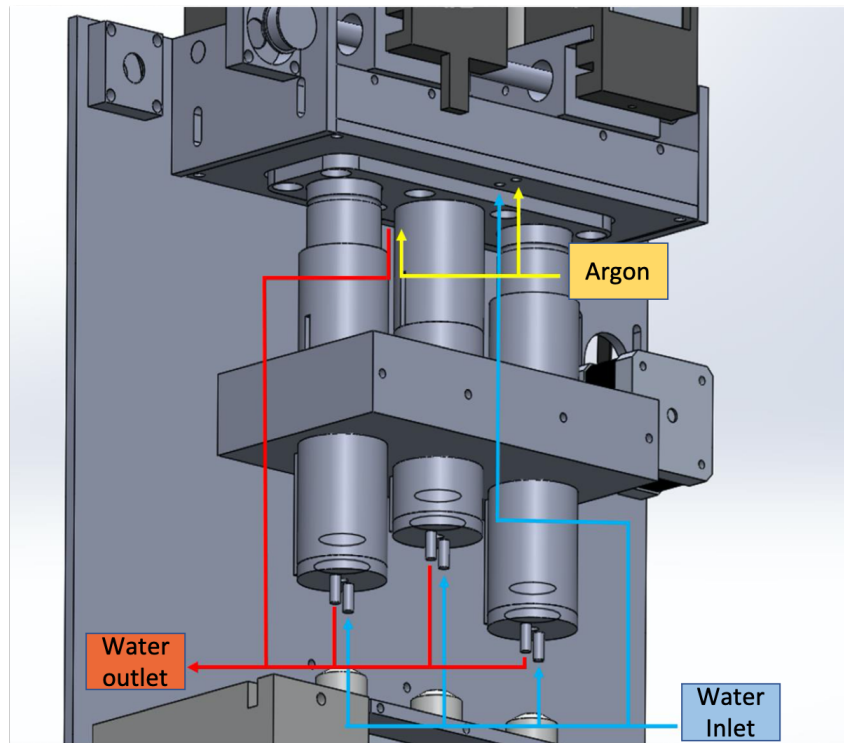


Figure 92: 3DMMLPBF machine v2.0: Water cooling and atmosphere control systems (adapted from [178])

4.4.5.1 Testing and Validation

The equipment's tests were divided in the following categories: mechanical – axes movements, movements precision; control – temperature, mechanical endstop triggering, and machine reset; laser – scanning and marking.

Mechanics For mechanical tests, two types of approaches were used: manual – free (manually driven) or induced motion (external motors) to test the axes; automatic – snippets of code to automatically test the axes movements and the movements precision. Only the latter will be discussed in detail.

To test the axes movements a snippet of code was written to control all five machine axes, either by direction and distance, either between mechanical endstop limits. The direction and distance control aforementioned also enabled the movements precision tests. The command protocol is presented in Fig. 94.

The axes resolution were determined taking into consideration the screws thread pitch of 1 millimeter and the number of steps per revolution of the stepper motor, combined with the excitation scheme. For full-step motors – all, except bed – the resolution is $5 \pm 0.02 \mu\text{m}$; for the bed axis the resolution is $0.32 \pm 0.016 \mu\text{m}$.

For the movements precision tests, the axes were driven to a mechanical endstop and then driven back to the other one. After determining the distance between the two mechanical endstops, the axes were placed at the home mechanical endstop and moved to the other one by the determined distance, checking if the mechanical endstop is triggered and at which distance. The motors presented good precision by consistently hitting the microswitch within a 1% margin. This result was even better for the bed deposit, due to the microstepping added resolution.

Control For temperature control testing, the temperature setpoint was varied from room temperature ($20 \text{ }^\circ\text{C}$) to operation temperature ($250 \text{ }^\circ\text{C}$) in increments of $30 \text{ }^\circ\text{C}$. Then, the rise time and settling time were registered and

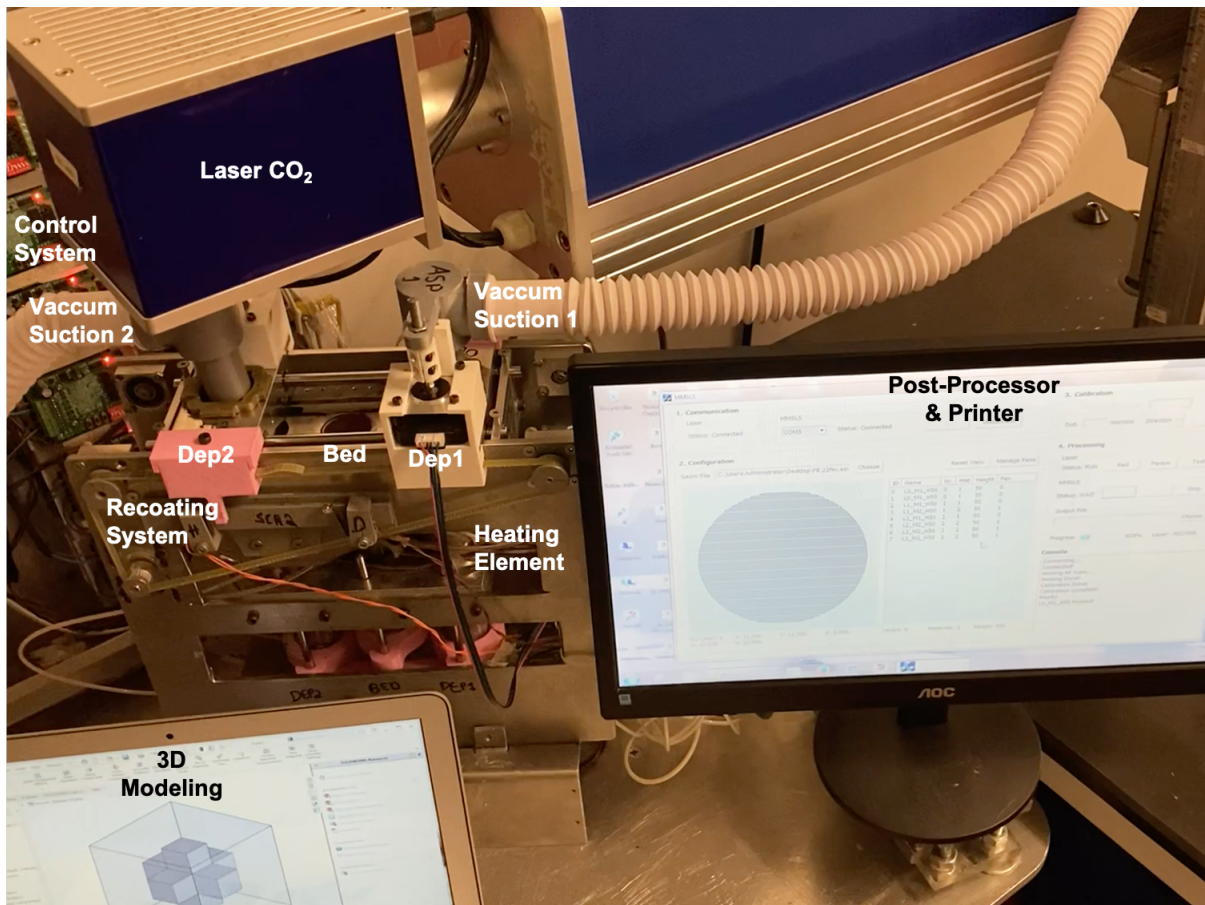


Figure 93: 3DMMLPBF machine v2.0 and supporting framework

```

Serial Monitor - /dev/cu.usbmodem14101 x
1 [SEND] #
2 C----- Free wheel test (# to abort) -----
3 --- Run stepper motors
4 --- aX<d,h,p,n>zYYY <0x0d>
5 --- X: axis nr: between 0 and 4<0x0d>
6 --- <d, h, p, n>: direction<0x0d>
7 ----- d: default<0x0d>
8 ----- h: home<0x0d>
9 ----- p: positive<0x0d>
10 ----- n: negative<0x0d>
11 --- YYY: distance to run

```

Figure 94: Automatic mechanical tests: command protocol

the temperature variation range. Finally, a full operation was performed between room temperature and operation temperature. The controller performance was very satisfactory with a settling time of three minutes and temperature range of 4 °C, especially considering that the radiation and conduction thermal losses are high. It should be noted that this could be achieved thanks to the auto-tuning function of the controller, which gains insight about the plant, despite its nature, and the robustness of the PID control.

The mechanical endstop testing was performed automatically, by sampling all associated pins through software and manually pressing each one, checking the result.

Finally, the machine reset operation could now be tested: first a small shell script stimulated the firmware executing on the microcontroller to perform the desired actions and retrieve the resulting messages; then, the printer software took over this task and stimulated directly the firmware, testing also the user relevant feedback

information.

Laser The scanning and marking were tested by using a dummy file with only one layer, as shown in Listing 4.8 and pressing the pushbuttons *Red* and *Test*, respectively. Furthermore, it also allowed to test different laser parameters by modifying the associated pen.

Listing 4.8: One layer manufacturing file to test the laser

```

1 <g id="LO_M1_H25" slic3r:z="0.0250" slic3r:slice -z="0.0125" slic3r:layer -height="0.0250"
  slic3r:mat="1">
2 <polyline points="20,0 0,0 0,20 20,20 20,0" style="fill: none; stroke: white; stroke -
  width: 0.1; fill -type: evenodd" slic3r:type="" />
3 </g>

```

Fig. 95 illustrates the laser marking testing procedure with multiple lasers. After the *User* select an layer ID to mark and press the *Test* button, the *Master* system will request to the list of lasers defined in the table to mark the entity with the designated laser actuation delay. As such, the entity ID = 4 is marked by laser 0 (controlled by the *Master*), and by laser 1 (controlled by the slave) after the *Master* system sends it the appropriate command.

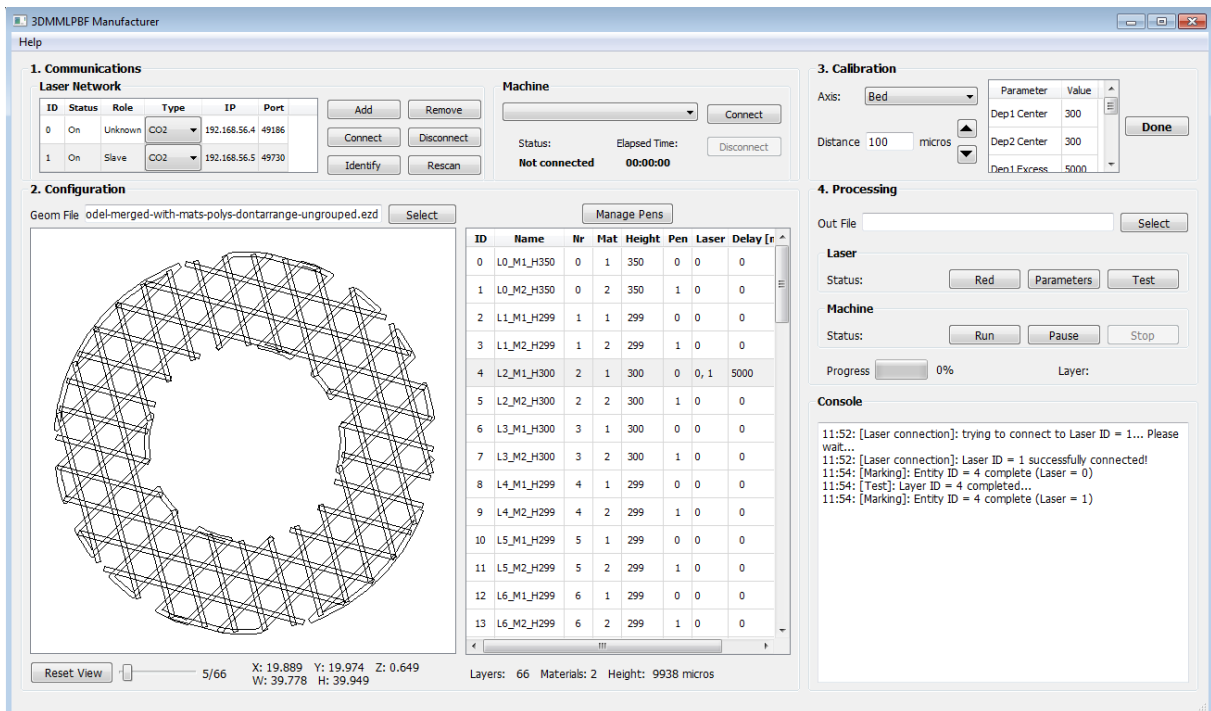
Manufacturing To fully test the machine operation, a dialog was added to the *Manufacturer's* software (see Fig. 96). All protocol commands are available for selection with the accompanying documentation. The commands were then issued with the respective parameters to stimulate the equipment and track its progress. The desired and real behaviours were then compared to validate the machine's operation in compliance to the designed state-machines and the *User's* requirements. For example, the *Debug Comm* command was used to validate the serial communication link between the equipment and the *Manufacturer's SW*: the message sent to the equipment should be looped back to the software with the same contents.

This is also a useful feature for future users of the equipment, allowing for the quick testing of the machine via software in a straightforward and transparent manner.

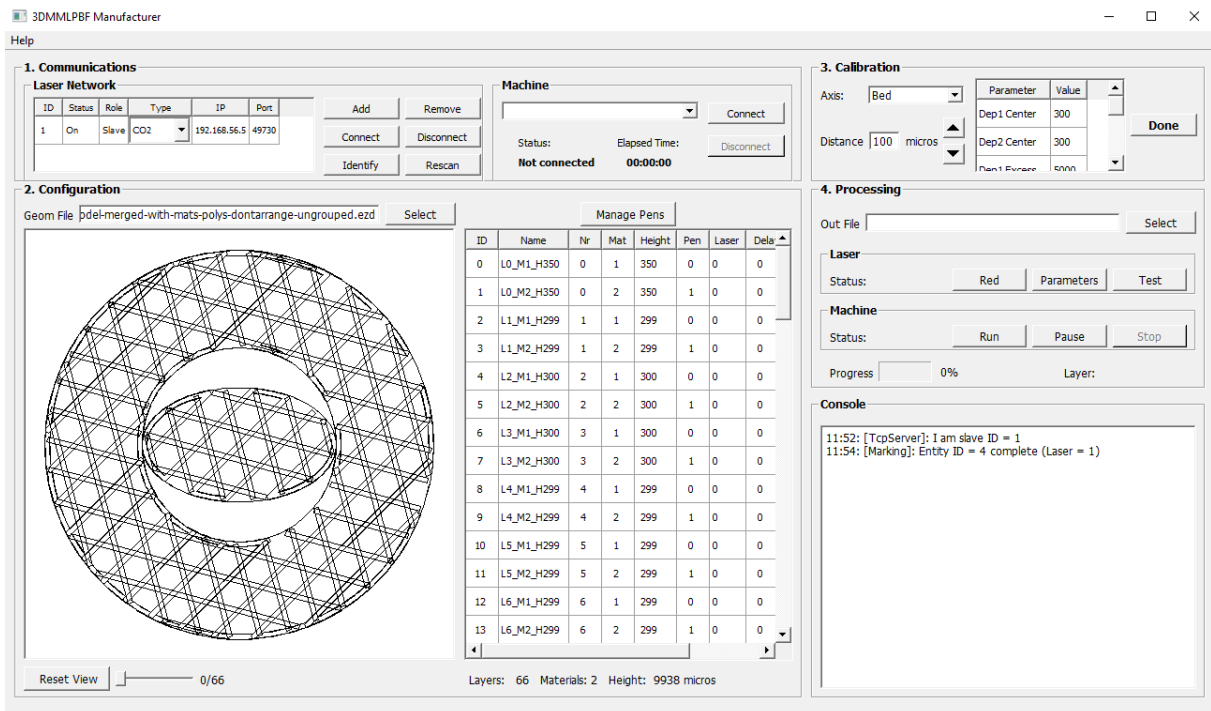
Validation The equipment tests conducted allowed to assess the mechanics, control and laser operating conditions. They were performed mainly automatically through software, and in isolation and integration. The axes movements and their precision was tested and validated. The temperature control was highly insensitive to the high thermal losses mainly by conduction and radiation within satisfactory timing and temperature range. The machine reset was tested: first by static stimulus and then dynamically by the printer, also validating the user messages. The laser scanning and marking were successfully tested, on a single and on multiple lasers, alongside with the marking parameters through the modification of the associated pen. The machine operation was thoroughly tested by software in a straightforward way, using a specially designed *UI* dialog. The equipment's firmware is available online [175] (see Fig. 97) and released under the AGPL v3 licence.

4.5 Summary

In this chapter a specialised workflow — *3DMMLPBF-C2P: CAD to Process* — was instantiated from the proposed methodology, integrating all the models from the manufacturing chain, but without the optimisation steps. The



(a) Master drives marking: it marks own laser and issues marking command to slave



(b) Slave extracts command and marks entity

Figure 95: 3DMMLPBF Laser marking testing

workflow is divided in three phases: manufacturing file generation, manufacturing file processing, and process knowledge feedback.



Figure 96: Manufacturing tests: machine's testing dialog

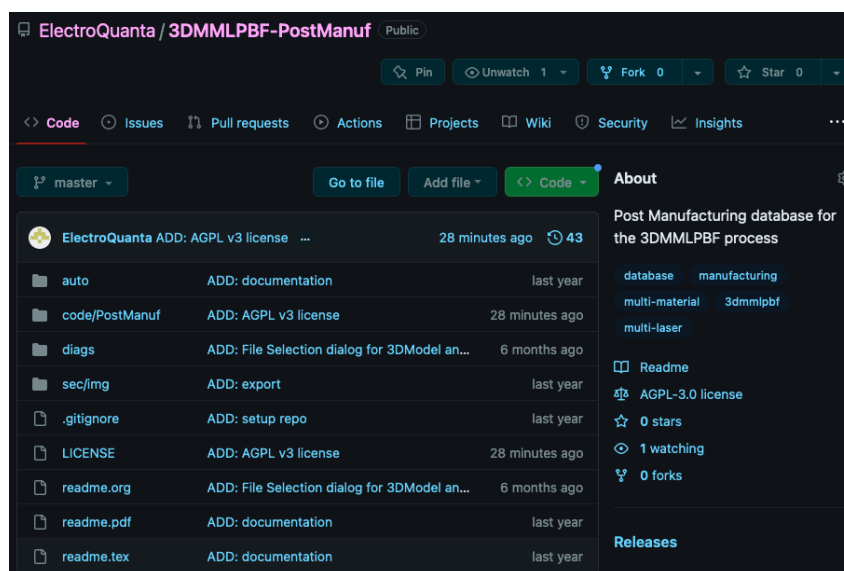


Figure 97: 3DMMLPBF equipment's firmware repository [179]

A software toolchain was developed to materialise the workflow, yielding the following components: **Pre-Manufacturer** – *slicer + path generator*; **Manufacturer** – *post-processor + printer*; and **Post-Manufacturer**.

The Pre-Manufacturer integrates a custom fork of the open-source software *Slic3r* for the slicing and path generation. The following features were added: merging of tridimensional geometric models enabling multi-material processing; toolpath exporting to *SVG*; preservation of model coordinates; custom tagging in *.svg* files to facilitate import by the post-processor. By using *Slic3r*, one benefits from a vast set of toolpaths and that can be extended to suit the *3DMMLPBF* needs.

The Manufacturer combines the *Post-Processor* and *Printer* to generate the manufacturing file from the 3D *CAD* models. The *Post-Processor* maps the topological data to the laser parameters to ensure the desired properties of the 3D part; the *Printer* controls the array of manufacturing lasers and the *3DMMLPBF* machine operation, interfacing both hardware subsystems and providing feedback to the user.

The Post-Manufacturer provides a process knowledge database that can be used by all manufacturing agents for process improvement. It enables models and manufacturing files to be directly imported, easing this process.

Furthermore, it can be used to bootstrap the process, as all information is readily available to use and test the equipment and the toolchain.

The **3DMMLPBF** machine was designed following the *V-model* methodology in two iterations, yielding two versions of the equipment. The working principle of the machine was established and the main subsystems were defined — axis; heating; shielding control; and powder-recovery — and the *global system* was assembled. Then, the subsystems were subject to an analysis, design and implementation loop for each domain area: mechanics, electronics and software.

In the mechanical domain, the machine was designed to fulfil the desired function, attending to the axes motions, the loads interacting in the system and the controlled environment for the materials powders.

In the electronics domain, the circuit drawings were performed in Autodesk Eagle for each subsystem and integrated for circuit assembly and future **PCB** production.

In the software domain, the system architecture was outlined comprised of three main systems: *Master* — controls the **MMLPBF** machine and the array of manufacturing lasers, and runs on the host computer; *Laser* — controls the path scanning driven by the *Master*; **MMLPBF** firmware — controls the multi-material processing, and runs on a microcontroller, commanded via serial interface. The *Manufacturer*, comprising the *Post-processor* and *Printer* software components, was designed and implemented to interface the **MMLPBF** and laser subsystems. Lastly, the firmware — low-level code — controlling the **MMLPBF** subsystem was developed.

The first version of the **3DMMLPBF** equipment was bulky, resulting in higher resource consumption, namely powder and energy (heat dissipation), which, in its present form, can make the operational costs unfeasible. Also, the powder recoating system was not very effective, making room for improvements. Thus, a second and more compact version was designed and built, optimizing powder consumption and recovery, and manufacturing efficiency, with relevant improvements in the powder delivery, heating, cooling, and powder removal systems.

Fig. 98 shows a synopsis of the **3DMMLPBF** ecosystem, illustrating the workflow, software toolchain and equipment interactions, alongside with the manufacturing agents, summarizing the development stage.

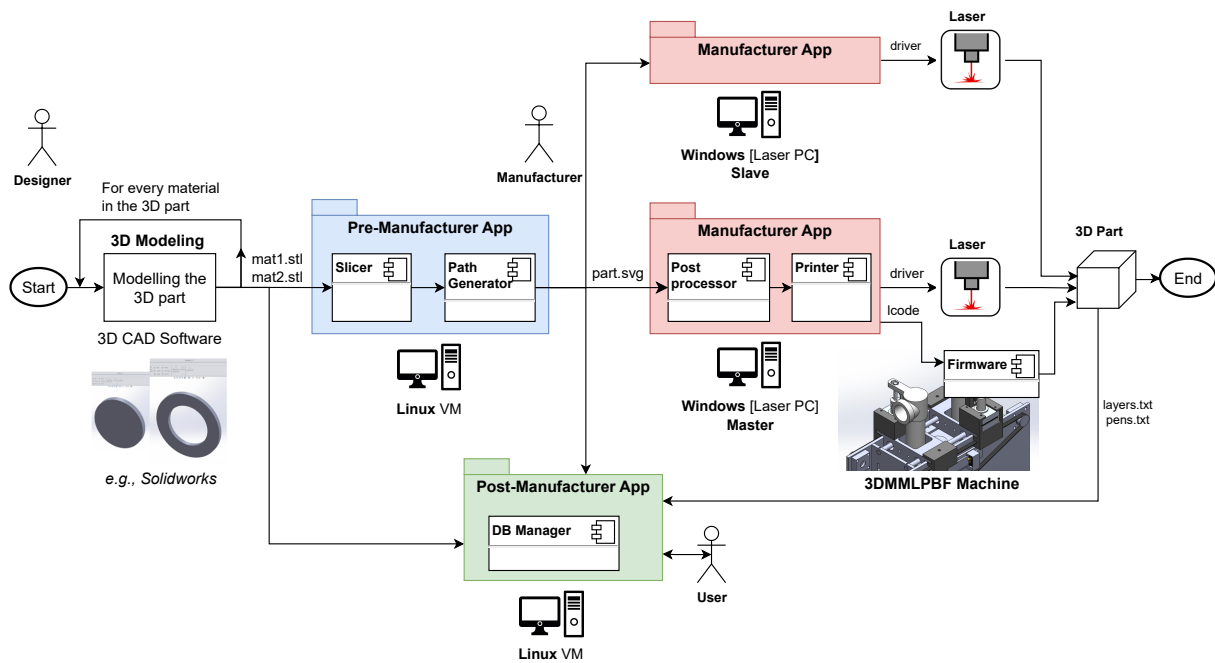


Figure 98: 3DMMLPBF ecosystem synopsis: Workflow, toolchain and equipment interactions

In this chapter, the [3DMMLPBF](#) methodology's is applied to multi-material fabrication, using one or multiple lasers. Thus, the complete process, from inception to produced part is tested as a whole, to ensure the full validation of the designed ecosystem, i.e., methodology, workflow, toolchain, and equipment. Lastly, the prospects for process improvement are outlined, leveraging the process knowledge acquired for systematic and consistent evolution of the [3DMMLPBF](#) manufacturing chain.

5.1 Multi-material mono-laser

The multi-material fabrication was tested out using a CO₂ laser or a Nd-YAG one. These tests are described next.

5.1.1 CO₂ Laser

As a proof-of-concept, a bi-material model — cylinder and cross — was designed in FreeCAD (see Fig. 99), and each material was exported to an [STL](#) file. The cylinder has 25 millimetres in diameter and 11 millimetres in height. The cross is an “assembly” of a parallelepiped with 7 x 7 x 2 mm, totalling a bounding volume of 21 x 21 x 6 mm. The cross referenced to the top plane of the cylinder, so that the cylinder's first layers act as support material.

5.1.1.1 Pre-Manufacturing

The [STL](#) files corresponding to each material were loaded in the [Pre-Manufacturer SW](#) for processing (Fig. 100a) and the results are displayed in Fig. 100. The same slicing and path generation parameters were defined for both entities (Fig. 100b): first layer height and layer height of 50 μm , null fill angle, fill density of 20%, and infill extrusion width of 50 μm , without connected paths. The manufacturing model was generated with 579 slices (Fig. 100c). Layer 0, located at $z = 50 \mu\text{m}$, shows the cylinder's bottom layers, without any intersecting slices belonging to the cross (Fig. 100d). Layer 100, located at $z = 5025 \mu\text{m}$, shows, as expected, the first bi-material layers (Fig. 100f, and Fig. 100e). Lastly, layer 120, located at $z = 7025 \mu\text{m}$, shows the first of the internal layers where the cross is fully displayed (Fig. 100g and Fig. 100h).

Thus, the slicing and path generation complied to the geometrical data (input [STL](#) models) and the configuration established, further validating the [Pre-Manufacturer SW](#).

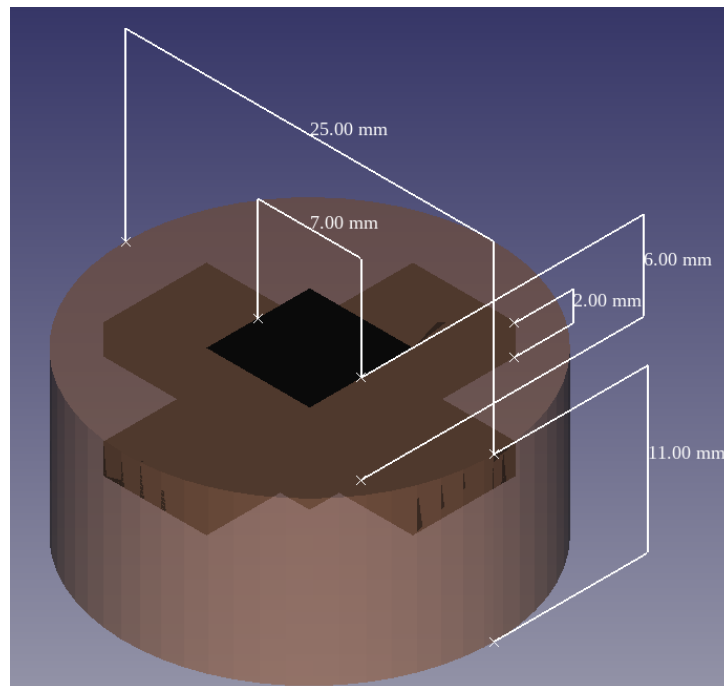


Figure 99: CO₂ laser – bi-material manufacturing test: FreeCAD modelling

5.1.1.2 Manufacturing

The resulting manufacturing model was then loaded to the Manufacturer's SW as illustrated in Fig. 101a. The master system was connected to the 3DMMLPBF machine via COM port. Upon the successful connection, the machine was automatically homed. The process parameters were mapped to each material through the Manage Pens pushbutton, as depicted in Fig. 101b. A calibration was also performed to minimise powder usage.

The filling procedure was executed for both materials. For easier demonstration, the same material was used for the cylinder and the cross – an electrostatic polymeric coating based on TGIC polyester [180] – but with different colours for better visualisation. After concluding these steps and validating the calibration, the machine's initialisation was complete.

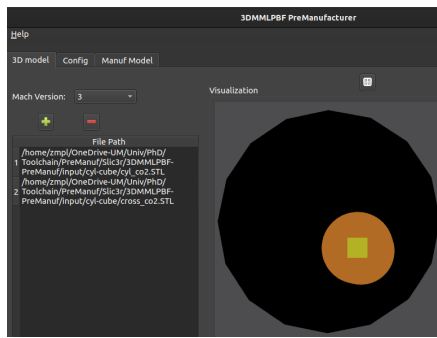
The manufacturing was then initiated by selecting all layers to manufacture and pressing the Run pushbutton. Fig. 101c and Fig. 101d illustrates the manufacturing: on the left the visualisation of the current layer and the corresponding UI status; on the right the result of the layer after being printed. As it can be seen, the layer is correctly printed, in compliance with the process and geometrical data provided. After more than two hours, the 579 layers were manufactured (Fig. 101e).

Fig. 102 illustrates the bi-material part produced, in cross-section (Fig. 102a) and orthogonal views (Fig. 102b), where it is clearly visible the tridimensional material variation, as defined by the original 3D CAD model.

5.1.1.3 Post-Manufacturing

After manufacturing was completed, several analysis were performed on the produced part to assess the manufacturing quality, namely on geometrical compliance and densification.

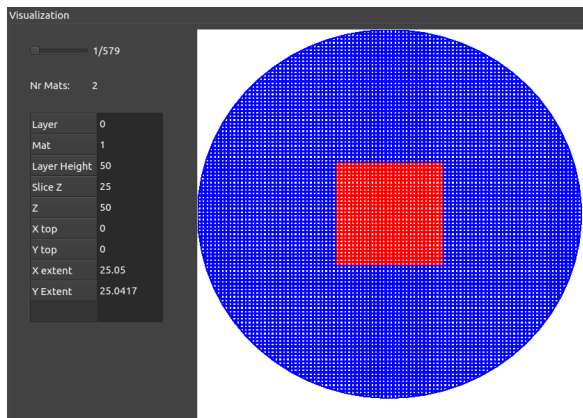
Geometrical compliance was assessed using a image processing SW package based on ImageJ – Fiji [181, 182] – using a 1 cent coin as a base for the measurements (Fig. 103). The measurements performed showed a



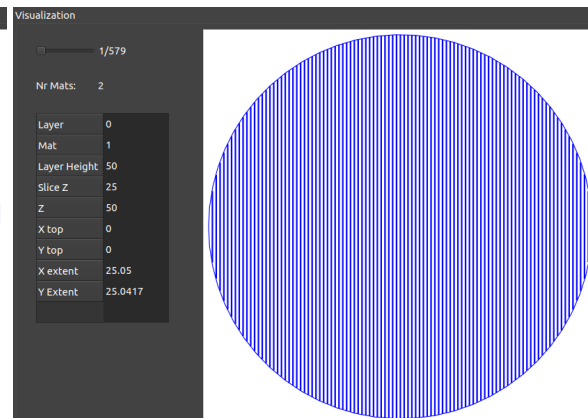
(a) 3D model preview

Generic		Specific	
<input checked="" type="checkbox"/> Enable			
STL ID	0	1	
First Layer Height (mm)	0.05	0.05	
Layer Height (mm)	0.05	0.05	
Fill Angle (deg)	0	0	
Fill Density (%)	20	20	
Fill Pattern	rectilinear	rectilinear	
Infill Extrusion Width (mm)	0.05	0.05	
Connect Paths	0	0	

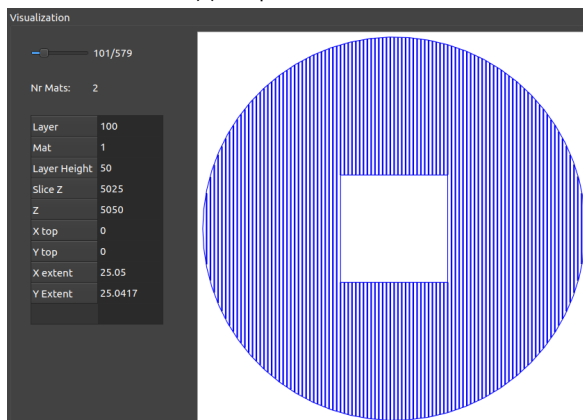
(b) Slicing and path generation setup



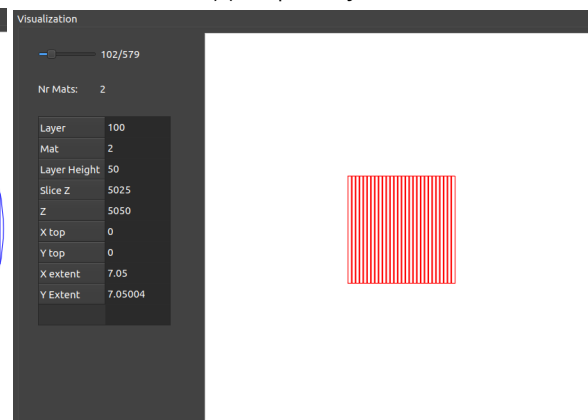
(c) Output: main view



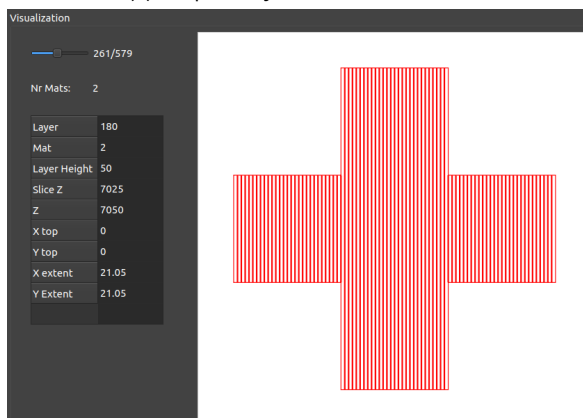
(d) Output: Layer 0



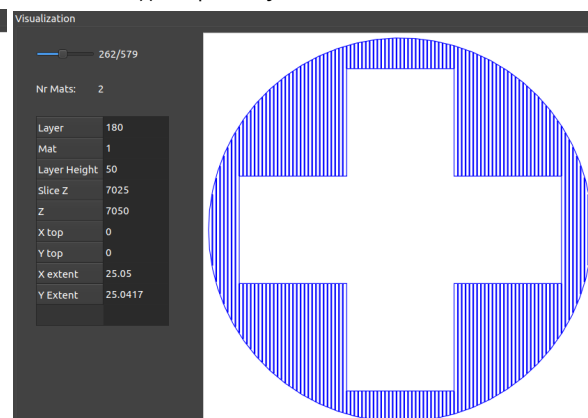
(e) Output: Layer 100 – material 1



(f) Output: Layer 100 – material 2

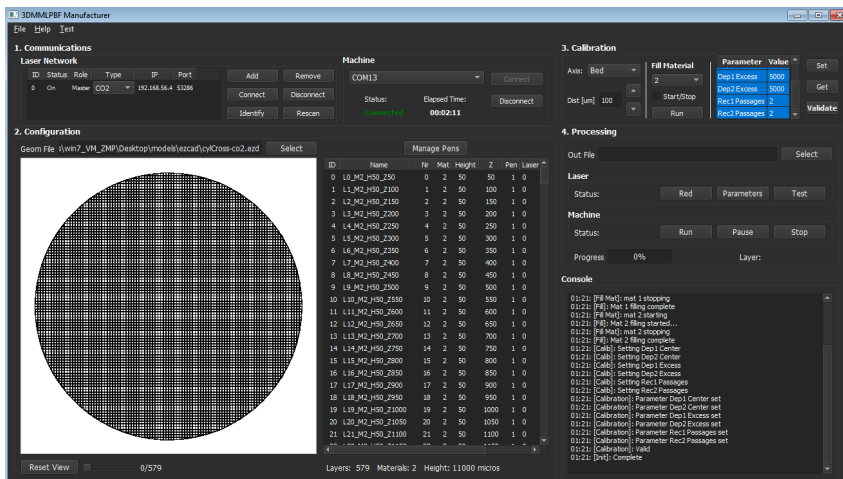


(g) Output: Layer 180 – material 2

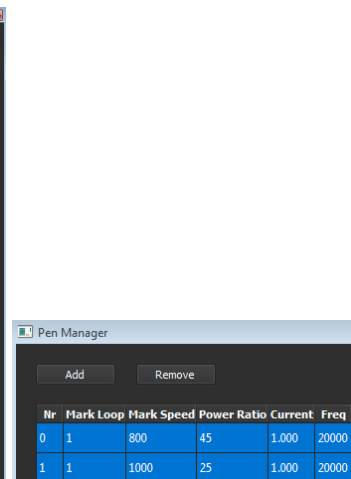


(h) Output: Layer 180 – material 1

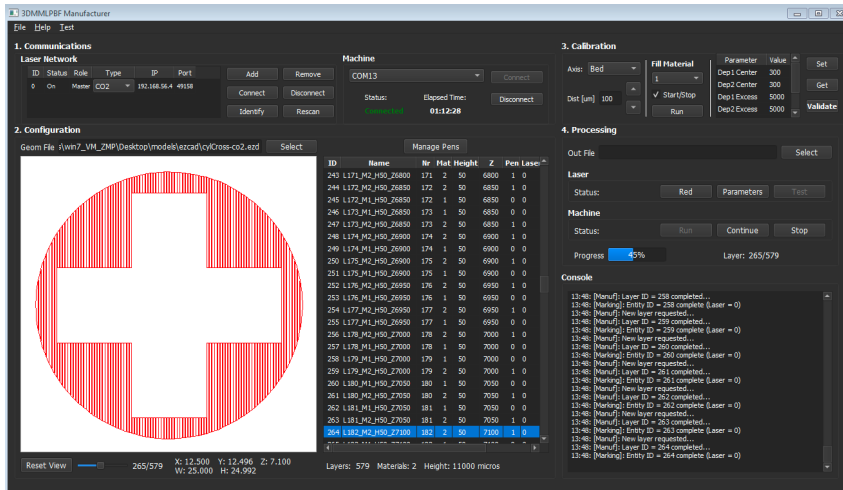
Figure 100: CO₂ laser – bi-material manufacturing test: Pre-Manufacturing processing



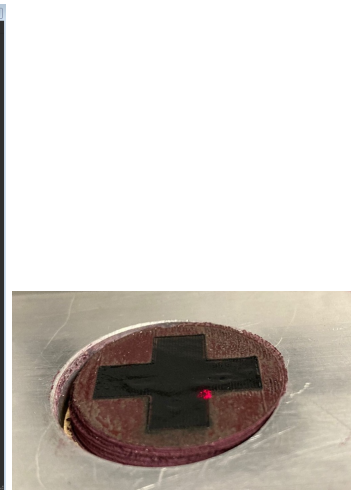
(a) Initialisation



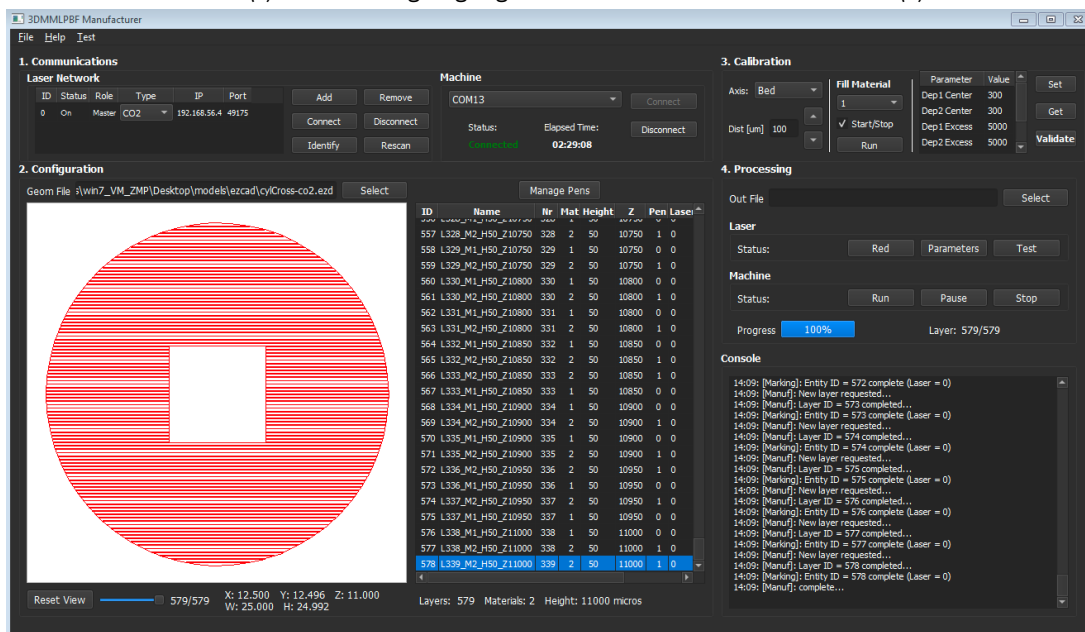
(b) Process parameters



(c) Manufacturing on-going



(d) Machine bed

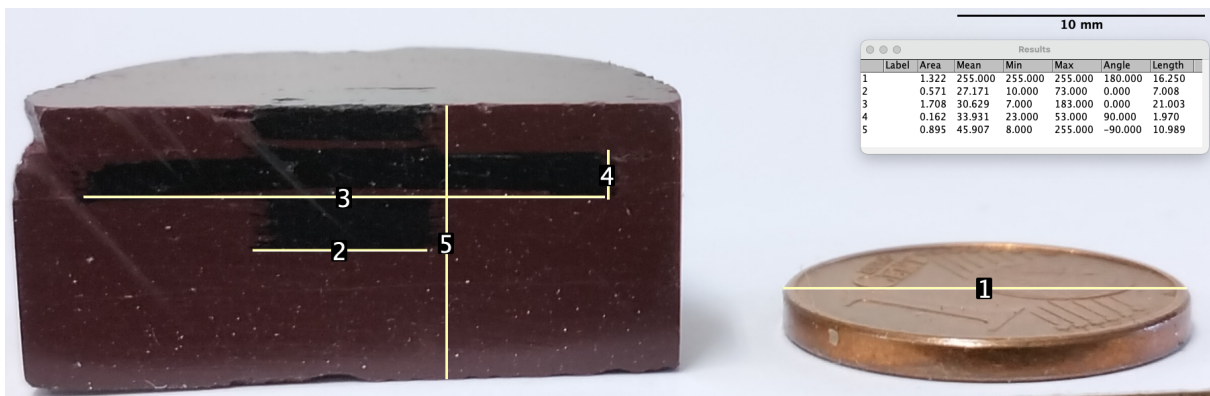


(e) Manufacturing complete

Figure 101: CO₂ laser – bi-material manufacturing test: Manufacturing

Figure 102: CO₂ laser – bi-material manufacturing test: Produced part

slight discrepancy, especially in the z-axis, which may be due to the densification effect or measurement errors, but overall the dimensions of the produced part match the ones from the 3D CAD model.

Figure 103: CO₂ laser – bi-material manufacturing test: Geometrical measurements using Fiji's SW

The SEM analysis performed on the part (Fig. 104) showed good densification, demonstrating the good manufacturing performance of the equipment.

Thus, the equipment is capable of producing multi-material components using the 3DMMLPBF process, in compliance to the 3D models geometry, and with good overall manufacturing performance by enabling the mapping of geometrical and topological data to process parameters and through robust control of the process.

The information concerning the manufacturing process as a whole was then collected and added to the *Post-Manufacturer*. Fig. 105 shows the *Pre-Manufacturer's* data collection, storing the input and output files' related information, respectively. It allows quick navigation and visualisation of these information flows, which are indexed to a produced part.

Fig. 106 shows the *Manufacturer's* data collection, storing the input, configuration and logs' related information, respectively. It allows quick navigation and visualisation of these information flows, which are also indexed to a produced part. The input and configuration data can be used in conjunction with the mechanical tests to analyse the manufacturing performance and behaviour. On the other hand, the logs can be used by the control/systems engineer to analyse the equipment and software behaviour, and improve it.

Fig. 107 depicts the Mechanical tests manager UI added to the *Post-Manufacturer* software to handle the mechanical tests performed on the produced components. These tests can be added to the database with an accompanying image, for example SEM, which can then be downloaded and used for analysis, for example, using AI. The analysis results can then be uploaded back to the database for tracking and process improvement.

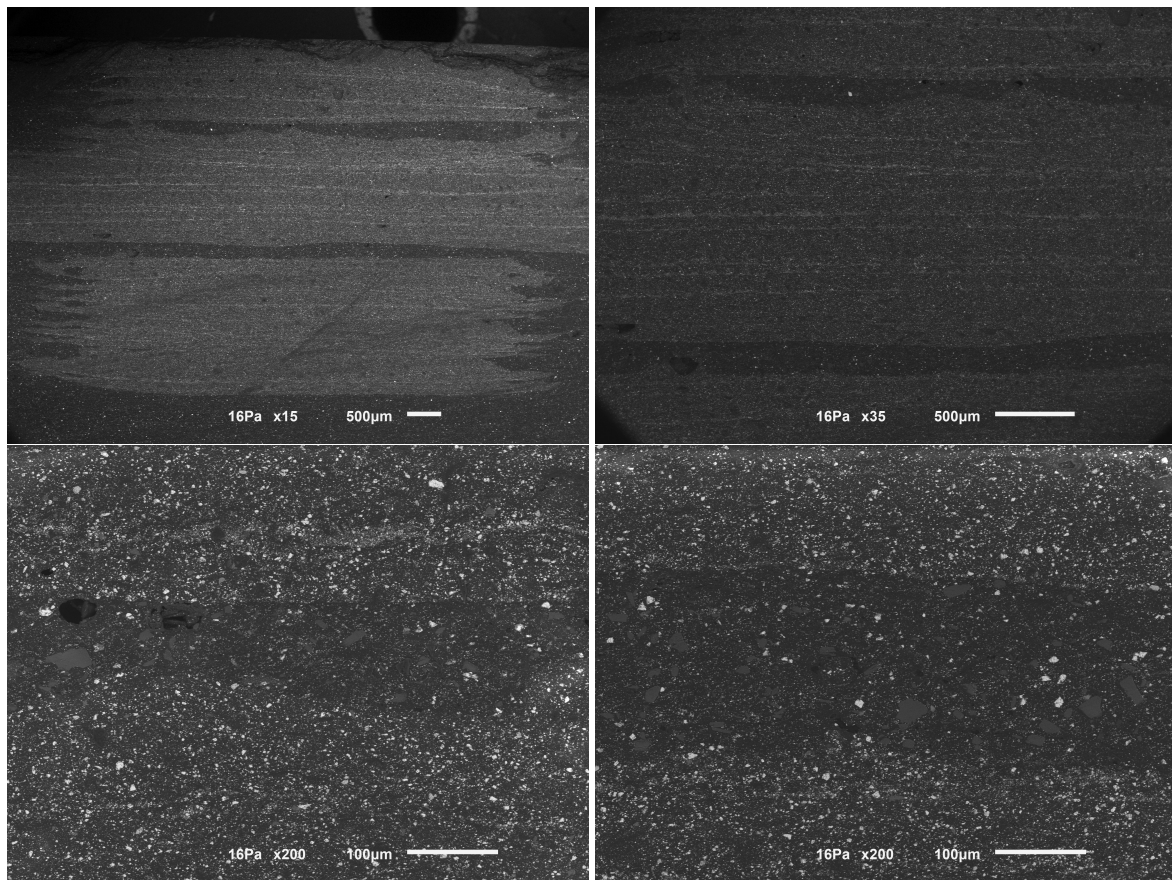


Figure 104: CO₂ laser – bi-material manufacturing test: SEM analysis

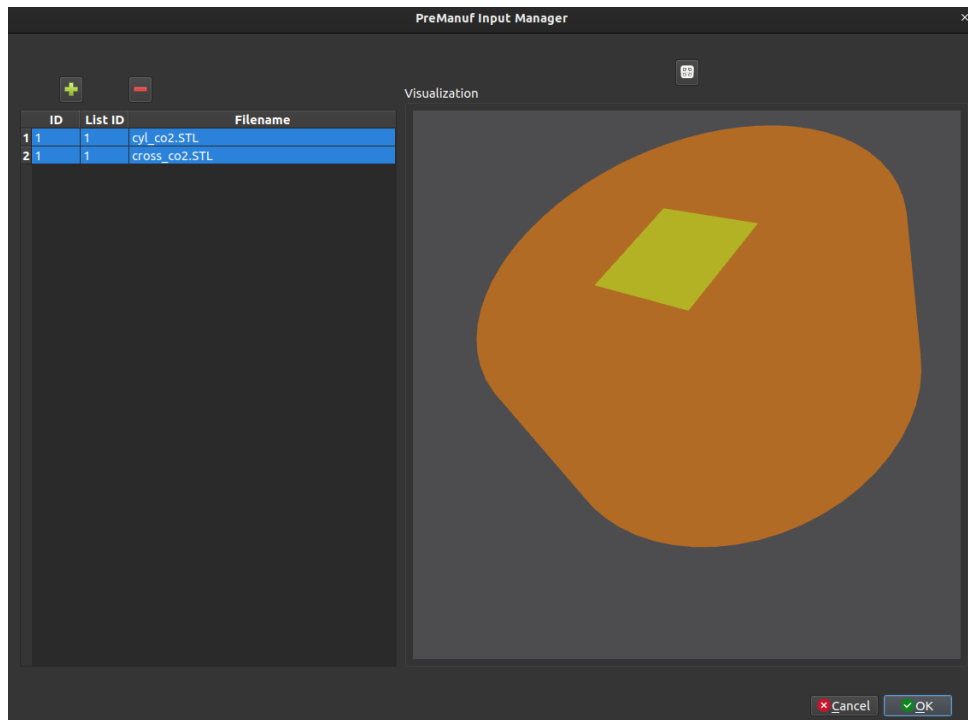
5.1.2 Nd-YAG Laser

After proving the correctness of the overall process – methodology, workflow, toolchain and equipment – more multi-material parts can be produced, but now, using metals.

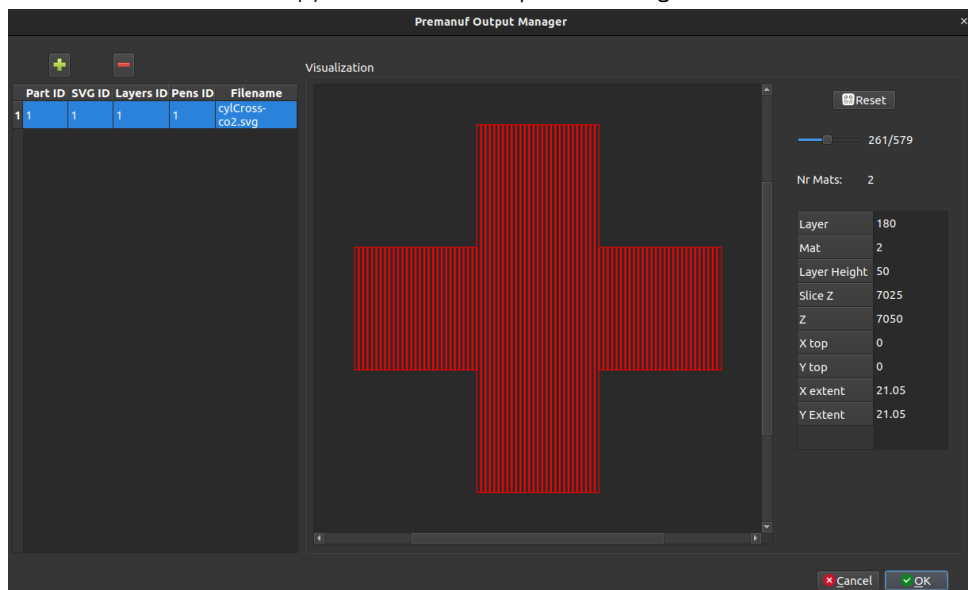
5.1.2.1 Pre-Manufacturing

Metallic powders have different absorption wavelength spectrum than the polymeric ones, which requires the usage of a different and suitable laser source, namely the Nd-YAG. In that sense, a multi-material metallic component was conceptualised for manufacturing.

However, this time, the conventional method was used to illustrate its difficulties. Thus, instead of 3D modelling and running the multi-material model through the Pre-Manufacturer software, the multi-material component was designed directly in a 2D vector drawing *SW*, EzCAD, in this case. This forced the designer to draw 2D layers and stack them on top of each other – mimicking the slicing – and manually perform the hatching – mimicking the path generation. With this approach the designer loses the 3D perspective, which makes it significantly harder for the conceptual design of the component. This downside is especially critical if multi-material is added to the equation, as now, the designer needs to be aware and track, not only, the tridimensional shape of the component, but also the materials' placement and its interfaces. As it becomes obvious, this completely defeats the purpose of functional design. Nonetheless, the *Manufacturer* is still able to process such models, as long as the layer



(a) Pre-Manufacturer input files manager

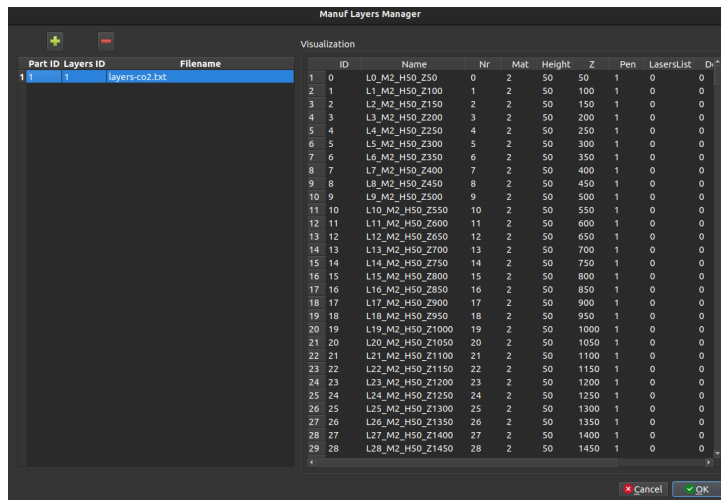


(b) Pre-Manufacturer output files manager

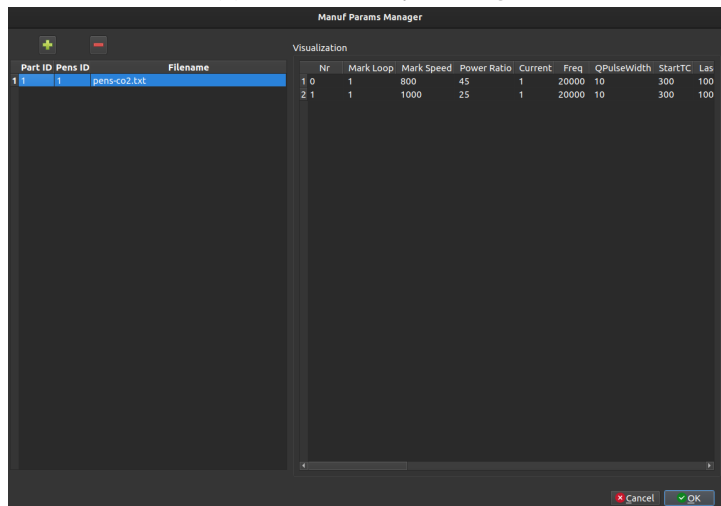
Figure 105: CO₂ laser – Post-Manufacturer: Pre-Manufacturer data management

naming convention is respected.

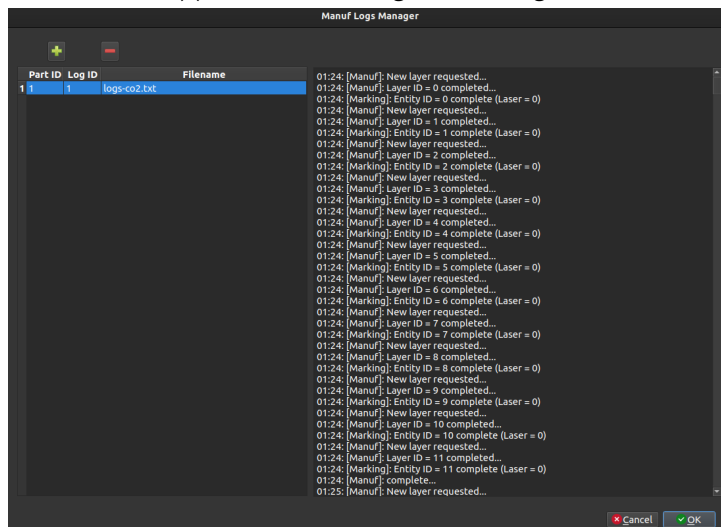
Fig. 108 illustrates the modelling procedure, with some layers containing sets of grouped points (pattern), and others being hatched (to act as a supporting layer), whose goal is to embed channels in the part and supporting pillars in the part [183]. It must be stressed out that the design methodology devised allows this component to be modelled directly in a 3D CAD software by adding intermediate models, abstracted as materials, and then processed normally across the manufacturing chain.



(a) Manufacturer input manager



(b) Manufacturer configuration manager



(c) Manufacturer logs manager

Figure 106: CO₂ laser – Post-Manufacturer: Manufacturer data management

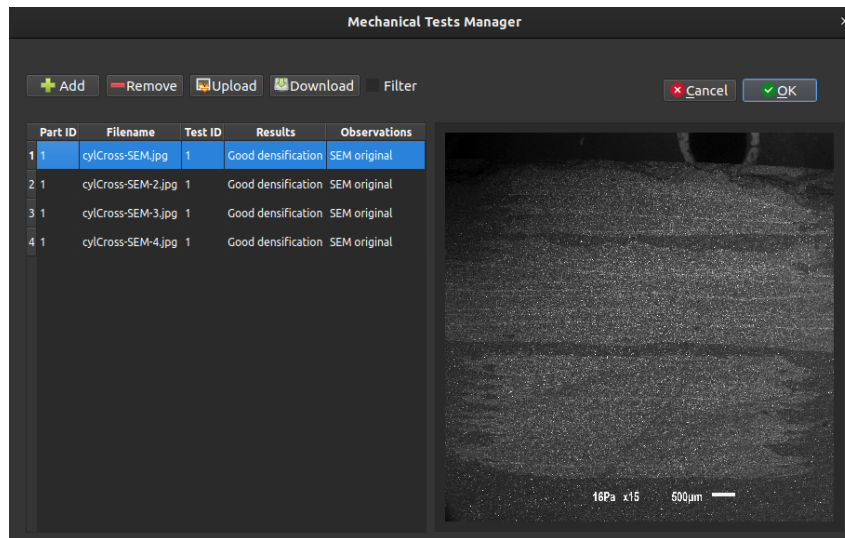


Figure 107: CO₂ laser – Post-Manufacturer: Mechanical tests manager

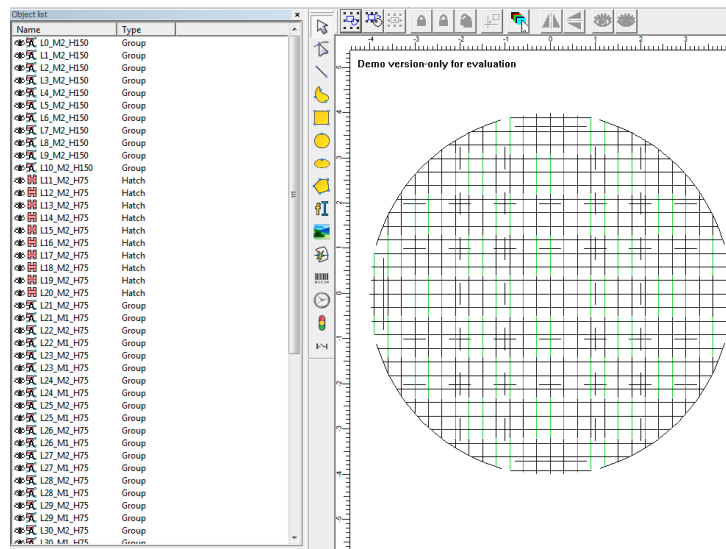


Figure 108: Nd-YAG laser: bi-material manufacturing test – Modelling in EzCAD

This model was then loaded into the Manufacturer SW for validation, as it eases the visualisation process. Fig. 109 shows the basic stratification of the model. The model has 62 slices totalling 4275 μm in height (Fig. 109a). The first ten layers (Fig 109b), with 150 μm in height, correspond to a cross pattern replicated across the whole area, acting as a support for the component. Then, from layer 11 to 20 (Fig. 109c), with 75 μm in height, we have a hatched pattern to act as a supporting substrate for the multi-material layers. From layer 21 to 31, we have slices containing both materials with a chess board pattern, but offsetted by 100 μm , to promote mechanical interlocking of the layers (see Fig. 109d, and Fig. 109e, respectively). Lastly, from layer 32 to the end, we have a hatched pattern to close off the part (Fig. 109).

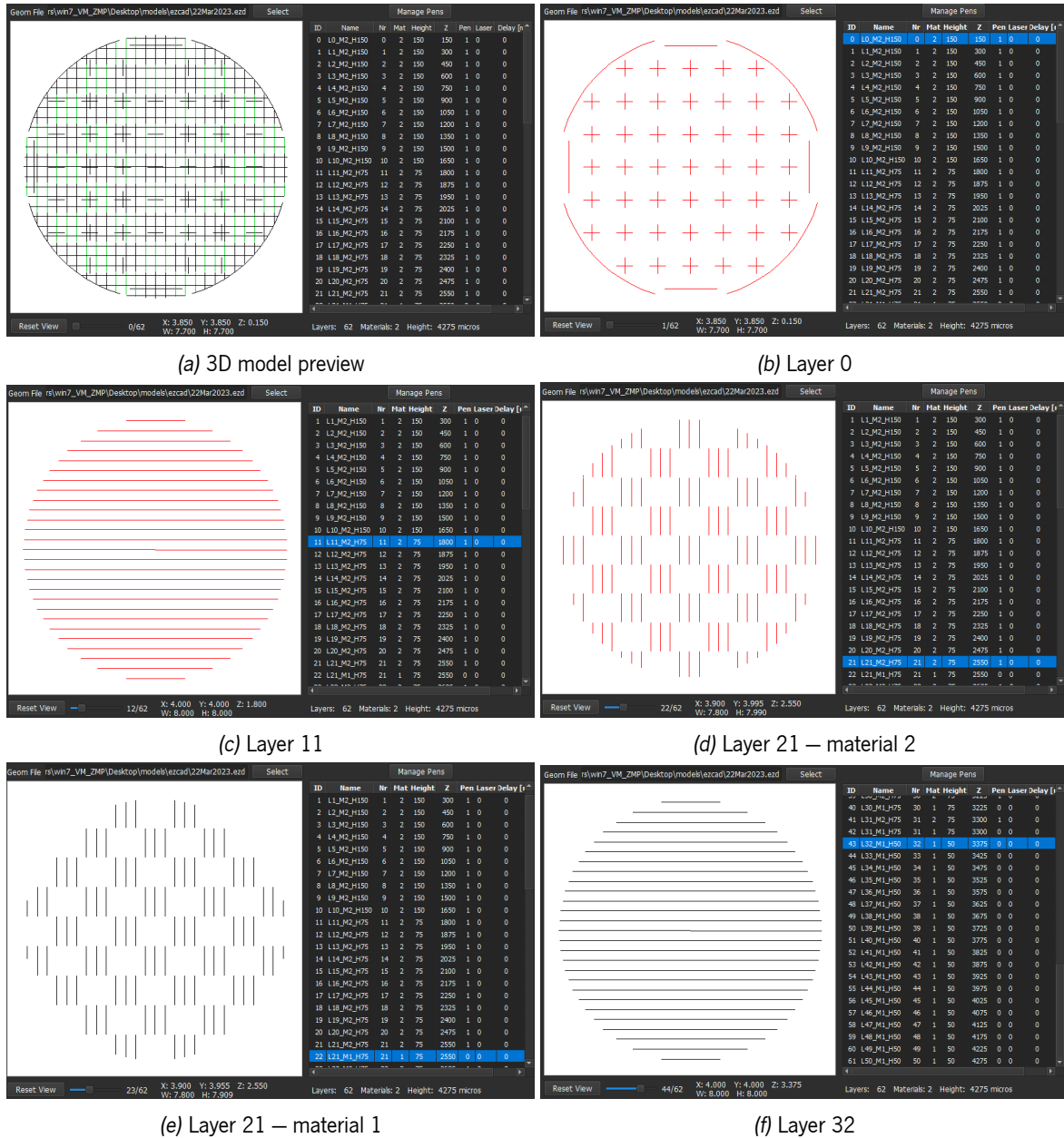
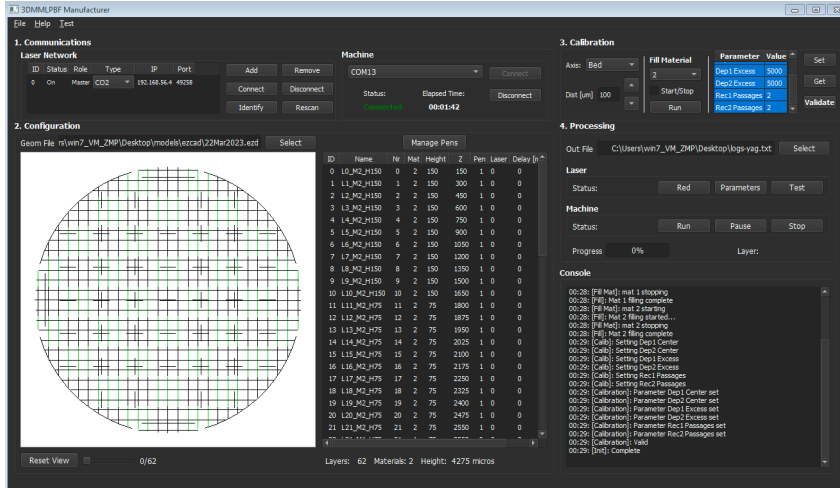


Figure 109: Nd-YAG laser – bi-material manufacturing test: Model preview

5.1.2.2 Manufacturing

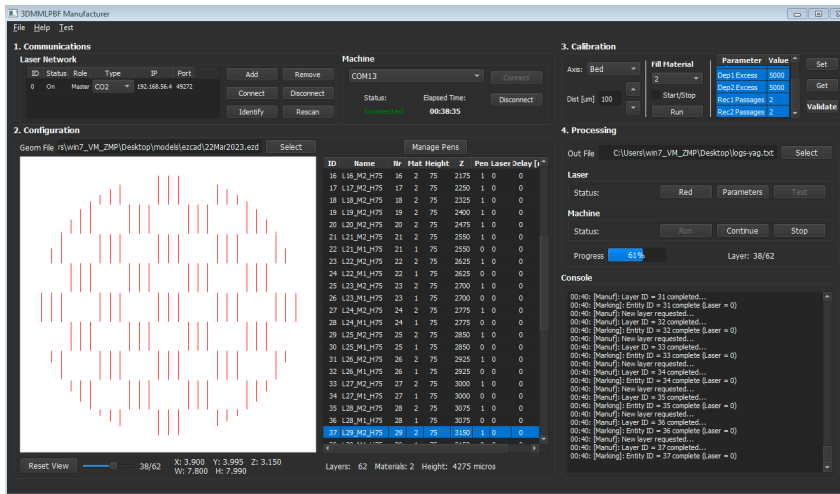
After loading the model, the initialisation procedure was performed, as illustrated in Fig. 110a, comprising the 3DMMLPBF machine communication setup and homing, the calibration for powder minimisation, and powder filling. The process parameters were mapped to each material, Ti6Al4V and CoCrMo, as shown in Fig. 110b. The same set of parameters were applied to both materials, with significantly slower marking speeds (10 mm/s) and higher power ratios (55%).



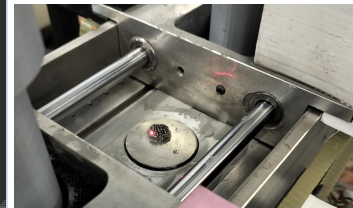
(a) Initialisation

Nr	Mark Loop	Mark Speed	Power Ratio	Current	Freq
0	1	10	55	1.000	35000
1	1	10	55	1.000	35000

(b) Process parameters



(c) Manufacturing halted



(d) Machine bed

Figure 110: Nd-YAG laser – bi-material manufacturing test: Manufacturing

The manufacturing was then initiated by selecting all layers to manufacture and pressing the Run pushbutton. More than half the layers were correctly manufactured, however, at layer 29, the process was halted (Fig. 110c), as some significant distortion were occurring at the interfaces between the two metals. Fig. 110d illustrates the machine bed when the halting occurred.

Fig. 111 shows the bi-material part produced, where it is clearly visible some of the distortions that took place and led to process aborting. Thus, more work in the 3D model design and manufacturing setup for this geometry with the designated metallic pair.



Figure 111: Nd-YAG laser – bi-material manufacturing test: Produced part

5.1.2.3 Post-Manufacturing

As important as documenting the successes, is the failed trials documentation. As such, the process information was collected and stored in the *Post-Manufacturer*.

Fig. 112 shows the *Manufacturer*'s data collection, storing the input, configuration and logs' related information, respectively. As can be seen, this information is appended to the already stored data.

Fig. 113 shows the *Electron Microscope (EM)* image analysis performed on the component added to the database. These images further support the manufacturing's halting decision, as the defects become clearer. Once again, data is appended, contributing to the increasing process knowledge base.

5.2 Multi-material multi-laser

The multi-material fabrication was also tested using multiple lasers, in this case, CO₂ and Nd-YAG. This is important because, as aforementioned, polymeric, ceramic and composite materials have different absorption wavelength spectrum than the metallic ones, which requires the usage of different laser types. Thus, for multi-material fabrication consisting of a combination of polymeric/ceramic materials with metallic ones, multiple lasers must be used efficiently.

The cylinder and cross model was used once again, but scaled, (see Fig. 99), and each material was exported to an *STL* file. The cylinder has 11 millimetres in diameter and 2.5 millimetres in height. The cross is an "assembly" of a parallelepiped with 2 x 2 x 0.4 mm, totalling a bounding volume of 6 x 6 x 1.2 mm. The cross referenced to the top plane of the cylinder, so that the cylinder's first layers act as support material.

One very interesting idea behind the usage of dissimilar types of materials is the *sacrificial substrate*. In this concrete example, the cross can be produced using a polymeric material, which could then be removed to yield its negative made out of a metallic alloy. The sacrificial substrate is significantly cheaper than the base material, and enables the production of a negative without manufacturing defects such as the ones resulting from hanging slices (without support material). This also limits cross contamination to the base material.

Part ID	Layers ID	Filename	ID	Name	Nr	Mat	Height	Z	Pen	LasersList	Delay(ms)
1	1	layers-co2.txt	0	L0_M2_H150	0	2	150	150	1	0	0
2	2	layers-yag.txt	1	L1_M2_H150	1	2	150	300	1	0	0
			2	L2_M2_H150	2	2	150	450	1	0	0
			3	L3_M2_H150	3	2	150	600	1	0	0
			4	L4_M2_H150	4	2	150	750	1	0	0
			5	L5_M2_H150	5	2	150	900	1	0	0
			6	L6_M2_H150	6	2	150	1050	1	0	0
			7	L7_M2_H150	7	2	150	1200	1	0	0
			8	L8_M2_H150	8	2	150	1350	1	0	0
			9	L9_M2_H150	9	2	150	1500	1	0	0
			10	L10_M2_H150	10	2	150	1650	1	0	0
			11	L11_M2_H75	11	2	75	1800	1	0	0
			12	L12_M2_H75	12	2	75	1875	1	0	0
			13	L13_M2_H75	13	2	75	1950	1	0	0
			14	L14_M2_H75	14	2	75	2025	1	0	0
			15	L15_M2_H75	15	2	75	2100	1	0	0
			16	L16_M2_H75	16	2	75	2175	1	0	0
			17	L17_M2_H75	17	2	75	2250	1	0	0
			18	L18_M2_H75	18	2	75	2325	1	0	0
			19	L19_M2_H75	19	2	75	2400	1	0	0
			20	L20_M2_H75	20	2	75	2475	1	0	0
			21	L21_M2_H75	21	2	75	2550	1	0	0
			22	L21_M1_H75	21	1	75	2550	0	0	0
			23	L22_M2_H75	22	2	75	2625	1	0	0
			24	L22_M1_H75	22	1	75	2625	0	0	0
			25	L23_M2_H75	23	2	75	2700	1	0	0
			26	L23_M1_H75	23	1	75	2700	0	0	0
			27	L24_M2_H75	24	2	75	2775	1	0	0
			28	L24_M1_H75	24	1	75	2775	0	0	0
			29	L24_M1_H75	24	1	75	2775	0	0	0

(a) Manufacturer input manager

Part ID	Pens ID	Filename	Nr	Mark Loop	Mark Speed	Power Ratio	Current	Freq	QPulsewidth	StartTC	Las	
1	1	pens-co2.txt	1	0	1	10	55	1	35000	10	300	100
2	2	pens-yag.txt	2	1	1	10	55	1	35000	10	300	100

(b) Manufacturer configuration manager

Part ID	Log ID	Filename
1	1	logs-co2.txt
2	2	logs-yag.txt

```

00:39: [Fill Mat]: mat 1 starting
00:39: [Fill]: Mat 1 filling started...
00:39: [Fill Mat]: mat 1 stopping
00:39: [Fill]: Mat 1 filling complete
00:39: [Fill Mat]: mat 2 starting
00:39: [Fill]: Mat 2 filling started...
00:39: [Fill Mat]: mat 2 stopping
00:39: [Fill]: Mat 2 filling complete
00:39: [Calib]: Setting Dep1 Center
00:39: [Calib]: Setting Dep2 Center
00:39: [Calib]: Setting Dep1 Excess
00:39: [Calib]: Setting Dep2 Excess
00:39: [Calib]: Setting Rec1 Passages
00:39: [Calib]: Setting Rec2 Passages
00:39: [Calibration]: Parameter Dep1 Center set
00:39: [Calibration]: Parameter Dep2 Center set
00:39: [Calibration]: Parameter Dep1 Excess set
00:39: [Calibration]: Parameter Dep2 Excess set
00:39: [Calibration]: Parameter Rec1 Passages set
00:39: [Calibration]: Parameter Rec2 Passages set
00:39: [Calibration]: Valid
00:39: [inj]: Complete
00:39: [Manuf]: New layer requested...
00:39: [Manuf]: Layer ID = 0 completed...
00:39: [Marking]: Entity ID = 0 complete (Laser = 0)
00:39: [Manuf]: New layer requested...
00:39: [Manuf]: Layer ID = 1 completed...
00:39: [Marking]: Entity ID = 1 complete (Laser = 0)
00:39: [Manuf]: New layer requested...
00:39: [Manuf]: Layer ID = 2 completed...
00:39: [Marking]: Entity ID = 2 complete (Laser = 0)
00:39: [Manuf]: New layer requested...
00:39: [Manuf]: Layer ID = 3 completed...
00:39: [Marking]: Entity ID = 3 complete (Laser = 0)
00:39: [Manuf]: New layer requested...
00:39: [Manuf]: Layer ID = 4 completed...
00:39: [Marking]: Entity ID = 4 complete (Laser = 0)
00:39: [Manuf]: New layer requested...

```

(c) Manufacturer logs manager

Figure 112: Nd-YAG laser – Post-Manufacturer: Manufacturer data management

5.2.1 Pre-Manufacturing

The STL files corresponding to each material were loaded in the Pre-Manufacturer SW for processing (Fig. 115a) and the results are displayed in Fig. 115. The same slicing and path generation parameters were defined for both entities (Fig. 115b): first layer height and layer height of $50 \mu\text{m}$, null fill angle, fill density of 10%, and infill extrusion width of $20 \mu\text{m}$, without connected paths. The manufacturing model was generated with 103 slices (Fig. 115c). Layer 0, located at $z = 50 \mu\text{m}$, shows the cylinder's bottom layers, without any intersecting slices belonging to the cross (Fig. 115d). Layer 27, located at $z = 1325 \mu\text{m}$, shows, as expected, the first bi-material layers (Fig. 115e, and Fig. 115f). Lastly, layer 42, located at $z = 1725 \mu\text{m}$, shows the first of the internal layers where the cross is fully displayed (Fig. 115g and Fig. 115h).

Thus, once again, the slicing and path generation complied to the geometrical data (input STL models) and the

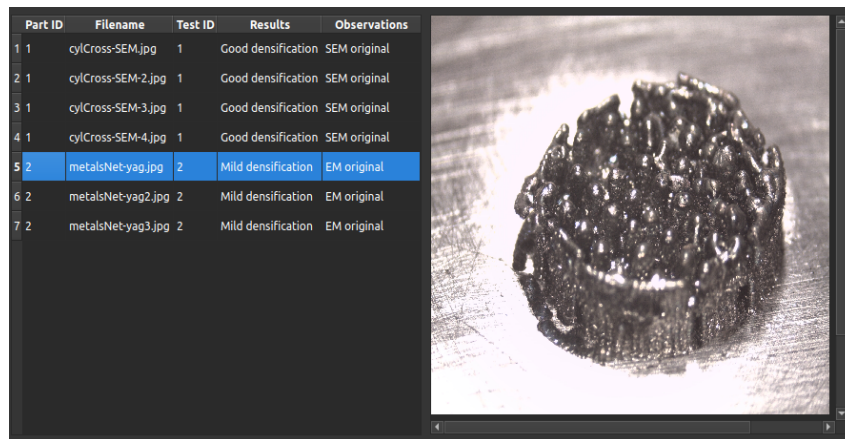


Figure 113: Nd-YAG laser – Post-Manufacturer: Mechanical tests manager

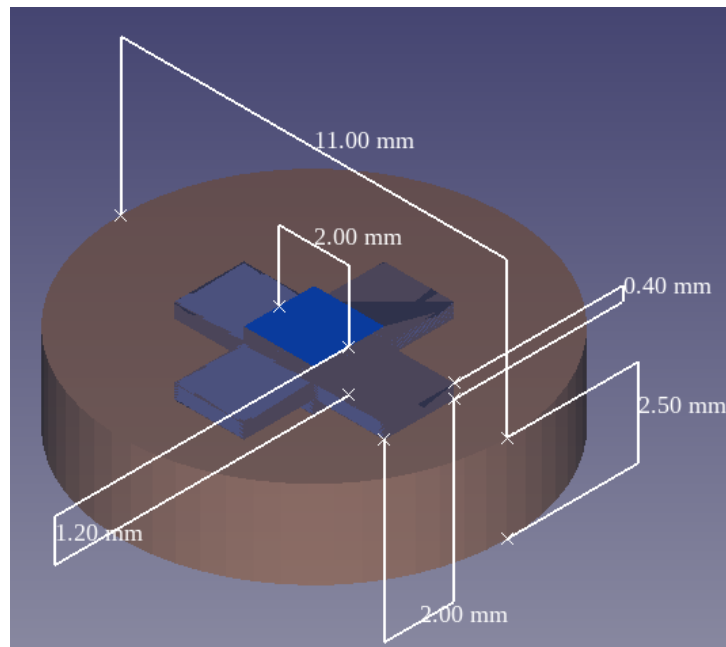


Figure 114: Multi-laser – bi-material manufacturing test: FreeCAD modelling

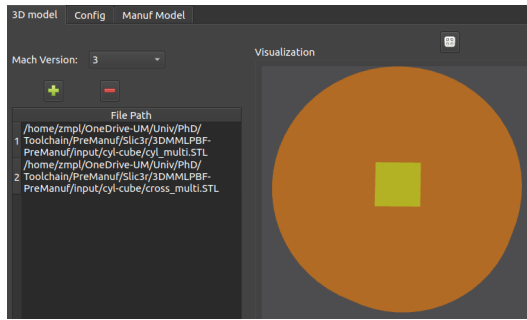
defined configuration, further validating the [Pre-Manufacturer SW](#).

5.2.2 Manufacturing

Multi-laser manufacturing requires a special setup, due to the available lasers' characteristics and its specifics, namely, bulky laser generation systems, and different focus distances.

Thus, firstly, the lasers arrangement was modelled in a CAD software for quick iteration (see Fig. 116). The bulkiness and different focus distances dictate that the lasers must be tilted in order to obtain a working overlapping area. However, the laser tilting produces focus field distortion, which must be corrected to limit geometrical deviations.

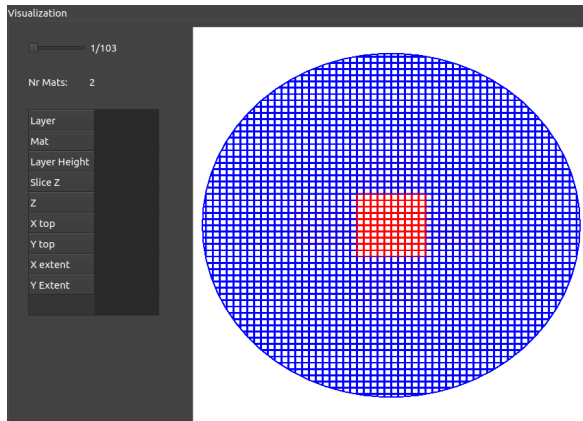
The lasers' focus cones were placed at the focus height and with a minimum offset apart (Fig. 116a), and the lasers were tilted (Fig. 116b), determining the intersection between them (Fig. 116c). The intersection plane must



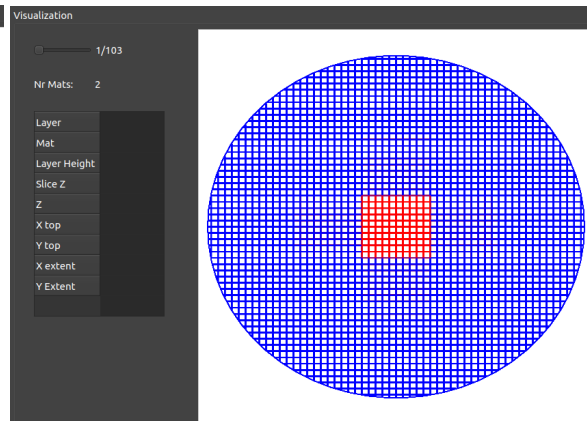
(a) 3D model preview

Generic		Specific	
✓ Enable			
STL ID	0	1	
First Layer Height (mm)	0.05	0.05	
Layer Height (mm)	0.05	0.05	
Fill Angle (deg)	0	0	
Fill Density (%)	10	10	
Fill Pattern	rectilinear	rectilinear	
Infill Extrusion Width (mm)	0.02	0.02	
Connect Paths	0	0	

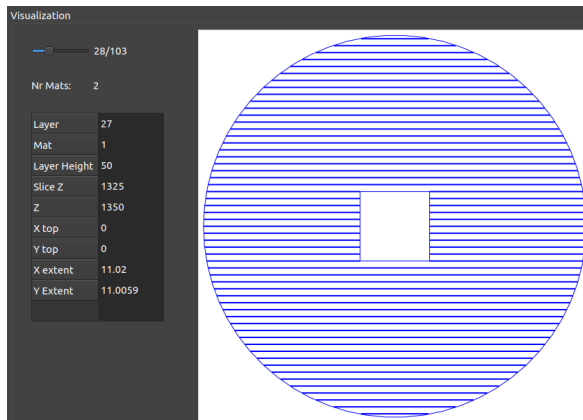
(b) Slicing and path generation setup



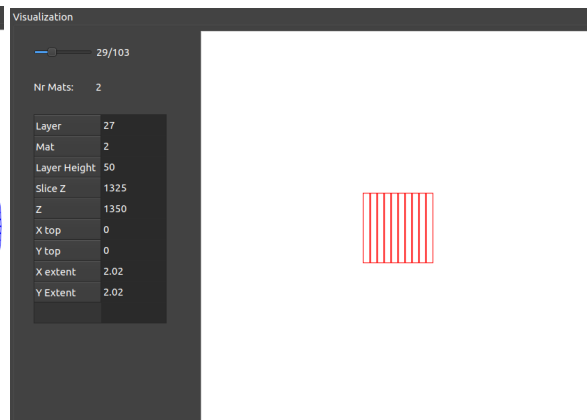
(c) Output: main view



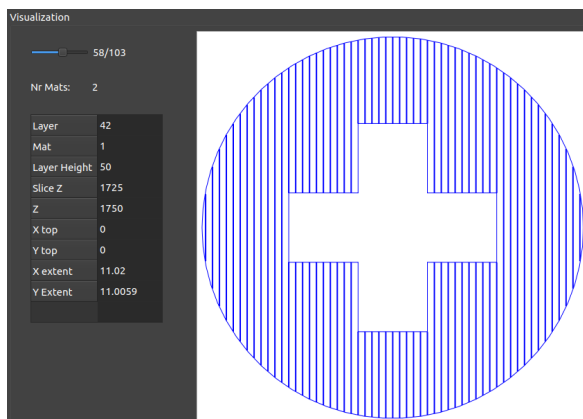
(d) Output: Layer 0



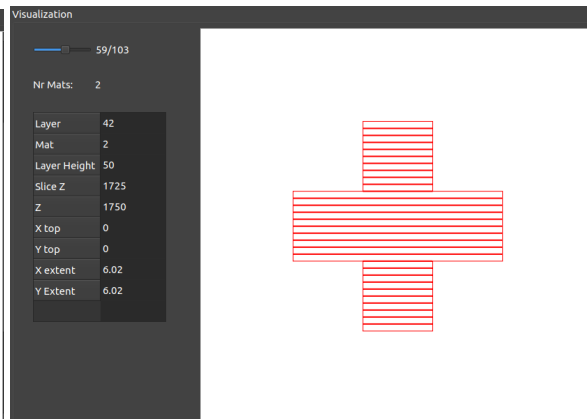
(e) Output: Layer 27 – material 1



(f) Output: Layer 27 – material 2



(g) Output: Layer 42 – material 1



(h) Output: Layer 42 – material 2

Figure 115: Multi-laser – bi-material manufacturing test: Pre-Manufacturing processing

have at least the area of the printing bed – a circle of 28 mm in diameter (Fig. 116d). The minimum tilting angle that yields a working overlapping area of 28 mm in diameter is circa 27 degrees.

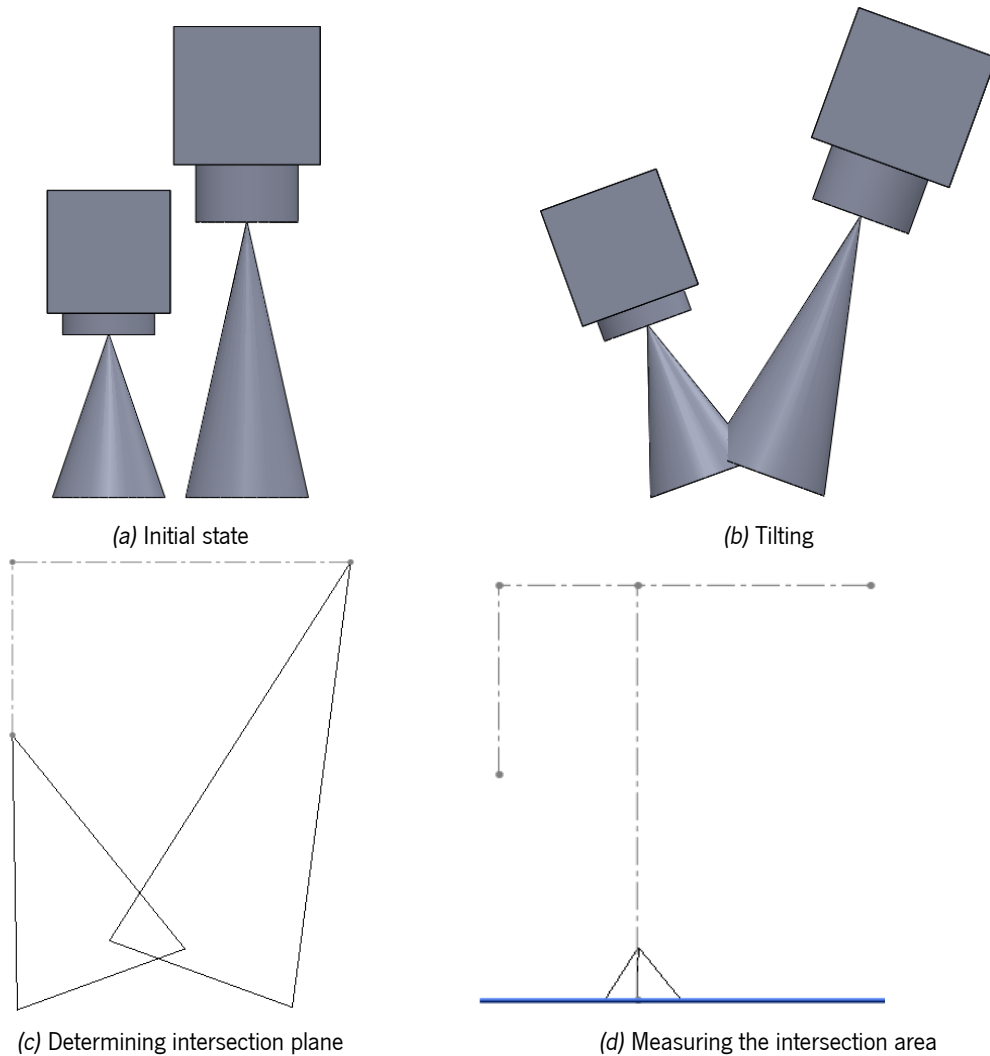


Figure 116: Multi-laser – bi-material manufacturing test: Lasers' setup modelling

However, for practical reasons, such as secure placement of both lasers and the collision with the powder recovery systems, only the CO₂ laser was tilted (Fig 117a). Then, both laser beams were calibrated and aligned to the centre of printing bed (Fig. 117b).

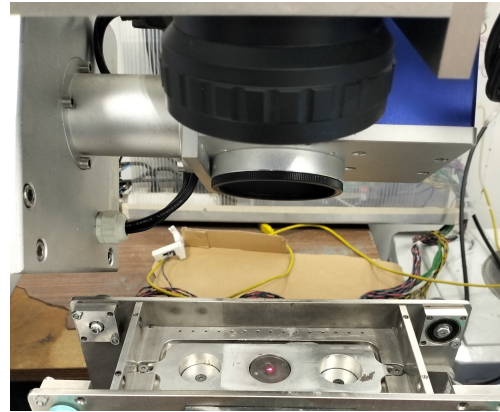
Following the Manufacturer's deployment diagram (see Fig. 49), one instance of the software was deployed to each laser's computer (Fig 118). The computers were connected using an Ethernet cable, and the main system (master) was connected to the machine via USB cable.

The resulting manufacturing model was then loaded to each Manufacturer's SW instance and the network was configured and setup for master and slave connection. Fig. 119 illustrates the network setup configuration: in the master system the slave network address and port is added (Fig. 119a), and the connection is established by pressing the Connect pushbutton. If the network configuration is correct, the master system connects to the slave, which then prints its network ID (Fig. 119b).

The manufacturing parameters were configured, as illustrated in Fig. 120a, with pen 0 being mapped to the



(a) Laser tilting



(b) Lasers' beam calibration

Figure 117: Multi-laser – bi-material manufacturing test: Lasers' setup

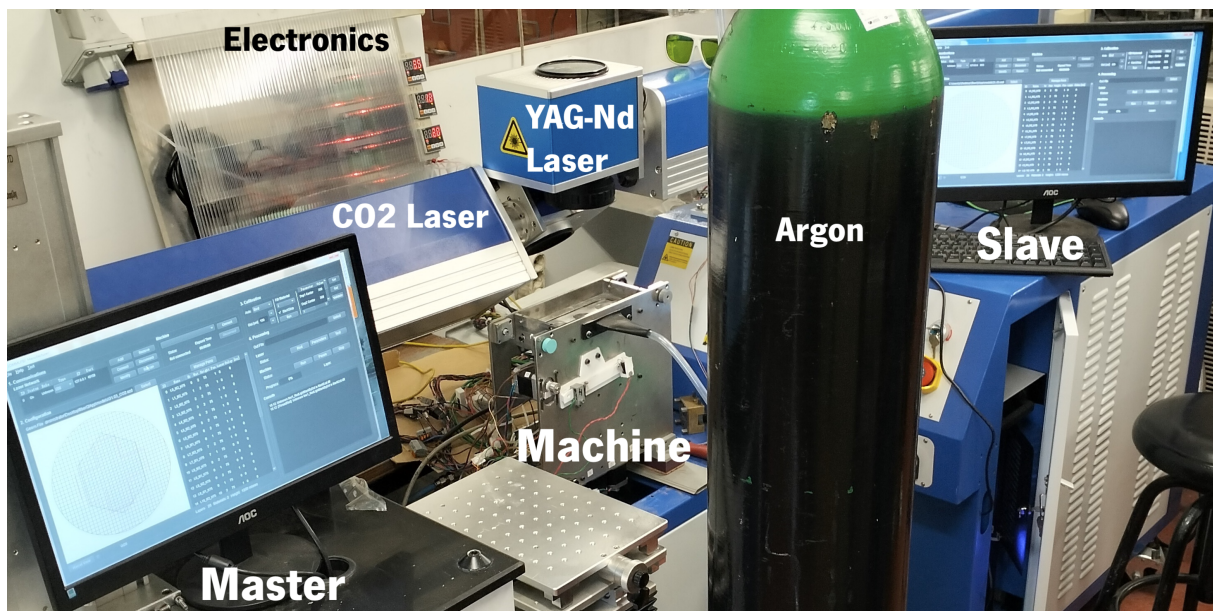
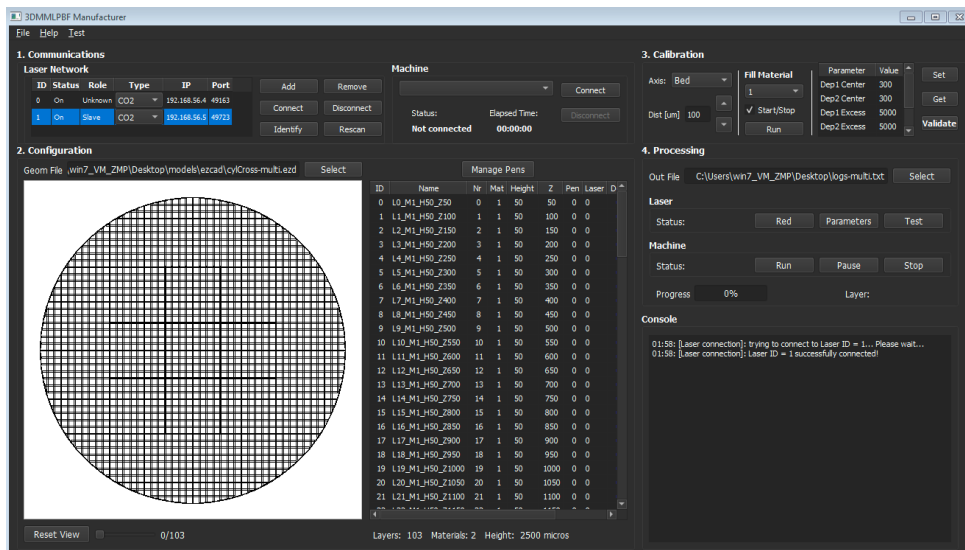


Figure 118: Multi-laser – bi-material manufacturing test: Manufacturing setup

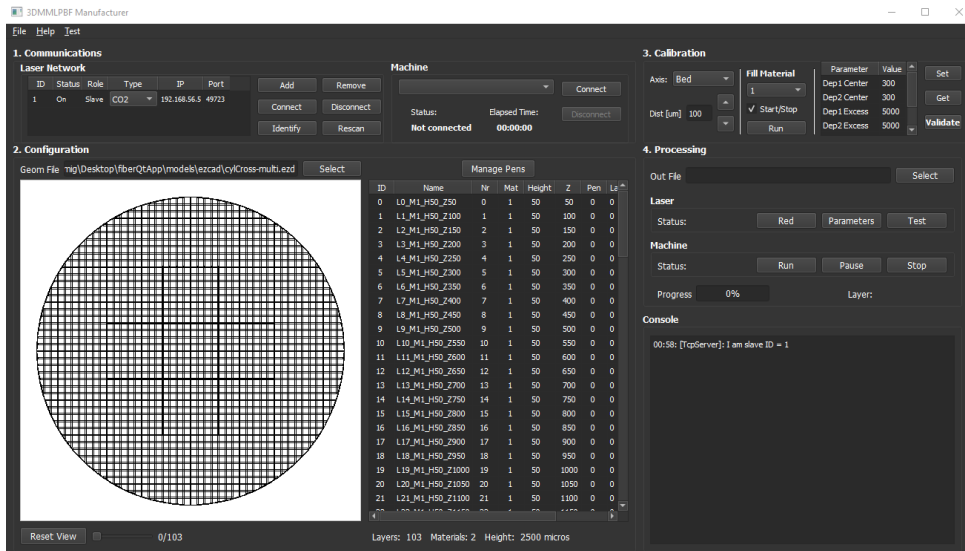
polymeric material (electrostatic coating based on TGIC polyester), and pen 1 to a metallic alloy of CoCrMo. Layers were then assigned to each laser, by sorting them by material and defining the laser, as shown in Fig. 120b.

The master system was connected to the 3DMMLPBF machine via COM port. Upon the successful connection, the machine was automatically homed. A calibration was performed to minimise powder usage and the filling procedure was executed for both materials. After concluding these steps and validating the calibration, the machine's initialisation was complete.

Fig. 121 illustrates the manufacturing procedure. The manufacturing was initiated by selecting all layers to manufacture and pressing the Run pushbutton 121a. Fig. 121b and Fig. 121c illustrates the on-going manufacturing, where it can be seen the multi-material part being built, first adding the material and then marking the paths with the laser. Fig. 121d and Fig. 121e shows the final manufacturing state: on layer 70 it was detected some defects on the polymeric sintering, which forced the process to be aborted. These defects may arise from the selected layer height (the same as the metallic alloy), from the powder's bed temperature, from the different



(a) Master configuration and connection establishment



(b) Slave accepts connection and prints its ID

Figure 119: Multi-laser – bi-material manufacturing test: Manufacturing (network setup)

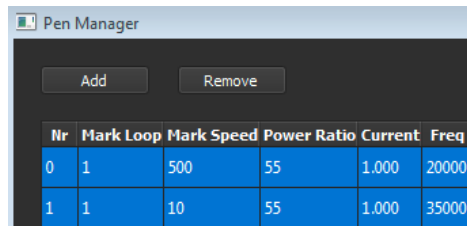
processing parameters, or from a combination of all of them.

Fig. 122 shows the bi-material part produced, where it is clearly visible the defects in the polymeric manufacturing.

5.2.3 Post-Manufacturing

Even though the part was not completely manufactured, it is important to document and analyse the reasons behind this. In that sense, several analysis were performed on the produced part to assess the manufacturing quality, namely on geometrical compliance and densification.

Geometrical compliance was assessed, once again, using Fiji [181] and using a 1 cent coin as a base for the measurements (Fig. 103). The measurements performed showed a higher discrepancy, which can be due to the laser focus distortion induced by the tilting. This must be further investigated and corrected. Nonetheless,



Nr	Mark Loop	Mark Speed	Power Ratio	Current	Freq
0	1	500	55	1.000	20000
1	1	10	55	1.000	35000

(a) Parameters setup

ID	Name	Nr	Mat	Height	Z	Pen	Laser	De
28	L27_M2_H50_Z1350	27	2	50	1350	1	1	
29	L28_M2_H50_Z1400	28	2	50	1400	1	1	
31	L29_M2_H50_Z1400	29	2	50	1400	1	1	
34	L30_M2_H50_Z1450	30	2	50	1450	1	1	
36	L31_M2_H50_Z1450	31	2	50	1450	1	1	
38	L32_M2_H50_Z1500	32	2	50	1500	1	1	
40	L33_M2_H50_Z1500	33	2	50	1500	1	1	
42	L34_M2_H50_Z1550	34	2	50	1550	1	1	
44	L35_M2_H50_Z1550	35	2	50	1550	1	1	
45	L36_M2_H50_Z1600	36	2	50	1600	1	1	
47	L37_M2_H50_Z1600	37	2	50	1600	1	1	
49	L38_M2_H50_Z1650	38	2	50	1650	1	1	
52	L39_M2_H50_Z1650	39	2	50	1650	1	1	
54	L40_M2_H50_Z1700	40	2	50	1700	1	1	
56	L41_M2_H50_Z1700	41	2	50	1700	1	1	
58	L42_M2_H50_Z1750	42	2	50	1750	1	1	
59	L43_M2_H50_Z1750	43	2	50	1750	1	1	
61	L44_M2_H50_Z1800	44	2	50	1800	1	1	
63	L45_M2_H50_Z1800	45	2	50	1800	1	1	
65	L46_M2_H50_Z1850	46	2	50	1850	1	1	
67	L47_M2_H50_Z1850	47	2	50	1850	1	1	
69	L48_M2_H50_Z1900	48	2	50	1900	1	1	
71	L49_M2_H50_Z1900	49	2	50	1900	1	1	

(b) Layers assignment to lasers

Figure 120: Multi-laser — bi-material manufacturing test: Manufacturing (Parameters and lasers setup)

overall, the geometry of the produced part matched the one from the 3D CAD model, but with a discrepancy in the dimensions.

The EM analysis performed on the part (Fig. 124) showed mild densification for the metallic alloy and poor densification for the polymeric material, further supporting the decision to halt the manufacturing. This may be a result of the degradation of the polymeric material under the thermal gradients induced by the selected processing parameters. This requires careful optimisation, especially if the polymer is not used only as a sacrificial material.

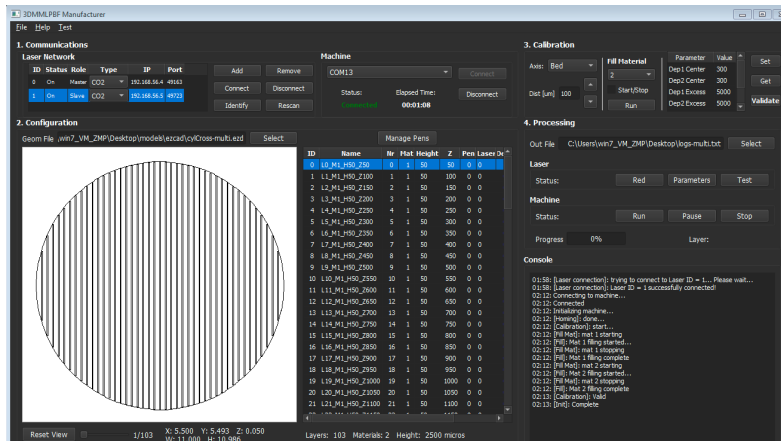
The multi-material part was also analysed using Energy-Dispersive x-ray Spectroscopy (EDS) (Fig. 125) for the two materials. Z1 represents the cross (polymer) and Z2 the cylinder (metallic alloy). This analysis showed that the chemical composition is accordingly to the expectations, with Z1 mainly composed of carbon and Z2 with Cobalt, Chromium, and Molybdenum. It can be further seen that the metallic densification is satisfactory, with the major issue being on the polymer degradation.

The information concerning the manufacturing process as a whole was then collected and added to the *Post-Manufacturer*. Fig. 126 shows the *Pre-Manufacturer's* data collection, storing the input and output files' related information, respectively. It allows quick navigation and visualisation of these information flows, which are indexed to a produced part.

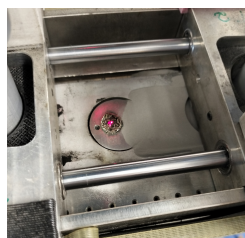
Fig. 127 shows the *Manufacturer's* data collection, storing the input, configuration and logs' related information, respectively. It allows quick navigation and visualisation of these information flows, which are also indexed to a produced part. The input and configuration data can be used in conjunction with the mechanical tests to analyse the manufacturing performance and behaviour. On the other hand, the logs can be used by the control/systems engineer to analyse the equipment and software behaviour, and improve it.

Fig. 128 shows the electron microscope image analysis performed on the component added to the database. Once again, data is appended, contributing to the increasing process knowledge base.

The equipment and manufacturing tests performed clearly demonstrates the feasibility of 3DMMLPBF process and validates the equipment developed, as well as the accompanying toolchain.



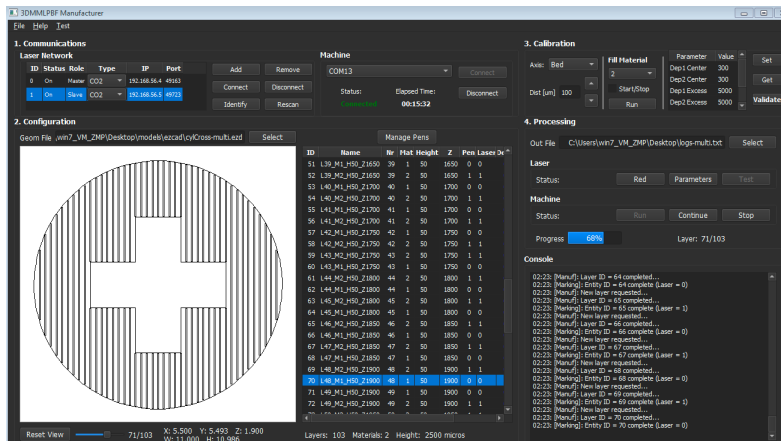
(a) Start



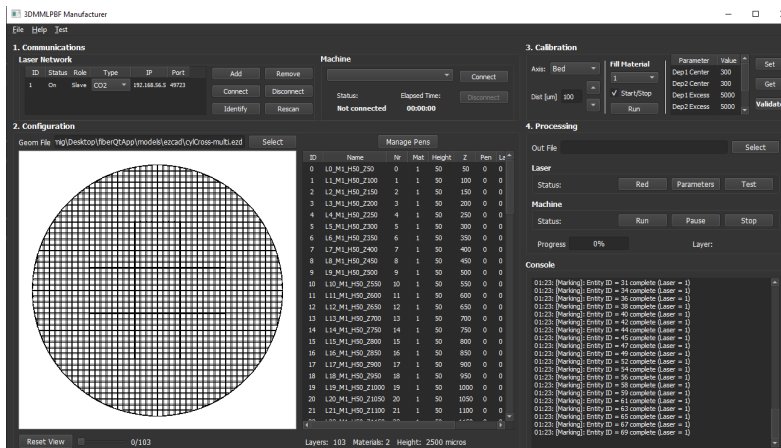
(b) Printing bed: Adding material



(c) Printing bed: Laser actuation



(d) Master final state



(e) Slave final state

Figure 121: Multi-laser – bi-material manufacturing test: Manufacturing procedure



Figure 122: Multi-laser – bi-material manufacturing test: Produced part

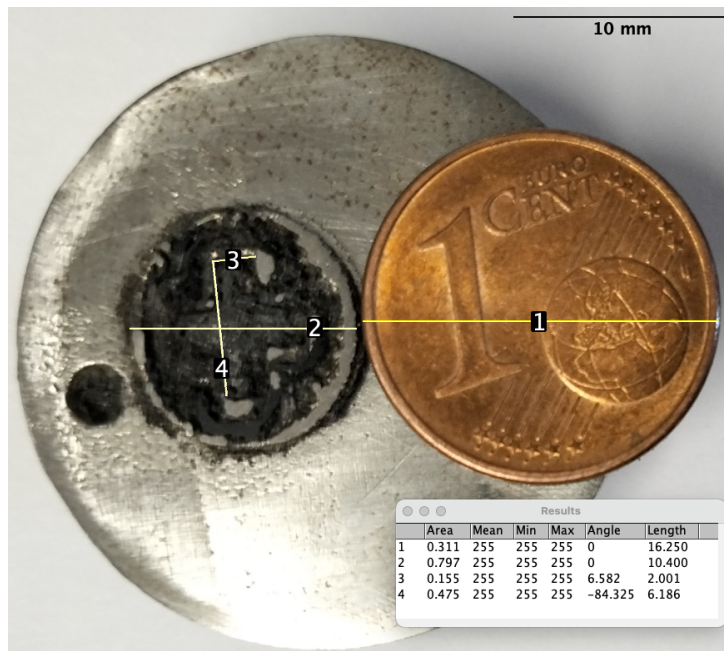


Figure 123: Multi-laser – bi-material manufacturing test: Geometrical measurements using Fiji's SW

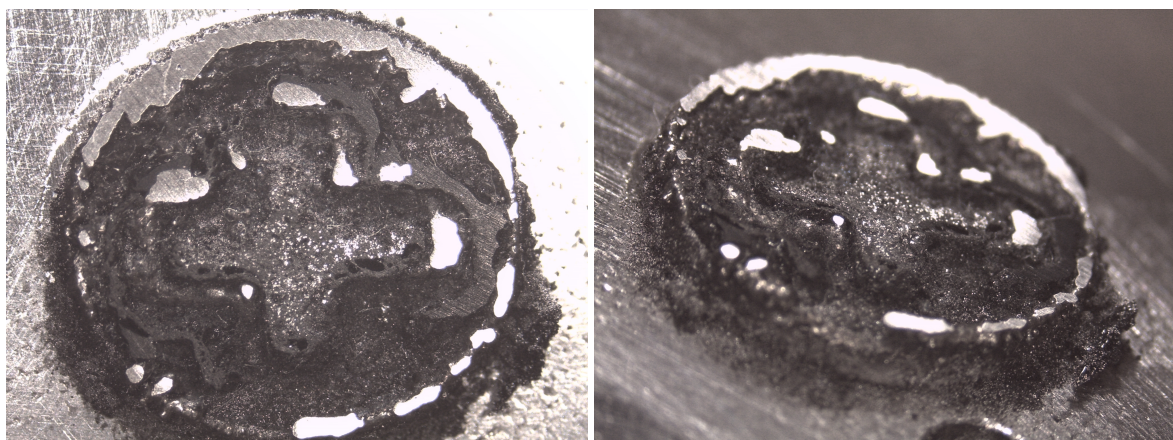


Figure 124: Multi-laser – bi-material manufacturing test: EM analysis

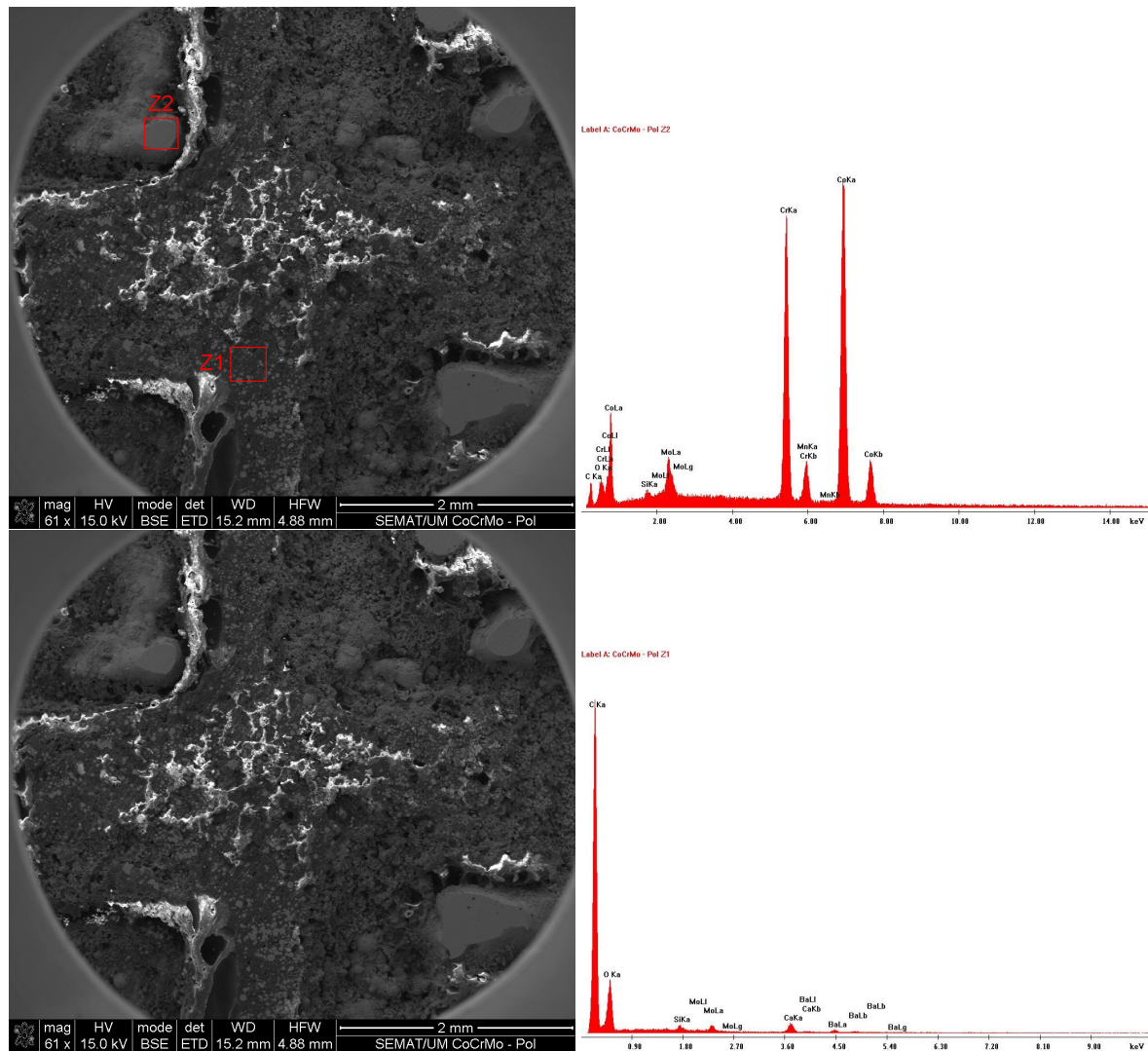
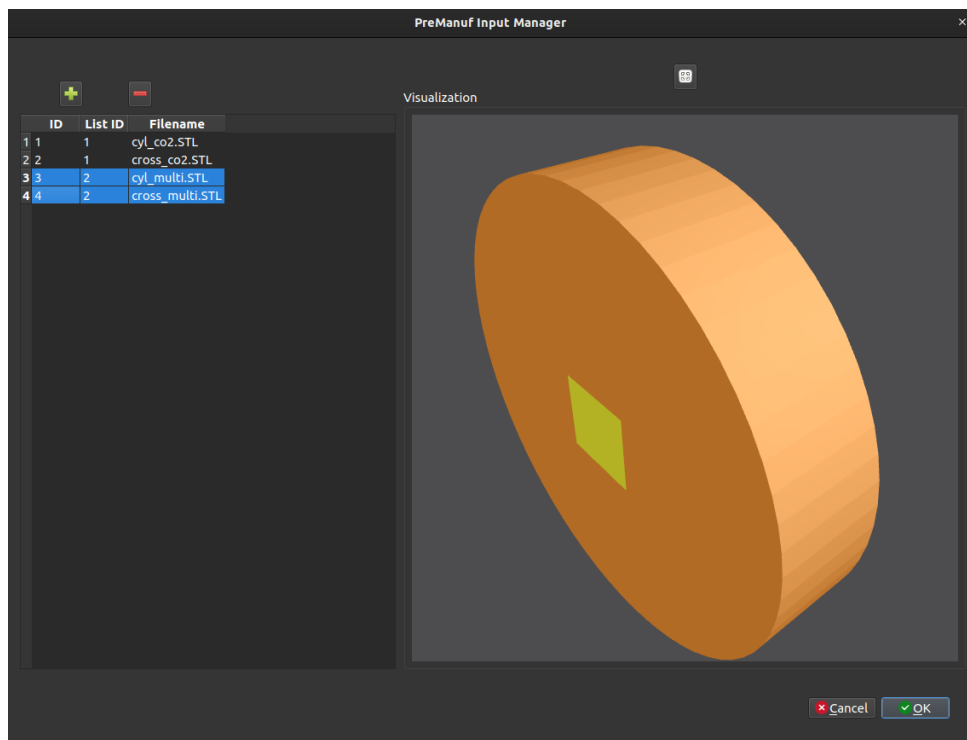


Figure 125: Multi-laser – bi-material manufacturing test: SEM analysis (EDS)

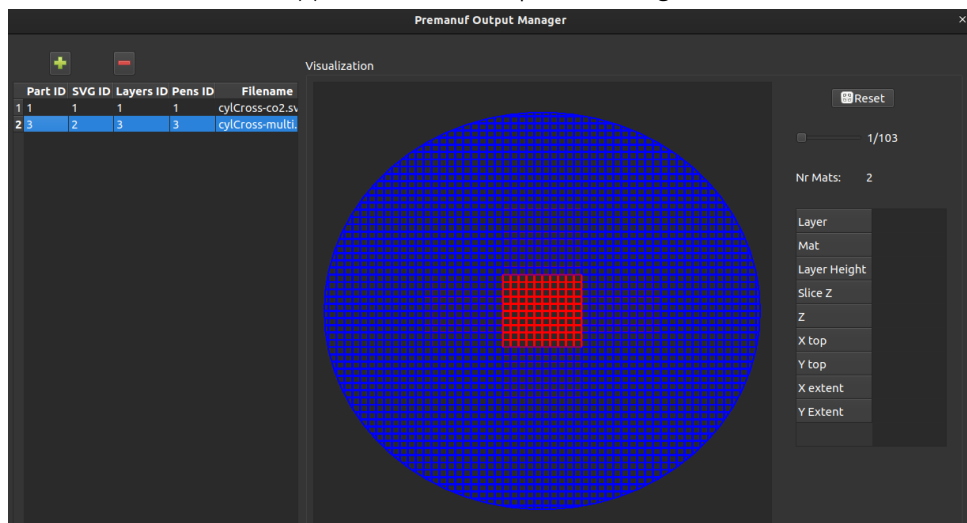
5.3 3DMMLPBF Improvement

The Post-Manufacturer's software provides a knowledge base for 3DMMLPBF process analysis and improvement in a myriad of ways. One such example is illustrated in Fig. 129, where AI is applied to the analysis of the SEM images that enable the assessment of the mechanical structure of the produced parts. It should be noted that this is only a possible venue, as tools and methodologies may differ.

In this example, the SEM analysis is performed through deep learning using Convolutional Neural Network (CNN). The conventional image processing methods, such as traditional segmentation, threshold method, or watershed segmentation, rely on the similarity or intensity (or both) of the image's pixels to locate or delineate the boundaries of objects [184]. Thus, when image's pixels lack intensity or contrast it becomes extremely difficult to distinguish boundaries, even for trained professionals. On the other hand, deep learning tries to mimic the human expert's analysis. By building computational models that can learn representations of data without such requirements, they can be used to perform tasks as efficiently as human experts in specialised fields, saving time and money [184]. For this purpose, deep learning network architecture comprises multiple layers of artificial neural net



(a) Pre-Manufacturer input files manager



(b) Pre-Manufacturer output files manager

Figure 126: Multi-laser – Post-Manufacturer: Pre-Manufacturer data management

units – convolutional neural networks [184].

One paradigmatic example of a fully convolutional network architecture is the *U-Net*, initially developed in 2014 for biomedical image segmentation [185]. It provides more precise segmentation maps using fewer training images [185]. As machine-learning may still be a daunting subject, in 2019 Falk and Mai [186] designed a plugin module to the image processing software *ImageJ* that enables non-expert personnel to design their own training model with the *U-Net*.

Since then the *U-Net* has been used for segmenting image data of non-medical materials. For example, Chen et

Part ID	Layers ID	Filename
1	1	layers-co2.txt
2	2	layers-yag.txt
3	3	layers-multi.txt

ID	Name	Nr	Mat	Height	Z	Pen	LasersList	Delta
1	L0_M1_H50_Z50	0	1	50	50	0	0	0
2	L1_M1_H50_Z100	1	1	50	100	0	0	0
3	L2_M1_H50_Z150	2	1	50	150	0	0	0
4	L3_M1_H50_Z200	3	1	50	200	0	0	0
5	L4_M1_H50_Z250	4	1	50	250	0	0	0
6	L5_M1_H50_Z300	5	1	50	300	0	0	0
7	L6_M1_H50_Z350	6	1	50	350	0	0	0
8	L7_M1_H50_Z400	7	1	50	400	0	0	0
9	L8_M1_H50_Z450	8	1	50	450	0	0	0
10	L9_M1_H50_Z500	9	1	50	500	0	0	0
11	L10_M1_H50_Z550	10	1	50	550	0	0	0
12	L11_M1_H50_Z600	11	1	50	600	0	0	0
13	L12_M1_H50_Z650	12	1	50	650	0	0	0
14	L13_M1_H50_Z700	13	1	50	700	0	0	0
15	L14_M1_H50_Z750	14	1	50	750	0	0	0
16	L15_M1_H50_Z800	15	1	50	800	0	0	0
17	L16_M1_H50_Z850	16	1	50	850	0	0	0
18	L17_M1_H50_Z900	17	1	50	900	0	0	0
19	L18_M1_H50_Z950	18	1	50	950	0	0	0
20	L19_M1_H50_Z1000	19	1	50	1000	0	0	0
21	L20_M1_H50_Z1050	20	1	50	1050	0	0	0
22	L21_M1_H50_Z1100	21	1	50	1100	0	0	0
23	L22_M1_H50_Z1150	22	1	50	1150	0	0	0
24	L23_M1_H50_Z1200	23	1	50	1200	0	0	0
25	L24_M1_H50_Z1250	24	1	50	1250	0	0	0
26	L25_M1_H50_Z1300	25	1	50	1300	0	0	0
27	L26_M1_H50_Z1350	26	1	50	1350	0	0	0
28	L27_M1_H50_Z1350	27	1	50	1350	0	0	0
29	L27_M2_H50_Z1350	27	2	50	1350	1	1	0

(a) Manufacturer input manager

Part ID	Params ID	Filename
1	1	pens-co2.txt
2	2	pens-yag.txt
3	3	pens-multi.txt

Nr	Mark Loop	Mark Speed	Power Ratio	Current	Freq	QPulseWidth	StartTC	Las
1	0	500	55	1	20000	10	300	100
2	1	10	55	1	35000	10	300	100

(b) Manufacturer configuration manager

Part ID	Log ID	Filename
1	1	logs-co2.txt


```

01:24: [Manuf]: New layer requested...
01:24: [Manuf]: Layer ID = 0 completed...
01:24: [Marking]: Entity ID = 0 complete (Laser = 0)
01:24: [Manuf]: New layer requested...
01:24: [Manuf]: Layer ID = 1 completed...
01:24: [Marking]: Entity ID = 1 complete (Laser = 0)
01:24: [Manuf]: New layer requested...
01:24: [Manuf]: Layer ID = 2 completed...
01:24: [Marking]: Entity ID = 2 complete (Laser = 0)
01:24: [Manuf]: New layer requested...
01:24: [Manuf]: Layer ID = 3 completed...
01:24: [Marking]: Entity ID = 3 complete (Laser = 0)
01:24: [Manuf]: New layer requested...
01:24: [Manuf]: Layer ID = 4 completed...
01:24: [Marking]: Entity ID = 4 complete (Laser = 0)
01:24: [Manuf]: New layer requested...
01:24: [Manuf]: Layer ID = 5 completed...
01:24: [Marking]: Entity ID = 5 complete (Laser = 0)
01:24: [Manuf]: New layer requested...
01:24: [Manuf]: Layer ID = 6 completed...
01:24: [Marking]: Entity ID = 6 complete (Laser = 0)
01:24: [Manuf]: New layer requested...
01:24: [Manuf]: Layer ID = 7 completed...
01:24: [Marking]: Entity ID = 7 complete (Laser = 0)
01:24: [Manuf]: New layer requested...
01:24: [Manuf]: Layer ID = 8 completed...
01:24: [Marking]: Entity ID = 8 complete (Laser = 0)
01:24: [Manuf]: New layer requested...
01:24: [Manuf]: Layer ID = 9 completed...
01:24: [Marking]: Entity ID = 9 complete (Laser = 0)
01:24: [Manuf]: New layer requested...
01:24: [Manuf]: Layer ID = 10 completed...
01:24: [Marking]: Entity ID = 10 complete (Laser = 0)
01:24: [Manuf]: New layer requested...
01:24: [Manuf]: Layer ID = 11 completed...
01:24: [Marking]: Entity ID = 11 complete (Laser = 0)
01:24: [Manuf]: complete...
01:25: [Manuf]: New layer requested...

```

(c) Manufacturer logs manager

Figure 127: Multi-laser – Post-Manufacturer: Manufacturer data management

al. [184] presented a strategy to segment clay particles from matrix mineral grains in SEM images of shale samples using the U-Net architecture with a revised weighting algorithm, where no obvious grayscale contrast can be used to differentiate between the two interlocked minerals.

Based on these considerations, Fig. 129 illustrates a possible AI application to SEM images' analysis using the U-Net deep learning CNN architecture and the U-Net ImageJ plugin. The plugin is the front-end, interacting directly with the User, while the deep learning neural network runs on the back-end for performance reasons. These components use the client-server model, connected by a TCP/IP link. The plugin runs on any main OS (Linux, MacOS, Windows), while the back-end may run on a cloud-service or even a Linux workstation.

The Post-Manufacturer stores the SEM images associated to the mechanical tests performed on the

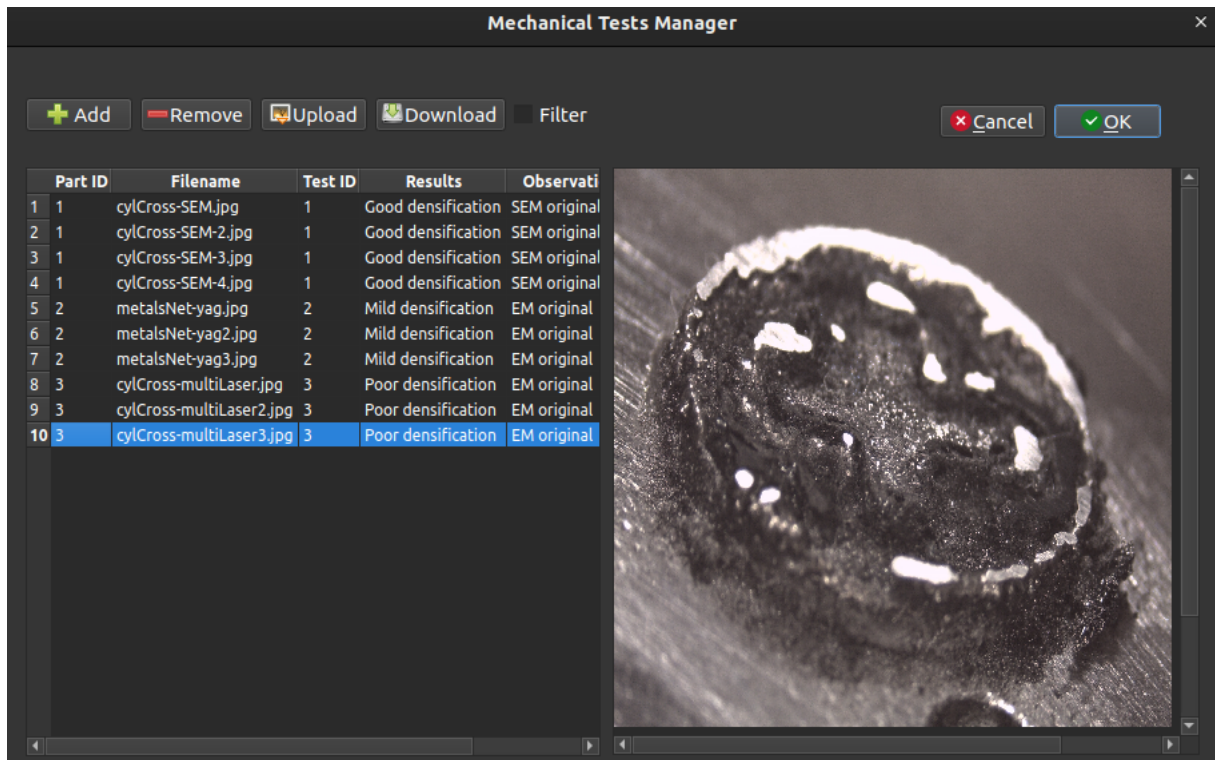


Figure 128: Multi-laser – Post-Manufacturer: Mechanical tests manager

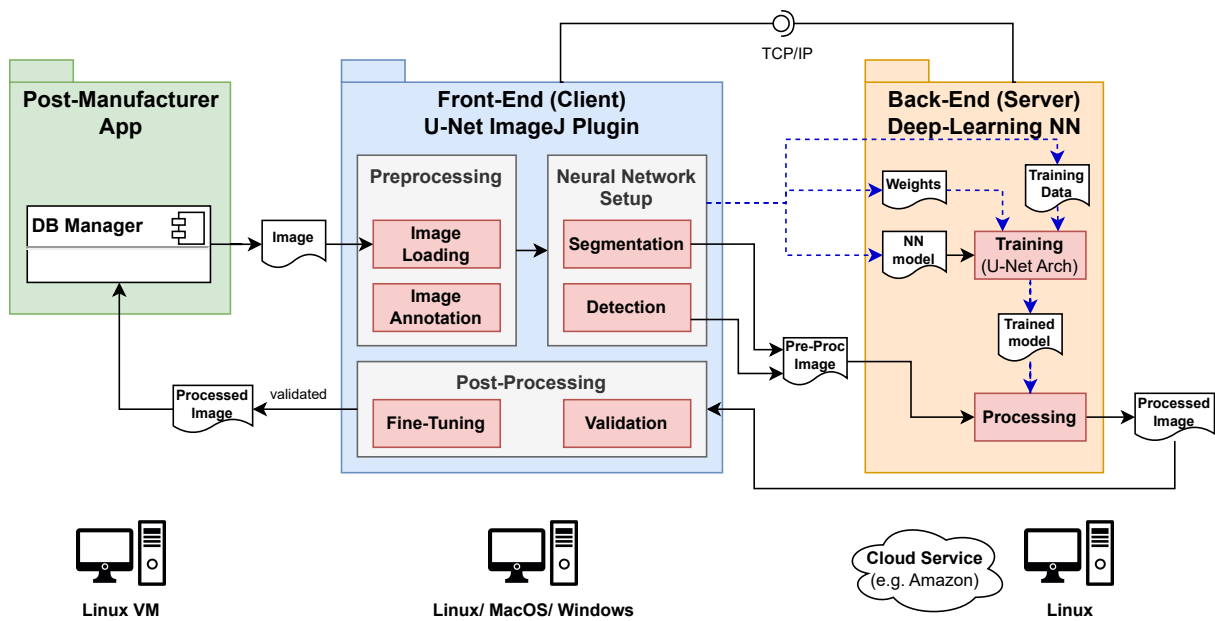


Figure 129: AI application for process improvement: SEM image analysis example

manufactured components. These images can then be loaded into the U-Net ImageJ plugin for pre-processing. For example, image annotation may be required to identify relevant areas to account for or to ignore when the neural network is learning. Then, the neural network is setup initially for training, providing the neural network model, the weights, and the training data. The training yields the trained model, which can now be used to segment or detect features in the pre-processed images. After processing, the output image is analysed and validated. If valid, it is stored in the `Post-Manufacturer` database (see also Fig. 107). Otherwise, the model is fine-tuned until significant accuracy is attained.

Another interesting option is the addition of more manufacturing data collection, which could be used on-line and in real-time — for adaptative control of the process — or off-line — for structured improvement of the process's control through heuristics or new control models sustained by AI data mining. For example, the inclusion of infrared thermal cameras or LSP. The former allows to assess the stability of the process, but not on the material condition. On the other hand, LSP analyses the change in the interference patterns of the laser (speckles) to identify inhomogeneities in 3D printing and even “invisible” defects [119]. Obviously, this requires a significant investment and resources, but could greatly benefit the manufacturing quality.

5.4 Results

The manufacturing tests performed validated the 3DMMLPBF's methodology devised. The 3DMMLPBF equipment was successfully tested and deployed, serving as a means to produce multi-material components via laser powder bed fusion process, thanks to the devised 3DMMLPBF methodology, the instantiated workflow and the supporting toolchain. Furthermore, the manufacturing is highly customisable and extensible due to the open source nature of the toolchain, acting as a ramp for fast prototyping.

However, the manufacturing tests also suggested that more investigation is required for attaining a reliable manufacturing quality, especially when handling dissimilar types of materials, such as polymeric and metal alloys. The scope of action can be varied, as different layer heights or path topologies can be needed — pre-manufacturing — or different process parameters, such as laser related, powder bed's temperature, shielding atmosphere control — manufacturing. This highlights the importance of the `Post-Manufacturer` software, storing and tracking the different information flows, enabling quick analysis and iteration.

Multi-material fabrication using the 3DMMLPBF process can also leverage from the usage of multiple lasers for different material types, in a scalable and reliable architecture, although contingent to the proper arrangement of the lasers' set over the printing bed. Using lasers with different beam generation systems, such as solid-state, can significantly reduce its volume, and facilitate this integration.

5.5 Summary

In this chapter the 3DMMLPBF's manufacturing was tested, and by extension also the whole ecosystem — methodology, workflow, toolchain, and equipment.

The workflow and accompanying toolchain proved itself capable of: handling various 3D models — irrespective of the number of materials, layer height, path topology and layer number; supporting different materials processing and with multiple lasers; and conveniently storing all process related information for posterior analysis and process improvement.

A manual and naive procedure for the manufacturing file generation was also used — in the Nd-YAG laser testing — to further illustrate the difficulty of generating such files without the appropriate tooling. Even though it may serve as a quick workaround for testing some geometries, it is extremely complex to apply this to functional design, as it would require the `Designer` to think in a 2D fashion, which defeats the purpose of using a 3D multi-material fabrication process.

The modifications performed on the slicer and path generator enabled the adaptation of 3D paths topologies for the `3DMMLPBF` process. This paves the way for quick iteration of the different path topologies and the associated parameters to assess its impact on the overall manufacturing quality of the produced component.

The `Pre-Manufacturer` slices and generates the manufacturing paths for each input model (material) in compliance to the user-defined configuration and merges them, yielding a 3D multi-material manufacturing file.

This file is then loaded into the `Manufacturer's SW`, and the manufacturing is configured by mapping the process parameters to each layer and assigning it to one or multiple lasers simultaneously. This `SW` efficiently handles the manufacturing process, controlling the equipment and the laser network. Furthermore, the generated data streams — layers, configuration, and logs — can be easily exported for storing and analysis.

The `Post-Manufacturer` allows the `User` to manage the process knowledge database by importing manufacturing chain files (models, manufacturing output, mechanical tests) and to export database, enabling the widespread of the `3DMMLPBF` technology through bootstrapping.

The manufacturing tests yielded varied results. The polymeric bi-material (CO_2 laser) showed good densification and geometrical compliance to the 3D model. On the other hand, the metallic alloy bi-material and polymeric/metallic alloy bi-material components, showed mild to poor densification and discrepancies in geometrical compliance. These unsatisfactory results mandate further investigation on the topic, especially on the parametrisation of the process.

Lastly, some venues were presented for `3DMMLPBF's` improvement, utilising the collected data by the `Post-Manufacturer` application, namely manufacturing quality assessment off-line — using `SEM` analysis supported by deep learning `CNN` — manufacturing quality assessment on-line and adaptative control — using infrared thermography or `LSP`.

In this chapter the conclusions and prospect for future work are outlined.

6.1 Conclusions

Functional design represents a shift in the product design paradigm, because the focus is on overall components' functionality instead of on the manufacturing process or materials to achieve it. This means that material is only added where it is strictly required to perform its function, optimising resources, such as materials and energy, and frees the designer to use its creativity and ingenuity.

On one hand, functional design may dictate the usage of several materials or a combination of them to fulfil its goal, which is hindered by the current manufacturing methodologies. On the other hand, functional design is very attractive for the design of high-value products, such as the biomedical implants. As a consequence, in the present work, the functional design is applied to the multi-material manufacturing using metals and ceramics to pursuit a path for the easier design and manufacturing of such relevant components.

For this purpose, laser-powder bed fusion proves to be the most well suitable technology for the job. However, current L-PBF technology only is guided towards mono-material fabrication. Adding to that, functional design is hard and complex, especially if requiring multiple materials, which drives away the end user, preventing widespread adoption.

Thus, the present work aimed to close the gap between design and fabrication of multi-material components like the aforementioned implants, by: proposing a design methodology for multi-material fabrication of metals/ceramics using the L-PBF process – 3DMMLPBF-CAD2Part; instantiating a practical workflow and the respective toolchain from the methodology; building a proof-of-concept low-cost equipment able to produce such components.

The 3DMMLPBF-CAD2Part methodology devised tries to address the high complexity associated with the design and manufacturing of multi-material parts and fill the gap in this domain, as no such methodology was found in the literature. It uses a model-driven approach to reduce the problem's complexity, taking into account all key agents in the process and enabling fast prototyping and testing. Four models and the relevant agents were considered: design model – designer; pre-manufacturing model – manufacturer; manufacturing model – manufacturer; post-manufacturing model – designer, manufacturer, material engineer, mechanical engineer, control engineer, physicist and data scientist.

At plain sight the methodology may seem trivial, but it provided a bird's eye view over the whole process: the

knowledge acquired through its models was crucial for the development of a specialised workflow for the 3DMMLPBF process and the respective toolchain, and to the development of a machine capable of producing multi-material components from metallic/ceramic powders matching the designed workflow.

Then, a toolchain was assembled and the missing software components were developed, following the waterfall model, namely:

- Pre-Manufacturer: The 3DMMLPBF-CAD2Part methodology views each 3D multi-material model as an assembly of 3D mono-material models. Each model is exported into an STL file and imported to the Pre-Manufacturer, where it is sliced and infilled with the manufacturing paths, according to the user-defined configuration. These infilled slices are then merged into a single manufacturing model, sorting them by z-value, and encoding the material and topological data into a custom version of an SVG file.
- Manufacturer: the manufacturing model is loaded into the Manufacturer SW, where its topological and material information is mapped to the relevant process parameters, enabling the accurate and adequate manufacturing of the parts. Furthermore, it also allows the assignment of the component's layers into different lasers, widening the scope of multi-material fabrication to different types of materials. This application controls the 3DMMLPBF's machine and the network of lasers, responsible for the actual multi-material fabrication. Lastly, process related information can be exported for storing and posterior analysis.
- Post-Manufacturer: the *post-manufacturer* provides a process knowledge database that can be used by all manufacturing agents for process improvement. It enables models, manufacturing files, and mechanical tests images to be directly imported, easing this process. Furthermore, it can be used to bootstrap the process, as all information is readily available to use and test the equipment and the toolchain.

The toolchain was extensively tested and validated. The Pre-Manufacturer tests demonstrated that this tool is capable of slicing and generating paths for various 3D models, irrespective of their provenance, the configuration used and the number of materials. It preserves the models coordinates and supports different parameters for each model, even different layer heights. It also pointed out that the fill density and infill extrusion width can be varied to mimic the required path filling for L-PBF trajectories. The Manufacturer tests showed that it accurately maps the geometrical and topological data to process parameters and that it efficiently handles the 3DMMLPBF manufacturing, driving both the machine and the array of lasers. The Post-Manufacturer tests proved that it can efficiently store the process related information and displaying it a convenient way to each manufacturing agent for further analysis.

The machine was developed using the V-model methodology in the three domain areas: mechanics, electronics and software. The overall equipment was divided into smaller subsystems. The mechanics were designed by another member of the laboratory staff and assembled. The electronics were designed to control the machine operation: motions, temperature, shielding and powder removal. The machine's firmware was developed to handle the low-level tasks of the system, responding to Manufacturer's commands.

The equipment's tests performed allowed to assess the mechanics, control and laser domains on operating conditions. A testing dialog was created in the Manufacturer's application to enable on-line testing of the equipment in a straightforward and easy way. The tests conducted demonstrated the good performance of these subsystems.

In the product manufacturing tests, several bi-material components were fabricated using one or multiple lasers. The polymeric bi-material component manufactured using the CO₂ laser was correctly produced, in compliance

with the process and geometrical data provided. The cross-sectioning and SEM analysis performed on the part demonstrated the tridimensional material variation in both horizontal and vertical directions, alongside with good densification. The metallic alloy bi-material component manufactured followed a manual pre-manufacturing strategy as a quick workaround, which demonstrated the difficulty of generating such files without proper tooling. This component was produced using an Nd-YAG laser and the results showed mild densification and some geometric discrepancy between the model and the produced component. Nonetheless, the devised methodology supports the modelling of such components containing support pillars and channels, using intermediate models abstracted as materials. Lastly, a multi-material component made out of one polymeric and one metallic alloy material was manufactured using a CO₂ laser and a Nd-YAG one. The multi-laser setup was cumbersome and, in the present format, it induces focus field distortion that must be corrected. The results showed poor densification and higher geometrical deviations, which are mostly due to these distortions. Nonetheless, the concept was proven and may be applied using lasers with less bulky beam generation systems, such as solid-state.

Lastly, some paths for 3DMMLPBF's process improvement were outlined, leveraging from the process knowledge database established by the Post-Manufacturer. Data mining can be applied using AI, for example, for the assessment of manufacturing quality within the available SEM analysis sets. This can be used to infer heuristics regarding process parameters. The assessment of the manufacturing quality can also be performed on-line using infrared thermography or LSP technology, which can be used for the adaptative control of the process.

Overall, the main goals of this work were fulfilled. A global 3DMMLPBF methodology was devised and laid the foundations for the instantiation of a practical workflow and the derived toolchain, as an effective means to materialise the functional design using multiple materials. A low-cost equipment was designed and built as proof-of-concept enabling the multi-material fabrication of parts through the L-PBF technology, for only a very small fraction of the cost – 10 k€ when compared to the commercial equipments costing hundreds of thousands dollars or more. The manufacturing chain information feeds a growing process knowledge database that can be used for process improvement. Furthermore, the 3DMMLPBF ecosystem assembled can be easily and conveniently bootstrapped and replicated, due to its the open-source nature, enabling a more widespread adoption of multi-material fabrication and functional design.

6.2 Prospect for future work

The 3DMMLPBF methodology devised and implemented is still on its infancy. This work represents only the first stone on paving the way for multi-material manufacturing of materials and ceramics in a sustained way, approaching the problem from a wider perspective and including all the key agents in the manufacturing chain. The envisioned future work goals are listed as follows, accordingly to its priority:

1. High

- Perform more tests on multi-material fabrication with: different materials, namely metallic and ceramics; processing parameters; topologies, including custom ones; manufacturing strategies. The manufacturing strategies may include sacrificial substrate, preheat treatments, chemical (oxidation) or thermochemical treatments (nitration).
- Improve shielding and temperature control, centrally managed by the microcontroller's firmware.

2. **Medium**

- Design a [PCB](#) to integrate the electronic components in a single board.
- Investigate the possibility of adding a third laser to remove material (subtractive), thus yielding a hybrid [AM](#) + [SM MMLPBF](#) technology. The ecosystem designed is flexible and can be extended to accommodate for this procedure.

3. **Low**

- Abstract from Laser API — design an open-source controller for lasers with a custom gcode language, as *grbl* — a no-compromise, high performance, low cost alternative to parallel-port-based motion control for CNC milling — is already doing [[187](#)].
- Implement database mining for process optimisation through heuristics and guidelines.
- Investigate alternative and more compact methods to store the manufacturing file information, migrating from the user-readable [SVG](#) file to a more machine-readable version.

Bibliography

- [1] J. M. Lourenço. *The NOVAthesis L^AT_EX Template User's Manual*. NOVA University Lisbon. 2021. url: <https://github.com/joaomlourenco/novathesis/raw/main/template.pdf> (cit. on p. ii).
- [2] *AconityMIDI+ product description*. accessed: 2023-01-28. url: <https://aconity3d.com/products/aconity-midi-plus/> (cit. on pp. vi, vii, 1, 24, 25).
- [3] *SLM Solutions 280 2.0 product description*. accessed: 2023-01-28. url: <https://www.eos.info/en/industrial-3d-printer/metal/eos-m-300-4> (cit. on pp. vi, vii, 1, 24, 25).
- [4] T. Bareth et al. "Implementation of a multi-material mechanism in a laser-based powder bed fusion (PBF-LB) machine". In: *Procedia CIRP* 107 (2022). Leading manufacturing systems transformation – Proceedings of the 55th CIRP Conference on Manufacturing Systems 2022, pp. 558–563. doi: <https://doi.org/10.1016/j.procir.2022.05.025>. url: <https://www.sciencedirect.com/science/article/pii/S2212827122003092> (cit. on pp. vi, vii, 2, 14, 16, 17, 25).
- [5] M. Schneck et al. "Capability of multi-material laser-based powder bed fusion—development and analysis of a prototype large bore engine component". In: *Metals* 12.1 (2022), p. 44 (cit. on pp. vi, vii, 2, 14, 16, 25).
- [6] V. Nadimpalli et al. "Multi-material additive manufacturing of steels using laser powder bed fusion". English. In: *Proceedings of the 19th International Conference and Exhibition (EUSPEN 2019)*. The European Society for Precision Engineering and Nanotechnology, 2019, pp. 240–243 (cit. on pp. vi, vii, 2, 14–16, 22, 24, 25).
- [7] C. Anstaett, C. Seidel, and G. Reinhart. "Fabrication of 3D multi-material parts using laser-based powder bed fusion". In: *2017 International Solid Freeform Fabrication Symposium*. University of Texas at Austin. 2017 (cit. on pp. vi, vii, 2, 14, 25, 26).
- [8] S. Sing et al. "Interfacial characterization of SLM parts in multi-material processing: Intermetallic phase formation between AlSi10Mg and C18400 copper alloy". In: *Materials Characterization* 107 (2015), pp. 220–227 (cit. on pp. vi, vii, 2, 14, 25).
- [9] Z. Liu et al. "Interfacial characterization of SLM parts in multi-material processing: Metallurgical diffusion between 316L stainless steel and C18400 copper alloy". In: *Materials Characterization* 94 (2014), pp. 116–125 (cit. on pp. vi, vii, 2, 14, 25).

- [10] M. Schneck et al. "Review on additive hybrid-and multi-material-manufacturing of metals by powder bed fusion: state of technology and development potential". In: *Progress in Additive Manufacturing* (2021), pp. 1–14 (cit. on pp. vi, vii, 1, 2, 22, 26, 27).
- [11] M. M. Soliman et al. "A Review of Biomaterials and Associated Performance Metrics Analysis in Pre-Clinical Finite Element Model and in Implementation Stages for Total Hip Implant System". In: *Polymers* 14.20 (2022), p. 4308 (cit. on pp. 1, 27).
- [12] S. M. Thompson et al. "An overview of Direct Laser Deposition for additive manufacturing; Part I: Transport phenomena, modeling and diagnostics". In: *Additive Manufacturing* 8 (2015), pp. 36–62 (cit. on pp. 1, 9, 10, 12, 15, 31).
- [13] *Multi-Material LPBF: 2x Faster with Machine Learning*. accessed: 2023-03-28. url: https://www.fujifilm.com/fbglobal/eng/company/technology/production/solution_service/fav.html (cit. on pp. 2, 26).
- [14] P. Ciraud. "Process and Device for the Manufacture of any Objects Desired from any Meltable Material". In: *FRG Disclosure Publication* 2263777 (1972) (cit. on p. 4).
- [15] *History of the RepRap project*. accessed: 2022-03-28. url: <https://all3dp.com/history-of-the-reprap-project/> (cit. on p. 4).
- [16] Y. Yang et al. "Biomimetic anisotropic reinforcement architectures by electrically assisted nanocomposite 3D printing". In: *Advanced materials (Deerfield Beach, Fla.)* 29.11 (2017) (cit. on p. 8).
- [17] K. Wang et al. "Dual-material 3D printed metamaterials with tunable mechanical properties for patient-specific tissue-mimicking phantoms". In: *Additive Manufacturing* 12 (2016), pp. 31–37 (cit. on p. 8).
- [18] I. M. El-Sherbiny and M. H. Yacoub. "Hydrogel scaffolds for tissue engineering: Progress and challenges". In: *Global Cardiology Science and Practice* 2013.3 (2013), p. 38 (cit. on p. 8).
- [19] A. Marques et al. "Inconel 718–copper parts fabricated by 3D multi-material laser powder bed fusion: a novel technological and designing approach for rocket engine". In: *The International Journal of Advanced Manufacturing Technology* 122.3 (2022-09-01), pp. 2113–2123. doi: [10.1007/s00170-022-10011-x](https://doi.org/10.1007/s00170-022-10011-x). url: <https://doi.org/10.1007/s00170-022-10011-x> (cit. on pp. 8, 9, 14, 17, 26).
- [20] L. Zhu, N. Li, and P. Childs. "Light-weighting in aerospace component and system design". In: *Propulsion and Power Research* 7.2 (2018), pp. 103–119 (cit. on p. 8).
- [21] Z. Hu et al. "Design of ultra-lightweight and high-strength cellular structural composites inspired by biomimetics". In: *Composites Part B: Engineering* 121 (2017), pp. 108–121 (cit. on pp. 8, 9).
- [22] S. Portanguen et al. "Toward the design of functional foods and biobased products by 3D printing: A review". In: *Trends in Food Science & Technology* 86 (2019), pp. 188–198 (cit. on p. 8).
- [23] H.-Z. Jin et al. "Structural and functional design of geopolymer adsorbents: a review". In: *Tungsten* (2023), pp. 1–29 (cit. on p. 8).
- [24] D. Gupta. "Design and engineering of functional clothing". In: (2011) (cit. on p. 8).

- [25] E. McKinney, A. Martindale, and M. Miller. "Inclusion of functional design characteristics in current children's pants: differences by gender". In: *International Journal of Fashion Design, Technology and Education* (2023), pp. 1–12 (cit. on p. 8).
- [26] A. du Plessis et al. "Beautiful and Functional: A Review of Biomimetic Design in Additive Manufacturing". In: *Additive Manufacturing* 27 (2019), pp. 408–427. issn: 2214-8604. doi: <https://doi.org/10.1016/j.addma.2019.03.033>. url: <https://www.sciencedirect.com/science/article/pii/S2214860419302611> (cit. on p. 8).
- [27] W.-C. Chiang, A. Pennathur, and A. Mital. "Designing and manufacturing consumer products for functionality: a literature review of current function definitions and design support tools". In: *Integrated Manufacturing Systems* 12.6 (2001), pp. 430–448 (cit. on p. 8).
- [28] J. Plocher and A. Panesar. "Review on design and structural optimisation in additive manufacturing: Towards next-generation lightweight structures". In: *Materials & Design* 183 (2019), p. 108164 (cit. on p. 8).
- [29] Y.-S. Leung et al. "Challenges and status on design and computation for emerging additive manufacturing technologies". In: *Journal of Computing and Information Science in Engineering* 19.2 (2019) (cit. on p. 8).
- [30] N. M. Rafiq et al. "A review on multifunctional bioceramic coatings in hip implants for osteointegration enhancement". In: *Applied Surface Science Advances* 13 (2023), p. 100353. issn: 2666-5239. doi: <https://doi.org/10.1016/j.apsadv.2022.100353>. url: <https://www.sciencedirect.com/science/article/pii/S266652392200143X> (cit. on p. 9).
- [31] Y. Yang et al. "3D-printed biomimetic super-hydrophobic structure for microdroplet manipulation and oil/water separation". In: *Advanced materials* 30.9 (2018), p. 1704912 (cit. on p. 9).
- [32] Z. X. Khoo et al. "3D printing of smart materials: A review on recent progresses in 4D printing". In: *Virtual and Physical Prototyping* 10.3 (2015), pp. 103–122 (cit. on p. 9).
- [33] M. P. Chae et al. "Four-dimensional (4D) printing: a new evolution in computed tomography-guided stereolithographic modeling. Principles and application". In: *Journal of Reconstructive Microsurgery* 31.06 (2015), pp. 458–463 (cit. on p. 9).
- [34] Y. Liu et al. "Sequential self-folding of polymer sheets". In: *Science Advances* 3.3 (2017), e1602417 (cit. on p. 9).
- [35] A. Sydney Gladman et al. "Biomimetic 4D printing". In: *Nature materials* 15.4 (2016), pp. 413–418 (cit. on pp. 9, 13).
- [36] K. Senthil Kumar, P.-Y. Chen, and H. Ren. "A review of printable flexible and stretchable tactile sensors". In: *Research* 2019 (2019) (cit. on p. 9).
- [37] I. Tirado-Garcia et al. "Conductive 3D printed PLA composites: On the interplay of mechanical, electrical and thermal behaviours". In: *Composite Structures* 265 (2021), p. 113744 (cit. on p. 9).
- [38] E. Fornells et al. "Integrated 3D printed heaters for microfluidic applications: Ammonium analysis within environmental water". In: *Analytica Chimica Acta* 1098 (2020), pp. 94–101 (cit. on p. 9).
- [39] Y. Liu et al. "3D-printed bionic superhydrophobic surface with petal-like microstructures for droplet manipulation, oil-water separation, and drag reduction". In: *Materials & Design* 219 (2022), p. 110765 (cit. on p. 9).

- [40] M. C. Freyman et al. "3D printing of living bacteria electrode". In: *Nano Research* 13 (2020), pp. 1318–1323 (cit. on p. 9).
- [41] M. Wajahat et al. "Three-dimensional printing of silver nanoparticle-decorated graphene microarchitectures". In: *Additive Manufacturing* 60 (2022), p. 103249 (cit. on p. 9).
- [42] F. Fu et al. "Functional conductive hydrogels for bioelectronics". In: *ACS Materials Letters* 2.10 (2020), pp. 1287–1301 (cit. on p. 9).
- [43] M. Danish et al. "An experimental investigations on effects of cooling/lubrication conditions in micro milling of additively manufactured Inconel 718". In: *Tribology International* 173 (2022), p. 107620 (cit. on p. 9).
- [44] H. Hegab et al. "Design for sustainable additive manufacturing: a review". In: *Sustainable Materials and Technologies* (2023), e00576 (cit. on p. 9).
- [45] B. Lauwers et al. "Hybrid processes in manufacturing". In: *CIRP Annals* 63.2 (2014), pp. 561–583. issn: 0007-8506. doi: <https://doi.org/10.1016/j.cirp.2014.05.003>. url: <https://www.sciencedirect.com/science/article/pii/S0007850614001851> (cit. on p. 9).
- [46] *3D-printed titanium parts could save Boeing up to \$3 million per plane*. accessed: 2021-11-28. url: <https://www.theverge.com/2017/4/11/15256008/3d-printed-titanium-parts-boeing-dreamliner-787> (cit. on p. 9).
- [47] M. Bronz et al. "Mission-oriented additive manufacturing of modular mini-UAVs". In: *AIAA Scitech 2020 Forum*. 2020, p. 0064 (cit. on p. 9).
- [48] Y. Tadjeh. "Navy beefs up 3D printing efforts with new 'Print the Fleet' program". In: *National Defense* 99.731 (2014), pp. 24–26 (cit. on p. 9).
- [49] R. Scott. *Chinese Company Showcases Ten 3D-Printed Houses*, *ArchDaily*. <http://www.archdaily.com/543518/chinese-company-showcases-ten-3d-printed-houses>. accessed: 2017-09-25. 2014 (cit. on p. 9).
- [50] L.-E. Rännar, A. Glad, and C.-G. Gustafson. "Efficient cooling with tool inserts manufactured by electron beam melting". In: *Rapid Prototyping Journal* 13.3 (2007), pp. 128–135 (cit. on p. 9).
- [51] K. Dalgarno and T. Stewart. "Production tooling for polymer moulding using the RapidSteel process". In: *Rapid Prototyping Journal* 7.3 (2001), pp. 173–179 (cit. on p. 9).
- [52] F. Bartolomeu et al. "Additive manufacturing of NiTi-Ti6Al4V multi-material cellular structures targeting orthopedic implants". In: *Optics and Lasers in Engineering* 134 (2020), p. 106208 (cit. on pp. 9, 13, 14, 16, 26).
- [53] S. Esmaeili et al. "An artificial blood vessel fabricated by 3D printing for pharmaceutical application". In: *Nanomedicine Journal* 6.3 (2019), pp. 183–194 (cit. on p. 9).
- [54] E. Cansiz, F. Turan, and Y. Z. Arslan. "Computer-aided design and manufacturing of a novel maxillofacial surgery instrument: application in the sagittal split osteotomy". In: *Journal of Medical Devices* 10.4 (2016) (cit. on p. 9).
- [55] R. McCann et al. "In-situ sensing, process monitoring and machine control in Laser Powder Bed Fusion: A review". In: *Additive Manufacturing* 45 (2021), p. 102058 (cit. on pp. 10, 26).

- [56] B. Vayre, F. Vignat, and F. Villeneuve. “Metallic additive manufacturing: state-of-the-art review and prospects”. In: *Mechanics & Industry* 13.2 (2012), pp. 89–96 (cit. on p. 10).
- [57] *ISO/ASTM 52900:2021 Additive manufacturing – General principles – Fundamentals and vocabulary*. accessed: 2021-11-29. url: <https://www.iso.org/obp/ui/#iso:std:iso-astm:52900:ed-2:v1:en> (cit. on p. 10).
- [58] E. M. Sefene, Y. M. Hailu, and A. A. Tsegaw. “Metal hybrid additive manufacturing: state-of-the-art”. In: *Progress in Additive Manufacturing* (2022), pp. 1–13 (cit. on pp. 10, 11).
- [59] N. Guo and M. C. Leu. “Additive manufacturing: technology, applications and research needs”. In: *Frontiers of mechanical engineering* 8.3 (2013), pp. 215–243 (cit. on p. 10).
- [60] S. Radel et al. “Skeleton arc additive manufacturing with closed loop control”. In: *Additive Manufacturing* 26 (2019), pp. 106–116 (cit. on p. 10).
- [61] K. Garanger, T. Khamvilai, and E. Feron. “3D printing of a leaf spring: A demonstration of closed-loop control in additive manufacturing”. In: *2018 IEEE conference on control technology and applications (CCTA)*. IEEE, 2018, pp. 465–470 (cit. on p. 10).
- [62] T. Purtonen, A. Kalliosaari, and A. Salminen. “Monitoring and adaptive control of laser processes”. In: *Physics Procedia* 56 (2014), pp. 1218–1231 (cit. on p. 10).
- [63] M. Vaezi et al. “Multiple material additive manufacturing–Part 1: a review: this review paper covers a decade of research on multiple material additive manufacturing technologies which can produce complex geometry parts with different materials”. In: *Virtual and Physical Prototyping* 8.1 (2013), pp. 19–50 (cit. on pp. 10, 13, 14).
- [64] J. Yang et al. “Role of molten pool mode on formability, microstructure and mechanical properties of selective laser melted Ti-6Al-4V alloy”. In: *Materials & Design* 110 (2016), pp. 558–570 (cit. on p. 10).
- [65] P. Collins et al. “Microstructural control of additively manufactured metallic materials”. In: *Annual Review of Materials Research* 46 (2016), pp. 63–91 (cit. on p. 10).
- [66] C. Wei et al. “An overview of laser-based multiple metallic material additive manufacturing: from macro-to micro-scales”. In: *International Journal of Extreme Manufacturing* 3.1 (2020), p. 012003 (cit. on pp. 10, 13, 26).
- [67] *Aconity3D Machines*. accessed: 2023-01-28. url: <https://aconity3d.com/machines> (cit. on pp. 10, 14, 16, 21, 22, 24).
- [68] *SLM Solutions 500 product description*. accessed: 2023-01-28. url: <https://www.eos.info/en/industrial-3d-printer/metal/eos-m-300-4> (cit. on pp. 10, 14, 21).
- [69] *EOS M 300 product description*. accessed: 2023-01-28. url: <https://www.eos.info/en/industrial-3d-printer/metal/eos-m-300-4> (cit. on pp. 10, 14, 21, 24, 25).
- [70] *Trumpf Truprint 500 product description*. accessed: 2023-01-28. url: https://www.trumpf.com/en_INT/products/machines-systems/additive-production-systems/truprint-5000/ (cit. on pp. 10, 14, 21).

- [71] Aurora Labs RMP1 product description. accessed: 2023-01-28. url: <https://www.design-industry.com.au/aurora-labs-rmp1> (cit. on pp. 10, 14, 21).
- [72] A. Mussatto. "Research progress in multi-material laser-powder bed fusion additive manufacturing: A review of the state-of-the-art techniques for depositing multiple powders with spatial selectivity in a single layer". In: *Results in Engineering* (2022), p. 100769 (cit. on pp. 10, 14, 16, 17, 19, 20, 24, 26, 29, 30, 33).
- [73] P. Pratt et al. "Residual stress measurement of laser-engineered net shaping AISI 410 thin plates using neutron diffraction". In: *Metallurgical and Materials Transactions A* 39.13 (2008), pp. 3155–3163 (cit. on p. 12).
- [74] S. L. Sing, W. Y. Yeong, and F. E. Wiria. "Selective laser melting of titanium alloy with 50 wt% tantalum: Microstructure and mechanical properties". In: *Journal of Alloys and Compounds* 660 (2016), pp. 461–470 (cit. on p. 12).
- [75] W. Yu et al. "Influence of re-melting on surface roughness and porosity of AISi10Mg parts fabricated by selective laser melting". In: *Journal of Alloys and Compounds* 792 (2019), pp. 574–581 (cit. on pp. 12, 13).
- [76] S. Zou et al. "Numerical analysis of the effect of the scan strategy on the residual stress in the multi-laser selective laser melting". In: *Results in Physics* 16 (2020), p. 103005 (cit. on pp. 12, 13).
- [77] J.-P. Kruth et al. "Selective laser melting of iron-based powder". In: *Journal of materials processing technology* 149.1-3 (2004), pp. 616–622 (cit. on p. 12).
- [78] B. Cheng, S. Shrestha, and K. Chou. "Stress and deformation evaluations of scanning strategy effect in selective laser melting". In: *Additive Manufacturing* 12 (2016), pp. 240–251 (cit. on p. 12).
- [79] H. Wan et al. "Effect of scanning strategy on grain structure and crystallographic texture of Inconel 718 processed by selective laser melting". In: *Journal of materials science & technology* 34.10 (2018), pp. 1799–1804 (cit. on p. 12).
- [80] S. Sing et al. "Emerging metallic systems for additive manufacturing: In-situ alloying and multi-metal processing in laser powder bed fusion". In: *Progress in Materials Science* 119 (2021), p. 100795 (cit. on p. 13).
- [81] D. Han and H. Lee. "Recent advances in multi-material additive manufacturing: Methods and applications". In: *Current Opinion in Chemical Engineering* 28 (2020), pp. 158–166 (cit. on p. 13).
- [82] A. Bandyopadhyay and B. Heer. "Additive manufacturing of multi-material structures". In: *Materials Science and Engineering: R: Reports* 129 (2018), pp. 1–16 (cit. on p. 13).
- [83] D. Joung et al. "3D printed stem-cell derived neural progenitors generate spinal cord scaffolds". In: *Advanced functional materials* 28.39 (2018), p. 1801850 (cit. on p. 13).
- [84] Y. Lu et al. "Microstereolithography and characterization of poly (propylene fumarate)-based drug-loaded microneedle arrays". In: *Biofabrication* 7.4 (2015), p. 045001 (cit. on p. 13).
- [85] F. Li et al. "Multimaterial 3D printed fluidic device for measuring pharmaceuticals in biological fluids". In: *Analytical chemistry* 91.3 (2018), pp. 1758–1763 (cit. on p. 13).

- [86] G. Coelho et al. "Multimaterial 3D printing preoperative planning for frontoethmoidal meningoencephalocele surgery". In: *Child's Nervous System* 34.4 (2018), pp. 749–756 (cit. on p. 13).
- [87] A. Cresswell-Boyes et al. "Approaches to 3D printing teeth from X-ray microtomography". In: *Journal of Microscopy* 272.3 (2018), pp. 207–212 (cit. on p. 13).
- [88] C. Yuan et al. "3D printed reversible shape changing soft actuators assisted by liquid crystal elastomers". In: *Soft Matter* 13.33 (2017), pp. 5558–5568 (cit. on p. 13).
- [89] D. Espalin et al. "3D Printing multifunctionality: structures with electronics". In: *The International Journal of Advanced Manufacturing Technology* 72.5 (2014), pp. 963–978 (cit. on p. 14).
- [90] A. D. Valentine et al. "Hybrid 3D printing of soft electronics". In: *advanced Materials* 29.40 (2017), p. 1703817 (cit. on p. 14).
- [91] W. HuangáGoh, A. HoseináSakhaei, et al. "Highly stretchable hydrogels for UV curing based high-resolution multimaterial 3D printing". In: *Journal of Materials Chemistry B* 6.20 (2018), pp. 3246–3253 (cit. on p. 14).
- [92] T.-S. Wei et al. "3D printing of customized li-ion batteries with thick electrodes". In: *Advanced Materials* 30.16 (2018), p. 1703027 (cit. on pp. 14, 22, 23).
- [93] F. Brueckner et al. "Enhanced manufacturing possibilities using multi-materials in laser metal deposition". In: *Journal of Laser Applications* 30.3 (2018), p. 032308 (cit. on p. 14).
- [94] K. Shah et al. "Parametric study of development of Inconel-steel functionally graded materials by laser direct metal deposition". In: *Materials & Design (1980-2015)* 54 (2014), pp. 531–538 (cit. on p. 14).
- [95] S. Liu and Y. C. Shin. "Additive manufacturing of Ti6Al4V alloy: A review". In: *Materials & Design* 164 (2019), p. 107552 (cit. on p. 14).
- [96] F. Bartolomeu et al. "Selective Laser Melting of Ti6Al4V sub-millimetric cellular structures: Prediction of dimensional deviations and mechanical performance". In: *journal of the mechanical behavior of biomedical materials* 113 (2021), p. 104123 (cit. on p. 14).
- [97] N. Shamsaei et al. "An overview of Direct Laser Deposition for additive manufacturing; Part II: Mechanical behavior, process parameter optimization and control". In: *Additive Manufacturing* 8 (2015), pp. 12–35 (cit. on pp. 14, 32, 33).
- [98] J. Walker et al. "Multi-material laser powder bed fusion additive manufacturing in 3-dimensions". In: *Manufacturing Letters* 31 (2022), pp. 74–77 (cit. on pp. 14, 17, 18).
- [99] Z. Liu et al. "Interfacial characterization of SLM parts in multi-material processing: Metallurgical diffusion between 316L stainless steel and C18400 copper alloy". In: *Materials Characterization* 94 (2014), pp. 116–125. issn: 1044-5803. doi: <https://doi.org/10.1016/j.matchar.2014.05.001>. url: <https://www.sciencedirect.com/science/article/pii/S1044580314001351> (cit. on p. 14).
- [100] *Renishaw AM 500 product description*. accessed: 2023-01-28. url: <https://www.renishaw.com/en/renam-500-metal-additive-manufacturing-3d-printing-systems--37011> (cit. on pp. 14, 16, 21, 22, 24, 25).
- [101] J. Edgar and S. Tint. "Additive manufacturing technologies: 3D printing, rapid prototyping, and direct digital manufacturing". In: *Johnson Matthey Technology Review* 59.3 (2015), pp. 193–198 (cit. on p. 14).

- [102] Y. Bai et al. "Dual interfacial characterization and property in multi-material selective laser melting of 316L stainless steel and C52400 copper alloy". In: *Materials Characterization* 167 (2020), p. 110489 (cit. on pp. 14, 16).
- [103] J. Koopmann, J. Voigt, and T. Niendorf. "Additive manufacturing of a steel–ceramic multi-material by selective laser melting". In: *Metallurgical and Materials Transactions B* 50 (2019), pp. 1042–1051 (cit. on pp. 14, 16).
- [104] *Aerosint and InfraTrac partner to prevent part counterfeiting in powder bed additive manufacturing*. accessed: 2022-11-29. url: <https://3dprintingindustry.com/news/aerosint-and-infratrac-partner-to-prevent-part-counterfeiting-in-powder-bed-additive-manufacturing-158090/> (cit. on pp. 14, 16, 19, 20, 24).
- [105] X. Zhang et al. "An integrated dual ultrasonic selective powder dispensing platform for three-dimensional printing of multiple material metal/glass objects in selective laser melting". In: *Journal of Manufacturing Science and Engineering* 141.1 (2019) (cit. on pp. 14, 17).
- [106] C. Wei et al. "Additive manufacturing of horizontal and 3D functionally graded 316L/Cu10Sn components via multiple material selective laser melting". In: *Journal of Manufacturing Science and Engineering* 141.8 (2019), p. 081014 (cit. on pp. 14, 17, 26).
- [107] A. G. Demir and B. Previtali. "Multi-material selective laser melting of Fe/Al-12Si components". In: *Manufacturing letters* 11 (2017), pp. 8–11 (cit. on pp. 14, 17, 19).
- [108] R. Wang et al. "Multi-material additive manufacturing of a bio-inspired layered ceramic/metal structure: Formation mechanisms and mechanical properties". In: *International Journal of Machine Tools and Manufacture* 175 (2022), p. 103872 (cit. on pp. 14, 17).
- [109] T. Stichel et al. "Electrophotographic multilayer powder pattern deposition for additive manufacturing". In: *Jom* 72.3 (2020), pp. 1366–1375 (cit. on pp. 14, 18).
- [110] J. Foerster et al. "Aspects of Developing a Powder Application Module Based on Electrophotography for Additive Powder Bed Based Processes". In: *Proceedings of the Machining Innovations Conference (MIC)*. 2020 (cit. on p. 14).
- [111] M. J. Benning and K. Dalgarno. "Proof of concept of a novel combined consolidation and transfer mechanism for electrophotographic 3D printing". In: *Rapid Prototyping Journal* (2018) (cit. on pp. 14, 19).
- [112] T. Stichel et al. "Electrophotographic multi-material powder deposition for additive manufacturing". In: *Journal of Laser Applications* 30.3 (2018), p. 032306 (cit. on p. 14).
- [113] Y. Chivel. "New Approach to Multi-material Processing in Selective Laser Melting". In: *Physics Procedia* 83 (2016), pp. 891–898 (cit. on p. 15).
- [114] C. Seidel et al. "Status quo der metallischen multimaterialverarbeitung mittels Laserstrahlschmelzen". In: *DGM-Fachtagung Werkstoffe und Additive Fertigung-Conference Presentation*. 2018 (cit. on p. 15).
- [115] J. Woidasky. "Recyclingtechnik–Fachbuch für Lehre und Praxis. Von H. Martens, D. Goldmann". In: *Chemie Ingenieur Technik* 3.89 (2017), pp. 346–346 (cit. on p. 15).

- [116] H. Ullrich. *Mechanische Verfahrenstechnik: Berechnung und Projektierung*. Springer-Verlag, 2013 (cit. on p. 15).
- [117] M. A. Obeidi. "Metal additive manufacturing by laser-powder bed fusion: Guidelines for process optimisation". In: *Results in Engineering* 15 (2022), p. 100473. issn: 2590-1230. doi: <https://doi.org/10.1016/j.rineng.2022.100473>. url: <https://www.sciencedirect.com/science/article/pii/S2590123022001438> (cit. on pp. 15, 16, 23).
- [118] K. Zeng et al. "Layer by layer validation of geometrical accuracy in additive manufacturing processes". In: *2013 International Solid Freeform Fabrication Symposium*. University of Texas at Austin. 2013 (cit. on pp. 16, 22).
- [119] L. Chen et al. "Laser speckle photometry—Optical sensor systems for condition and process monitoring". In: *Materials Testing* 61.3 (2019), pp. 213–219 (cit. on pp. 16, 143).
- [120] R. Mahamood and E. T. Akinlabi. "Laser metal deposition of functionally graded Ti6Al4V/TiC". In: *Materials & Design* 84 (2015), pp. 402–410 (cit. on p. 16).
- [121] R. Wang et al. "Formation mechanisms of TiB₂ tracks on Ti6Al4V alloy during selective laser melting of ceramic-metal multi-material". In: *Powder technology* 367 (2020), pp. 597–607 (cit. on p. 17).
- [122] D. Goll et al. "Additive manufacturing of soft magnetic materials and components". In: *Additive Manufacturing* 27 (2019), pp. 428–439 (cit. on p. 17).
- [123] J. Chen et al. "Influence mechanism of process parameters on the interfacial characterization of selective laser melting 316L/CuSn10". In: *Materials Science and Engineering: A* 792 (2020), p. 139316 (cit. on p. 17).
- [124] T. Stichel et al. "Powder layer preparation using vibration-controlled capillary steel nozzles for additive manufacturing". In: *Physics Procedia* 56 (2014), pp. 157–166 (cit. on p. 17).
- [125] C. Wei et al. "Easy-To-Remove composite support material and procedure in additive manufacturing of metallic components using multiple material laser-based powder bed fusion". In: *Journal of Manufacturing Science and Engineering* 141.7 (2019) (cit. on p. 17).
- [126] P. Kumar et al. "Direct-write deposition of fine powders through miniature hopper-nozzles for multi-material solid freeform fabrication". In: *Rapid Prototyping Journal* (2004), p. . (Cit. on p. 18).
- [127] C. van der Eijk et al. "Metal printing process: a rapid manufacturing process based on xerography using metal powders". In: *MATERIALS SCIENCE AND TECHNOLOGY-ASSOCIATION FOR IRON AND STEEL TECHNOLOGY-3* (2005), p. 8 (cit. on p. 18).
- [128] J. Bakkelund, R. Karlsen, and Ø. Bjørke. "Fabrication metal objects using layer manufacturing technology and powder metallurgy science". In: *CIRP Annals* 46.1 (1997), pp. 135–138 (cit. on p. 18).
- [129] F. Psarommatis and G.-C. Vosniakos. "Systematic Development of a Powder Deposition System for an Open Selective Laser Sintering Machine Using Analytic Hierarchy Process". In: *Journal of Manufacturing and Materials Processing* 6.1 (2022), p. 22 (cit. on p. 18).
- [130] M. Mehrpouya et al. "Multimaterial powder bed fusion techniques". In: *Rapid prototyping journal* (2022) (cit. on p. 19).

- [131] D. Wang et al. "Recent progress on additive manufacturing of multi-material structures with laser powder bed fusion". In: *Virtual and Physical Prototyping* 17.2 (2022), pp. 329–365 (cit. on pp. 19, 21–23).
- [132] K. Eckes. "How multi-powder deposition will transform industrial 3D printing". In: *Aerosint* 15 (2018), p. 44 (cit. on p. 19).
- [133] *Aerosint - Home page*. accessed: 2021-11-28. url: <https://aerosint.com/> (cit. on pp. 19, 20).
- [134] *Aerosint: Multi-material L-PBF*. accessed: 2021-11-28. url: <https://aerosint.com/multi-material-3d-printing-bundle/> (cit. on p. 20).
- [135] C. Seidel. "Multi-material metal parts by powder bed fusion: new application opportunities". In: *Metal Additive Manufacturing* (2022) (cit. on pp. 21, 26).
- [136] C. Altenhofen et al. "Continuous property gradation for multi-material 3D-printed objects". In: *2018 International Solid Freeform Fabrication Symposium*. University of Texas at Austin. 2018 (cit. on p. 21).
- [137] X. Yao et al. "A multi-material part design framework in additive manufacturing". In: *The International Journal of Advanced Manufacturing Technology* 99 (2018), pp. 2111–2119 (cit. on p. 21).
- [138] *GraMMaCAD - Graded Multi-Material CAD*. accessed: 2021-11-28. url: <https://www.igd.fraunhofer.de/en/products/information-technology/grammacad---graded-multi-material-cad.html> (cit. on pp. 21, 23).
- [139] G. H. Loh et al. "An overview of functionally graded additive manufacturing". In: *Additive Manufacturing* 23 (2018), pp. 34–44 (cit. on pp. 21, 23).
- [140] D. Moreno Nieto and D. Moreno Sánchez. "Design for additive manufacturing: Tool review and a case study". In: *Applied Sciences* 11.4 (2021), p. 1571 (cit. on p. 22).
- [141] M. Binder et al. "Potentials and challenges of multi-material processing by laser-based powder bed fusion". In: *2018 International Solid Freeform Fabrication Symposium*. University of Texas at Austin. 2018 (cit. on pp. 22, 26).
- [142] J. D. Hiller and H. Lipson. "STL 2.0: a proposal for a universal multi-material additive manufacturing file format". In: *2009 International Solid Freeform Fabrication Symposium*. University of Texas at Austin. 2009 (cit. on p. 23).
- [143] L. Chenyan and J. Shikai. "Multi-attribute voxelization technology of AMF for 3D printing". In: *2019 IEEE 6th International Conference on Industrial Engineering and Applications (ICIEA)*. IEEE. 2019, pp. 81–85 (cit. on p. 23).
- [144] J. Shi, J. Yang, and X. Wang. "Status and trend of 3D printing technology for heterogeneous objects". In: *Machine Design and Manufacturing Engineering* 46.02 (2017), pp. 11–17 (cit. on p. 23).
- [145] Z. Xiaowei and W. Congjun. "A new file format for multiple material additive manufacturing". In: *Modern Manufacturing Engineering* 445.10 (2017), p. 30 (cit. on p. 23).
- [146] A. Mussatto et al. "Laser-powder bed fusion of silicon carbide reinforced 316L stainless steel using a sinusoidal laser scanning strategy". In: *Journal of Materials Research and Technology* 18 (2022), pp. 2672–2698 (cit. on p. 23).

- [147] *The New 3D Data Format FAV*. accessed: 2023-03-28. url: https://www.fujifilm.com/fbglobal/eng/company/technology/production/solution_service/fav.html (cit. on p. 24).
- [148] *AconityMINI product description*. accessed: 2023-01-28. url: <https://aconity3d.com/products/aconity-mini/> (cit. on pp. 24, 25).
- [149] *Trumpf TruPrint300 product description*. accessed: 2023-01-28. url: https://www.trumpf.com/en_INT/products/machines-systems/additive-production-systems/truprint-3000/ (cit. on pp. 24, 25).
- [150] *SLM Solutions 280 2.0 product review*. accessed: 2023-01-28. url: <http://badrsystem-t.com/en/product/slm-280-en/> (cit. on pp. 24, 25).
- [151] C. Wei and L. Li. "Recent progress and scientific challenges in multi-material additive manufacturing via laser-based powder bed fusion". In: *Virtual and Physical Prototyping* 16.3 (2021), pp. 347–371 (cit. on p. 26).
- [152] S. Mao et al. "Effects of process parameters on interfacial characterization and mechanical properties of 316L/CuCrZr functionally graded material by selective laser melting". In: *Journal of Alloys and Compounds* 899 (2022), p. 163256 (cit. on p. 26).
- [153] H. Fayazfar et al. "A critical review of powder-based additive manufacturing of ferrous alloys: Process parameters, microstructure and mechanical properties". In: *Materials & Design* 144 (2018), pp. 98–128 (cit. on p. 26).
- [154] C. F. Tey et al. "Additive manufacturing of multiple materials by selective laser melting: Ti-alloy to stainless steel via a Cu-alloy interlayer". In: *Additive Manufacturing* 31 (2020), p. 100970 (cit. on p. 26).
- [155] C. Wei et al. "Understanding of process and material behaviours in additive manufacturing of Invar36/Cu10Sn multiple material components via laser-based powder bed fusion". In: *Additive Manufacturing* 37 (2021), p. 101683 (cit. on p. 26).
- [156] D. Gu et al. "Laser additive manufacturing of metallic components: materials, processes and mechanisms". In: *International materials reviews* 57.3 (2012), pp. 133–164 (cit. on pp. 26, 29).
- [157] P. Yadav et al. "In situ monitoring systems of the SLM process: On the need to develop machine learning models for data processing". In: *Crystals* 10.6 (2020), p. 524 (cit. on p. 26).
- [158] H. Derar and M. Shahinpoor. "Recent patents and designs on hip replacement prostheses". In: *The open biomedical engineering journal* 9 (2015), p. 92 (cit. on p. 27).
- [159] F. Eltit, Q. Wang, and R. Wang. "Mechanisms of adverse local tissue reactions to hip implants". In: *Frontiers in bioengineering and biotechnology* 7 (2019), p. 176 (cit. on pp. 27, 28).
- [160] N. M. Rafiq et al. "A review on multifunctional bioceramic coatings in hip implants for osteointegration enhancement". In: *Applied Surface Science Advances* (2022), p. 100353 (cit. on p. 27).
- [161] B. Bruegge and A. H. Dutoit. *Object-Oriented Software Engineering Using UML, Patterns and Java-(Required)*. Vol. 2004. Prentice Hall, 2004 (cit. on pp. 30–32, 39).
- [162] M. A. Cusumano and S. A. Smith. "Beyond the waterfall: Software development at Microsoft". In: (1995) (cit. on p. 38).

- [163] J. Gausemeier and S. Moehringer. "NEW GUIDELINE VDI 2206-A FLEXIBLE PROCEDURE MODEL FOR THE DESIGN OF MECHATRONIC SYSTEMS". In: *DS 31: Proceedings of ICED 03, the 14th International Conference on Engineering Design, Stockholm*. 2003 (cit. on p. 39).
- [164] *Scalable Vector Graphics (SVG) 1.1. - Second Edition*. <https://www.w3.org/TR/SVG/>. accessed: 2017-09-25 (cit. on p. 42).
- [165] *Slic3r - G-code generator for 3D printers*. <http://slic3r.org/>. accessed: 2017-09-25 (cit. on pp. 42, 44).
- [166] A. Ranelluci. *Slic3r Github repository*. <https://github.com/slic3r/Slic3r>. accessed: 2018-05-25. 2011 (cit. on p. 44).
- [167] W3C. *SVG Path*. https://www.w3schools.com/graphics/svg_path.asp. accessed: 2018-06-05. 2016 (cit. on p. 48).
- [168] F. team. *FreeCAD: 3D parametric modeler*. <https://www.freecadweb.org/>. accessed: 2019-10-31. 2016 (cit. on p. 53).
- [169] *Open-source toolpath generator for the 3DMMMLPBF process*. accessed: 2023-03-28. url: <https://github.com/ElectroQuanta/Slic3r> (cit. on p. 64).
- [170] *Open-source manufacturer manager for the 3DMMMLPBF process*. accessed: 2023-03-28. url: <https://github.com/ElectroQuanta/3DMMLPBF-Manuf> (cit. on pp. 79, 80).
- [171] R. Ramakrishnan, J. Gehrke, and J. Gehrke. *Database management systems*. Vol. 3. McGraw-Hill New York, 2003 (cit. on p. 81).
- [172] *Which Modern Database Is Right for Your Use Case?* accessed: 2021-11-30. url: <https://www.xplenty.com/blog/which-database/> (cit. on p. 81).
- [173] C. Coronel and S. Morris. *Database systems: design, implementation, & management*. Cengage Learning, 2016 (cit. on p. 82).
- [174] *MySQL Connectors and APIs*. accessed: 2021-11-30. url: <https://dev.mysql.com/doc/index-connectors.html> (cit. on p. 82).
- [175] *Open-source post-manufacturer database for the 3DMMMLPBF process*. accessed: 2023-03-28. url: <https://github.com/ElectroQuanta/3DMMLPBF-PostManuf> (cit. on pp. 88, 113).
- [176] N. N. M. Peek. "Making machines that make: object-oriented hardware meets object-oriented software". PhD thesis. Massachusetts Institute of Technology, 2016 (cit. on p. 93).
- [177] X. Wang et al. "Direct Selective Laser Sintering of Hard Metal Powders: Experimental Study and Simulation". In: *International Journal of Advanced Manufacturing Technology* 19 (2002-03), pp. 351–357. doi: [10.1007/s001700200024](https://doi.org/10.1007/s001700200024) (cit. on p. 101).
- [178] D. A. Figueiredo. "Desenvolvimento de um sistema de deposição de pós metálicos para manufatura aditiva multimaterial". MA thesis. University of Minho, 2021 (cit. on pp. 109–111).
- [179] *Open-source firmware to control the 3DMMMLPBF equipment*. accessed: 2023-03-28. url: <https://github.com/ElectroQuanta/3DMMLPBF-firmware> (cit. on p. 115).

-
- [180] *HotCoat powder coating*. accessed: 2022-02-17. url: <https://www.eastwood.com/hotcoat-powder-coating/powders/purple-powders-1.html> (cit. on p. 119).
- [181] *Fiji, an image processing package of distribution of ImageJ2*. accessed: 2022-11-28. url: <https://imagej.net/software/fiji/> (cit. on pp. 119, 135).
- [182] J. Schindelin et al. “Fiji: an open-source platform for biological-image analysis”. In: *Nature methods* 9.7 (2012), pp. 676–682. doi: [10.1038/nmeth.2019](https://doi.org/10.1038/nmeth.2019). url: <https://doi.org/10.1038/nmeth.2019> (cit. on p. 119).
- [183] S. R. S. Rodrigues. “Sinterizacao laser de porcelanas dentarias”. MA thesis. University of Minho, 2017 (cit. on p. 124).
- [184] Z. Chen et al. “Deep learning-based method for SEM image segmentation in mineral characterization, an example from Duvernay Shale samples in Western Canada Sedimentary Basin”. In: *Computers & Geosciences* 138 (2020), p. 104450. issn: 0098-3004. doi: <https://doi.org/10.1016/j.cageo.2020.104450>. url: <https://www.sciencedirect.com/science/article/pii/S0098300419304819> (cit. on pp. 139–141).
- [185] O. Ronneberger, P. Fischer, and T. Brox. “U-Net: Convolutional Networks for Biomedical Image Segmentation”. In: *Medical Image Computing and Computer-Assisted Intervention – MICCAI 2015*. Ed. by N. Navab et al. Cham: Springer International Publishing, 2015, pp. 234–241. isbn: 978-3-319-24574-4 (cit. on p. 140).
- [186] T. Falk et al. “U-Net – Deep Learning for Cell Counting, Detection, and Morphometry”. In: *Nature Methods* 16 (2019), pp. 67–70. url: <http://lmb.informatik.uni-freiburg.de/Publications/2019/FMBCAMBBR19> (cit. on p. 140).
- [187] G. team. *Grbl: Open-source CNC G-Code parser and controller*. <https://github.com/gnea/grbl/wiki>. accessed: 2019-10-31. 2019 (cit. on p. 148).
- [188] J. Pires et al. “A Global Methodology for 3d Multi-Material Laser Powder Bed Fusion Processes”. In: *Available at SSRN 4156726* (). doi: <https://dx.doi.org/10.2139/ssrn.4156726>. url: https://papers.ssrn.com/sol3/papers.cfm?abstract_id=4156726 (cit. on p. 165).

Ezcad API

The relevant part of the Ezcad API for this project is extensively presented below, with a self-documenting prototypes, thus self-explanatory.

Listing A.1: Ezcad API

```

1  #ifndef MARKEZDLL_H
2  #define MARKEZDLL_H

4  // Return Values
5  #define LMC1_ERR_SUCCESS      0 // Success
6  #define LMC1_ERR_EZCADRUN    1 // Find EZCAD running
7  #define LMC1_ERR_NOFINDCFGFILE 2 // Can not find EZCAD.CFG
8  #define LMC1_ERR_FAILEDOPEN  3 // Open LMC1 board failed
9  #define LMC1_ERR_NODEVICE     4 // Can not find valid lmc1 device
10 #define LMC1_ERR_HARDVER      5 // Lmc1's version is error.
11 #define LMC1_ERR_DEVCFG       6 // Can not find configuration files
12 #define LMC1_ERR_STOPSIGNAL   7 // Alarm signal
13 #define LMC1_ERR_USERSTOP     8 // User stops
14 #define LMC1_ERR_UNKNOW       9 // Unknown error
15 #define LMC1_ERR_OUTTIME     10 // Overtime
16 #define LMC1_ERR_NOINITIAL    11 // Un-initialized
17 #define LMC1_ERR_READFILE     12 // Read file error
18 #define LMC1_ERR_OWENWNDNULL  13 // Window handle is NULL
19 #define LMC1_ERR_NOFINDFONT   14 // Can not find designated font
20 #define LMC1_ERR_PENNO        15 // Wrong pen number
21 #define LMC1_ERR_NOTTEXT      16 // Object is not text
22 #define LMC1_ERR_SAVEFILE     17 // Save file failed
23 #define LMC1_ERR_NOFINDENT    18 // Can not find designated object
24 #define LMC1_ERR_STATUE       19 // Can not run operation in current state

26 //INTENTION: initialize lmc1 control board
27 typedef int (*LMC1_INITIAL)(TCHAR* strEzCadPath, BOOL bTestMode, HWND hOwenWnd);

29 //INTENTION: Close lmc1 board
30 typedef int (*LMC1_CLOSE)();

32 //INTENTION: open the appointed ezd file, and clear all the object in database.
33 typedef int (*LMC1_LOADZDFILE)(TCHAR* strFileName);

35 //INTENTION: mark all the data in database
36 typedef int (*LMC1_MARK)(BOOL bFlyMark);

```

```

38 //INTENTION: mark the appointed named object in database
39 typedef int (*LMC1_MARKENTITY)(TCHAR* strEntName);

41 //INTENTION: read the input port of the lmc1
42 typedef int (*LMC1_READPORT)(WORD& data);

44 //INTENTION: write data to output port on the lmc1
45 typedef int (*LMC1_WRITEPORT)(WORD data);

47 //INTENTION: Get the preview picture of all the objects in database.
48 typedef CBitmap* (*LMC1_GETPREVBITMAP)(HWND hwnd,int nBMPWIDTH,int nBMPHEIGHT);

50 //INTENTION: get the parameter of appointed pen
51 typedef int (*LMC1_GETPENPARAM)(int nPenNo, //(0-255)
52                                 int&      nMarkLoop, //
53                                 double&    dMarkSpeed, //mm/s
54                                 double&    dPowerRatio, //(0-100%)
55                                 double&    dCurrent, //A
56                                 int&      nFreq, //HZ
57                                 double&    dQPulseWidth, //Qus
58                                 int&      nStartTC, //us
59                                 int&      nLaserOffTC, //us
60                                 int&      nEndTC, //us
61                                 int&      nPolyTC, //us //
62                                 double&    dJumpSpeed, //mm/s
63                                 int&      nJumpPostTC, //us
64                                 int&      nJumpDistTC, //us
65                                 double&    dEndComp, //mm
66                                 double&    dAccDist, //mm
67                                 double&    dPointTime, //ms
68                                 BOOL&     bPulsePointMode, //
69                                 int&      nPulseNum, //
70                                 double&    dFlySpeed);

72 //INTENTION: Set the pen parameter
73 typedef int (*LMC1_SETPENPARAM)(int nPenNo, //(0-255)
74                                 int      nMarkLoop, //
75                                 double   dMarkSpeed, //mm/s
76                                 double   dPowerRatio, //(0-100%)
77                                 double   dCurrent, //A
78                                 int      nFreq, //HZ
79                                 //int    nQPulseWidth, //Qus
80                                 double   dQPulseWidth, //Qus
81                                 int      nStartTC, //us
82                                 int      nLaserOffTC, //us
83                                 int      nEndTC, //us
84                                 int      nPolyTC, //us //
85                                 double   dJumpSpeed, //mm/s
86                                 int      nJumpPostTC, //us
87                                 int      nJumpDistTC, //us
88                                 double   dEndComp, //mm
89                                 double   dAccDist, //mm
90                                 double   dPointTime, // ms
91                                 BOOL     bPulsePointMode, //
92                                 int      nPulseNum,
93                                 double   dFlySpeed); //

```



```
95 //INTENTION: clear all object in database
96 typedef int (*LMC1_CLEARENTLIB)();

98 //INTENTION: add the appointed file into database.
99 typedef int (*LMC1_ADDFILETOLIB)(TCHAR* pFileName, //
100                                  TCHAR* pEntName, //
101                                  double dPosX, //x
102                                  double dPosY, //y
103                                  double dPosZ, //z
104                                  int nAlign, //08
105                                  double dRatio, //
106                                  int nPenNo, //
107                                  BOOL bHatchFile); // ezd

110 //INTENTION: add new curve object into database.
111 typedef int (*LMC1_ADDCURVETOLIB)(double ptBuf[][2], //
112                                   int ptNum, //
113                                   TCHAR* pEntName, //
114                                   int nPenNo, //
115                                   int bHatch); //

117 //INTENTION: enable and reset the coordinate of extend axis
118 typedef double (*LMC1_RESET)(BOOL bEnAxis0 , BOOL bEnAxis1);

120 //INTENTION: save all objects in database to the appointed .ezd file.
121 typedef int (*LMC1_SAVEENTLIBTOFILE)(TCHAR* strFileName);

123 //INTENTION: move object appointed distance
124 typedef int (*LMC1_MOVEENT)(TCHAR* pEntName,
125                             double dMovex,
126                             double dMovey);

128 //INTENTION: get the total number of objects in database.
129 typedef int (*LMC1_GETENTITYCOUNT)();

131 //INTENTION: get the name of the object that has appointed serial number
132 typedef int (*LMC1_GETENTITYNAME)(int nEntityIndex, TCHAR szEntName[256]);

134 #endif
```



A global methodology for 3DMMLPBF processes

The paper submitted to *Journal of Robotics and Computer Integrated Manufacturing* is presented next [188].

A global methodology for 3D multi-material Laser Powder Bed Fusion processes

José Pires^{a,b}, Paulo Pinto^{a,b}, Flávio Bartolomeu^{a,b}, Filipe Silva^{a,b}, Óscar Carvalho^{a,b,*}

^a*Centre for Micro Electrical Mechanical Systems (CMEMS), Azurém, 4800-058 Guimarães, Portugal*

^b*LABELS — Associate Laboratory, Braga/Guimarães, Portugal*

Abstract

Laser Powder Bed Fusion (LPBF) processes emerge as one of the most feasible and flexible Additive Manufacturing (AM) technologies of metallic and composites parts, as they enable the layer-wise production of complex-shaped, functionally graded or custom-tailored parts by material deposition and subsequent or simultaneous melting via a focused laser beam. Furthermore, LPBF processes also enable the fabrication of multi-material parts, highly desirable for enhancing even further the performance of such parts, by varying compositions or type within layers, unachievable by conventional manufacturing processes. However, most current commercially available systems are mono-material only, which could be partially explained by the added complexity of the multi-material processing to an already complex multi-physics problem. The trend is for the problem to get worse, as the techniques to solve it will become increasingly complex. Still, the reported methodologies seem to address only specific parts of the problem, disregarding the ‘whole picture’ scenario. In the present work, a global methodology for tackling the complexity of LPBF processes is proposed, demonstrating the added benefits for all the agents in the manufacturing chain. The design of this methodology will be discussed in detail with special focus in its core principles and tools. The methodology is then applied specifically

*Corresponding author

Email address: `oscar.carvalho@dem.uminho.pt` (Óscar Carvalho)

to LPBF process, adding the multi-material aspect in all directions, yielding a novel 3D Multi-Material Laser Powder Bed Fusion (3DMMLPBF) process. As a result, a simplified workflow — CAD to 3DMMLBPF-PART — is established. The software toolchain was derived from the workflow, comprising the slicer and path generator, post-processor and printer, and the post-manufacturer. A low-budget, highly customizable 3DMMLPBF equipment was built as a proof-of-concept. The workflow and associated toolchain, and the equipment were tested and validated.

Keywords: methodology, multi-material, powder bed fusion, equipment

Acronyms

3DMMLPBF 3D Multi-Material Laser Powder Bed Fusion

AI Artificial Intelligence

AM Additive Manufacturing

ASTM American Society for Testing and Materials

CAD Computer-Aided Design

CAE Computer-Aided Engineering

CAM Computer-Aided Manufacturing

CNC Computer Numerical Control

DED Direct Energy Deposition

DLD Direct Laser Deposition

DOE Design Of Experiments

EBM Electron Beam Melting

FDM Fused Deposition Material

FGM Functionally Graded Material

GUI Graphical User Interface

LMD Laser Metal Deposition

LOM Laminated Object Manufacturing

LPBF Laser Powder Bed Fusion

MMAM Multi-Material Additive Manufacturing

MMFGM Multi-Material Functionally Graded Material

NC Numerical Control

PBF Powder Bed Fusion

SEM Scanning Electron microscope

SLM Selective Laser Melting

SLS Selective Laser Sintering

STL Standard Tessellation Language

SVG Scalable Vector Graphics

UAV Unmanned Aerial Vehicles

UML Unified Modeling Language

XML eXtensible Markup Language

1. Introduction

AM is revolutionizing the way we manufacture products by providing the designer the freedom to bring the conceptualized ideas to life from ground-up, contrarily to the traditional (subtractive) manufacturing techniques which impose a pre-shape. With this theoretically ‘unlimited’ freedom comes a greater responsibility, and aid should be provided to the designer in the form of guidelines and design criteria, as a means to unlock AM full potential: as material is only added where is functionally needed, waste is minimized and the overall properties of the component being built are enhanced [1].

This idea meets its pinnacle with the concept of an Multi-Material Functionally Graded Material (MMFGM) — multi material components with materials gradations in between. The great interest on using MMFGMs is the possibility of controlling composition or structure and thus obtain components with desired local properties, as regarding mechanical, tribological, thermal properties, and others [2].

However, most current commercially available systems have been designed for mono-material part fabrication [3] and are unprepared for multi-material processing due to the lack of flexibility and processing capability. In the field of metallic and composite components the panorama is worst due to: the complexity of the multi-physics problem associated with the process used — for example, LPBF processes — which exhibit multiple modes of heat and mass transfer [4, 5, 6, 7, 8, 9] and in some instances chemical reactions [10, 11]; the vast number of process parameters [12]; and the lack of a global infrastructure that supports the development of the multi-material processes in this field, as the solutions are from proprietary nature, and therefore closed-environment, hindering the technological advances in the area.

Thus, a global methodology for the fabrication of multi-material metallic and composite parts is required to handle the inherent complexity and leverage the process’s knowledge, providing an AM process database — as suggested by Gu et al. [13] — to all key agents in the manufacturing chain.

2. Reviews

2.1. Additive Manufacturing

The fundamental premise of AM is quite simple: adding and bonding the material(s) to create the part only where it is/are needed, typically in a layer-
35 by-layer fashion via Computer Numerical Control (CNC) displacement, from imported three-dimensional (3D) model data [14]. The 3D part is ‘assembled’ by bonding materials, either like or dissimilar, with each new layer of material being a manifestation of the 3D model cross-sectional data. These models are typically in the Computer-Aided Design (CAD) form in Standard Tessellation Language
40 (STL) file format and are numerically sliced into many fictitious layers/cross-sectional data from which the manufacturing paths can be generated, dictating the CNC displacement. A wide variety of AM application have been reported namely: Unmanned Aerial Vehicleless (UAVs) [15], fuel nozzles [16], houses [17], tooling [18, 19], biomedical implants [20], among others.

45 To accomplish the effective material bonding, the successful combination of material and energy delivery is required, differing with the material and the AM process[14, 21]. The AM processes can be classified by [22]:

- *state of raw material*: liquid, solid sheet or discrete particle;
- *type of material*: metal (layer or direct deposition); polymer (Fused De-
50 position Material (FDM), stereolithography, polyjet); paper (Laminated Object Manufacturing (LOM); wood (stratoconception).

Sometimes, terminology will differ but American Society for Testing and Materials (ASTM) in attempt to standardize this classification recognizes the following AM methods [14]: material extrusion, material jetting, sheet lamination, vat
55 polymerisation, binder jetting, Direct Energy Deposition (DED) and Powder Bed Fusion (PBF).

The AM process is traditionally ‘open-loop’ due to its lower complexity and lower cost; however feedback control is being introduced to ensure better part quality, in some cases with real-time characteristics [23, 24].

60 *2.2. Laser-based Additive Manufacturing*

When it comes to the additive manufacturing of metallic parts and composites DED and PBF are the most proven and feasible methods [14, 25]. Both processes involve the deposition of powder metal (or less common preforms such as wire) and their simultaneous or subsequent melting, respectively, via a focused thermal energy source, namely an electron beam or a laser beam. In case a laser beam is used the processes can be referred as form of LPBF, while DED can be further specified as Direct Laser Deposition (DLD) [14]. The usage of an electron beam (Electron Beam Melting (EBM)) makes high scanning speed possible (up to several km/s) due to the lack of moving parts to guide the building spot [22]; however, the increased complexity and cost does not make it commercially viable yet. As a result, LPBF processes are the current bet for commercial and industrial applications.

2.3. Multi-Material Additive Manufacturing

The capability to fabricate multiple material parts is highly desirable as it allows for the accurate placement of material according to its functionality, providing custom-tailored parts for specific applications with enhancement of its mechanical properties and behaviour in service. However, most current commercially available systems have been designed for mono-material part fabrication [3]. The emerging Multi-Material Additive Manufacturing (MMAM) technology can enhance the AM parts performance by varying compositions or type within layers, unachievable by conventional manufacturing processes [25], without the need for complex manufacturing process and expensive tooling [26, 27].

The range of applications are vast and pivotal. In the biomedical engineering field, MMAM enabled the production of 3D engineered tissue (3D spinal cord [28]), biomedical devices such as microneedle arrays [29] and diagnostic devices [30], multi-material cellular structures targeting orthopedic implants [31], and 3D artificial models for preclinical or preoperative surgical training [32, 33], among others. In the soft robotics field, where flexibility is key for complex actuations and motions, MMAM enabled the production of pneumatillcay driven

90 elastomeric actuators [34] and direct integration of functional components re-
quired for it (e.g., a silver-nanoparticle ink acting acting as a resistive heating
element [35]). In electronics MMAM is critical for direct manufacturing of 3D
electronic devices where electrically dissimilar materials including conductors,
semiconductors, and dielectrics are integrated together [26]. Some examples are
95 a 3D magnetic sensor with integrated electronics components and conductive
paths [36], stretchable strain or pressure sensors [37] and a highly stretchable
electronic LED board [38], yielding high potential for wearable electronics, and
even an fully 3D printed and package Li-ion battery [39].

To achieve this superior performance over AM, different materials or chemi-
100 cals need to be physically delivered to any point in the 3D space during the ad-
ditive manufacturing. In some processes, like direct 3D printing in Objet, FDM,
this is relatively straight-forward to achieve as the materials are deposited in
the platform dot-by-dot or line-by-line via nozzles; to incorporate multi-material
fabrication multiple nozzles can be added [25].

105 For multi-material fabrication of metals, a similar result could be achieved
through the use of LENS process or DLD, as they can use multiple nozzles/hop-
pers in the part fabrication. For example, multi-material components manu-
factured by Laser Metal Deposition (LMD) has been demonstrated in litera-
ture [40, 41]. However, in other processes, like Selective Laser Sintering (SLS),
110 Selective Laser Melting (SLM), LOM, this is not trivial, as the materials are
delivered as whole layer by a scraper or as a solid sheet, requiring new material
delivery systems to be first developed [25]. Nonetheless, SLM provides higher
precision, smaller feature size and the ability to produce lightweight structures
based on lattices, which are appealing features for turbine blades that cannot be
115 easily achieved by LMD [42, 43]. On top of that, DLD is a more difficult process
to master due to added complexity of deposition control, on top of the melt-
pool control, which can cause variations in the laser spot due to local increase
of part's height as a result of the deposition [44].

Focusing on the SLM process, the key process parameters are laser power,
120 scanning speed, layer thickness and hatch spacing [45]. Recent works demon-

strated its feasibility for multi-material manufacturing, by using modified industrial machines or self-developed prototypes, but with material variation obtained layerwise only. Using a modified industrial machine, C18400 copper have been successfully deposited on top of 316L stainless steel and AlSi10Mg [46, 47]. However, there is no control of the transition zone between the two materials, which is the most critical in a multi-material part. As aforementioned the powder delivery system is critical for the multi-material fabrication using SLM and must be carefully designed to prevent cross-contamination between materials, thus, special focus was given to it. Demir and Previtali developed a double hopper powder delivery system based on piezoelectric transducers which enabled the manufacturing of a Fe/Al-12Si specimen, with an intermixed region between the two materials [48]. Kumar et al. used glass pipettes as ‘hopper-nozzles’ to spread powder, by means of gas pressure or vibration feed, allowing a precise powder delivery, without the need to vacuuming the excess [49]. Another approach towards a graded transition is the use of selective recoaters combined with a special processing scheme for powder removal, where one material is selectively deposited, then melted before the other one is delivered, and finally excess powder is vacuumed [50, 51, 52]. Anstaett et al. proposed an SLM system capable of depositing two different powders, combining a Cu-alloy and a tool steel to produce a multi-material component [53].

On the commercial field, Admatec developed an industrial SLM machine which spreads the raw material as a slurry, thus allowing to combine multiple materials [54]. By heating the feedstock the binder eventually evaporates and the metal powder can be successively processed.

Very recently, Walker et al. [55] developed a LPBF machine technology for graded alloy processing, with the capability to deposit location specific powder of varying material composition in any 3-dimensional location, thanks to multiple powder hoppers. The Open Additive Open Machine Control TM (OMC) software is used (proprietary source) to control all process operations, namely, powder deposition, control of the vacuum nozzle, and application of location specific processing parameters. Furthermore, the composition mixtures are cre-

ated prior to processing and separated into individual hoppers or the powder supply, for multi-material processing, but no design guidelines are provided for the common user: how to design a multi-material part that the machine is able
155 to produce, with the required functionality?

Thus, in the first iteration of the methodology proposed SLM process will be considered, contingent of the need for a better powder delivery system.

2.4. Methodologies

Some methodologies for multi-material processing have been proposed in the
160 literature [56, 57, 52]. Chiu et al. [56] proposed a methodology for direct digital manufacturing of 3D Functionally Graded Material (FGM) objects via 3D printing based on the geometrical — 3D CAD model — and material information — color property. The resultant colors are determined by Computer-Aided Engineering (CAE) analysis results which convert the design criteria (strength)
165 requirements, binder concentration requirements, primary binder requirements using 3D pixels — voxels. The design of the FGM model then becomes the problem of determining the average binder concentration applied to each pixel of the model. It also reports the problems of the current FGM model representation using plain STL files as it only conveys geometrical information and
170 reviews some alternatives like material tree structure [58], ‘grading source’ representation [59], vector valued function spanning a material space [60], STEP + data planning model [61], among others. However, this methodology is limited to direct deposition technologies and the range of change of the binder concentration is narrow.

175 Ponche et al. [57] proposed a new methodology of design for AM applied to LPBF processes, organized into three main steps — part orientation, functional optimisation and manufacturing paths optimisation — that takes into account the geometrical deviations induced by the physical phenomena occurring during the process as means to produce more accurate and reliable parts. However, it
180 is only suited for DLD process, it uses a considerable amount of different tools (Morfeo, Topostruct, MATLAB) and it uses empirical manufacturing rules.

Chivel [52] proposed a new approach to multi-material processing in SLM introducing a new SLM machine concept with improved build platform cleaning and optical systems, including a monitoring system with a high speed digital
185 CCD camera and pyrometer for melt-pool control. The multi-material fabrication was conducted through a clever cleaning and powder recovery system design via granulometric sieving (according to particle diameter) and alternate descent and ascent of the printing bed to remove the powder. To avoid wash out of solid-melt interface, a special strategy of scanning was proposed to reduce
190 the time of solid-melt contact, consisting of a spiral scanning path carried out from the centre to the periphery. However, the alternate descent and ascent of the printing bed seems to be unnecessary, which suggests improvements can be made, and the machine is patent-protected which inhibits any modification, hindering the customisation requirement of the manufacturing process.

195 The proposed methodology in the present work borrows some concepts from the preceding methodologies, aiming to fill the gaps left by them through a global perspective over LPBF processes, leveraging the process's knowledge throughout the manufacturing chain.

3. LPBF methodology

200 3.1. Motivation

The proposed methodology arises mainly from three important aspects: the lack of a methodology that encompasses the LPBF process as a whole, considering the key agents and leveraging the overall existing knowledge; the need to build an equipment to fabricate MMFGMs, as the currently available processing
205 technology does not fit the desired customization and freedom requirements; the inherent complexity of LPBF processes, even for a single material, and, since the trend is for the complexity to increase as we enter the field of multiple materials and FGMs, an efficient way to handle the complexity is required.

Furthermore, the current commercial equipments are expensive and not very
210 customizable, undermining the machine's full potential, as the end-user has

limited access to the machine and process parameters. This is especially critical in the research environment, diminishing the research opportunities, increasing inequalities in the field, and, most important of all, hindering the evolution of the LPBF processes.

215 The underlying philosophy follows, in a sense, the open-source one, as transparency is undoubtedly a desirable feature, enabling the convenient scrutiny of all stages of the process, which is a science's premise. This holds valid for both software and hardware tools.

3.2. Core Principles

220 Knowledge, the theoretical or practical understanding of a subject, is the most important human asset. However, knowledge acquisition is a nonlinear process, as a single piece of additional data can invalidate complete models [62]. Still, LPBF knowledge is scattered around its agents without an apparent connection. Moreover, some employed techniques in LPBF processes are empirical-
225 based [14], which obviously requires the capture of the context and the rationale behind these decisions. The key idea here is to capture the knowledge and the associated context and delivery it to the appropriate handler, leveraging its efficient usage in favour of the overall process.

The core principles of the methodology are:

- 230 • *Abstraction*: layer(s) to abstract from the internal specifics of the process should be provided by means of tractable interfaces;
- *Modularity*: every component of the process should be replaceable by another of identical functionality;
- *Independence*: the process should be agnostic about the inputs, as long as
235 the valid interfaces are respected;
- *Flexibility*: capable of handling different inputs/components as new parameters or the conjunction of its effects can be used in the process; it should support different materials, machines modules, slicing strategies, etc.;

- 240 • *Extensibility*: new components should be added without compromising the process;
- *High customization*: both software and hardware based components should allow a high customization of its operation;
- 245 • *Capability of managing the different information flows*: pre-process, process and post-process data should be collected and delivered to its handler in a convenient way;
- *Evolution*: The acquired knowledge should be used for improvement of the process;
- 250 • *Guidance to end-users*: the acquired knowledge should enable the creation of guidelines and heuristics to aid the end-user;
- *Maximization of process's control*: an open developing environment enhances end-user's capabilities to control the process — normal users can evolve to power users, as opposed to closed environments.

3.3. Concept

255 An effective way to handle complexity is through a model, an abstract representation of a system that enables us to answer questions about it [62]. To create the relevant models, a modeling language will be used, more specifically, the Unified Modeling Language (UML), as it enables the modeling of a variety of artifacts, from software systems to processes and work products [62]. First, 260 the actors of the process are identified as the key agents that interact with it, classified in:

- *Internal* — that takes effective action in the process, namely:
 - *Designer* — idealizes a concept and translates it to a virtual 3D representation (CAD model).
 - 265 – *Manufacturer* — takes the virtual 3D model and employs the appropriate materials, techniques and tools to materialize into a physical object.

- *External* — that benefit from or induce actions in the process, e.g.:
 - *Physicist* — studies all physical phenomena in the process and contributes with a greater knowledge about them in the form of physics models and parameters, enabling better control strategies, better materials properties, faster process, etc;
 - *Materials/Mechanical Engineer* — studies all materials/mechanical properties of the produced part in service and contributes usually in the form of empirical knowledge as a set of rules that enhance the part properties and performance;
 - *Control Engineer* — studies the process control, i.e., an effective means of reaching the system goals in a regulated and bounded way, generating the control strategies to be used in the processed [44];
 - *Mathematician* — studies, among other subjects, the manufacturing path topology and the geometric and interchange data representation of the 3D virtual model for the machine execution.
 - *Data Scientist* — studies all process generated data, via data-driven models, leveraging the fact there is an immense quantity of data available to identify data patterns to produce more efficient and accurate empirical knowledge. It can be used to design better experiments, via Design Of Experiments (DOE), and to better control the process, via Artificial Intelligence (AI)[44].

Next, the manufacturing chain was decomposed into four models that will be detailed next, namely: design model, pre-manufacturing model, manufacturing model and post-manufacturing model.

3.3.1. Design Model

Fig. 1 illustrates the design model of the manufacturing chain. The designer initiates this phase by identifying a function/application of the object to be designed. Then, a requirements analysis is performed and the design criteria are

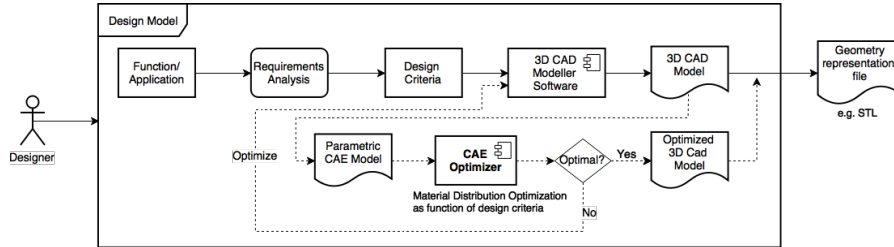


Figure 1: Model of the design activity

established. Now, the object can be modeled in a 3D CAD software, yielding a 3D CAD model of the object. The 3D CAD model ideally, although not necessary, goes through an optimization stage, where it is converted into a parametric CAE model and fed to a CAE optimizer, optimizing the material distribution as a function of the design criteria: if the optimal configuration is not achieved, the designer should optimize the 3D CAD model. Otherwise, for both optimized and unoptimized 3D CAD model, a data file representing the geometry of the 3D CAD is generated, with the most common being an STL file.

3.3.2. Pre-Manufacturing Model

Fig. 2 depicts the pre-manufacturing phase. All internal components of the model are software ones. The manufacturer starts by feeding the geometry representation file to the Computer-Aided Manufacturing (CAM) optimizer (ideal setup — shown in dashed lines) or directly to the slicer (conventional setup — shown in continuous lines). The CAM optimizer, as well as the advisor, are included as a recommended way of optimizing the manufacturing process: the former is used to optimize it as a function of the process based on systematized knowledge originary from the machine, process and material information; the latter is used to optimize through convenient part orientation, file data sanity check and the conformation to the standards based on empirical knowledge also originary from the machine, process and material information. Both these optional components can be used to optimize the 3D CAD model from the design

stage; however, the first, as it is based on systematized knowledge should issue the recommendations as errors or warnings, stopping the process, while the last, as it based on heuristics and guidelines, should issue them as tips.

Then, the 3D model is sliced using cross xy planes into 2D layers — slicer. Some problems can occur in this stage, especially if the geometry representation file is a tessellation of the surface (STL), as it is unable to accurately represent holes, porosity and discontinuities. This will be addressed in more detail ahead.

The final software component — the post-processor — deserves special attention. The pre-manufacturing and manufacturing models are linked together by a common principle that dates back to the beginning of the Numerical Control (NC) machinery, even before the advent of the computer (and thus the CNC) — the compiler/interpreter. The principle is simple: the instructions to run the machine have to be compiled into a standard code that can be interpreted by the machine (the first was called G-code). Therefore, the code as to be known by both parts — the compiler and the interpreter — represented by language tokens, originating the manufacturing instructions tokens, based on the machine, process and material tokens; the compiler utilize them to compile machine-compliant instruction code; the interpreter is built based on them, incrementing the firmware. The post-processor, before handling the compilation, is also responsible for the layers merging and the inclusion of the process parameters as a means to execute the correct compilation. After the compilation, a file containing machine instructions for manufacturing is generated, which in this case conveniently named *.lcode*.

3.3.3. Manufacturing Model

The manufacturing model, in charge of the manufacturer, includes the control model and the manufacturing process model (Fig. 3) tightly coupled together. The manufacturer feeds the manufacturing instruction file, containing the manufacturing process relevant data for the part fabrication, to the interpreter — a software sub-component of the machine's firmware. The interpreter then, reads, parses and interprets the *.lcode* instructions. If the End-of-File

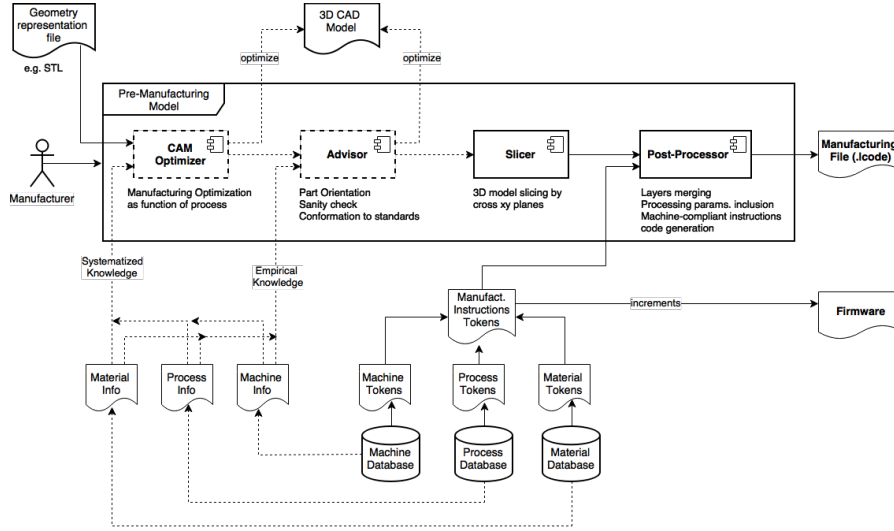


Figure 2: Model of pre-manufacturing activity

(EOF) has not been reached it issues commands to the control board which, in turn, issues controls for the controlled parts like motors, the laser, the heating elements, etc. This yields an effect on the manipulated variable which affects the manufacturing process, represented as a transfer function, different for each process variable. The result of the control action will be a variation in the controlled variable state (e.g., temperature, laser speed, etc.), affecting the manufactured part, which is measured by a sensor (e.g. encoder, thermocouple, pyrometer, etc.) and feed back to the control board for comparison with the desired values for the process variables, with the control action being adjusted accordingly. Additionally, the process variables are registered by another software component — the logger — which reads, converts and logs the relevant parameters as a process info data file to be stored in the process trials database. When the manufacturing file reaches the end, the part is produced and ready for the next stage — the post-manufacturing phase.

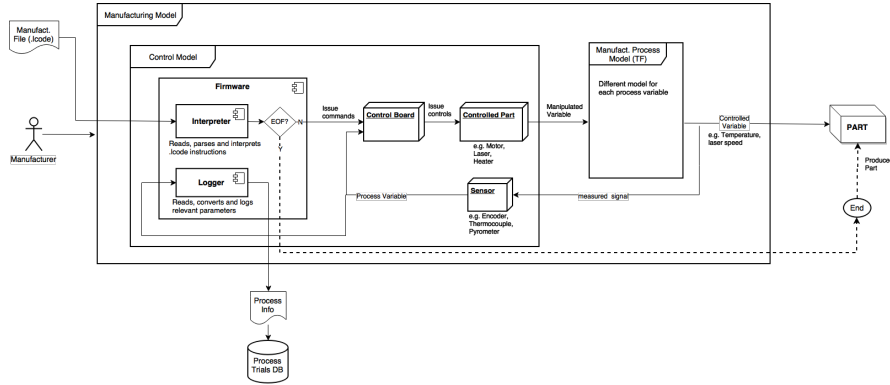


Figure 3: Model of manufacturing activity

3.3.4. Post-Manufacturing Model

The post manufacturing stage (Fig. 4) is probably the most important one in the chain, and often the most neglected, as the quality analysis of the process and of the produced part are conducted in this phase, with the relevant outputs cascading to the precedent stages. With the produced part, the material and mechanical engineers can conduct, respectively, the material analysis and mechanical behaviour analysis; from the former will result the relevant material information and from the latter the mechanical properties of the produced part, to be stored in the respective databases.

The mechanical properties and material information will aid the physicist to conduct the physical analysis via simulation or modeling techniques yielding physical models, which ultimately result in physical laws or theories, predicting what happens or proposing why it happens.

Another often neglected role in the manufacturing chain is of the data scientist which conducts process data analysis, typically in one of two ways: via DOE or AI. Analysing process data history via DOE enables the design of more effective and statistically relevant experiments, resulting in another iteration of the manufacturing phase; analysing via AI enables the recognition of data patterns, yielding empirical models which can lead to empirical laws or theories,

generating heuristics and guidelines that update the *advisor* software component.

The process models will then be generated from both physical and empirical laws/theories that together with the process trials data information enable the control engineer to conduct the control analysis. From this analysis stems an integrated model of the *control + process* combination, which yields control algorithms and parameters. Both these outputs are used to update the machine's firmware and are stored in the process control database. Additionally, they are also used, together with the material information, the mechanical properties and physical laws/theories to update the CAM optimizer.

Lastly, the specification analysis is conducted by the designer and the manufacturer, taken into account the compliance to the function/application in question of the produced part and its mechanical properties. If the function/application is not fulfilled, then the design should be repeated. Otherwise, and if the quality of the part produced namely, mechanical properties, dimensions or surface finishing, etc., is not fulfilled, better manufacturing paths or better process control may be required, leading to a new iteration starting at the pre-manufacturing or manufacturing phases. This information should be properly depured to conveniently and correctly deliver it to the appropriate agent: if the former is verified, this information should be conveyed to the mathematician for topology optimization; if the latter is true, the relevant information should be conveyed to all the agents responsible, directly or indirectly for the control, like the physicist, data scientist and control engineer. If the quality is according to the specifications, the result will be a produced part there is ready for service, and this trial should be signaled as successful, with the relevant information cascading to all databases for further improvement of all involved models.

4. Application of the methodology to 3DMMLPBF

The proposed methodology is complex and extense, and therefore needs to be implemented by stages, where only the most essential features are considered

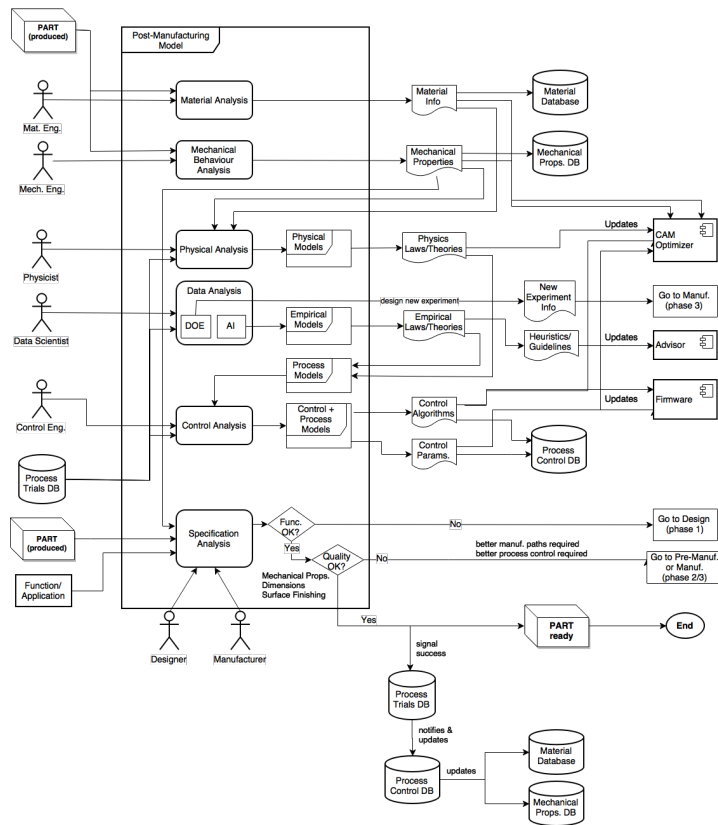


Figure 4: Model of post-manufacturing activity

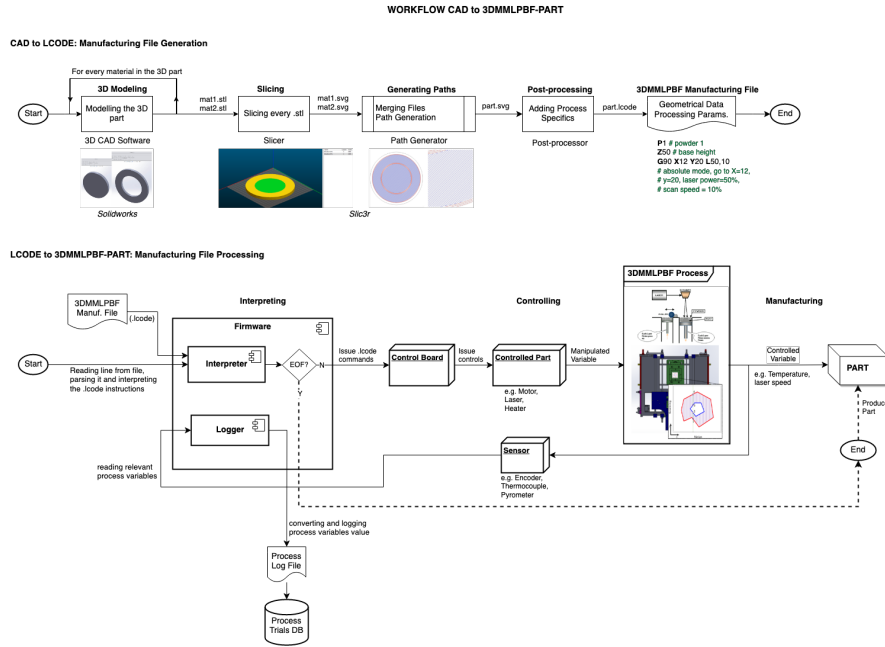


Figure 5: Workflow CAD to 3DMMLPBF-PART

410 in each development phase, being intensively tested before the integration in the framework. Furthermore, the manufacturing process chosen for the multi-material fabrication of tridimensional metallic and composite parts is the LPBF, yielding a novel process named 3DMMLPBF.

Thus, a simplified workflow for this process is proposed (fig. 5) as a means
 415 to: produce customized 3D multi-material parts with freedom of shape and process control; test the proposed methodology; increase the process's knowledge; quickly iterate over the manufacturing chain with different part's design and different processing solutions, as will be detailed further ahead. This workflow, together with the methodology proposed, paved the way for the correct development and deployment of both software and hardware (mechanical/electronic)
 420 components.

The workflow — named *CAD to 3DMMLPBF-PART* — integrates the design model and pre-manufacturing model without the CAE and CAM optimiza-

tion steps, respectively, and does not implement the post-processing model yet.
425 This will be reserved for future iterations. The workflow is divided in two phases:
the manufacturing file generation and the manufacturing file processing.

4.1. CAD to LCODE — Manufacturing File Generation

The goal of the first phase — *CAD to LCODE* — of the proposed workflow is
the generation of the file containing the manufacturing instructions. Each mate-
430 rial of the 3D model is modelled individually, in a common 3D CAD modelling
software (e.g. SolidWorks), and a tessellation file of the surface is produced,
containing the geometric information. In this initial stage, the 3D model is
considered to have no holes, porosity or discontinuities, as this would invalidate
the usage of the surface tessellation, i.e., the multi-material modelled parts are
435 considered to be completely filled in.

The next phases — *Slicing and Path Generation* — use an open-source tool
named Slic3r[63], due to the underlying philosophy of transparency, extensibil-
ity, reusability, adaptability, flexibility, and modularity desired. Furthermore,
Slic3r is a highly configurable and robust slicer, allowing for the fine control of
440 the multiple types of scan paths — rectilinear, line, concentric, 3D honeycomb,
Hilbert Curve, etc.—, generating customized G-code for multiple target plat-
forms and scriptable (for batch mode). We will be working with a cloned version
of the project to integrate the custom scan paths algorithms. Additionally, pre-
scanning paths will be added to deal with the high thermal gradients induced in
445 a single passage of the laser beam. The output of both these phases is an Scal-
able Vector Graphics (SVG) file; the choice of this file format is due to the use of
markup language, namely eXtensible Markup Language (XML), for describing
two-dimensional vector and mixed vector/raster graphics[64]. This allows the
conveying of extra information besides the geometry, that can be packed in a
450 structure node, for example line color attribute to represent different materials,
addressing the multi-material representation ambiguity. In respect of the oper-
ations' logic, each material is sliced in layers and output as a SVG file. Then
the files are combined for each layer and the scan paths are generated, yielding

a complete SVG file of the part.

455 This file, containing the geometry information pertaining to the scan paths,
will be post-processed to add the process relevant parameters, like material and
process parameters with the former being pulled from the material database
and the latter being defined by the end-user. The result will be a file — `.lcode`
— containing the manufacturing instructions for the 3DMMLPBF process with
460 the geometrical data and process parameters. The post-processor is currently
under development, but an extract sample is provided in 5, illustrating the
tokens used:

- P1 — Powder 1
- Z50 — base height
- 465 • G90 X12 Y20 L50,10 — absolute mode, go to X=12, Y=20, with laser
power at 50% and scan speed at 10%.

4.2. *LCODE to 3DMMLPBF-PART — Manufacturing File Processing*

The goal of the second phase — *LCODE to 3DMMLPBF-PART* — of the
proposed workflow is the processing of the file containing the manufacturing
470 instructions. This file will be read line-by-line, parsed and interpreted, issuing
commands to the control board based on the *lcode* instructions of the file. The
remainder of the operation — controlling and manufacturing — is similar to the
one described in the manufacturing model (Section 3.3.4), with the controlled
part inducing an effect in the 3DMMLPBF process and the controlled variable
475 that affects the manufactured part being measured and logged by the logger
software component to a process log file, which is stored in the process trials
database. When the *End-of-File* is reached, the process terminates and the part
is manufactured.

This workflow represents the typical simplified one for the 3DMMLPBF
480 manufacturing process. However, currently there is a major restriction for the
implementation of this workflow as is, due to the closed nature of the proprietary
software of our CO₂, YAG-Nd and fiber lasers. In the future, we will implement

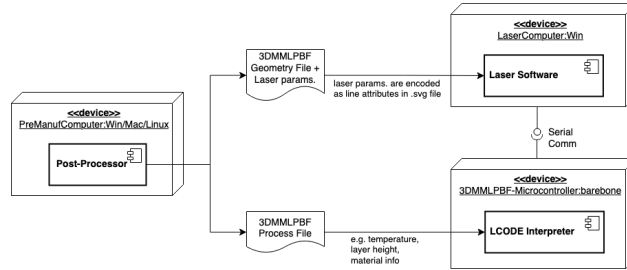


Figure 6: Workaround for the proposed workflow: two separate data files — geometry and process — are used by the laser software and LCODE interpreter for scanning paths marking and process related tasks, respectively

our own software to control the lasers hence integrating in the 3DMMLPBF machine, but for now a workaround was used. This workaround consists in separating the geometric data from the process data at the post-processing stage and assigning it, respectively, to the laser and the 3DMMLPBF machine. The processing parameters of the laser are encoded in the SVG file as line attributes that the laser software is able to recognize and use for the scan paths marking.

Fig. 6 illustrates the architecture of this solution with the representation of the data streams, the software components that use those streams, the hardware nodes where the software components are assigned and the protocols under which they communicate, namely serial communication for laser and 3DMMLPBF machine synchronization.

4.3. 3DMMLPBF machine for multi-material processing

Based on the requirements imposed by the 3DMMLPBF process, namely the freedom of shape and of control and the specifics of the multi-material processing, an equipment was developed and built (version 2.0), as illustrated in Fig. 7. This equipment is a more compact version, optimizing powder consumption and recovery, and manufacturing efficiency.

The equipment includes: the *powder recoating system*; the *powder reservoirs*; the *heating elements* for bed and reservoirs heating; *powder recovery system*

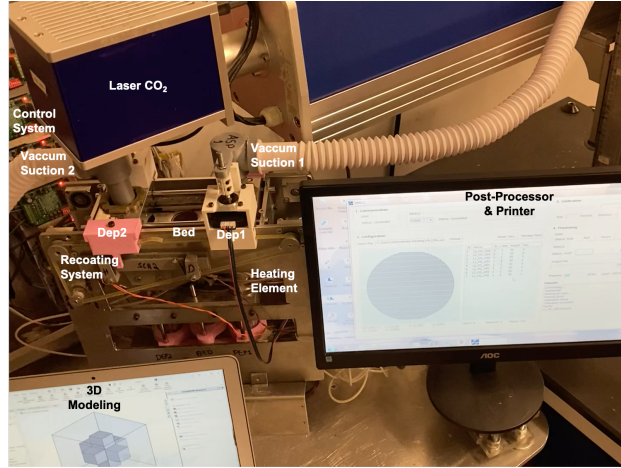


Figure 7: 3DMMLPBF machine — version 2.0

consisting of a vacuum suction system; *atmosphere control system* consisting of a pressurized inert gas system; and the *control system*.

The working principle is similar to one of the typical LPBF machines, but
 505 it includes some tweaks for multi-material processing:

1. the printing bed lowers by layer height;
2. the powder reservoir goes up by layer height and powder is dragged by the recoating system to the printing bed; machine signals to the laser that it is ready for printing;
- 510 3. the laser marks the scanning paths; when a layer is finished or material changes the geometry file changes layer and the laser stops; the laser signals this fact to the machine;
4. the machine proceeds with the *lcode* instructions processing: if a new material is needed, the powder is recovered via powder recovery system and a new material is fetched from the respective reservoir and fed to the
 515 printing bed; the machine signals to the laser that is ready for printing;
5. the process repeats itself for each new layer and for each new material in a layer until the *End-of-File* is reached.

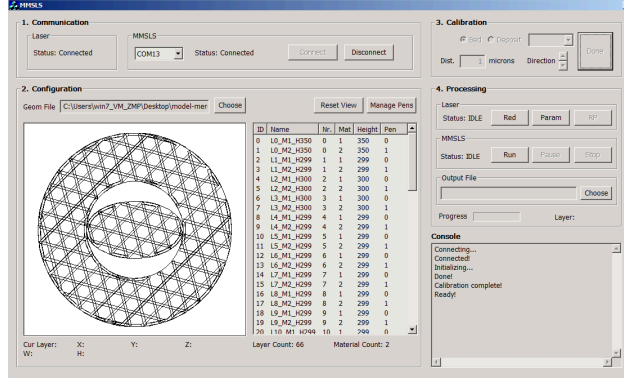


Figure 8: GUI to interface the 3DMMLPBF machine

It should be noted that, due to selective each material before a new one is added, the processing paradigm shifts from layer to layer to a point-by-point manufacturing.

A Graphical User Interface (GUI) was developed (Fig. 8) to interface the 3DMMLPBF machine, comprising the following software artifacts: post-processor — maps the geometrical data into process parameters through associated pens; printer — handles the communication with the equipment, command interpretation and data logging.

Table 1 lists the 3DMMLPBF machine specifications.

Lastly, the post-manufacturer software was developed to feedback relevant information to all agents in the manufacturing chain. Fig. 9 illustrates the manufacturing model view, comprising the model, the scan pattern, its layers and the associated materials and pens. The manufacturing model can be loaded and previewed, alongside with the manufacturing output file (the output from the equipment). The top-level entities are shown as the top tabs, namely part, 3D model, manufacturing model, laser, and mechanical tests. All databases can be exported separately for appropriate handling by each process' agent.

Table 1: 3DMMLPBF machine final specifications

Dimensions (l x w x h)[mm]	320 x 100 x 400
Power supply	Laser: 400 VAC, 10 A
	Machine: 24 V, 15 A
Build dimensions [mm]	25 \varnothing x 100
Nr. of materials	2
Temperature	Tested up to 250°C (higher temperatures can be used)
Laser	Type: CO_2
	Power: 30 W
	Spot size: 50 μ m
Resolution [μ m]	Full-step (all axes, except bed): 5 ± 0.25
	1/16-step (bed): 0.32 ± 0.016
Estimated cost [EURO]	Laser: 7500
	Machine: 1500
	Total: 9000

5. Tests

In this chapter, the 3DMMLPBF methodology devised was tested and the results are presented, namely: tests to the software toolchain instantiated and the workflow, and equipment and product manufacturing tests.

⁵⁴⁰ 5.1. Workflow

The workflow tests contemplate two types of tests: unit tests — tests to each software component independently, to assess if the functionality of each component meets its specific requirements; integrated tests — tests to the pipelining of the software components, to assess if the overall workflow specifications are

⁵⁴⁵ met.

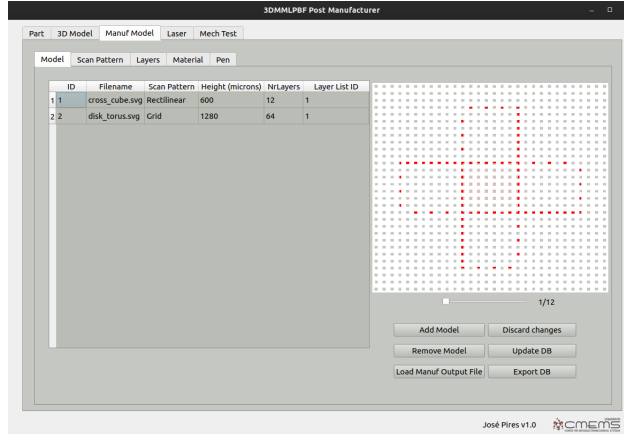


Figure 9: 3DMMLPBF Post-Manufacturer

5.1.1. Slicer and Path generator

The unit tests performed fall in the following categories: different path topologies; different slicing and path generation parameters; different 3D models.

550 The `.stl` input models used for the testing were: `mod1.stl` — a torus, simply called a *ring*; `mod2.stl` — a disk (see fig. 10). These models aims to represent two different materials and the simplest of the cases of multi-material processing: filled and unfilled regions without overlapping, but close enough that the bonding can occur via welding.

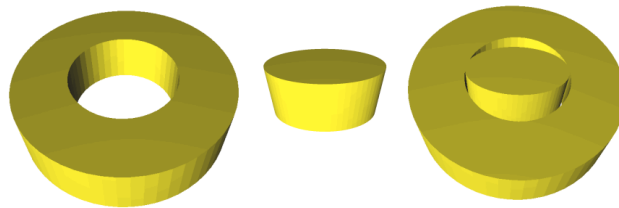


Figure 10: Input `.stl` models: `mod1.stl` (left); `mod2.stl` (center); assembled (right)

555 *Path topologies.* The slicer supports different path topologies, namely: rectilinear; aligned-rectilinear; grid; triangles; cubic; concentric; honeycomb 3d-

honeycomb; hilbert-curve; archimedean-chords; octagram-spiral.

Due to intrinsic open nature of the slicer and path generator, shell scripting was used to automatically test all path topologies in a batch.

560 As a common denominator between the tests, the following main parameters were fixed (see table 2): fill angle, fill density and infill extrusion width. The path topologies tests results are presented in fig. 11 for the different topologies. It can be seen that the slicer + path generator is able to generate the different topologies for multi material components.

Table 2: Path topology main fixed parameters

fill angle	fill density	infill extrusion width
45°	15 %	0.1 mm

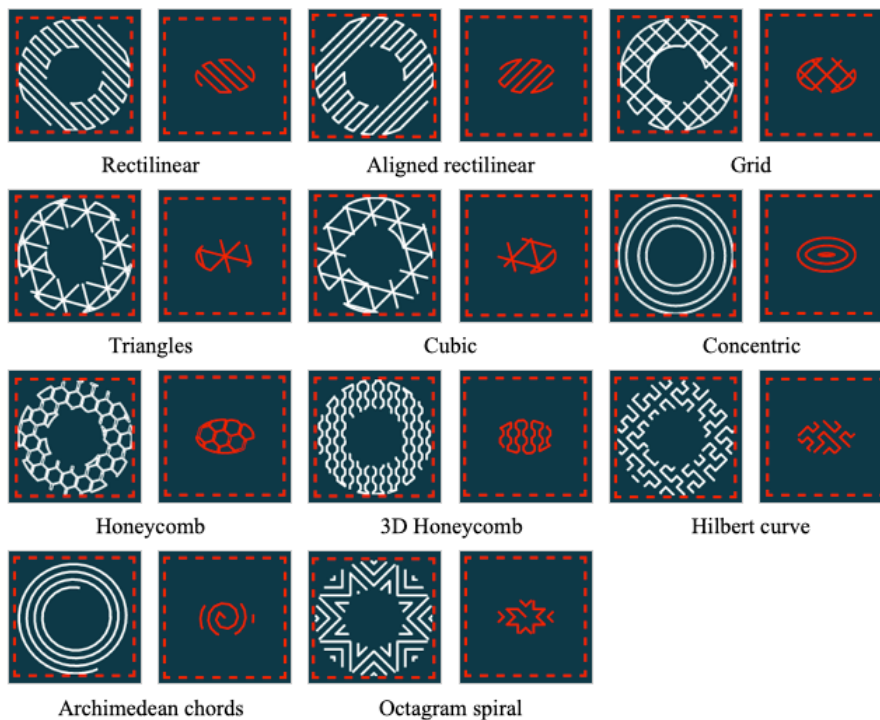


Figure 11: Path topologies test

565 *Slicing and Path generation parameters.* For the slicing and path generation parameters testing the 3D models are the same and the path topology selected was the rectilinear one. The following parameters were varied: fill angle, fill density, infill extrusion width (for path generation); layer height (for slicer). Once again, the scripting technique previously mentioned was used.

570 The fill angle was varied from 0% to 90%. Only one material is presented, as the slicing and path generation for multi material was previously validated. As can be seen in fig. 12, the fill angle is successfully modified.

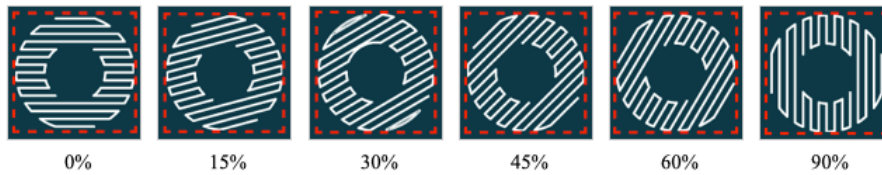


Figure 12: Fill angle test: 0% to 90%

The fill density was varied from 1% to 40%. As can be seen in fig. 13, for very low fill densities, e.g. 1–5%, the slice is only partially filled; increasing the fill density from 20 to 40%, the slice is almost completely filled. These higher fill densities (40% for the models in analysis) can be helpful in enabling the porting of the 3D printing path topologies to SLS ones, as the reduced distance between fillings (fill spacing) helps to promote powder melting in small gaps.

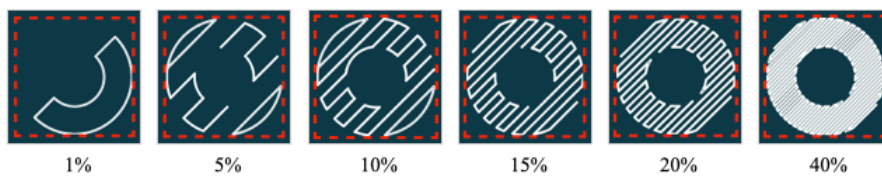


Figure 13: Fill density test: 1% to 40%

580 The infill extrusion width was varied from 0.01 to 0.5 millimeters. As can be seen in fig. 14, for very low extrusion widths, e.g. 0.01–0.02 mm, the slice is almost completely filled, which can be beneficial for SLS paths. For higher infill extrusions widths, e.g. 0.5 mm, the part is only partially filled.

Although related, fill density and infill extrusion width are conceptually different: infill extrusion width is the filling width, which can be lowered to
 585 mimic the laser marking path width; fill density is the amount of filling paths per slice area.

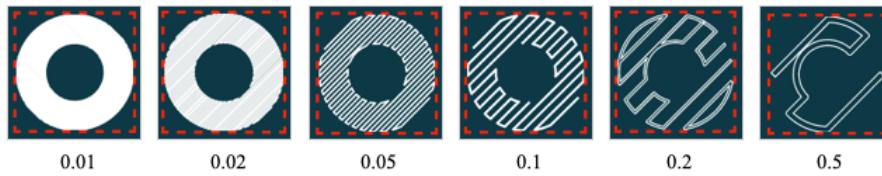


Figure 14: Infill extrusion width test: 0.01–0.5 mm

To analyse the slicer performance, the layer height was varied from 0.025 to 0.001 millimeters, and the number of layers, execution time, and file size were registered in table 3. As can be seen, for 25 micrometers, the number of
 590 layers is 120, taking 2.86 seconds to compute and yielding a file size of 1.3 MB. Decreasing the layer height, increases the number of layers as expected, as well as the computation time and file size. Even more interesting is that the slicer is capable of slicing layers with 1 micrometer height within a reasonable amount of time (79.4 seconds), which excels the fabrication requirements. However, the
 595 file size is penalised as expected, yet, is still tolerable.

Table 3: Layer height tests: 0.025–0.001 mm

Layer height [mm]	Nr. of layers	Computation time [s]	File Size [kB]
0.025	120	2.86	1300
0.020	150	3.84	1600
0.015	198	5.52	2100
0.010	298	7.12	3100
0.005	592	14.50	6200
0.001	1456	79.39	29400

Models. In this section is analysed the response of the slicer and path generation to different input models:

- *Cross and cube:* a bi-material component with an internal cavity belonging to one material and the external component to another; this is a good example of a multi-material component that is only feasible via additive manufacturing (fig. 15);
- *3 cubes:* a three material component, with each cube being enclosed by an outer one. Once again, this a typical example of a component only feasible using AM (fig. 17).

Furthermore, the integrity of the `.stl` file format produced and the agnostic behaviour of the slicer and path generator in respect of the inputs was tested by using a different 3D CAD modelling tool — FreeCAD — an open source 3D parametric modeller [65].

The cross and cube component 3D model is illustrated in fig. 15. Consists of a cross of one material inserted in a cube of another material. The component was exported as two `.stl` files corresponding to each material and fed to the the slicer and path generator, using the default values. The result can be seen in fig.16, with both sub-components being sliced and filled with the rectilinear pattern in consecutive layers corresponding to the center of the part. Thus, the slicer and path generator performs well with a different input model and is agnostic about the provenance of the `.stl` input files.

The 3 cubes 3D model is illustrated in fig. 17. Consists of a three cubes, each one inside of the outer one. The component was exported as three `.stl` files corresponding to each material and fed to the the slicer and path generator, using the default values. The result can be seen in fig.18, with all sub-components being sliced and filled with the rectilinear pattern in consecutive layers corresponding to the three materials. An excerpt of the output `.svg` file is presented in Listing 1, where it can be seen that the slicing and path generation occurred for all three materials.

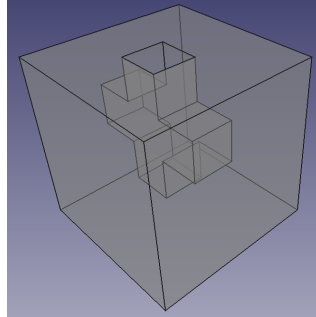


Figure 15: Cross and Cube 3D model

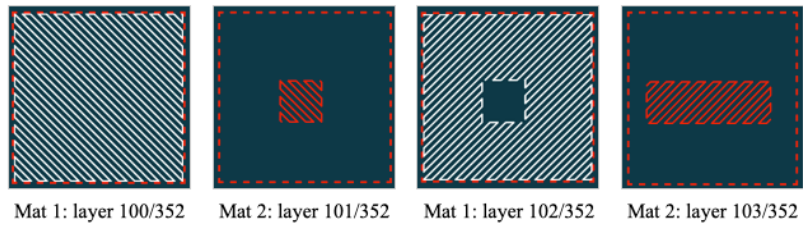


Figure 16: Cross and cube slicing test

625 Once again, the slicer and path generator performs well with a different input
 model and is agnostic about the provenance of the `.stl` input files. Furthermore,
 it is capable of handling models with more than two materials.

```

630 <g id="L0_M1_H25" slic3r:z="0.0250" slic3r:slice-z="0.0125" slic3r:layer-height=
      "0.0250" slic3r:mat="1">
    <polyline points= "20,0 0,0 0,20 20,20 20,0 " style="fill: none; stroke: white;
      stroke-width: 0.1; fill-type: evenodd" slic3r:type="" />
  </g>
635 <g id="L0_M2_H25" slic3r:z="0.0250" slic3r:slice-z="0.0125" slic3r:layer-height=
      "0.0250" slic3r:mat="2">
    <polyline points= "15,5 0,5 0,20 15,20 15,5 " style="fill: none; stroke: red;
      stroke-width: 0.1; fill-type: evenodd" slic3r:type="" />
  </g>
640 <g id="L0_M3_H25" slic3r:z="0.0250" slic3r:slice-z="0.0125" slic3r:layer-height=
      "0.0250" slic3r:mat="3">
    <polyline points= "10,10 0,10 0,20 10,20 10,10 " style="fill: none; stroke: blue
      ; stroke-width: 0.1; fill-type: evenodd" slic3r:type="" />
  </g>
  
```

Listing 1: 3cubes.svg (excerpt)

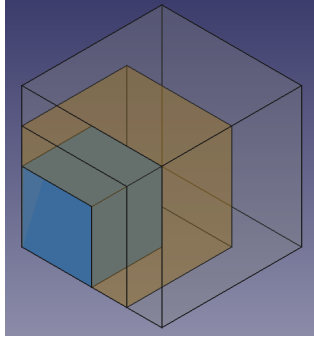


Figure 17: 3 cubes 3D model

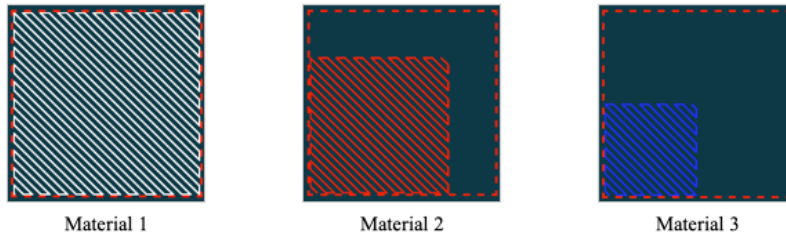


Figure 18: 3 cubes slicing test

645 *5.1.2. Discussion*

The workflow tests performed on the slicer and path generator, and on the post-processor and printer, helped to improve the respective tools by feeding back relevant information. More importantly, these tests allowed to validate the toolchain:

- 650 • Slicer and path generator: the slicer and path generator are capable of slicing and generating paths for various 3D models with different fill angle, fill density, infill extrusion width, layer height, and number of materials. The slicer is agnostic about the input files. It was also seen that a significant number of path topologies are available and that the fill density and infill extrusion width can be varied to mimic the required path filling for laser trajectories. Due to the high number of path topologies available off-the-shelf and the possible adaptation from the 3D printing area to

the SLS one, fast iteration on part production is possible. Lastly, due to the open source nature of the slicer and path generator, the modification of the available path topologies or the addition of new ones is relatively straightforward.

- Post-processor and printer: the post-processor is capable of processing the geometric and material data in the manufacturing file and mapping them to the desired processing parameters, irrespective of the material, layer height and layer number. The printer was successfully tested on offline mode to produce the part. Additionally, it was also seen the tight coupling between post-processor and printer, signalled by the restriction on the production of parts with more than two materials.

5.2. *Equipment and Manufacturing*

In this section the tests conducted on the equipment and part manufacturing are presented. As a proof-of-concept, the cross and cube model was used. This bimaterial model was sliced in 6 layers for easier process demonstration, with a height of 50 micrometers and the rectilinear toolpath was used. For easier demonstration, the same material was used, but with different colors for better visualization.

The resulting manufacturing model was then loaded to the Post-Processor and Printer GUI as illustrated in Fig. 19. The master system is connected to the 3DMMLPBF machine via COM port. The process parameters are mapped to each material through the **Manage Pens** pushbutton, as depicted in Table 4. A calibration can also be performed to minimize powder usage. After all these steps are completed and the machine homing is done, the manufacturing can start by pressing the **Run** pushbutton.

Fig 20 illustrates the manufacturing: on the left the visualization of the current layer and the corresponding GUI status; on the right the result of the layer after being printed. As it can be seen, the layer is correctly printed, in compliance with the process and geometrical data provided.

Table 4: Manufacturing parameters for each material

Process Parameters	Mat 1 (Purple)	Mat 2 (Black)
Speed [mm/s]	850	1000
Power (%)	45	25
Pulse frequency (kHz)	20	20

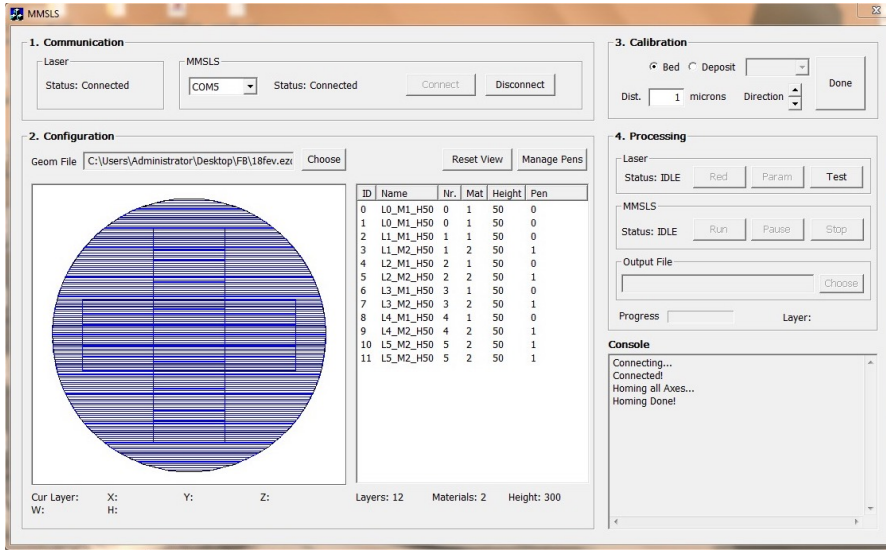
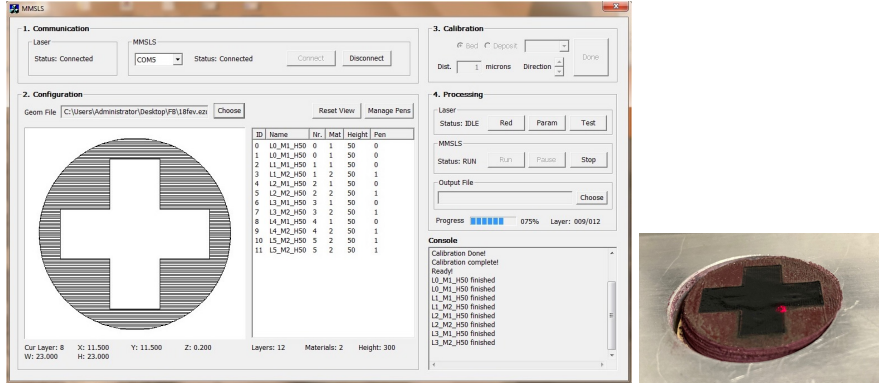


Figure 19: Post-Processor & Printer GUI: Initialization

Finally, Fig. 21 illustrates the bimaterial cross and cube part produced after being cross-sectioned, where it is clearly visible the tridimensional material variation, as defined by the original 3D CAD model. Furthermore, the Scanning Electron microscope (SEM) analysis performed on the part (Fig. 22) showed good densification, demonstrating the good manufacturing performance of the equipment.

Additionally, the 3DMMLPBF equipment was tested in conjunction with a fiber laser to verify its agnosticism. Unfortunately, no suitable powder material was available, thus the tests comprised only the scanning paths and process parameters. This test was successful, proving the 3DMMLPBF can be used with multiple lasers without any modification. Hence, this opens new prospects on



(a) GUI

(b) Machine bed

Figure 20: Post-Processor & Printer: Manufacturing

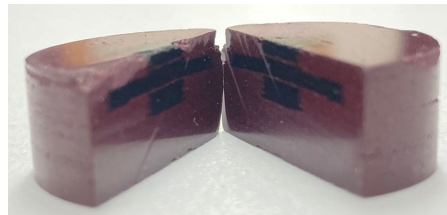


Figure 21: Cross and cube part: final result

the use of the equipment, where the combination of multiple laser sources of different wavelength can further support the fabrication of multi-material components of very distinct powder granulometric size, contingent of their flowability and an adequate powder dispensing system.

The equipment and manufacturing tests performed clearly demonstrate the feasibility of 3DMMLPBF process and validate the equipment developed, as well as the accompanying toolchain.

6. Conclusion

Current LPBF based processes' workflow lies in a closed environment that does not take into account all involved agents, limiting their access to relevant information which consequently hinders the technological development. Fur-

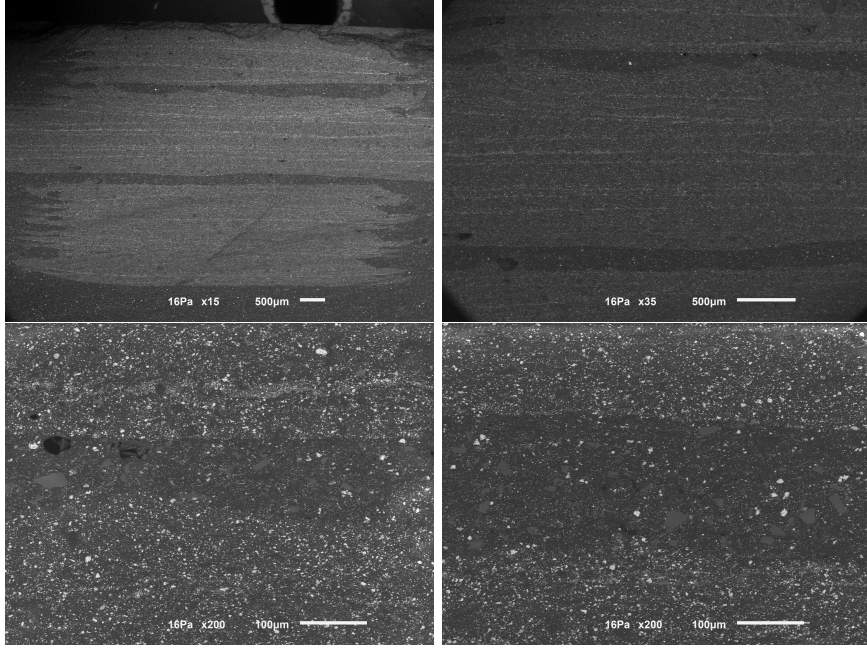


Figure 22: Cross and cube part: SEM analysis

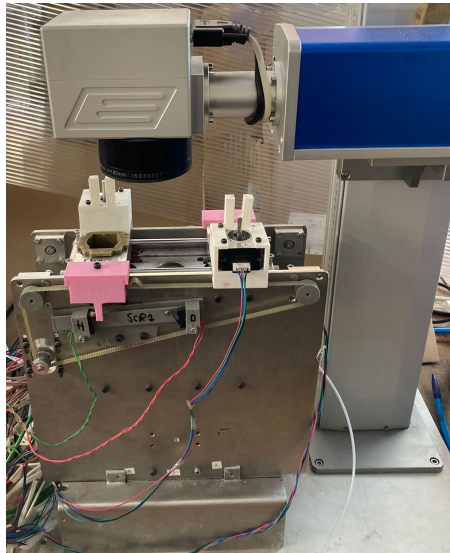


Figure 23: Laser agnostic: the 3DMMLPBF equipment was tested with a fiber laser

thermore, as often this workflow resides in the chaining of intransparent blocks
710 of software and/or hardware, the complexity is very difficult to handle, as it
does not provide a flexible, modular and reusable infrastructure. If one adds the
multi-material processing to this already complex equation, it becomes nearly
impossible to handle.

The transparency of the tools used and a deep level of control over them,
715 alongside with a systematic and global perspective of LBAM processes without
the limitation of specific tools is of the utmost importance. Thus, in the present
work a methodology is proposed in order to cope with the identified difficulties
and to provide some desirable features, namely: abstraction, modularity, flex-
ibility, extensibility, high customisation, capability of managing the different
720 information flows, guidance to end-users and maximization of process's con-
trol. This methodology works by considering the relevant actors in LPBF pro-
cesses and the relevant data flows and their transformation in the manufacturing
chain. Four models were created for this purpose: design, pre-manufacturing,
manufacturing and post-manufacturing. As a result, the information flows are
725 conveniently and accurately handled by the relevant agent improving the man-
ufacturing chain, and the software components and hardware components were
identified.

Then, this methodology was applied specifically to the LPBF process for
multi-material processing. A simple workflow was presented with the minimum
730 features required for the task, implementing the pre-manufacturing, manufac-
turing stages and post-manufacturing stages, whereas the optimizations will be
implemented in the near future. Based on this methodology an equipment for
LPBF multi-material processing was designed and built.

Lastly, tests were conducted over the workflow, and equipment and manu-
735 facturing, proving the feasibility and correctness of the methodology and the
associated outputs — the software toolchain and the equipment — for the pro-
duction of 3D multi-material components by the LPBF process.

7. Future work

In the near future the remainder of the methodology will be implemented.
740 The optimizations in the manufacturing chain will be addressed by the inclusion
of the CAE and CAM optimizers, as well as the advisor.

Concerning the 3DMMLPBF equipment developed, the intention is to re-
place the laser software by our own custom software, enabling the integration
of the laser in the current equipment yielding a unique equipment for multi-
745 material processing. This will enable the generation of a single *lcode* file with
manufacturing instructions and reduce the complexity of the software compo-
nents and the synchronization protocol involved, while providing a deeper level
of control and customisation. As a result, the post-processor will be optimized.

It is also expected that the post-manufacturing chain will allow improve-
750 ments in the manufacturing chains by performing the relevant analysis. Lastly,
some additional solutions for multi-material processing and specially MMFGMs
will be tested based on different hardware and software solutions — e.g., com-
bination of multiple laser sources — which is supported by the modularity and
flexibility features of the proposed methodology, at both the software and hard-
755 ware level.

Declaration of Competing Interest

The authors declare that they have no known competing financial interests or
personal relationships that could have appeared to influence the work reported
in this paper.

760 Acknowledgements

This work was supported by Portuguese Foundation of Science and Technol-
ogy national funds, under the national support to R&D units grant, through the
reference projects UIDB/04436/2020 and UIDP/04436/2020), and also, through
the project ‘HAMaBICo — Hybrid Additive Manufacturing for Bio-Inspired

765 Components', reference NORTE-01-0145-FEDER-000018 and by the project
Add.Additive_Manufacturing to Portuguese Industry_POCI-01-0247-FEDER-
024533.

References

- [1] G. Liu, X. Zhang, X. Chen, Y. He, L. Cheng, M. Huo, J. Yin, F. Hao,
770 S. Chen, P. Wang, et al., Additive manufacturing of structural materials,
Materials Science and Engineering: R: Reports 145 (2021) 100596.
- [2] O. Carvalho, M. Buciumeanu, S. Madeira, D. Soares, F. Silva, G. Miranda,
Optimization of alsicnts functionally graded material composites for en-
gine piston rings, Materials & Design 80 (2015) 163–173.
- 775 [3] T. Wohlers, Wohlers report 2011: Additive manufacturing and 3d printing,
state of the industry, wohlers associates, ft, Collins, CO.
- [4] H. Chen, Y. Sun, W. Yuan, S. Pang, W. Yan, Y. Shi, A review on discrete
element method simulation in laser powder bed fusion additive manufactur-
ing, Chinese Journal of Mechanical Engineering: Additive Manufacturing
780 Frontiers (2022) 100017.
- [5] M. Bayat, W. Dong, J. Thorborg, A. C. To, J. H. Hattel, A review of
multi-scale and multi-physics simulations of metal additive manufacturing
processes with focus on modeling strategies, Additive Manufacturing 47
(2021) 102278.
- 785 [6] B. Xiao, Y. Zhang, Numerical simulation of direct metal laser sintering of
single-component powder on top of sintered layers, Journal of Manufactur-
ing Science and Engineering 130 (4) (2008) 041002.
- [7] K. Dai, L. Shaw, Thermal and mechanical finite element modeling of laser
forming from metal and ceramic powders, Acta Materialia 52 (1) (2004)
790 69–80.

- [8] X. He, J. Mazumder, Transport phenomena during direct metal deposition, *Journal of Applied Physics* 101 (5) (2007) 053113.
- [9] X. He, G. Yu, J. Mazumder, Temperature and composition profile during double-track laser cladding of h13 tool steel, *Journal of Physics D: Applied Physics* 43 (1) (2009) 015502.
- 795
- [10] A. Manthiram, D. Bourell, H. Marcus, Nanophase materials in solid freeform fabrication, *JOM Journal of the Minerals, Metals and Materials Society* 45 (11) (1993) 66–70.
- [11] H. Asgharzadeh, A. Simchi, Effect of sintering atmosphere and carbon content on the densification and microstructure of laser-sintered m2 high-speed steel powder, *Materials Science and Engineering: A* 403 (1) (2005) 290–298.
- 800
- [12] P. Avrampos, G.-C. Vosniakos, A review of powder deposition in additive manufacturing by powder bed fusion, *Journal of Manufacturing Processes* 74 (2022) 332–352.
- [13] D. Gu, W. Meiners, K. Wissenbach, R. Poprawe, Laser additive manufacturing of metallic components: materials, processes and mechanisms, *International materials reviews* 57 (3) (2012) 133–164.
- 805
- [14] S. M. Thompson, L. Bian, N. Shamsaei, A. Yadollahi, An overview of direct laser deposition for additive manufacturing; part i: Transport phenomena, modeling and diagnostics, *Additive Manufacturing* 8 (2015) 36–62.
- 810
- [15] Y. Tadjdeh, Navy beefs up 3d printing efforts with new ‘print the fleet’ program, *National Defense* 99 (731) (2014) 24–26.
- [16] M. J. Foust, D. Thomsen, R. Stickles, C. Cooper, W. Dodds, Development of the ge aviation low emissions taps combustor for next generation aircraft engines, *AIAA Paper* 936 (2012) 2012.
- 815
- [17] R. Scott, Chinese Company Showcases Ten 3D-Printed Houses, *ArchDaily*, <http://www.archdaily.com/543518/>

chinese-company-showcases-ten-3d-printed-houses, accessed:
2017-09-25 (2014).

- 820 [18] K. Dalgarno, T. Stewart, Production tooling for polymer moulding using
the rapidsteel process, *Rapid Prototyping Journal* 7 (3) (2001) 173–179.
- [19] L.-E. Rännar, A. Glad, C.-G. Gustafson, Efficient cooling with tool inserts
manufactured by electron beam melting, *Rapid Prototyping Journal* 13 (3)
(2007) 128–135.
- 825 [20] L. Murr, S. Gaytan, F. Medina, H. Lopez, E. Martinez, B. Machado,
D. Hernandez, L. Martinez, M. Lopez, R. Wicker, et al., Next-generation
biomedical implants using additive manufacturing of complex, cellular and
functional mesh arrays, *Philosophical Transactions of the Royal Society of
London A: Mathematical, Physical and Engineering Sciences* 368 (1917)
830 (2010) 1999–2032.
- [21] R. McCann, M. A. Obeidi, C. Hughes, É. McCarthy, D. S. Egan, R. K.
Vijayaraghavan, A. M. Joshi, V. A. Garzon, D. P. Dowling, P. J. McNally,
et al., In-situ sensing, process monitoring and machine control in laser
powder bed fusion: A review, *Additive Manufacturing* 45 (2021) 102058.
- 835 [22] B. Vayre, F. Vignat, F. Villeneuve, Metallic additive manufacturing: state-
of-the-art review and prospects, *Mechanics & Industry* 13 (2) (2012) 89–96.
- [23] D. Salehi, M. Brandt, Melt pool temperature control using labview in nd:
Yag laser blown powder cladding process, *The international journal of ad-
vanced manufacturing technology* 29 (3) (2006) 273–278.
- 840 [24] T. Purtonen, A. Kalliosaari, A. Salminen, Monitoring and adaptive control
of laser processes, *Physics Procedia* 56 (2014) 1218–1231.
- [25] M. Vaezi, S. Chianrabutra, B. Mellor, S. Yang, Multiple material addi-
tive manufacturing—part 1: a review: this review paper covers a decade of
research on multiple material additive manufacturing technologies which

- 845 can produce complex geometry parts with different materials, *Virtual and Physical Prototyping* 8 (1) (2013) 19–50.
- [26] D. Han, H. Lee, Recent advances in multi-material additive manufacturing: Methods and applications, *Current Opinion in Chemical Engineering* 28 (2020) 158–166.
- 850 [27] A. Bandyopadhyay, B. Heer, Additive manufacturing of multi-material structures, *Materials Science and Engineering: R: Reports* 129 (2018) 1–16.
- [28] D. Joung, V. Truong, C. C. Neitzke, S.-Z. Guo, P. J. Walsh, J. R. Monat, F. Meng, S. H. Park, J. R. Dutton, A. M. Parr, et al., 3d printed stem-cell derived neural progenitors generate spinal cord scaffolds, *Advanced functional materials* 28 (39) (2018) 1801850.
- 855 [29] Y. Lu, S. N. Mantha, D. C. Crowder, S. Chinchilla, K. N. Shah, Y. H. Yun, R. B. Wicker, J.-W. Choi, Microstereolithography and characterization of poly (propylene fumarate)-based drug-loaded microneedle arrays, *Biofabrication* 7 (4) (2015) 045001.
- 860 [30] F. Li, N. P. Macdonald, R. M. Guijt, M. C. Breadmore, Multimaterial 3d printed fluidic device for measuring pharmaceuticals in biological fluids, *Analytical chemistry* 91 (3) (2018) 1758–1763.
- [31] F. Bartolomeu, M. Costa, N. Alves, G. Miranda, F. S. Silva, Additive manufacturing of niti-ti6al4v multi-material cellular structures targeting
- 865 orthopedic implants, *Optics and Lasers in Engineering* 134 (2020) 106208.
- [32] G. Coelho, T. M. F. Chaves, A. F. Goes, E. C. Del Massa, O. Moraes, M. Yoshida, Multimaterial 3d printing preoperative planning for frontoethmoidal meningoencephalocele surgery, *Child’s Nervous System* 34 (4) (2018) 749–756.
- 870 [33] A. Cresswell-Boyes, A. Barber, D. Mills, A. Tatla, G. Davis, Approaches to 3d printing teeth from x-ray microtomography, *Journal of Microscopy* 272 (3) (2018) 207–212.

- [34] A. Sydney Gladman, E. A. Matsumoto, R. G. Nuzzo, L. Mahadevan, J. A. Lewis, Biomimetic 4d printing, *Nature materials* 15 (4) (2016) 413–418.
- 875 [35] C. Yuan, D. J. Roach, C. K. Dunn, Q. Mu, X. Kuang, C. M. Yakacki, T. Wang, K. Yu, H. J. Qi, 3d printed reversible shape changing soft actuators assisted by liquid crystal elastomers, *Soft Matter* 13 (33) (2017) 5558–5568.
- [36] D. Espalin, D. W. Muse, E. MacDonald, R. B. Wicker, 3d printing multifunctionality: structures with electronics, *The International Journal of Advanced Manufacturing Technology* 72 (5) (2014) 963–978.
- 880 [37] A. D. Valentine, T. A. Busbee, J. W. Boley, J. R. Raney, A. Chortos, A. Kotikian, J. D. Berrigan, M. F. Durstock, J. A. Lewis, Hybrid 3d printing of soft electronics, *advanced Materials* 29 (40) (2017) 1703817.
- [38] W. HuangáGoh, A. HoseináSakhaei, et al., Highly stretchable hydrogels for uv curing based high-resolution multimaterial 3d printing, *Journal of Materials Chemistry B* 6 (20) (2018) 3246–3253.
- 885 [39] T.-S. Wei, B. Y. Ahn, J. Grotto, J. A. Lewis, 3d printing of customized li-ion batteries with thick electrodes, *Advanced Materials* 30 (16) (2018) 1703027.
- 890 [40] F. Brueckner, M. Riede, M. Müller, F. Marquardt, R. Willner, A. Seidel, E. Lopéz, C. Leyens, E. Beyer, Enhanced manufacturing possibilities using multi-materials in laser metal deposition, *Journal of Laser Applications* 30 (3) (2018) 032308.
- [41] K. Shah, I. ul Haq, A. Khan, S. A. Shah, M. Khan, A. J. Pinkerton, Parametric study of development of inconel-steel functionally graded materials by laser direct metal deposition, *Materials & Design (1980-2015)* 54 (2014) 531–538.
- 895 [42] S. Liu, Y. C. Shin, Additive manufacturing of ti6al4v alloy: A review, *Materials & Design* 164 (2019) 107552.
- 900

- [43] F. Bartolomeu, M. Costa, N. Alves, G. Miranda, F. S. Silva, Selective laser melting of ti6al4v sub-millimetric cellular structures: Prediction of dimensional deviations and mechanical performance, *Journal of the Mechanical Behavior of Biomedical Materials* 113 (2021) 104123.
- 905 [44] N. Shamsaei, A. Yadollahi, L. Bian, S. M. Thompson, An overview of direct laser deposition for additive manufacturing; part ii: Mechanical behavior, process parameter optimization and control, *Additive Manufacturing* 8 (2015) 12–35.
- [45] S. Sing, S. Huang, G. Goh, G. Goh, C. Tey, J. Tan, W. Yeong, Emerging
910 metallic systems for additive manufacturing: In-situ alloying and multi-metal processing in laser powder bed fusion, *Progress in Materials Science* 119 (2021) 100795.
- [46] Z. Liu, D. Zhang, S. Sing, C. Chua, L. Loh, Interfacial characterization of slm parts in multi-material processing: Metallurgical diffusion between 316l stainless steel and c18400 copper alloy,
915 *Materials Characterization* 94 (2014) 116–125. doi:<https://doi.org/10.1016/j.matchar.2014.05.001>.
URL <https://www.sciencedirect.com/science/article/pii/S1044580314001351>
- 920 [47] S. Sing, L. Lam, D. Zhang, Z. Liu, C. Chua, Interfacial characterization of slm parts in multi-material processing: Intermetallic phase formation between als10mg and c18400 copper alloy, *Materials Characterization* 107 (2015) 220–227.
- [48] A. G. Demir, B. Previtali, Multi-material selective laser melting of fe/al-
925 12si components, *Manufacturing Letters* 11 (2017) 8–11.
- [49] P. Kumar, J. K. Santosa, E. Beck, S. Das, Direct-write deposition of fine powders through miniature hopper-nozzles for multi-material solid freeform fabrication, *Rapid Prototyping Journal* (2004) .

- [50] K. A. Mumtaz, N. Hopkinson, Laser melting functionally graded composition of waspaloy® and zirconia powders, *Journal of materials science* 42 (18) (2007) 7647–7656.
- [51] M. Ott, M. Zach, Multi-material processing in additive manufacturing, in: 2010 International Solid Freeform Fabrication Symposium, University of Texas at Austin, 2010.
- [52] Y. Chivel, New approach to multi-material processing in selective laser melting, *Physics Procedia* 83 (2016) 891–898.
- [53] C. Anstaett, C. Seidel, G. Reinhart, Fabrication of 3d multi-material parts using laser-based powder bed fusion, in: 2017 International Solid Freeform Fabrication Symposium, University of Texas at Austin, 2017.
- [54] Admatec, laserflux conflux, <https://admateceurope.com/#laserflex>, accessed: 2022-02-25.
- [55] J. Walker, J. R. Middendorf, C. C. Lesko, J. Gockel, Multi-material laser powder bed fusion additive manufacturing in 3-dimensions, *Manufacturing Letters* 31 (2022) 74–77.
- [56] W. Chiu, K. Yu, Direct digital manufacturing of three-dimensional functionally graded material objects, *Computer-Aided Design* 40 (12) (2008) 1080–1093.
- [57] R. Ponche, O. Kerbrat, P. Mognol, J.-Y. Hascoet, A novel methodology of design for additive manufacturing applied to additive laser manufacturing process, *Robotics and Computer-Integrated Manufacturing* 30 (4) (2014) 389–398.
- [58] W. Chiu, S. Tan, Multiple material objects: from cad representation to data format for rapid prototyping, *Computer-aided design* 32 (12) (2000) 707–717.

- 955 [59] Y. Siu, S. Tan, 'source-based' heterogeneous solid modeling, *Computer-Aided Design* 34 (1) (2002) 41–55.
- [60] T. R. Jackson, Analysis of functionally graded material object representation methods, Ph.D. thesis, Massachusetts Institute of Technology (2000).
- [61] L. Patil, D. Dutta, A. D. Bhatt, K. Jurrens, K. Lyons, M. Pratt, R. D. Sri-
960 ram, A proposed standards-based approach for representing heterogeneous
objects for layered manufacturing, *Rapid Prototyping Journal* 8 (3) (2002)
134–146.
- [62] B. Bruegge, A. H. Dutoit, *Object-Oriented Software Engineering Using
UML, Patterns and Java-(Required)*, Vol. 2004, Prentice Hall, 2004.
- 965 [63] Slic3r - g-code generator for 3d printers, <http://slic3r.org/>, accessed:
2017-09-25.
- [64] Scalable Vector Graphics (SVG) 1.1. - second edition, [https://www.w3.
org/TR/SVG/](https://www.w3.org/TR/SVG/), accessed: 2017-09-25.
- [65] F. team, FreeCAD: 3D parametric modeler, [https://www.freecadweb.
970 org/](https://www.freecadweb.org/), accessed: 2019-10-31 (2016).



Graphical Abstract

The graphical abstract of paper submitted to *Journal of Robotics and Computer Integrated Manufacturing*, showcasing the present work, is presented next.

